INFORMATION TO USERS

This manuscript has been reproduced from the microfilm master. UMI films the text directly from the original or copy submitted. Thus, some thesis and dissertation copies are in typewriter face, while others may be from any type of computer printer.

The quality of this reproduction is dependent upon the quality of the copy submitted. Broken or indistinct print, colored or poor quality illustrations and photographs, print bleedthrough, substandard margins, and improper alignment can adversely affect reproduction.

In the unlikely event that the author did not send UMI a complete manuscript and there are missing pages, these will be noted. Also, if unauthorized copyright material had to be removed, a note will indicate the deletion.

Oversize materials (e.g., maps, drawings, charts) are reproduced by sectioning the original, beginning at the upper left-hand corner and continuing from left to right in equal sections with small overlaps.

Photographs included in the original manuscript have been reproduced xerographically in this copy. Higher quality 6" x 9" black and white photographic prints are available for any photographs or illustrations appearing in this copy for an additional charge. Contact UMI directly to order.

Bell & Howell Information and Learning
300 North Zeeb Road, Ann Arbor, MI 48106-1346 USA
800-521-0600

Université d'Ottawa • University of Ottawa

MINERAL CHEMISTRY AND MÖSSBAUER SPECTROSCOPY OF MICAS FROM GRANITIC ROCKS OF THE CANADIAN APPALACHIANS

by

Amir Ali Tabbakh Shabani

A thesis submitted to the School of Graduate Studies and Research

in partial fulfillment of the requirements

for the degree of Ph.D. in Earth Sciences

OTTAWA-CARLETON GEOSCIENCE CENTRE

AND

UNIVERSITY OF OTTAWA

OTTAWA, CANADA

Abstract

This thesis represents the results of a mineral chemical and crystal chemical investigation of trioctahedral and dioctahedral micas from the Paleozoic granitic rocks of the Dunnage, Gander, Avalon and Meguma tectonic zones of the Canadian Appalachians. These minerals were studied by wavelength-dispersive X-ray microanalyses, X-ray powder diffractometry and ^{57}Fe Mössbauer spectroscopy. The objectives of the thesis were: 1) to investigate the relationships between the composition of biotite and the tectonic origin of the host granitic rock, 2) to investigate the significance of quadrupole splitting distributions in the Mössbauer spectra of these Appalachian and other biotite specimens and, 3) to investigate the cis and trans- octahedral Fe^{2+} Mössbauer spectral contributions of dioctahedral (muscovite) micas from the granitic rocks of the Gander zone in New Brunswick. These results of the study are presented as three manuscripts intended for submission to peer-reviewed journals.

In the first manuscript, the author document the mineral chemistry of biotite occurring in granitic rocks of the Canadian Appalachians that range from gabbro, to diorite, syenite and granite. The most significant variations are changes in total Al contents and Fe/(Fe+Mg) values, both sensitive indicators of conditions that prevailed in the host magmas. Using common oxygen geobarometers, the biotite from the granitic rocks of most zones plot on or above the NNO buffer, indicating moderate oxidizing conditions, whereas biotite from the Meguma zone plots between the QFM and NNO buffers implying fairly reducing conditions during crystallization.

By comparing with the biotite from other well-documented granitic suites of the world, the author conclude that the composition of biotite in Appalachian granitic rocks reflects primarily the nature of the host magmas and cannot be readily used for interpreting the tectonic setting of these rocks without the aid of whole-rock trace-element geochemistry, isotopic data and other geological constraints.

In the second manuscript, the methodology of quadrupole splitting distribution (QSD) analysis was used to describe the room temperature ^{57}Fe Mössbauer spectra of 71 specimens of trioctahedral micas from the Paleozoic granitic rocks of the Canadian Appalachians, the granitic rocks of the Hepburn and Bishop intrusive suites of the Early Proterozoic Wopmay orogen, Northwest Territories, and the nepheline syenite of the Cretaceous Mont Saint-Hilaire alkaline intrusion, Québec. The possible range of values and morphology of Fe^{2+} QSDs in biotite specimens has been established. The author extrapolate these QSD parameters to biotites in general.

To the author, the details of the crystallochemical controls of the observed QSDs in biotite are not well understood because of a lack of electronic structure calculations that link local distortion environments to quadrupole splitting values. Furthermore, several chemical parameters that are key crystal chemical parameters of the synthetic phlogopite-biotite-annite solid solution (e.g., Fe/(Fe+Mg), Fe^{3+}/Fe_{total}) do not correlate with any of the QSD features of natural biotites. The most strongly-correlated chemical parameter is found to be Al_{total}, which is related to several crystal chemical features such as calculated average octahedral cation radius [R], tetrahedral rotation angle (α) and average octahedral flattening angle (Ψ).

Finally, in the third manuscript, QSD analysis of specimens of muscovite from granites of the Gander zone in New Brunswick shows that the Mössbauer spectra of these dioctahedral micas fall into two distinct groups, despite an absence of systematic differences in chemical composition, X-ray patterns, unit-cell parameters, and Fe^{3+}/Fe_{total} ratios. In the first group, two well-resolved octahedral Fe^{2+} spectral contributions occur whereas, in the second group, a single but broader octahedral Fe^{2+} contribution occurs. Furthermore, spectra from the first group clearly show bimodal QSDs for Fe^{2+}, with a dominant contribution at ~3.0 mm/s and a minor one at ~2.1 mm/s that are attributable to cis- and trans-octahedral sites, respectively. In the second group, the spectra show broad unimodal QSDs for Fe^{2+}. These muscovite specimens from the second group may have Fe^{2+} in both cis- and trans-sites but these cannot be resolved, as is usually the case, for example, with trioctahedral micas. In group one, cis/trans populations provide measures of the degree of cation order and the density of vacancies on the cis sites.

Sommaire

Cette thèse présente les résultats d'une étude de la composition chimique et de la cristallochimie des micas trioctaédriques et dioctaédriques provenant des granites paléozoïques des zones tectoniques de Dunnage, Gander, Avalon et Meguma des Appalaches canadiennes. Ces minéraux furent caractérisés par spectrométrie de rayons-X avec la microsonde électronique ainsi que par diffraction de rayons X et par spectrométrie de Mössbauer. Les buts de l'étude étaient: 1) d'explorer les relations entre la composition de la biotite et le cadre tectonique des granites où elle se retrouve, 2) de chercher les causes et significations des distributions d'éclatements quadrupolaires extraites des spectres Mössbauer des biotites des Appalaches et d'ailleurs et, 3) de documenter les contributions spectrales Mössbauer attribuées au Fe^{2+} des sites octaédriques cis et trans des micas dioctaédriques (muscovite) de la zone Gander du Nouveau-Brunswick. Les résultats de l'étude sont présentés sous forme de trois manuscrits destinés à des revues scientifiques avec comité de lecture.

Le premier manuscrit explore la composition chimique de la biotite des roches granitiques (gabbro, diorite, granite, syénite) des Appalaches canadiennes. Les variations compositionelles les plus marquées sont des changements de la teneur totale en Al et du rapport Fe/(Fe+Mg), deux paramètres étroitements liés aux conditions existantes lors de la cristallisation magmatique de ces roches. En utilisant les géobaromètres d'oxygène les plus communs, la biotite des roches granitiques de la majorité des zones se situe près ou

légèrement au-dessus des valeurs attribuables au tampon NNO, indiquant des conditions relativement oxydantes alors que la biotite de la zone Méguma se situe entre les tampons QFM et NNO témoignant ainsi de conditions beaucoup plus réductrices lors de la cristallisation.

Une comparaison de ces biotites avec celles des suites granitiques bien documentées du monde permet de conclure que la composition de la biotite des granites des Appalaches reflète surtout la nature des magmas plutôt que leur cadre tectonique. La composition de la biotite ne peut donc être utilisée par elle-même pour déterminer le cadre tectonique de ces roches granitiques sans l'aide d'autres données telles que la géochimie des oligoéléments, des isotopes ou d'autres contraintes géologiques.

Dans le second manuscrit, la méthode d'extraction de distributions d'éclatements quadrupolaires est utilisée pour décrire les spectres Mössbauer de 71 échantillions de micas trioctaédriques provenant des granites paléozoïques des Appalaches canadiennes, des suites intrusives Hepburn et Bishop de l'orogène protérozoïque Wopmay des Territoires du Nord-Ouest et de l'intrusion alcaline crétacée du Mont Saint-Hilaire au Québec. Les écarts de valeurs possibles et les caractéristiques morphologiques de ces distributions d'éclatements quadrupolaires sont établies pour ces échantillions de biotite et sont extrapolées à toutes les biotites en général.

Les facteurs cristallochimiques qui contrôlent la forme des éclatements observés sont mal compris, surtout à cause du manque de calculs théoriques des structures électroniques qui relient les environnements locaux de distortion à ces éclatements quadrupolaires. En plus, plusieurs des propriétés compositionelles les plus importantes des micas synthétiques de

la série phlogopite-biotite-annite (e.g. Fe/(Fe+Mg), Fe^{3+}/Fe_{total}) ne montrent aucune corrélation avec les propriétés des distributions d'éclatements des biotites naturelles. Le paramètre compositionel ayant la plus grande corrélation avec les éclatements est la teneur totale en aluminium, qui est reliée elle-même à plusieurs paramètres cristallochimiques comme le rayon moyen calculé des cations octaédriques [R], l'angle de rotation tétraédrique (α) et la valeur moyenne de l'écrasement octaédrique (ψ).

Finalement, au troisième manuscrit l'analyse des distributions d'éclatements quadrupolaires des spectres Mössbauer des spécimens de muscovite provenant des granites de la zone Gander du Nouveau-Brunswick démontre que ces micas définissent deux groupes distincts malgré l'absence de différences observables de composition chimique, de patrons de diffraction de rayons X, de paramètres de maille élémentaire, et de valeurs de Fe^{3+}/Fe_{total}. Les micas du premier groupe démontrent deux contributions bien distinctes pour le Fe^{2+} octaédrique alors que les micas du deuxième groupe ont qu'une seule contribution élargie pour le Fe^{2+} octaédrique. De plus, les spectres du premier groupe ont une distribution d'éclatements quadrupolaires qui est clairement bimodale, avec une dominante à ~3.0 mm/s et une mineure à ~2.1 mm/s qui sont attribuables respectivement au sites octaédriques de géométrie cis et trans. Les spectres du deuxième groupe ont des distributions d'éclatements qui sont unimodales et élargies. Il est possible que les spécimens de muscovite du deuxième groupe aient du Fe^{2+} dans des sites cis et trans, cependant, les contributions de ces deux types de sites ne peuvent être discernées comme c'est le cas pour la plupart des micas trioctaédriques. Pour les micas du premier groupe, les populations attribuables aux sites cis

et trans permettent d'évaluer le niveau de mise en ordre des cations ainsi que la densité de sites vacants parmi les sites cis.

Acknowledgments

I would like to sincerely acknowledge some of the people whom without their help this thesis would never have been completed.

I would like first to express my sincere appreciation and gratitude to my supervisor, Dr. André E. Lalonde, for his continuous encouragement, guidance and support throughout the course of this study.

I am very grateful to Dr. Denis G. Rancourt, Department of Physics, who was always available for helpful discussion, guidance to solve the research problems, and for reviewing critically two parts of the thesis.

This study would not have been possible without the samples and data provided generously by Dr. J. B. Whalen of the Geological Survey of Canada; Dr. A. Kerr of the Geological Survey of Newfoundland and Labrador and Dr. D. B. Clarke of Dalhousie University, Nova Scotia.

I would also like to sincerely thank Dr. J. B. Whalen for his advice and reviewing one part of the thesis, in addition to contributing a large number of mineral specimens for this thesis.

Special thanks also to Drs. R. Kretz, K. Benn and R. Taylor for their advice on my research.

I wish to extend my sincere thanks to G. Poirier, McGill University, for instruction on the use of the electron microprobe, R. Hartree for XRF analyses of rocks, G. Mrazek for his assistance with the preparation of polished thin sections and J. Loop for his help on rock staining and titration analyses.

I would like also to thank my friends, colleagues and the support staff of the Department of Earth Sciences and graduate students K. Lagarec, P. Mercier and M. Z. Dang in the Mössbauer Laboratory of the Department of Physics, for their help on numerous occasions.

The author acknowledges a generous graduate scholarship from the Ministry of Culture and Higher Education of Iran. Research expenditures were covered by the Natural Sciences and Engineering Council of Canada through research grants to André E. Lalonde and Denis G. Rancourt.

Finally, I am enormously grateful to my wife, Shahrzad, for her patience, support and understanding during my studies in Canada.

Statement of Original Contribution

This thesis was done under the supervision of Dr. André E. Lalonde, from the Department of Earth Sciences (principal supervisor) and Dr. Denis G. Rancourt from the Department of Physics of the University of Ottawa. The following describes the extent of my personal involvement in the thesis.

1. Collection of rock samples from granitic plutons of the Gander zone in Newfoundland, assisted by Dr. André E. Lalonde, in August, 1995 and acquisition of rock samples from various sources.

2. Compilation of a comprehensive data set of mica analyses and Mössbauer parameters from theses and published papers which were used in the first and second manuscripts.

3. Preparation of samples for microprobe analysis (cutting the rocks, making polished thin sections and navigation maps of the sections), Mössbauer spectroscopy (crushing the rock, sieving, separation of mica and its final purification), XRF and XRD analyses (crushing and powdering).

4. Thin section petrography of all specimens.

5. Analysis of all mica specimens by Mössbauer spectroscopy, from preparing and running the sample, to collecting the spectrum, to fitting and analysis of the spectrum. Training provided by Drs. André E. Lalonde and Denis G. Rancourt.

6. Microprobe analysis of all micas. G. Poirier, Microprobe laboratory of the McGill University, provided instruction on the use of the JEOL electron microprobe.

7. Powder XRD analysis and cell-refinements of muscovite specimens from preparing

and running the sample, through the collecting of the XRD diffractogram and analysis. Dr. André E. Lalonde provided training in the use of the powder diffractometer and the computer cell-refinement program.

8. Preparation of the map of granitoid rocks of the Canadian Appalachians by compilation from various sources.

Finally, data presentation, analysis, interpretation and writing was performed by the author with the guidance and editing of the co-authors.

Table of Contents

Manuscript 2

Correlations between Octahedral - Fe^{2+} Quadrupole Splitting Distributions from Mössbauer Spectroscopy and Chemical Parameters in Biotite

Manuscript 3

Determination of Cis- and Trans- Fe^{2+} Populations in $2M_1$ Muscovite by Mössbauer Spectroscopy

List of Figures

Manuscript 1

Manuscript 2

Manuscript 3

List of Tables

Manuscript 1

Manuscript 2

Manuscript 3

List of Appendices

Appendices of Manuscript 1

Appendices of Manuscript 2

Appendix of Manuscript 3

List of abbreviations and symbols

A/CNK	molar $Al_2O_3/(CaO + Na_2O + K_2O)$
AFC	assimilation-fractional crystallization
a.p.f.u.	atoms per formula unit
ASPE	annite- siderophyllite-phlogopite-eastonite
BG	background
CS	center shift
$f(O_2)$	fugacity of oxygen
Ga	10^9 years
HM	hematite-magnetite ($f(O_2)$ buffer)
I-WC	weakly-contaminated I-type granites from classification of Ague and Brimhall (1988)
I-MC	moderately-contaminated I-type granites from classification of Ague and Brimhall (1988)
I-SC	strongly-contaminated I-type granites from classification of Ague and Brimhall (1988)
I-SCR	strongly-contaminated and reduced I-type granites from classification of Ague and Brimhall (1988)
LDE	local distortion environment
Ma	10^6 years
MS	Mössbauer spectroscopy
MSH	Mont Saint-Hilaire

NB	New Brunswick
Nfld	Newfoundland
NNO	Ni-NiO ($f(O_2)$ buffer)
NS	Nova Scotia
P(Δ)	probability density
QC	Québec
QFM	quartz-fayalite-magnetite ($f(O_2)$ buffer)
QS	quadrupole splitting
QSD	quadrupole splitting distribution
<QS>	average quadrupole splitting
$QS_{H\text{-}edge}$	quadrupole splitting at half maximum of P(Δ) at the high edge of QSD
$QS_{L\text{-}edge}$	quadrupole splitting at half maximum of P(Δ) at the low edge of QSD
QS_{peak}	quadrupole splitting value at which the probability density is the largest
[R]	average octahedral cation radius
RT	room temprature (~22 °C)
SI	solidification index; $MgO*100/(MgO+FeO+Fe_2O_3+Na_2O+K_2O)$
S_k	QS_{peak} - <QS>
S_t	skewness
XRF	X-ray fluorescence spectrometry
VAG	volcanic-arc granite
WPG	within-plate granite
W_{QSD}	width of QSD at half maximum of P(Δ)

α	tetrahedral rotation angle
σ_{QSD}	standard deviation of QSD
Ψ	average octahedral flattening angle
Γ	Lorentzian width

General Introduction

Biotite is a profusely common rock-forming mineral in granitic rocks. The mineral has a complex phyllosilicate structure that allows it to accommodate most of the common elements in granitic magmas, a feature that makes it a valuable probe of magma compositions. Several recent studies (Nachit et al. 1985, Lalonde and Bernard 1993, Burkhard 1993, Abdel-Rahman 1994) have indicated that biotite also has the potential to be used as a tectonomagmatic indicator for granites, being capable of recognizing for example granites generated in continental arcs from those resulting from crustal anatexis in continent-continent collisional settings.

Recently, the Siluro-Devonian granitic rocks of the Canadian Appalachians have been the object of several detailed geological, geochemical, isotopic and geochronological investigations aimed at understanding their petrogenetic source materials and relationships with tectonism. With such a comprehensive data set, the granitic rocks of the Canadian Appalachian orogen provide an ideal framework to explore the relationships between biotite mineral chemistry and tectonic settings.

This thesis, which consists of three individual manuscripts, represents the results of a mineral chemical and Mössbauer spectroscopic investigation of the micas from the Siluro-Devonian granitic rocks of the Dunnage, Gander, Avalon and Meguma zones of the Appalachian orogen in the provinces of Québec, New Brunswick, Nova Scotia and Newfoundland. The first manuscript is a study of the mineral chemistry of biotite from the granitic rocks of the Canadian Appalachians. In this manuscript, the composition of 156

biotite specimens from 76 different sites in the provinces of Québec, New Brunswick, Nova Scotia and Newfoundland was documented by wavelength-dispersive X-ray spectrometry for major elements and by ^{57}Fe Mössbauer spectroscopy for the oxidation and coordination states of iron. Relationships between the mineral composition of the biotite and the bulk-rock granite composition were explored to evaluate the potential of biotite as a tectonomagmatic indicator. Comparisons were also made with biotites from granitic rocks of other well-documented orogens in the world.

In the second and third manuscripts, by-products of the above study, two distinct areas of investigations pertaining to the Mössbauer spectroscopy of true micas were addressed. In the second manuscript the methodology of quadrupole splitting distribution (QSD) analysis was used for the first time to study a large number of natural biotite samples from rocks of differing geographic locations, geologic age and petrogenetic origin. Until now, only synthetic specimens from the phlogopite-annite series had been analyzed by this powerful new spectrum analysis method capable of extracting information related to the local distortion and local chemical environments in the mineral. A thorough investigation of the relationships between Mössbauer spectral parameters and mineral composition was also performed as part of this study.

The third manuscript of the thesis constitutes the first study to clearly demonstrate the possibility and limits of quantitative determinations of cis- and trans-Fe^{2+} populations in $2M_1$ muscovite. This study shows that a group of dioctahedral micas have spectra in which the octahedral Fe^{2+} contribution is resolved into two unique contributions attributable to cis and

trans octahedral sites. This is important since recent studies have rigorously demonstrated, against popular belief, that Mössbauer spectroscopy cannot resolve cis and trans Fe^{2+} contributions in trioctahedral and some dioctahedral micas because of spectral overlap.

COMPOSITION OF BIOTITE FROM GRANITIC ROCKS OF THE CANADIAN APPALACHIANS: A POTENTIAL TECTONOMAGMATIC INDICATOR?

Amir A. T. Shabani[1], André E. Lalonde[1], and Joseph B. Whalen[2]

1) Ottawa-Carleton Geoscience Centre, Department of Earth Sciences,

University of Ottawa, Ottawa, Ontario, Canada, K1N 6N5

2) Geological Survey of Canada, 601 Booth street, Ottawa, Ontario, Canada, K1A 0E8

Abstract

The composition of biotite, the dominant ferromagnesian mineral in the Paleozoic granitic rocks of the Canadian Appalachians, has been investigated by wavelength-dispersive X-ray microanalyses for major elements and by ^{57}Fe Mössbauer spectroscopy for the oxidation state and coordination of Fe.

The biotite studied is from a wide variety of rock types ranging from gabbro, diorite, syenite to granite. The mineral generally exhibits magmatic textures, however, in Ordovician foliated rocks it is considered as a metamorphosed or recrystallized phase.

The most pronounced variations in composition of biotite in these rocks are differences in total Al contents and Fe/(Fe+Mg) values, both sensitive indicators of conditions that prevailed in the host magmas. In the biotite quadrilateral (annite-siderophyllite-phlogopite-eastonite) diagram, the composition of biotite from the A-type granites of the Humber and Avalon zones in GaspJsie (Québec) and New Brunswick is characterized by low mean Al contents ~ 2.3 (a.p.f.u.) and variable Fe/(Fe+Mg) values from 0.4 to 0.9. In the granites of the Notre-Dame arc, formed within a subduction-related environment, biotite has moderate mean values of Al (~ 2.8 a.p.f.u.) and Fe/(Fe+Mg) (~ 0.58). In the granites of the Gander zone of New Brunswick and Newfoundland, the biotite has a mean Fe/(Fe+Mg) value of 0.6 and shows a pronounced trend of increasing total Al (2.1 to 3.5 a.p.f.u.), confirming a significant contribution of aluminous supracrustal material, either by assimilation or anatexis, to the granitic rocks. Finally, in the Meguma zone granites, derived entirely from crustal

metasedimentary material, the biotite exhibits a remarkable increase in total Al (2.6 to 4 a.p.f.u.) and considerable iron-enrichment (Fe/(Fe+Mg) = 0.4 to 1), with compositions nearing the siderophyllite end-member.

Using common oxygen geobarometers, the biotite from the granites of most zones plots on or above the NNO buffer, indicating moderate oxidizing conditions, whereas that from the Meguma zone plots between the QFM and NNO buffers implying fairly reducing conditions during biotite crystallization. Assuming a reasonable range of crystallization temperatures of 750 to 900 °C, oxygen fugacities ranged from 10^{-10} to $10^{-16.9}$ bars during the crystallization of these rocks.

By comparing these with biotite from other well-documented granitic suites from various localities worldwide, we conclude that the composition of biotite in Appalachian granitic rocks reflects primarily the nature of the host magmas and cannot be readily used for interpreting the tectonic setting of these rocks without the aid of whole-rock trace-element geochemistry, isotopic data and other geological constraints.

1. Introduction

The systematic study of biotite in granitic rocks and the recognition of compositional variations and trends began with the development of rapid microbeam analytical methods in the early 1960's. Numerous studies have been published that demonstrate the use of biotite composition as a valuable guide to granite petrogenesis [e.g., Peikert (1963), Haslam (1968), Dodge et al. (1969), Kabesh and Refaat (1972), de Albuquerque (1973), Kabesh and Ragab (1974), Stallard (1975), Sapountzis (1976), Neiva (1976, 1981), De Pieri and Jobstraibizer (1977, 1983), Barrière and Cotton (1979), Kabesh and Aly (1980), Phillips et al. (1981), Speer (1981), Mahmood (1983), Mason (1985), Konings et al. (1988), Ague and Brimhall (1988), Hecht, (1994a, 1994b) and Stone et al. (1997)]. In addition, the classical experimental work of Wones and Eugster (1965) clearly established the relationship between biotite composition and oxygen fugacity, thereby making this mineral a valuable indicator of redox conditions in granitic magmas. More recently, studies by Nachit et al. (1985), Lalonde and Bernard (1993), Burkhard (1993) and Abdel-Rahman (1994) have shown that biotite also has potential to be used as a tectonomagmatic indicator in granites, capable of recognizing, for example, granites generated in continental arcs from those resulting from crustal anatexis in continent-continent collisional settings. Other methods or attempts to tectonomagmatically characterize granites of unknown affinity via various approaches such as whole-rock major element composition (e.g., Lameyre and Bowden 1982, Pitcher 1983, Batchelor and Bowden 1985, Maniar and Piccoli

1989), or trace element discrimination diagrams (e.g., Pearce et al. 1984) have met with variable success.

Biotite, an extremely widespread mineral, occurring in nearly all granite types, is a phyllosilicate mineral with a complex structure that can accommodate most of the common elements present in granitic magmas, a feature which makes it a valuable probe of magma composition. However, the rationale for selecting biotite as a tectonomagmatic indicator is that it is the most important host of any excess aluminum in granites and therefore, reflects directly the peraluminosity of the host magma. In addition, it is also the most readily available indicator of oxidation state of the rock. Peraluminosity and relative oxidation state of the magma have been the basis for the classification of granites into I- and S-types (Chappell and White 1974) and ilmenite- and magnetite-series (Ishihara 1977, 1981), respectively.

Recently the granitic rocks of the Canadian Appalachians have been the object of several detailed geological, geochemical and isotopic investigations aimed at defining their source materials. This is because it is recognized that granites represent samples of large volumes of lower crustal and/or mantle-derived source rocks (e.g., Whalen 1993). In addition, these studies have investigated the relationships between granitic magmatism and tectonism in the orogen. The comprehensive data set that exists for Canadian Appalachian granites provides an ideal framework to explore the compositional relationships of biotite in granites of differing tectonic settings and to further elucidate the petrogenesis of these intrusive rocks.

In this study, we document by electron microprobe the composition of over 156 granitic biotite specimens taken from 76 different sites from the Appalachian orogen in the provinces of Québec, New Brunswick, Nova Scotia and Newfoundland. Of these specimens, 56 were studied by Mössbauer spectroscopy to document their Fe^{3+}/Fe composition. Furthermore, 195 biotite analyses from the literature, mostly from the Meguma zone of Nova Scotia, were added to our data base. This constitutes the most complete analytical data set of igneous biotites ever undertaken in the Appalachian orogen.

2. Sources of Data and Material

This study became feasible through a fairly large number of rock specimens, as well as corresponding major, minor, trace element and isotopic whole-rock analyses from the granitic rocks of the Dunnage, Gander and Avalon zones of New Brunswick as well as the Dunnage zone of Newfoundland, that were provided by Dr. J. B. Whalen of the Geological Survey of Canada. Additional hand specimens and corresponding whole-rock analyses and reports from granitic rocks of the Gander zone in Newfoundland were provided by Dr. A. Kerr of the Geological Survey of Newfoundland and Labrador. A number of rock specimens from the Halifax pluton of the South Mountain batholith of the Meguma zone in Nova Scotia were supplied by Dr. D. B. Clarke of Dalhousie University.

In addition to these materials, specimens of the granitic plutons of the Gander zone in Newfoundland were sampled by the first two authors in August 1995. The plutons or intrusive

suites from which biotites were studied are listed in Table 1 and the location and description of their rock samples are tabulated in Appendix I. Furthermore, a fairly large number of biotite analyses and in some cases corresponding host rock analyses reported mainly in theses were included in the study. Their sources and localities are given in Table 2.

3. Analytical Methods

3.1 Electron Microprobe Analysis

Mineral analyses were obtained by wavelength-dispersive X-ray spectrometry for 11 elements (K, Na, Ca, Mg, Mn, Fe, Al, Ti, Si, F, and Cl) using the JEOL 8900 Superprobe of the McGill University Microprobe Laboratory. Typical beam operating conditions were 15 kV and 20 nA. The chemical composition of each of the 351 specimens analyzed is presented in Appendix II along with its respective structural formula based on 20 oxygen atoms and OH+F+Cl=4. Contents of FeO and Fe_2O_3 for some of the specimens were determined by applying the $Fe^{3+}/(Fe^{2+}+ Fe^{3+})$ ratios determined by Mössbauer spectroscopy (MS). For those samples not measured by MS, the above mentioned ratios were extrapolated from those of similar petrographic units.

3.2 Mössbauer Spectroscopy

Transmission ^{57}Fe Mössbauer spectra of 57 samples were obtained at room temperature (RT=22°C) using a ^{57}Co rhodium matrix source on a velocity range of ±4 mm/s with a constant acceleration transducer. Data were collected on 1024 channels, which covered twice the Doppler velocity range of ±4 mm/s. Calibrations of spectra were obtained with a ^{57}Fe-enriched iron foil, both before and after each experiment. All positions are reported with respect to this calibration spectrum, i.e., with respect to the centre shift (CS) of metallic α-Fe at RT. All spectra were folded to give a flat background (BG).

Absorbers were prepared as follows. Whole-rock samples were crushed using both jaw crusher and pulverizer. The crushed samples were then sieved to retain the size fraction between 45 and 60 mesh (350-250 mm). All samples were washed with water or acetone to remove dust. Magnetite was removed with a strong permanent magnet and the mafic and felsic grains were then separated using a Frantz magnetic separator. Further purification in some cases was achieved using heavy liquids (methylene iodide, specific gravity = 3.33). Final shaking on a tilted paper sheet and hand-picking were performed for all samples until the concentrates appeared at least 99% pure under the binocular microscope. However, impurities such as minute crystals of apatite, zircon and interleaved muscovite or chlorite in some of the specimens could not be avoided.

The amount of sample used in the absorbers varied between 70 to 130 mg and was determined by the method of Rancourt et al. (1993) to maximize the signal to noise ratio. The

above-mentioned amount of granulated mica corresponding to the ideal (or near-ideal) absorber thickness was then mixed with petroleum jelly in a 5 mm thick and 0.5 inch inside diameter holder. This method has been shown to give random orientation of the mica grains in the absorbers and allows one to impose equality in area of corresponding high and low-energy lines in site-specific doublets (Rancourt, 1994).

The new Voigt-based model of arbitrary-shape quadrupole splitting distributions (QSD) of Rancourt and Ping (1991) was used to fit the spectra. This model assumed that the true underlying QSD for a given valence state and coordination number, i.e., for a given site, is composed of a given number N of Gaussian components as can be justified on statistical grounds and used. Unique distributions are thereby obtained (Rancourt and Ping, 1991).

None of the spectra were thickness corrected, a method which takes into account the spectral distortions that occur because of finite absorber thickness (Rancourt et al. 1993; Ping and Rancourt 1992; Rancourt 1989). Although we know that thickness effects are minimal for these types of absorbers.

3.3 Whole-Rock XRF Analyses

Whole-rock major, minor and trace elements were determined by sequential wavelength-dispersive X-ray fluorescence (XRF) with a Philips PW2400 automated spectrometer. Major, minor and trace element analyses were performed on glass discs of fused rock samples and are tabulated in Appendix III.

4. Plutonic Suites of the Canadian Appalachians

4.1 Tectonic Overview

The Appalachian orogen in Newfoundland, New Brunswick and Gaspésie, Québec comprises four main tectonostratigraphic zones (Williams 1979; Williams et al. 1988). From west to east, these are the **Humber zone** (the western margin of Iapetus or the ancient North American continental margin), the **Dunnage zone** (allochthonous remnants of the Iapetus, mostly comprising rocks of island arcs and back-arc basins), the **Gander zone** (a metamorphic belt of sedimentary protholiths possibly representing an opposing Gondwanan continental margin) and the **Avalon zone** (a Late Proterozoic orogenic province with a thin Paleozoic cover sequence; probably a fragment of Gondwanaland developed during the Pan-African cycle) (Fig. 1).

In addition to these four main zones, the **Meguma zone** is the easternmost lithotectonic terrain in the Appalachian orogen. It is situated south of the Avalon zone of northern Nova Scotia and consists largely of Paleozoic rocks (Williams, 1979). The unique lithologies and deformational and intrusive history of the Meguma zone within the northern Appalachians suggest that it is an exotic terrane (Schenk 1971).

The Dunnage zone in New Brunswick is poorly exposed, being obscured by young cover sequences, whereas in Newfoundland, where it is well exposed, it has been subdivided into two segments, termed the Notre Dame subzone and the Exploits subzone, each of which

have distinct lithological, faunal and evolutionary characteristics (Williams et al. 1988). The southern portion of the Notre Dame subzone, a region underlain mainly by high grade ortho- and para-gneisses, was redefined as the Dashwoods subzone by Piasecki et al. (1990).

Based on earlier interpretations of marine seismic-reflection profiles, three lower crustal blocks were recognized underlying these zones (Keen et al. 1986; Marillier et al. 1989). These are the Grenville block, interpreted to underlie the Humber and western Dunnage zones, the Avalon block, interpreted to coincide with the surface expression of the Avalon zone and the enigmatic intervening region termed Central block which underlies the Gander and much of the Dunnage zones. Based on the interpretation of more recent onland seismic-reflection profiles (Quinlan et al. 1992), only two lower crustal blocks, termed the Laurentian and Gondwanan blocks, are recognized beneath the orogen. The Central block of the marine profiles has been partly interpreted as a region where Laurentian and Gondwanan crust is tectonically interleaved as a result of opposing Ordovician (Taconic) and Silurian (Salinic) structures.

Plutonic rocks comprise about one quarter of the exposed Canadian Appalachians, occurring in all tectonostratigraphic zones (Currie, 1995). Most of the granitic plutonism in the orogen occurred during the Middle Ordovician to Early Devonian periods (Whalen, 1993). It should be mentioned that the Humber and Avalon zones of Newfoundland and Cape Breton were not included in this study, principally because of a lack of specimens or the severe alteration of biotite in their granitic rocks.

4.2 Plutonism within the Zones

Humber Zone, Gaspésie (Québec)

The Humber zone is composed of Cambro-Ordovician sedimentary, basic volcanic, and ultramafic allochthons. These allochthons were collectively emplaced onto the Laurentian margin by Late Ordovician time (Williams and Hatcher 1983). The Devonian McGeriggle complex truncates deformation fabrics in the allochthons.

The complex can be roughly subdivided into granitic and hybrid suites. The hybrid suite includes a component lithologically similar to the granitic suite rocks but which is distinguished by common mafic inclusions. Contacts between the granitic and hybrid suites are both sharp and gradational in nature. The granitic rocks vary in color from scarlet red to white and their main mafic mineral is biotite with local hornblende ± pyroxene. Magnetite, apatite, zircon, titanite and allanite are minor accessory minerals. The hybrid suite is compositionally variable and includes most intrusive rock types from gabbro to granite.

According to Whalen (1993) this group of metaluminous, amphibole-bearing plutonic rocks was derived from igneous or reworked mantle-derived (infracrustal) protoliths. Values of $\delta^{18}O$, ε_{Nd} and $^{207}Pb/^{204}Pb$ of these rocks overlap those of mantle-derived magmas, eliminating supracrustal rocks as a significant source component.

Dunnage Zone

South of the Baie-Verte-Brompton Line in Gaspésie, Dunnage zone Ordovician rocks composed of arc and back-arc remnants of the Iapetus, are unconformably overlain by gently folded Siluro-Devonian, marine and terrestrial sedimentary rocks of the Connecticut Valley-Gaspé synclinorium (Williams and Hatcher 1983). Granitic rocks, a volumetrically minor rock type in this area, are Siluro-Devonian in age. Some of these are high-level porphyry intrusions that have undergone deuteric and (or) hydrothermal alteration. This restricts the mineralogical study to plutons D3, D5, and D6 (Table 1) that have fresh biotite.

In Newfoundland, the Early to Middle Ordovician age plutonic rocks of the Notre Dame subzone are both lithologically and compositionally variable, even at the outcrop scale. They range in texture from fine- to coarse-grained, equigranular to porphyritic, and in composition from gabbro to diorite to tonalite and granodiorite. Blue quartz-eye porphyritic tonalite is the predominant lithology and granite, sensu-stricto, is rare (Whalen et al. 1997). Most plutons have rocks that are slightly to moderately foliated, some, especially in the Dashwood subzone, are metamorphosed and recrystallized. In these rocks amphibole is normally the principal mafic mineral, even at high silica contents. Fine- to medium-grained, angular to ovoid inclusions of hornblende-rich gabbro and diorite, probably of cognate origin are common and locally abundant. Based on geochemical and isotopic signatures, Whalen et al. (1997) interpreted these rocks as both mantle-, and slab-derived magmas modified through assimilation-fractional crystallization (AFC) processes in the lower crust, and also partial melts of solidified, previously hybridized, lower crustal rocks.

In the Exploits subzone, Silurian plutonic rocks are grouped as the Mount Peyton association by Williams et. al. (1989) which is bimodal in nature. A limited number of specimens of the plutonic rocks of Fogo Island, which belong to this association, were included in this study.

Gander Zone

The Gander zone in New Brunswick, which has also been termed the Miramichi terrane (Fyffe and Fricker, 1987), was the site of voluminous granitic plutonism during the Middle Ordovician, Silurian and Devonian periods. The Ordovician granitic plutons constitute a striking pattern of elongated bodies deformed into broad open folds, during Late Ordovician to Silurian deformation. Following regional metamorphism and deformation, the area was intruded by a number of Silurian and scarce Devonian granitic plutons.

The Siluro-Devonian plutons, in general, are relatively undeformed, although some exhibit local cataclastic features near their margins. They are predominantly biotite granite, sensu stricto, with subordinate biotite granodiorite. Tonalite and quartz-poor plutonic rocks, including gabbro, are a volumetrically minor component of a number of Silurian plutons. Some Siluro-Devonian plutons include amphibole-bearing granodiorite, whereas other plutons contain felsic, magmatic-muscovite-bearing, and rarely cordierite-bearing rocks.

These Ordovician and Siluro-Devonian metaluminous to moderately peraluminous intrusive igneous rocks belong to an alumino-cafemic magmatic association derived from a mixture of supracrustal and mantle-derived source components. Negative ε_{Nd} and elevated

$^{207}Pb/^{204}Pb$, $\delta^{18}O$ values and Proterozoic xenocrystic zircons within Gander granites are consistent with reworking of old crust (T_{DM}=1.1 to 1.8 Ga).

In Newfoundland, granites of the Gander zone have a broadly syntectonic relationship to major Silurian deformation throughout this region (e.g., Dunning et al. 1990). Williams et al. (1989) distinguished two compositional groups within this zone, which they termed the Burgeo and Middle Ridge associations. The dominant rock type of the Burgeo association is a coarse-grained, K-feldspar megacrystic, biotite (± hornblende) granite. The Middle Ridge association is dominated by leucocratic muscovite-biotite granite, which also locally intrudes nearby parts of the Exploits subzone, and is most abundant in the interior, lower-grade portions of the region.

In Newfoundland, Devonian plutonic suites are a major component of the Gander zone and south coast regions, and also the adjacent Avalon zone. Williams et al. (1989) grouped all these rocks within the Ackley association, named after the largest pluton. These rocks were discussed in detail by Kerr et al. (1993).

Within the Gander zone, K-feldspar megacrystic biotite granite and muscovite-biotite granite form a compositional continuum, and are intermixed on different scales. The K-feldspar megacrystic suites range from tonalite to granite and their composition is broadly calc-alkaline. However, they are dominated by granite and are strongly potassic. In their study of the Nd-isotope systematic of these rocks, Kerr et al. (1995) suggested that these rocks were derived from supracrustal sources of ancient provenance along with more juvenile infracrustal sources of inferred late Precambrian basement.

Devonian granites of the Gander zone are compositionally restricted, more evolved and more agpaitic compared to the Silurian suites. They have similar Nd isotopic signatures to the Silurian K-feldspar megacrystic suites. Kerr et al. (1993, 1995) suggest a 3-component origin consisting of mantle-derived magmas, mixed with anatectic melts of both Precambrian basement and Paleozoic cover rocks. These granites postdate juxtaposition of the Gander and Avalon zones and their geochemical features are typical of granites developed in post-collisional environments of uplift and extension (Kerr 1997).

Avalon Zone

The Avalon zone, distinguished by rocks ranging from Late Precambrian to Cambrian, is composed of volcanic, sedimentary and gabbroic to granitic rocks. These rocks are intruded by Siluro-Devonian granites and are overlain unconformably or structurally by post-Cambrian supracrustal rocks. All the Siluro-Devonian granites within the Avalon zone of New Brunswick represent different components or phases of the northeast-trending Saint-George batholith (Table 1), that was emplaced at or near the tectonic junction between the Gander and Avalon zones.

According to Whalen (1993), this group of Siluro-Devonian metaluminous, mainly felsic biotite ± amphibole granites forms a cafemic (in the sense of Debon and Le Fort, 1982) granite association derived from I-type (infracrustal) or mantle-derived sources. Some granites are peralkaline A-type granites and most others have some A-type affinities. However, their $\delta^{18}O$ values which are only slightly lower than those of Gander granites, may reflect the

presence of a supracrustal component. Positive ε_{Nd} (0.4 Ga) values indicate derivation from relatively young juvenile sources, whereas elevated $^{207}Pb/^{204}Pb$ signatures and xenocrystic zircon data indicate an ancient crustal component.

Meguma Zone

About one third of the Meguma zone is underlain by granitic plutons (Whalen and Currie 1995) that fall into two spatial-chemical genetic types (Clarke et al. 1997). The central plutons, including the giant South Mountain batholith, crop out throughout central areas and the peripheral plutons crop out in the peripheral onshore areas of the Meguma zone to the southwest and northeast (Fig. 1). According to Clarke et al. (1997), the best estimates for the granite intrusion ages are 372 ± 3 Ma for central plutons and 378 ± 3 for the peripheral plutons. The central plutons consist of exclusively peraluminous (A/CNK; molar $Al_2O_3/(CaO + Na_2O + K_2O)$ = 1.1-1.3), garnet-bearing biotite-granodiorite, cordierite- and andalusite-bearing two mica monzogranite and leucomonzogranite. They are late-tectonic to post-tectonic, predominantly unfoliated plutons emplaced into low-grade metamorphic host rocks. The peripheral plutons, which include the Barrington Passage, Shelburne, Port Mouton and Canso plutons, are dominantly peraluminous (A/CNK = 0.9-1.3), late-tectonic, moderately foliated and emplaced into higher grade metamorphic host rocks. Lithologies within these plutons include hornblende-biotite-tonalite, biotite-granodiorite and two-mica monzogranite. In addition, some of these plutons are associated with synchronous, mafic-intermediate intrusions which form dykes, plugs and synplutonic bodies; spessartite, lamprophyre, gabbro-diorite and diorite are the

most abundant lithologies (Tate and Clarke 1997). Preservation of mingled mafic-intermediate pillows and hybrids within three synplutonic intrusions suggests that the hornblende-bearing tonalites formed locally as the products of magma mingling and mixing (Tate et al. 1997; Clarke et al. 1997).

The general mineral assemblage of unaltered granite in the Meguma zone is quartz + alkali feldspar + plagiocalse + muscovite ± biotite ± cordierite ± garnet ± andalusite ± topaz ± ilmenite. Magnetite is rare to absent. The granitic rocks of the Meguma zone are best classified as ilmenite-series or S-type granites (Clarke and Muecke, 1985).

4.3 Tectonic Models of Granite Magmatism

The geology of the Canadian Appalachians is generally interpreted in terms of the opening and closing of the Late Precambrian-Early Paleozoic Iapetus ocean. While a Late Precambrian timing for Iapetus opening is generally accepted, interpretations differ as to whether the closure of the Iapetus was complete by the Middle Ordovician or Silurian or even the Devonian. Because most of the granitic plutonism in the orogen occurred during this Middle Ordovician to Early Devonian period, these rocks are particularly relevant to understanding the later stages of Iapetus closure.

It is believed that the closure of the Iapetus ocean, with the subsequent collision of the Taconic arc with Laurentia, occurred during the Late Ordovician to the Early Silurian. The

problem with this model is the enigmatic nature of the heat source driving the widespread Siluro-Devonian granite magmatism.

Recent tectonic models of granite genesis for the Canadian Appalachians have been proposed by Kerr et al. (1992, 1997) for Newfoundland and by Whalen (1993, 1997) for New Brunswick. In both models, the wide distribution of Siluro-Devonian plutons is attributed to a major thermal anomaly that extended onwards from mid-Silurian time, following the closure of the Iapetus ocean. In this context, both models attribute the thermal anomaly to post-collisional delamination of the lithosphere. At the beginning of collision, the descending slab may undergo rifting processes leading to detachment of the continental lithosphere from the subducting oceanic lithosphere. This detachment leads to short-lived extension and thinning of the lithosphere followed by continued convergence driven by mantle convection. During lithospheric delamination, the base of the crust is brought into contact with the hot asthenosphere leading to high-temperature metamorphism, crustal melting and extensive emplacement of synkinematic granitic magmas. Lithospheric delamination accompanying the closure of the Iapetus and its back-arc basin(s) could have provided the widespread thermal anomaly beneath the orogen. Localized and temporal variations in tectonic regime from extensional to compressional could have accounted for slight differences in the mineralogical and chemical characteristics of some granitic rocks across the orogen.

5. Description of Biotite in Plutonic Rocks

Biotite is, in general, the principal mafic mineral in granitic rocks of the Canadian Appalachian orogen. This mineral also occurs in the gabbroic and dioritic rocks. In what follows, the mode of occurrence and textural relationships of biotite are described separately for the granitic rocks of each zone. However, it is important to note that chlorite is almost ubiquitous in these rocks as an alteration product interleaved with, or completely replacing biotite.

After chlorite, prehnite is the most widespread secondary Ca-Al silicate associated with biotite. It forms lenticular patches along the {001} cleavage of biotite. Other minor Ca-Al silicates are pumpellyite and an intermediate grossular-andradite garnet ("grandite") which occur as lenses or pods within biotite or chloritized biotite, also elongated parallel to the cleavage.

Humber Zone, Gaspésie (Québec)

In his study of the McGeriggle complex, Wallace (1988) described the biotite in mafic to felsic plutonic rocks as light tan to dark brown pleochroic, commonly interstitial to subhedral grains. Apatite, opaque oxides and zircon are common inclusions. In nepheline syenite, the biotite forms light tan to dark greenish brown pleochroic, anhedral to euhedral, partly interstitial flakes.

Dunnage Zone

In Dunnage zone plutonic rocks, biotite is not usually the only mafic phase. It generally occurs as part of a amphibole, biotite, " titanite, apatite and opaque assemblage. Minor postmagmatic replacement of amphibole by biotite may be observed but, overall, the well-defined planar boundaries between the two minerals indicate magmatic crystallization. The dominant pleochroic color is dark brown; greenish and reddish brown colors are minor. In general, two texturally different groups of biotite are recognized. In foliated rocks, biotite is fine-grained, defines the planar fabric of the rock, and is considered a metamorphosed and recrystallized phase. In massive rocks, it is medium-grained, subhedral to euhedral, and interpreted as primary. Inclusions of apatite, zircon and opaque minerals are common in this latter biotite group.

Gander Zone

In Gander zone plutonic rocks, biotite is the sole mafic mineral within felsic compositions, whereas in intermediate rocks it coexists with amphibole and pyroxene. Here also, texturally-distinct biotite groups are recognized associated with foliated and undeformed granites. The foliated granites of New Brunswick and Newfoundland are of different ages and textures.

In the Middle Ordovician foliated granites of New Brunswick, anhedral to subhedral flakes of biotite up to 1 or 2 mm across are interstitial to other felsic minerals and define a strong planar fabric to the rock. These biotites are pleochroic from yellow to dark brown or

greenish brown and appear metamorphosed and recrystallized. In contrast, in the Silurian foliated K-feldspar megacrystic granites of Newfoundland, subhedral biotite flakes reaching up to 5 mm across are interstitial to large megacrysts of feldspar and define the moderate to strong planar fabric of the rock. Bending and rupturing of the cleavage of the biotite are common evidence of strain. In these rocks, biotite is interpreted as being essentially primary and oriented by the syntectonic relationship of the host granite to the major Silurian deformation throughout this region.

Biotite in the massive Siluro-Devonian plutons occurs as subhedral to euhedral flakes interstitial to the felsic minerals and is considered primary in nature. Inclusions of apatite, zircon and opaque minerals are also common in this biotite.

In general, biotite grains from Newfoundland granitic rocks are coarser than their counterparts from New Brunswick granitic rocks. In a similar comparison, the dominant pleochroic color for biotite in Newfoundland granites is from dark brown to greenish brown, whereas in New Brunswick, it is from dark brown to reddish brown.

Avalon Zone

In Avalon zone granites, biotite occurs either as the sole mafic mineral or as part of a amphibole , biotite, " titanite, apatite, and opaque assemblage. In general, light tan to dark brown pleochroic biotite forms anhedral to subhedral flakes reaching up to 4 mm across and showing no evidence of strain. Although some of the small grains of biotite clustered with amphibole could have originated in part by postmagmatic replacement of amphibole, the well-

defined planar boundaries between these two minerals suggests that it crystallized from a residual volatile-enriched magma. Inclusions of apatite, zircon and opaque minerals are generally common in biotite.

In syenite, yellow to deep reddish brown pleochroic biotite occurs mainly as anhedral flakes reaching up to 0.5 mm across that replace amphibole. In gabbronorite, biotite is yellow to deep red pleochroic in color and is a late crystallizing phase, partly replacing the earlier primary pyroxene and amphibole.

Meguma Zone

A review of the literature on the granitic rocks of the Meguma zone (Stallard 1975; MacDonald 1981; Ham 1988; and Ding 1995), as well as our mineralogical study of a number of samples from the South Mountain batholith and the Port Mouton pluton, indicate that biotite is a ubiquitous ferromagnesian mineral in almost all granitic rocks, representing 2 to 15% (by volume) of the mode. It occurs as euhedral to subhedral crystals, generally 2-5 mm in diameter. Biotite may be intergrown with muscovite along its cleavage or crystal faces. It is pleochroic from brownish yellow to dark reddish brown. Inclusions which are found ubiquitously in biotite, are generally euhedral and very small, and consist of apatite, monazite, zircon with pleochroic halos, and tabular ilmenite, or rutile along the cleavage.

6. Mössbauer Spectroscopy of Biotite

Mössbauer spectroscopy (MS) has become a fairly common method for characterizing the local environment of Fe in iron-bearing minerals. Several other methods can be used to determine the amount of ferric iron, including wet-chemical titration-based methods (Amonette and Scott 1991), X-ray photoelectron spectroscopy (Stucki 1981; Stucki and Anderson 1981; Raeburn et al. 1997a, 1997b), and indirect methods such as refractive indices and unit-cell dimensions (Hazen and Wones, 1972) but the most precise determinations of Fe^{3+}/Fe ratio are by MS.

All RT spectra of biotites exhibit remarkable similarity and have three main absorption peaks centered at ≈ -0.1, +1.0 and +2.3 mm/s, which respectively correspond to 1) the low-energy lines of both octahedral Fe^{2+} and octahedral Fe^{3+} quadrupole doublets, 2) the high-energy lines of octahedral Fe^{3+} quadrupole doublets, and 3) the high-energy lines of octahedral Fe^{2+} quadrupole doublets. None of these spectra shows a shoulder at ≈ 0.4 mm/s corresponding to high energy-lines of quadrupole doublets of Fe^{3+} in tetrahedral sites (Rancourt et al. 1992).

Representative Mössbauer spectra of biotites are shown in Figure 2 and all spectra are displayed in Appendix IV. The solid line joining the data points of a given spectrum is the fit result. The other solid lines show the separate contributions from octahedral Fe^{2+} and octahedral Fe^{3+}. The difference spectra (or residuals) are shown with the same vertical scales as the respective spectra.

In all spectra, the octahedral Fe^{2+} contributions were assumed to be sums of three Gaussian components. The octahedral Fe^{3+} contributions were assumed to be composed of one or two Gaussian components depending on the structure of the spectra. Fitting parameters for the best fits of all spectra are given in Appendix V.

In a review of Mössbauer data on trioctahedral micas, Dyar (1987) proposed that the three Fe^{2+} Gaussian components observed in the spectra of many micas resulted from three types of Fe^{2+} sites, i.e., a distorted Fe^{2+} trans-site, Fe^{2+} cis-site and a regular Fe^{2+} trans-site. More recently, Rancourt (1994) demonstrated that the three Fe^{2+} components are part of a continuous distribution and that they cannot be unambiguously resolved into cis- and trans-site occupancies.

In this study, the spectra of 54 biotite and 2 phlogopite specimens from granitic rocks of the different tectonomagmatic zones of the Canadian Appalachians were analyzed by MS. Results show a considerable range of Fe^{3+}/Fe from 0.05 to 0.23.

MacKenzie and Clarke (1974) and Stallard (1975), in their study of biotite compositions from granitic rocks of the South Mountain batholith, determined the Fe^{3+}/Fe ratio of biotite by conventional wet-chemical methods. They obtained Fe^{3+}/Fe values ranging from 0.06 to 0.37 for the 18 specimens that they analyzed. The spread of Fe^{3+}/Fe values obtained by Mössbauer spectroscopy, from 0.09 to 0.19, on 8 specimens of the same batholith plus 3 specimens of the Port Mouton pluton, is considerably smaller. In fact, our Mössbauer determinations of the Fe^{3+}/Fe ratio of all 47 mica specimens from the granitic rocks of the entire Canadian Appalachians, whether oxidized or reduced, range from 0.05 to 0.23. We believe

this reflects the poor precision of conventional wet-chemical determinations as performed in most laboratories. Mössbauer spectroscopy is far more precise than most commonly-performed oxidimetric wet-chemical methods (Lalonde et al. 1998). In addition, the wet-chemical methods appear to overestimate ferric iron contents, probably because of oxidation of Fe^{2+} during the acid decomposition.

7. Mineral Chemistry

7.1 Chemistry of Biotite

The 351 micas analyzed from the granitic rocks of the Canadian Appalachians are all biotites in the sense of Deer et al. (1962), i.e. (Fe/(Fe+Mg) $\geq$ 0.33 and trioctahedral (5.02 < O-site < 5.97), except for few phlogopites from mafic or nepheline-bearing suites. Selected electron-microprobe analyses and structural formulae of 12 samples of biotite from granitic rocks are presented in Table 3. In addition, the composition of these micas is summarized in Table 4.

In his petrological study of the granitic rocks of Québec (Gaspésie) and New Brunswick, Whalen (1993) found that granitic rocks from the Humber-Dunnage, Gander and Avalon tectonic zones all show distinct compositional and isotopic characteristics. The same three zones were adopted in this study for these reasons, in addition to those of the Dunnage

zone from Newfoundland, the Gander zone from Newfoundland, and the Meguma zone from Nova Scotia (Table 4).

The compositions of biotite from Humber-Dunnage and Avalon groups are quite similar (Table 4). Because of the strong chloritization of biotite in the Avalonian granites, no Mˆssbauer investigation was performed on this mica.

The compositional characteristics of 106 mica samples of Gander zone granites in both New Brunswick and Newfoundland are recognized by a fairly wide range in total aluminum. In contrast, however, biotite Fe/(Fe+Mg) values exhibit a relatively narrow range in New Brunswick samples relative to those from Newfoundland. Biotite titanium contents, filling only the octahedral sites, are quite similar in both New Brunswick and Newfoundland Gander zone samples (Table 4).

Analyses of 38 biotite samples from Dunnage zone granites show that total aluminum content shows a relatively smaller range than in Gander zone samples, hence the smaller range of octahedral Al^{3+} . However, Fe/(Fe+Mg) and titanium values of biotite more closely resemble the Humber-Dunnage and Avalon groups than the Gander zone group.

The 146 biotite samples from Meguma zone granites are compositionally distinct for they are the most Al enriched and exhibit the widest range of Fe/(Fe+Mg) and titanium, relative to biotite from the other Canadian Appalachian zones. Also, the slightly smaller range of biotite Fe^{3+}/Fe ratios in Meguma zone samples is distinct from that of other zones.

7.2 Peraluminosity of Biotite and its Host Rock

Biotite is perhaps the most common mineralogical sink for excess aluminum in granitic rocks. This has been shown in a plot of peraluminosity index (A/CNK) of biotite versus that of whole-rock (Fig. 3). In all of these plots biotite falls above the line, indicating clearly its higher A/CNK value relative to that of its host rock value.

Compositions of Gander, Avalon and Meguma zone biotite clearly display a positive correlation between A/CNK values for biotite and host rock. In addition, ΣAl in biotite increases with A/CNK of the host rock. However, this relationship is poorly developed for the Humber-Dunnage group in New Brunswick and Dunnage zone granites in Newfoundland which are mainly metaluminous in nature. Furthermore, A/CNK values of biotite in the basic and intermediate rocks generally show a slight negative correlation with whole-rock A/CNK values, perhaps, because part of the aluminum of the rock is accommodated in amphibole, hence decreasing the A/CNK ratio of the coexisting biotite.

By comparison, the distribution pattern of biotite samples, shown in Figure 3, for the Humber-Dunnage granite group is fairly similar with the distribution pattern of biotite samples for Dunnage zone granites. Furthermore, a close look at Figure 3 reveals that a fairly clear positive correlation exists between the A/CNK value of biotite and whole-rock when biotite is the sole mafic mineral in the rocks.

7.3 Determination of Oxygen Fugacity

In Figure 4, biotite compositions, from granitic rocks of the Canadian Appalachians are plotted in Wones and Eugster's (1965) Fe^{2+} - Fe^{3+} - Mg diagram along with the three common oxygen fugacity buffers; quartz-fayalite-magnetite (QFM), nickel-nickel oxide (NNO) and hematite-magnetite (HM). In general, the majority of biotite compositions plot on or above the NNO buffer, a few fall on or above the QFM buffer. By comparison, these biotites as a group are not so reduced as those of the Aregos granites of Portugal, which plot close to the QFM buffer curve (de Albuquerque 1973).

Figure 4 shows that the Humber-Dunnage biotite group falls between the NNO and HM buffers. A few analyses plot near the HM line, indicating fairly oxidizing conditions. The oxide minerals in these rocks are magnetite and ilmenite coexisting together.

Biotite from the Dunnage zone in Newfoundland plots mainly between the NNO and HM lines, however, a few analyses fall between the NNO and QFM buffers. In general, these analyses define a zone of considerable variation on Figure 4. The oxide minerals coexisting with these micas are an assemblage of magnetite-ilmenite. In only a few exceptions was magnetite, or ilmenite observed as single phases. Other opaque minerals that may accompany magnetite and ilmenite are chalcopyrite, pyrite and hematite. Titanite, as a primary mineral, is not common but it may occur in some samples.

Similarly, the majority of biotite analyses from the Gander zone of New Brunswick fall on or above the NNO buffer. In contrast, biotite from the Newfoundland Gander zone defines

an elongate cluster that falls mainly on the NNO oxygen fugacity buffer (Fig. 4). The main opaque phases in these rocks are magnetite + ilmenite ± chalcopyrite ± pyrite ± hematite. The ratio of magnetite to ilmenite is variable from rock to rock. Titanite as a primary accessory mineral occurs mainly in biotite and hornblende-bearing granites.

In Figure 4, biotite analyses from Meguma zone granites plot between the QFM and NNO buffers, similar to biotite from Japanese granites belonging to the ilmenite-series of Ishihara (1977), indicating fairly reducing conditions. The oxide mineral in the Meguma rocks is ilmenite.

A qualitative evaluation of oxygen fugacity can be made from the Fe/(Fe+Mg) ratio of biotite by using the calibrated curve of Wones and Eugster (1965) in $f(O_2)$-T space for biotite + K-feldspar + magnetite equilibrium (Fig. 5). These three phases coexist in all granitic rocks studied in this report, except for the Meguma zone granites, in which magnetite is absent. Assuming a reasonable range of crystallization temperatures of 750 to 900 °C for these rocks, $f(O_2)$ values are presented in Table 5.

7.4 Reducing versus Oxidizing Trends

In their experimental work on biotite composition, Wones and Eugster (1965) recognized two contrasting trends in the $f(O_2)$-T diagram (their Fig. 13): an oxidizing trend, in which biotite becomes increasingly Mg-rich with falling temperature (or progressive crystallization), and a reducing trend, in which biotite becomes increasingly Fe-rich. The

occurrence of both of these trends was documented by Murakami (1969) in Japanese granites; this eventually led to the recognition of the ilmenite- and magnetite-series granites by Ishihara (1981).

Using the solidification index (SI) $100*MgO/(MgO + FeO + Fe_2O_3 + Na_2O + K_2O)$ as a measure of progressive crystallization, we compare the Fe/(Fe+Mg) trend of the rocks and their contained biotite (Fig. 6). In this diagram, magmatic suites display from right to left a general iron-enrichment trend with progressive fractionation. Suites that evolve under reducing conditions have trends of whole-rock and biotite Fe/(Fe+Mg) values that increase jointly with progressive fractionnation. In oxidized suites, Fe^{2+} is oxidized to Fe^{3+} which then partitions into oxide phases causes an iron depletion of the biotite, leading to increased Mg contents. This is reflected in the diagram by decoupled trends for whole-rock and biotite Fe/(Fe+Mg) values.

Biotite from the Humber-Dunnage shows a general trend of iron enrichment with decreasing SI mainly in the mafic to intermediate rocks. However, a slight decrease in Fe/(Fe+Mg) is recognizable for biotite from granites and quartz monzonites and also a strong decrease in biotite from nepheline syenite, indicating an increase of oxygen fugacity in felsic rocks. Biotite from the Dunnage zone of Newfoundland defines a general trend of Fe-enrichment, although few analyses may show a slight decrease in Fe/(Fe+Mg) relative to their host rocks.

Biotite from Gander zone granites in New Brunswick shows a reducing trend, i.e., becoming increasingly Fe-rich with decreasing SI, although a few samples show decreasing

Fe/(Fe+Mg) relative to their host rocks (Fig. 6). Similarly, the majority of Gander zone biotite analyses from Newfoundland exhibit a reducing trend, but a slightly oxidizing trend is nevertheless shown by a small number of specimens.

In Figure 6 two trends can be identified for Avalon zone biotite: the first is a trend of moderate iron enrichment with progressing crystallization (decreasing solidification index) in both biotite and host rock (reducing trend). The second trend is one in which the host rock becomes iron-rich whereas the biotite shows an overall Fe-depletion (oxidizing trend). The rocks from this latter trend are biotite or hornblende-biotite granites. They contain considerable amounts of titanite as an accessory phase and have pink or red, hematite-clouded K-feldspar megacrysts, all indications of oxidizing magmatic and postmagmatic conditions. These rocks contain both magnetite and ilmenite, but the amount of magnetite exceeds that of ilmenite. The rocks which define the reducing trend are mostly biotite to muscovite-biotite granites whose color ranges from cream to beige. There is no titanite in these rocks and ilmenite dominates over magnetite in some samples.

Finally, Meguma granitic biotite defines a good Fe-enrichment trend, i.e., a reducing trend, indicating that oxygen fugacity must have decreased with progressive crystallization. This is in agreement with Meguma granites being ilmenite-bearing and magnetite-free.

In their study on ilmenite- and magnetite-series of Japanese granites, Czamanske et al. (1981) observed a good correlation between Fe/(Fe+Mg) for biotite and host rocks in the ilmenite-series. Biotite from the magnetite-series does not show this correlation and shows no increase in Fe/(Fe+Mg) as this ratio increases in the corresponding host rocks. Our analyses of

biotite from all zones generally show a positive correlation between Fe/(Fe+Mg) for biotite and host rocks, although some scatter is present (Fig. 7). The scattered samples are generally from oxidized granites.

It can be concluded that in general Canadian Appalachian granitic rocks formed under reducing conditions, although some intrusions might have evolved under moderate oxidizing conditions.

8. Biotite Compositions in the ASPE Quadrilateral

The annite - siderophyllite - phlogopite - eastonite quadrilateral (ASPE) is commonly adopted to illustrate the total Al and Fe/(Fe+Mg) compositional relationships of trioctahedral micas from igneous rock suites (Speer 1984). This diagram is particularly powerful since these two variables represent, respectively, indicators of peraluminosity and redox state of the rock hosting the mica. Biotite compositions from all the zones defined in this study are plotted in the ASPE quadrilateral in Figure 8.

Biotite specimens from the Humber-Dunnage group of granitic rocks (Fig. 8) exhibit a fairly wide range of Fe/(Fe+Mg) values within a narrow range of low total Al contents, reaching up to ~2.5 atoms per formula unit (a.p.f.u). A negative correlation is observed for biotite from granite and quartz monzonite phases, indicating weak to moderate oxidizing conditions.

Biotite samples from the Dunnage zone form a field exhibiting a wide range of Fe/(Fe+Mg) values and a moderate range of total Al contents (Fig. 8). Analyses are randomly

distributed with regards to rock type such that no trend is recognizable. Specimens from Fogo Island are distinguished by their high Fe/(Fe+Mg) values and low Al-contents.

In contrast, biotite samples from granitic rocks of the Gander zone in New Brunswick occupy a field defined by a relatively narrow range of Fe/(Fe+Mg) values (except for phlogopite) but with a large range in total aluminum from 2.10 to 3.55 a.p.f.u. Note that biotite in mafic, intermediate and a small number of felsic rocks exhibits a slight decrease in Fe/(Fe+Mg) values with increasing total aluminum. However, most felsic rocks exhibit a trend of increasing total Al contents at relatively constant Fe/(Fe+Mg) values.

Biotite from Gander zone granitic rocks in Newfoundland shows a positive correlation between Fe and Al in the ASPE quad. In these rocks, biotite Fe and Al contents increase with host rock silica contents from mafic to felsic rocks.

Biotite samples from Avalon zone granitic rocks of New Brunswick occupy a field that, similar to the Humber-Dunnage group, is defined by a fairly wide range of Fe/(Fe+Mg) values within a narrow zone of low total Al contents (Fig. 8). The two contrasting trends of oxidation and reduction that were described in sub-section 7.4 can also be identified in the ASPE quadrilateral (see arrows in Fig. 8, Avalon zone). One trend consists of a positive correlation between total iron and Al, corresponding to a reducing trend, i.e., biotite becomes Fe-rich with increasing total Al. The other trend consists of a negative correlation between total iron and Al, corresponding to an oxidizing trend, i.e., biotite becomes Mg-rich with increasing total Al (see Fig. 6).

Finally, similar to the biotite trend defined by Newfoundland Gander zone granites, biotite analyses from Meguma zone granitic rocks define a field characterized by both Fe and Al enrichment in the ASPE quadrilateral, with some compositions approaching the siderophyllite end member (Fig. 8).

9. Discussion

Granites from the Canadian Appalachians were grouped in section 4 according to their tectonostratigraphic zone because of the direct correlation that exists between the zonal distribution of these rocks and their geochemical and isotopic characteristics. These major tectonostratigraphic associations of granitic rocks were then clearly distinguished by the composition of their biotite in the ASPE quadrilateral plots (Section 8). This illustrates the effectiveness of the ASPE quadrilateral for discriminating associations of plutonic rocks, particularly where assimilation and/or anatexis of metasedimentary rocks and oxidation are involved (Lalonde and Bernard, 1993). Below, we compare the compositional fields or trends of biotite from Appalachian granites with those of well-documented granitic suites from elsewhere and through syllogistic reasoning attempt to infer both the petrogenetic and tectonomagmatic characteristics of their host rocks.

Humber -Dunnage Zones

Granites which intrude the Humber and Dunnage zones in New Brunswick and Québec have compositional features generally consistent with an extensional tectonic environment. The McGerrigle suite of the Humber zone in Québec and several plutons of the Dunnage zone of New Brunswick plot on whole-rock discrimination diagrams mainly in the A-type granite field of Whalen et al. (1987) and, in the within-plate granite field (WPG) of Pearce et al. (1984). In this last diagram, only a few analyses from mafic dykes and hybrid rocks plot within the volcanic-arc granite field (VAG). Field evidence from Whalen (1993) suggests that WPG magmatism predated the VAG rocks in this area.

Biotite compositions from plutons of the Humber and Dunnage zones of Québec and New Brunswick are shown in the ASPE quadrilateral (Fig. 8). In Figure 9, we plot the biotite composition from classic A-type or WPG suites from the literature, such as the Ascutney Mountain igneous complex of the White Mountain magma series in New Hampshire (Schniderman 1991), the Klokken gabbro-syenite complex of Greenland (Parsons 1981, 1991), the Mboutou layered gabbro-syenite-granite complex of Cameroon (Parsons 1986) and, the Baie-des-Moutons syenite complex of Québec (Lalonde and Martin 1983). The two fields show remarkable similarity; both are characterized by low total Al contents, in some cases even being Al-deficient, with a wide range of Fe/(Fe+Mg) values that extend from the phlogopite field to extremely iron-rich compositions with Fe/(Fe+Mg) values approaching 1.

In his compilation of biotite compositions of plutonic rocks, Abdel-Rahman (1994) discriminated between: i) anorogenic extension-related alkaline rocks, ii) calc-alkaline I-type orogenic suites and iii) peraluminous rocks including S-type granites. Several useful diagrams were introduced to discriminate the composition of biotite from these different tectonic settings in terms of its FeO, MgO, and Al_2O_3 contents. Of all these diagrams, the ternary FeO*-MgO-Al_2O_3 plot is probably the most powerful discriminant since, much like the ASPE quadrilateral, it reflects variations in redox state and peraluminosity. In this plot (Fig. 10) analyses of biotite from the Humber-Dunnage zones fall mainly within the A-type field. This observation is consistent with their whole-rock geochemical signature which, in all common discrimination diagrams, plot mainly within the A-type field (or WPG) (see Whalen, 1993).

Finally, in the Ague and Brimhall (1988) classification which is described in detail below, the majority of biotite analyses from the Humber-Dunnage zones plot within the different fields of I-type granitic rocks, although some analyses have higher F/OH values, as expected for micas crystallizing from high-fluorine magmas generated in within-plate settings. However, as discussed below, the suitability of this discrimination scheme for biotite from WPG rocks is questionable.

Dunnage Zone (Nfld)

If we exclude samples from Fogo Island which belong to the bimodal gabbro-granite Peyton association of Williams et al. (1989), Cambro-Ordovician plutonic rocks of the Notre-

Dame subzone (of the Dunnage zone) in Newfoundland are predominantly intermediate and metaluminous diorites, quartz diorites and granodiorites, and volcanic equivalents that were formed contemporaneously in a supra-subduction setting (Whalen et al. 1997). The geochemical and isotopic signatures of these rocks indicate a major mantle contribution along with significant input from old continental crust. The subduction-related batholiths of California constitute an ideal suite of rocks for comparison with the plutonic rock units of the Notre-Dame arc because these batholiths were generated and emplaced at convergent margins where oceanic crust was being subducted under a continental margin.

Ague and Brimhall (1988) presented a classification scheme for granitic rocks within Californian batholiths that is based on biotite $\log(X_F/X_{OH})$ and $\log (X_{Mg}/X_{Fe})$ values. These variables reflect ubiquitous buffer assemblages of $f(HF)/f(H_2O)$ and $f(O_2)$ conditions that prevailed during biotite crystallization. Rocks that contain biotite with $\log(X_{Mg}/X_{Fe}) > -0.21$ are divided into three subgroups based on increasing $\log(X_F/X_{OH})$: i) I-WC type (weakly-contaminated I-type), ii) I-MC type (moderately-contaminated I-type), and iii) I-SC type (strongly-contaminated I-type). Reduced rocks containing biotite with $\log(X_{Mg}/X_{Fe}) < -0.21$ are classified as I-SCR type (strongly contaminated and reduced I-type). Although the Ague and Brimhall classification is capable of detecting different levels of contamination by metaluminous crustal material, the scheme is susceptible to large errors because it relies on OH contents that are estimated from mineral recalculations and also requires F determinations, which when performed on the electron probe, as is usually the case, are prone to poor reproducibility.

In the diagram of Ague and Brimhall (1988) the composition of some biotite specimens from Dunnage zone rocks of Newfoundland fall within the I-WC, I-MC and I-SC fields (Fig. 11). Other samples corresponding to Fe-enriched biotite from highly evolved rocks (SiO_2 > 71 wt.%), including those from Fogo Island, plot in the I-SCR field. The spread of biotite compositions from I-WC to I-MC and I-SC fields is consistent with the claim of Whalen et al. (1997) that Notre-Dame subzone rocks result from the mixing of a major mantle-derived component with old continental crust.

On the ASPE quadrilateral, the biotite compositions of the I-WC, I-MC, and I-SC groups from California batholiths (Fig. 12), define a compositional field which is nearly identical to that defined by biotite from Notre Dame subzone rocks (Fig. 8). Note that on this diagram, the I-WC, I-MC and I-SC groups cannot be distinguished by their Fe/(Fe+Mg) values and Al-contents. According to Ague and Brimhall (1988), the nature and amount of hydrous minerals present in source rocks undergoing partial melting control the H_2O + halogen contents and temperatures of the first-formed melts. The observed west-to-east increase in the F/OH of mafic silicates documented by these authors, corresponding to the systematic I-WC to I-MC and I-SC progression, are attributed to variations in the halogen contents of their respective source rocks. Low $f(HF)/f(H_2O)$ during the formation of the western I-WC type granites is consistent with their derivation from low-fluorine source rocks in the subducted oceanic slab or in the upper mantle overlying the subducting plate. In contrast, higher $f(HF)/f(H_2O)$ values of crystallization recorded by the I-MC and I-SC type micas to the east implies a genesis which involve progressively greater amounts of continental crustal material towards the continental

interior. Two notable characteristics of biotites from these three suites of rocks formed in a continental arc are firstly, that they have moderate values of Al-contents, with a relatively low range of Fe/(Fe+Mg) values, and secondly, that no progressive trend can be observed in their ASPE plot.

In the discrimination diagrams of Abdel-Rahman (1994), the biotite compositions from Dunnage rocks fall principally in the calc-alkaline I-type field with few data points in the peraluminous and alkaline A-type fields (Fig. 10). Those in the alkaline field belong to the Fogo Island suite which is bimodal, suggestive of a rift-type environment.

Analyses of biotite from documented continental arc suites such the Coastal batholith of Peru (Mason, 1985), the Bishop suite of Wopmay orogen (Lalonde and Bernard 1993), and the magnetite-series granites of Japan (Czamanske et al. 1981), all exhibit in the ASPE quadrilateral a nearly-identical range of Fe/(Fe+Mg) values with respect to the Notre-Dame arc biotites, but have lower Al-contents (Fig. 13) suggesting lesser contributions of aluminous metasedimentary material to their magma genesis.

Gander Zone (NB)

Within the Gander zone of New Brunswick, all Ordovician granites have within-plate granite whole-rock geochemical signatures. The younger Siluro-Devonian granitic rocks show mixed volcanic-arc to within-plate signatures. Biotite compositions from these rocks appear to reflect such a mixed derivation. In the ASPE quadrilateral, biotites from granitic rocks of the

Gander zone of New Brunswick define a nearly-horizontal trend of increasing total Al at relatively constant Fe/(Fe+Mg) (Fig. 8). This trend is relatively common in the literature and is observed in biotites of the Adamello massif (De Pieri and Jobstraibizer 1977), the Southern Piedmont granites of the Appalachians (Speer 1981, 1987), the Umm Naggat stock of Egypt (Kabesh et al. 1975), the Zaer granite of Morocco (Mahmood 1983), the granites of Northern Portugal (Neiva 1976), the I-SCR granites of the California batholiths (Ague and Brimhall 1988), and the Hepburn intrusive suite of Wopmay orogen (Lalonde and Bernard 1993). Of all these suites, those of the Wopmay orogen and of California batholiths were retained here for comparison with the Gander rocks of New Brunswick, because these two suites have been the objects of considerable geochemical, isotopic and tectonic characterization.

The Hepburn intrusive suite of the Early Proterozoic Wopmay orogen, Northwest Territories, ranges in composition from gabbro to granite but peraluminous granites are dominant. These form large plutons of biotite-muscovite granite with xenocrysts of garnet and porphyroblasts of sillimanite. Fe-Ti oxides are almost always absent; only in few instances is ilmenite observed. Pronounced peraluminosity and high values of $\delta^{18}O$ indicate the importance of a metasedimentary contribution to the felsic members of the suite. Emplacement of this suite originated in an arc-related setting which rapidly evolved into a closing back-arc basin, i.e., a collisional setting, with an associated anatectic event (Lalonde, 1989).

In the batholiths of California, the I-SCR granites are relatively similar to those of the Gander zone in New Brunswick. These Californian I-type granitic rocks are believed to have undergone significant Al-enrichment and reduction by assimilation of graphitic

metasedimentary wall-rocks during their intrusion. As mentioned earlier, Gander granitic rocks are I-type, mainly peraluminous felsic biotite granites with minor gabbroic and amphibole-bearing granodioritic rocks. These rocks were derived from a mixture of supracrustal and mantle-derived components. Isotopic data are also consistent with reworking of older crust containing a significant supracrustal component.

Gander granitic rocks of New Brunswick have an opaque mineral assemblage that is dominated by magnetite coexisting with ilmenite in variable proportions. A few rare exceptions only have ilmenite. This situation is also observed in the Australian I-type granites (Whalen and Chappell 1988). Primary titanite is rarely observed, so are sulphides; pyrite and chalcopyrite are only observed either as interstitial crystals or as inclusions within amphibole or magnetite.

In the ASPE quadrilateral, biotite compositions from the I-SCR and Hepburn suite granitic rocks both define pronounced trends of increasing total Al at relatively constant Fe/(Fe+Mg) values (Fig. 14). The field defined by biotites from New Brunswick Gander zone rocks overlaps considerably with the combined Hepburn and I-SCR fields but is located slightly below these, at lower Fe/(Fe+Mg) values, suggesting that Gander rocks evolved under slightly more oxidizing conditions. This is consistent with the coexistence of magnetite and ilmenite in Gander rocks, in contrast to the sole occurrence of ilmenite in the majority of I-SCR rocks.

In the diagram of Ague and Brimhall (1988), not surprisingly, most biotite compositions from granitic rocks of the New Brunswick Gander zone fall in the I-SCR field (Fig. 11). However, some analyses also plot in the I-MC and I-WC fields, which are generally associated

with biotites from more primitive mafic or intermediate rock compositions. Also, the concentration of data points at lower values of log (X_{Mg}/X_{Fe}) in this diagram indicates, as with the ASPE diagram, more oxidizing conditions for the granitic rocks of the Gander zone than in the Californian I-SCR type.

In the ternary FeO*-MgO-Al_2O_3 diagram of Abdel-Rahman (1994), biotite compositions from New Brunswick Gander zone rocks are distributed between the calc-alkaline and peraluminous fields (Fig. 10); biotite from the mafic to intermediate rocks falls principally in the C field while, that from the peraluminous granites plots in the P field.

Gander Zone (Nfld)

In the ASPE quadrilateral, biotites from granitic rocks of the Gander zone in Newfoundland define a compositional field characterized by progressive enrichment of Fe and Al from the mafic to the felsic or evolved rocks (Fig. 8).

The trends defined by biotites from Japanese ilmenite-series granites (Czamanske et al. 1981), as well as hybrid and calc-alkaline Hercynian granites of northern Portugal (de Albuqurque, 1973; Neiva, 1981; Konings et al. 1988), in the ASPE diagram are very similar; i.e. Fe- and Al-contents increase together, reflecting low oxygen fugacity conditions (at or below the Ni-NiO buffer) resulting from significant contributions from metasedimentry material, either by assimilation or anatexis.

Unlike biotites from the Gander zone in New Brunswick, biotite compositions from the Gander zone in Newfoundland fall mainly in the I-MC to I-SC fields (less Fe-content) of Ague

and Brimhall, although a few analyses plot in their I-SCR field (Fig. 11). Newfoundland and New Brunswick biotites also display an interesting contrast of pleochroism. In Newfoundland rocks, biotite is dark brown to greenish-brown pleochroic, whereas in New Brunswick rocks, it is more reddish, suggesting higher total Fe contents, since Ti values for both groups are identical.

In the Abdel-Rahman triangular plot, Newfoundland biotites fall in the peraluminous and calc-alkaline fields and define a somewhat more linear trend than the cluster defined by New Brunswick biotites (Fig. 10).

Avalon Zone

All Siluro-Devonian granites located in the Avalon zone represent different phases of the Saint George-batholith. According to Whalen (1993), A2 and A4 plutons display clear A-type characteristics, whereas A1 and A5 plutons are clearly of I-type. Other Avalon granites (A3, A6) display transitional I- to A-type features. The localization of these granites at or near the fault-controlled Gander-Avalon boundary suggests emplacement in an extensional zone.

In the discrimination diagram of Abdel-Rahman (1994), the compositions of Avalon biotite falls in the calc-alkaline I-type and within-plate A-type fields (Fig. 10). Avalon biotite compositions belonging to the oxidized trend outlined earlier, mostly from amphibole - biotite granites, fall in the calc-alkaline I-type field and those belonging to the reduced trend, mostly biotite granites, plot in the alkaline A-type field, clearly consistent with their tectonomagmatic characteristics.

Although some phases of the Saint George-batholith are clearly of A-type character, we nevertheless plot their biotite compositions on the Ague and Brimhall (1988) diagrams designed for micas from normal I-type granites. As illustrated in Figure 11, analyses from the I-type amphibole-biotite-bearing granites fall in the I-MC field and those from biotite granites with A-type affinities, having higher Fe- and F-contents, plot outside of the I-type field, except for a single sample that plots in the I-SCR type.

Meguma Zone

According to Clarke et al. (1997), the central plutons of the Meguma zone are derived entirely from crust material and probably owe their origin to crustal thickening associated with accretion of the Meguma zone to the Avalon zone. In contrast, the peripheral plutons are of mixed derivation (sub-Meguma Group source rocks and mantle-derived mafic magmas) and probably owe their origin to the lower to mid-crustal intrusion of subduction-related mafic magmas prior to final emplacement of the Meguma zone.

On the ASPE quadrilateral (Fig. 8), biotite from peripheral and central plutons of the Meguma zone shows a remarkable increase in both iron and aluminum as the siderophyllite end-member is approached. Gander biotites from Newfoundland exhibit a quite similar trend but differences include a lower range of Fe/(Fe+Mg) and Al contents, implying more oxidizing conditions and lesser crustal contributions for Gander magmas than Meguma ones. This is further confirmed by the occurrence of both magnetite, ilmenite and titanite (in variable

proportions) in the majority of Gander samples from Newfoundland. Ilmenite is the common oxide phase in Meguma rocks, while magnetite and titanite are usually absent.

In the Ague and Brimhall (1988) diagram, Meguma zone biotites plot principally in the I-SCR field (Fig. 11); their crystallization under reducing conditions is further substantiated by their Fe-enriched composition and reddish-brown pleochroic color. Note that several samples are not shown in this diagram because of lack of fluorine data.

Not surprisingly, on the discrimination diagrams of Abdel-Rahman (1994), Meguma biotites plot exclusively in the peraluminous field (Fig. 10). A few samples which plot in the calc-alkaline field are from mafic rocks such as lamprophyres (spessarite).

10. Conclusions

The results of this study show that the most pronounced biotite compositional differences between granitic rocks of the Canadian Appalachians are in their total Al-contents and in Fe/(Fe+Mg) values. Both features are sensitive indicators of conditions that prevailed in the host magmas and documented as follow:

1. Biotite compositions from A-type granites of the Humber and Avalon zones, whether reduced or oxidized, are distinctly depleted in aluminium and enriched in total iron. A few samples from the Fogo Island plutonic rocks (Dunnage zone in Newfoundland), attributed to extensional tectonic environments, show the same features. Biotite compositions from I-type units have the same Al-contents as A-type rocks, however, being moderately enriched

in Mg, they plot in the calc-alkaline I-type field of biotite discrimination diagrams. These biotite compositional features are consistent with the nature of their host rocks.

2. Biotites from Notre Dame arc granites (Dunnage zone in Newfoundland), formed within a subduction-related environment, are compositionally comparable with biotite from California batholiths, a typical continental magmatic arc. Compared to biotite compositions from other continental arc suites, such as the Coastal batholith of Peru, the Bishop suite of Wopmay orogen of Canada, and the magnetite-series granites of Japan, biotite from Notre Dame arc granites has moderate Al contents, suggestive of a significant contribution from aluminous metasedimentary material to the magma genesis, consistent with the petrological and geochemical data.
3. Biotite from New Brunswick and Newfoundland Gander zone granites, derived from a mixture of supracrustal and mantle-derived source components, shows a pronounced trend of increasing total Al, confirming significant contributions from aluminous supracrustal material, either by assimilation or anatexis.
4. Meguma zone peripheral plutons, derived from a mixture of supracrustal and mantle derived mafic magma, have biotite compositions which resemble those of the Gander zone granites from Newfoundland. However, biotite compositions from the central plutons, derived entirely from crustal material, show a remarkable increase in both total Al and Fe, approaching the siderophyllite end member. Biotite from the central plutons is generally associated with muscovite, and/or garnet, cordierite and andalusite.

These examples show that the composition of biotite can be a discriminating tool for identifying the nature of granites. However, can it also be used for interpreting tectonic settings?

The Siluro-Devonian peralkaline A-type, metaluminous I-type, peraluminous I-type, and in rare cases, S-type granites of the Appalachian orogen were all emplaced during the post-collisional stage and must, therefore, be products of a major thermal anomaly that followed the closure of the Iapetus Ocean. A model which has been proposed to explain this thermal anomaly is the post-collisional delamination of the lithosphere (Whalen, 1993; Whalen et al. 1994; Kerr 1997). Although the major- and trace-element composition of these different granitic rocks is comparable with that of granite suites from classical convergent, collisional or within-plate environments, the major-element chemistry of the biotite from these rocks probably should not, by itself, be used to interpret the tectonic origin of these rocks, since a single tectonic process may have been responsible for the generation of all these different granite types within the Canadian Appalachians. However, an alternative interpretation to a delamination model is still being made (van Staal et al. 1998) that may change our present interpretation. Our results show that the major element composition of biotite can serve as one tool among others (e.g., Lameyre and Bowden 1982, Pitcher 1983, Pearce et al. 1984, Batchelor and Bowden 1985, Maniar and Piccoli 1989) and none of these methods is infallible and none should be employed in isolation, but if employed in combination in a multifaceted approach, they have a good likelyhood of success. We therefore conclude like Abdel-Rahman

(1994) that biotite chemistry can be useful if coupled with other parameters, such as whole-rock, trace-element, isotopic geochemical data, field and other geological constraints.

Table 1. Petrology and age of plutonic suites of the Canadian Appalachians.

A) Granitic rocks of New Brunswick and Québec

Zone	Pluton No.	Batholith/Suite	Pluton, phase or unit	Lithology	Radiometric age (Ma)	method used
Humber	H 1		McGerrigle complex	gb,di,to,gd,mz,md,sy,ne,gr	391±3	U-Pb (Zm)
Dunnage	D 3	Charlo stocks	Benjamin River complex	gb,di,md,mz,gr	370±30	Rb-Sr (W-R)
	D 5		Anitouri Lake	gr	372±4	U-Pb (Zm)
	D 6		Nicholas Denys	gd	381±4	U-Pb (Zm)
Gander	G 3	Ordovician suite	Meridian Brook	gr	464±5	U-Pb (Zm)
	G 4	Ordovician suite	Sweat Hill	gr	476+6/-4	U-Pb (Zm)
	G 5	Ordovician suite	Serpentine River	gr,ag	455+10/-8	U-Pb (Zm)
	G 6	Ordovician suite	Mullin Stream Lake	gd,gr	458+9/-13	U-Pb (Zm)
	G 7	Ordovician suite	Fox Ridge	gd,gr	452+15/-1	U-Pb (Zm)
	G 8	Ordovician suite	South Renous River	gd,gr	448+15/-21	U-Pb (Zm)
	G 9a	Ordovician suite	Unnamed Ordovician granite	gr	-	
	G 9b	Ordovician suite	Unnamed Ordovician granite	gd	-	
	G 9c	Ordovician suite	Unnamed Ordovician granite	gr	-	
	G 11		Pabineau Falls	gr	394±1	U-Pb (Zm)
	G 12	Mt.Elizabeth complex	mafic and alkaline suite plus granite	gb,do,md,mz,gd,sy,gr,ag	418±1, 414+11/-1	U-Pb (Mnz & Zm)
	G 13		Miramichi	gr	-	
	G 14	North Pole Stream suite	granodiorite, granite and mafic suite	do,to,gd,gr	417±1	U-Pb (Zm)
	G 15		RedStone Mountain suite	gb,gr	409±11	Rb-Sr (W-R)
	G 16		North Dungarvan River	gb,do,gd,to,gr	382	K-Ar
	G 17		Lost Lake suite	to,gd,gr	408±7, 402±4	K-Ar(Ms),Rb-Sr(Ms)
	G 18	Burnthill Brook suite	Dungarvan and Burnthill plutons	gr	380	Ar^{40}/Ar^{39}
	G 19		Beadle Mountain	gd	-	
	G 20		Juniper Barren	gd,gr	433±4	Rb-Sr (Ms)
	G 21		Bogan Brook	to,gd	-	
	G 22		Nashwaak	gr	422±4	Rb-Sr (Ms)
	G 23	Pokiok batholith	Hartfield	do, to,gd	415±1	U-Pb (Ttn)
	G 24	Pokiok batholith	Skiff Lake	to,gd,g	409±2	U-Pb (Zm)
	G 25	Pokiok batholith	Hawkshaw	gr	411±1	U-Pb (Ttn)
	G 26	Pokiok batholith	Allandale	gr	402±1	U-Pb (Mnz)
	G 28	Pokiok batholith	Tower Hill; Pleasant Ridge	gr	422±15	Rb-Sr (W-R)
	G 29	Pokiok batholith	Beech Hill	gr	349±11	Rb-Sr (W-R)
Avalon	A 1	St. George batholith	Evandale	mz,gd,gr	364	K-Ar (Bt)
	A 2	St. George batholith	Welsford and Jake Lee Mountain complexes	sy,gr,ag	422±3	U-Pb (Zm)
	A 3	St. George batholith	Mount Douglas	gr	366±1	U-Pb (Zm)
	A 4	St. George batholith	Utopia	gr	430±3	U-Pb (Zm)
	A 5	St. George batholith	Magaguadavic	md,gd,gr	396±1	U-Pb (Zm)
	A 6	St. George batholith	Bocabec complex	gb,gd,gr	403±20	Rb-Sr (W-R)

B) Granitic rocks of Newfoundland

Zone	subzone	Batholith/Suite	Pluton, phase or unit	Lithology	Radiometric age (Ma)	method used
	NDZs	Pierre's Pond plutonic suite		gb, di, Qtz di, gd	470	
	DWZn	Dashwoods - Ordovician plutonic suite		gb, di, Qtz di, gd	470	
	NDZn		Wild Cove Pond granite	gb, di, Qtz di, gd	470	
	NDZn		Dungarven granite	gb, di, Qtz di, gd	455	
	NDZs	Star Lake intrusive suite			420	
	NDZn		Mansfield Cove granodiorite		470	
	DWZs		Red Rocks granite		470	
	DWZs		Port aux Basque granite		470	
	NDZs	Star Lake intrusive suite				
	NDZn	Hungry Mountain complex				
Dunnage	NDZs	Pierre's Pond plutonic suite				
	NDZs	Dashwoods - early mafic intrusive				
	NDZn		Hinds Brook granite			
	DWZn	Dashwoods - Ordovician plutonic suite				
	DWZn	Dashwoods - younger granite suite				
	NDZs		Glover Island pluton			
	NDZs		Halfway Mountain pluton			
	NDZs	Caribou Lakes gneiss complex				
	DWZs	Grand Bay granodiorite suite				
	Exploit Sz		Fogo Island gabbro			
	Exploit Sz		Fogo Island granite			
			Cape Freels	gr	417±2	U-Pb (Zrn)
			Lockers Bay	gr	460±20	U-Pb (Zrn)
			Maccles Lake	gr	343±10	Rb-Sr
			Gaulois granite	gr	421±2	U-Pb (Zrn)
		Burgeo intrusive suite		gr, gd, Qtz di, gb	429+5/-3	U-Pb (Zrn)
Gander			Otter Point granite	gr	419±2	U-Pb (Zrn)
			Middle Ridge granite	gr, gd	410±2	U-Pb (Mnz)
			Deadman's Bay granite	gr	404±4	K-Ar
			NewPort granite	gr	366±5	Rb-Sr
			Gander Lake granite	gr	ca. 360	K-Ar
			Ackley granite	gr, gd	378-374	Ar-Ar
			Chetwynd granite	gr	390±3	U-Pb (Zrn)
			Northwest Cove granite	gr	ca. 350	
			Northwest Brook granite	gr	ca. 350	
			Dolland Bight granite	gr	ca. 350	
			Northwest Bay granite	gr	430±4	Rb-Sr
			Rose Blanche granite	gr		
			Buck Lake granite	gr	420	
			Through Hill granite	gr	429±2	Rb-Sr

C) Granitic Rocks of Nova Scotia

Zone	Batholith/Suite	Pluton, phase or unit	Lithology	Radiometric age (Ma)	method used
Meguma	South Mountain		gd,gr	372±2	Rb-Sr
	Musquodoboit		gr	368±3	Ar-Ar
		Ellison Lake pluton	gr	346±12	K-Ar
		Halfway Cove Queensport pluton	gd		
		plutons of Canso and Forest Hill area	gd, gr		
		Port Mouton	gd,gr	325-395	Ar-Ar

Rock type abbreviations are as follows: gb=gabbro; di=diorite; mz=monzonite; md=monzodiorite; sy=syenite; ne=nepheline syenite; to=tonalite; gd=granodiorite; gr=granite; ag = alkaline granite.
Age is given in millions of years with determinative method on whole-rock (W-R), zircon (Zm), monazite (Mnz), biotite (Bt), muscovite (Ms), titanite (Ttn).
Location of batholiths or plutons of Humber (Québec), Dunnage (New Brunswick and Newfoundland), Gander and Avalon zones (New Brunswick) are given in Whalen 1993, Gander zone (Newfoundland) in Kerr 1997 and Meguma zone (Nova Scotia) in Tate et al. 1997.

Table 2. Location, number of specimens and sources of data included in this study.

zone	No. of samples	locality	source
Meguma zone (Nova Scotia)	24	South Mountain batholith	Stallard (1975)
	8	South Mountain batholith	Allan (1981
	14	South Mountain batholith	Maillet (1984)
	10	South Mountain batholith	Ding (1995)
	4	South Mountain batholith	Clarke (unpublished)
	12	Musquodoboit batholith	MacDonald (1981)
	12	plutons of Canso and Forest Hill area	Hill (1991)
	29	Port Mouton pluton	Dumas (1988)
	23	Halfway Cove-Qeensport pluton	Ham (1988)
Humber zone (Quebec)	25	McGeriggle complex	Wallace (1988)
Dunnage zone (Newfoundland)	6	Topsail igneous complex	Whalen (unpublished)
Gander zone (Newfoundland)	18	granitic rocks of the Bay D'Espoir region	Bennet (1990)

Table 3. Selected electron-microprobe analyses and structural formulae of biotites from the Canadian Appalachian granites.

zone	Avalon (NB)		Dunnage (NF)		Gander (NF)		Gander (NB)		Humber-Dunnage (NB - QC)		Meguma (NS)	
sample no.	nb-180	nb-206	nf-78	nf-49	ak-166	ak-291	nb-29	nb-166	nb-53	mg-44	ed3	pc2b
whole-rock SiO_2	74.10	67.17	73.60	68.15	75.19	68.46	72.35	64.45	74.95	66.09	73.75	68.07
mean*	3	5	3	4	2	5	7	6	4	7	3	5
SiO_2	34.95	37.23	33.76	35.64	37.65	36.12	34.57	34.65	34.83	37.38	34.38	34.83
TiO_2	3.45	4.20	2.23	4.74	2.22	2.32	2.01	2.90	3.69	3.39	2.97	3.57
Al_2O_3	12.59	13.17	17.59	14.33	17.52	14.92	18.10	19.36	12.82	11.93	19.47	18.59
Fe_2O_3	4.64	3.99	3.30	3.03	3.83	3.21	5.03	1.75	5.98	4.10	2.68	2.69
FeO	27.95	15.30	19.85	15.43	15.70	16.36	16.10	18.40	24.50	20.83	25.11	22.21
MnO	0.70	0.33	0.71	0.43	1.84	0.54	0.95	0.21	0.78	0.25	0.81	0.39
MgO	3.52	12.90	8.67	12.70	6.65	12.19	9.46	8.59	5.06	8.74	3.68	6.98
CaO	0.00	0.03	0.03	0.81	0.05	0.04	0.01	0.00	0.04	0.01	0.03	0.03
Na_2O	0.07	0.10	0.07	0.17	0.05	0.06	0.07	0.22	0.18	0.07	0.12	0.14
K_2O	9.37	9.93	9.70	8.48	9.31	9.96	9.44	9.66	9.18	9.79	9.83	10.08
H_2O	3.20	3.58	3.64	3.84	3.37	3.68	3.65	3.74	2.77	2.90	3.54	3.74
F	0.79	0.65	0.43	0.23	1.23	0.53	0.53	0.40	1.87	1.75	0.57	0.26
Cl	0.39	0.17	0.04	0.04	0.02	0.04	0.01	0.01	0.32	0.42	0.08	0.09
O=F	-0.33	-0.27	-0.18	-0.10	-0.20	-0.22	-0.22	-0.17	-0.79	-0.74	-0.24	-0.11
O=Cl	-0.09	-0.04	-0.01	-0.01	-0.01	-0.01	0.00	0.00	-0.07	-0.09	-0.02	-0.02
Total	101.22	101.29	99.83	99.75	98.93	99.72	99.71	99.74	101.16	100.73	103.01	103.45
^{IV}Si	5.58	5.56	5.23	5.38	5.73	5.50	5.27	5.27	5.50	5.77	5.24	5.22
^{IV}Al	2.37	2.32	2.77	2.55	2.27	2.50	2.73	2.73	2.38	2.17	2.76	2.78
^{IV}Ti	0.05	0.12	0.00	0.07	0.00	0.00	0.00	0.00	0.12	0.06	0.00	0.00
T site	8.00	8.00	8.00	8.00	8.00	8.00	8.00	8.00	8.00	8.00	8.00	8.00
^{VI}Al	0.00	0.00	0.44	0.00	0.87	0.18	0.52	0.74	0.00	0.00	0.74	0.50
^{VI}Ti	0.36	0.35	0.26	0.46	0.25	0.27	0.23	0.33	0.32	0.33	0.34	0.40
Fe^{+3}	0.56	0.45	0.38	0.34	0.44	0.37	0.58	0.20	0.71	0.48	0.31	0.30
Fe^{+2}	3.73	1.91	2.57	1.95	2.00	2.08	2.05	2.34	3.23	2.69	3.20	2.78
Mn^{+2}	0.09	0.04	0.09	0.05	0.24	0.07	0.12	0.03	0.10	0.03	0.11	0.05
Mg	0.84	2.87	2.00	2.86	1.51	2.77	2.15	1.95	1.19	2.01	0.84	1.56
O site	5.58	5.62	5.74	5.67	5.31	5.73	5.65	5.59	5.56	5.54	5.53	5.60
Ca	0.00	0.00	0.01	0.13	0.01	0.01	0.00	0.00	0.01	0.00	0.01	0.00
Na	0.02	0.03	0.02	0.05	0.01	0.02	0.02	0.07	0.05	0.02	0.04	0.04
K	1.91	1.69	1.91	1.63	1.81	1.93	1.84	1.87	1.85	1.93	1.91	1.93
A site	1.93	1.93	1.94	1.81	1.83	1.96	1.86	1.94	1.91	1.95	1.95	1.97
O	20.00	20.00	20.02	20.02	20.00	20.00	20.03	20.01	20.00	20.00	20.11	20.12
OH	3.50	3.65	3.75	3.86	3.40	3.73	3.71	3.80	2.98	3.04	3.60	3.74
F	0.40	0.31	0.21	0.11	0.59	0.26	0.25	0.19	0.93	0.85	0.28	0.12
Cl	0.11	0.04	0.01	0.01	0.01	0.01	0.00	0.00	0.09	0.11	0.02	0.02
Fe/(Fe+Mg)	0.84	0.45	0.60	0.44	0.62	0.47	0.55	0.57	0.77	0.61	0.81	0.66

* number of analyses included in mean

Table 4. Compositional features of biotite from plutonic rocks of the Canadian Appalachians.

zone	no. sam.*	O-site	Σ Al	$^{vi}Al^{3+}$	$^{vi}Ti^{4+}$	Fe/(Fe+Mg)	Fe^{3+}/Fe
Hum-Dun (NB - QC)	30	5.35-5.72 (5.58)	2.01-2.52 (2.29)	0.00-0.35 (0.02)	0.39-0.59 (0.44)	0.37-0.87 (0.58)	0.09-0.26 (0.16)
Dunnage (NF)	38	5.41-5.83 (5.61)	2.37-3.20 (2.80)	0.00-0.55 (0.26)	0.19-0.55 (0.35)	0.37-0.87 (0.58)	0.10-0.23 (0.16)
Gander (NB)	56	5.38-5.78 (5.58)	2.10-3.55 (2.93)	0.00-0.90 (0.35)	0.17-0.54 (0.35)	0.42-0.76 (0.64)	0.06-0.23 (0.15)
Gander (NF)	50	5.30-5.81 (5.61)	2.35-3.54 (2.99)	0.00-0.99 (0.47)	0.15-0.48 (0.29)	0.36-0.80 (0.60)	0.09-0.22 (0.14)
Avalon (NB)	18	5.42-5.82 (5.61)	2.10-2.69 (2.36)	0.00-0.24 (0.03)	0.30-0.52 (0.41)	0.42-0.91 (0.64)	not determined
Meguma (NS)	146	4.91-5.97 (5.50)	2.63-4.01 (3.44)	0.36-1.55 (0.86)	0.04-0.53 (0.35)	0.37-0.99 (0.69)	0.08-0.19 (0.12)

* Number of determinations included in mean.

O-site, Σ Al, $^{vi}Al^{3+}$ and $^{vi}Ti^{4+}$ are in atomes per formula unit. Values in parantheses are means.

Table 5. Estimated oxygen fugacities for crystallization of plutonic rocks based on biotite composition.

zone	Fe/(Fe+Mg)	f (O_2) bars
Hum-Dun (QC-NB)	0.41-0.60	10^{-12}-10^{-15}
Dunnage (NF)	0.40-0.84	$10^{-11.6}$-$10^{-16.7}$
Gander (NB)	0.53-0.76	$10^{-13.7}$ -$10^{-16.4}$
Gander (NF)	0.49-0.60	$10^{-13.2}$ -$10^{-14.7}$
Avalon (NB)	0.42-0.91	10^{-12} -$10^{-16.8}$
Meguma (NS)	0.37-0.99	10^{-10} -$10^{-16.9}$

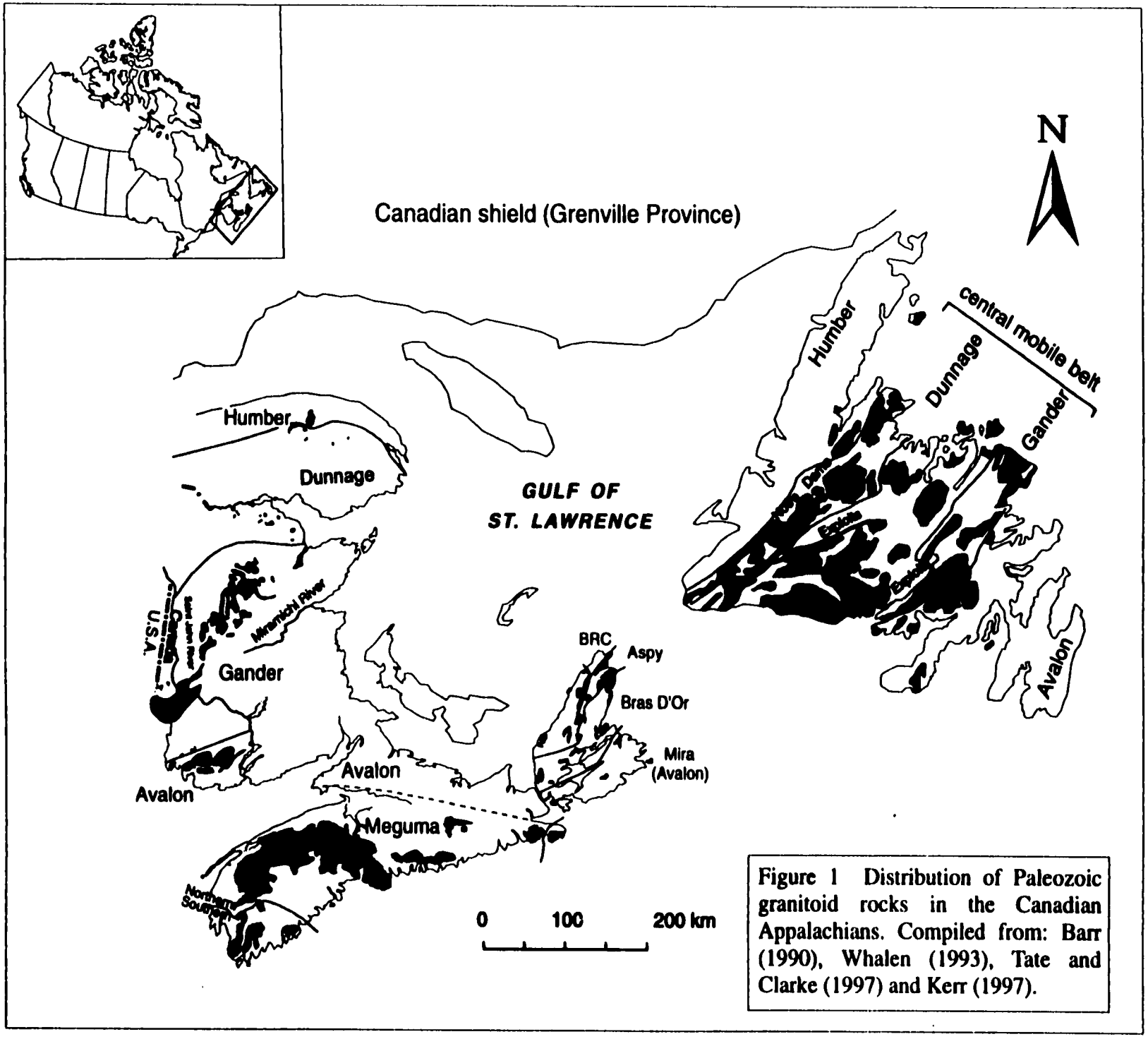

Figure 1 Distribution of Paleozoic granitoid rocks in the Canadian Appalachians. Compiled from: Barr (1990), Whalen (1993), Tate and Clarke (1997) and Kerr (1997).

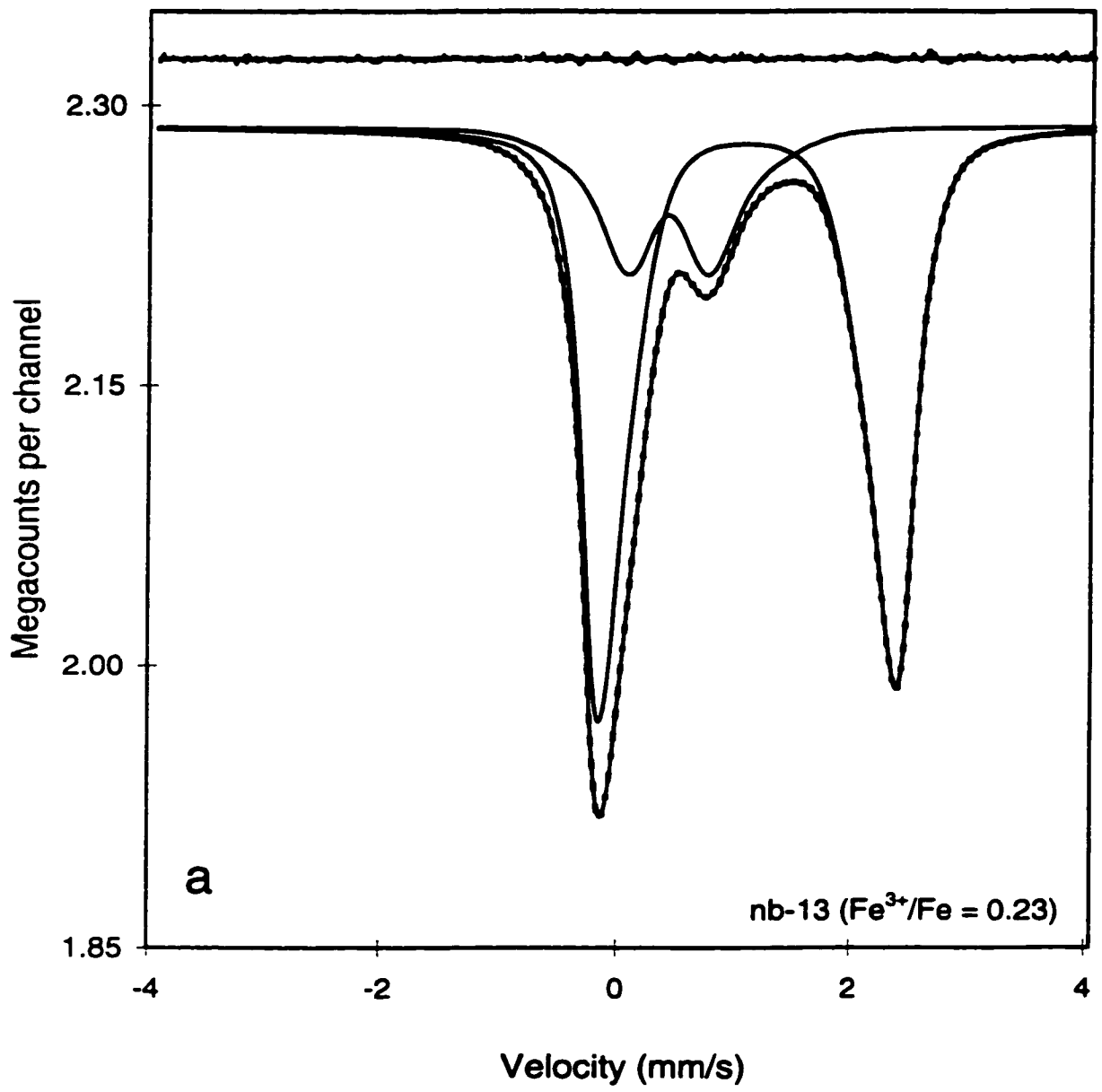

Figure 2 (a-b) Fitted RT raw folded spectra of two representative biotite samples from granitic rocks of the Canadian Appalachians. The line joining the data points is the fit result. The other solid lines show the separate contributions from octahedral Fe^{2+} and Fe^{3+}. The different spectra are shown with the same vertical scales.

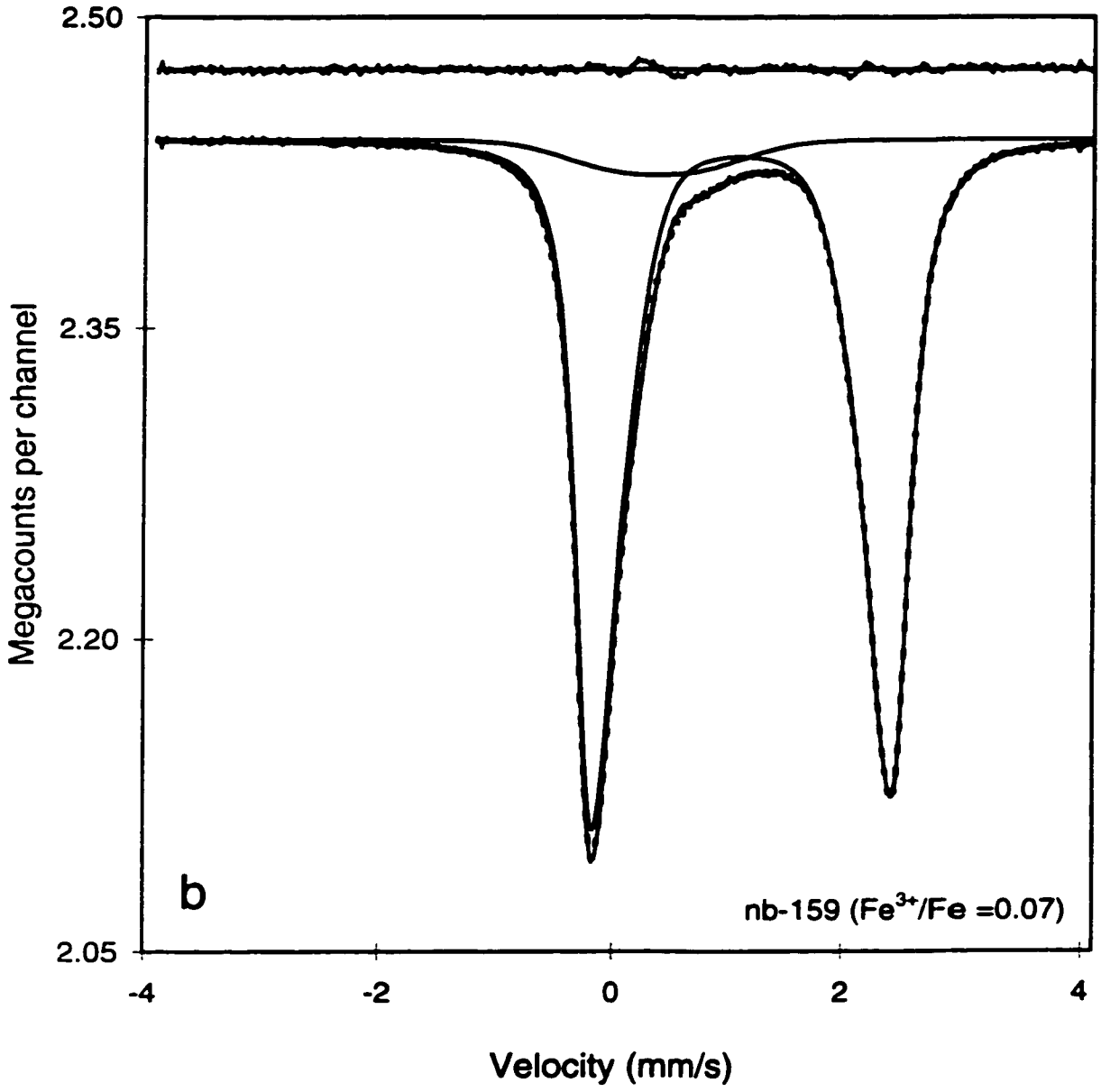
2.50
2.35
2.20
2.05
Megacounts per channel
b
nb-159 (Fe3+/Fe =0.07)
-4
-2
0
2
4
Velocity (mm/s)

Figure 2 (b).

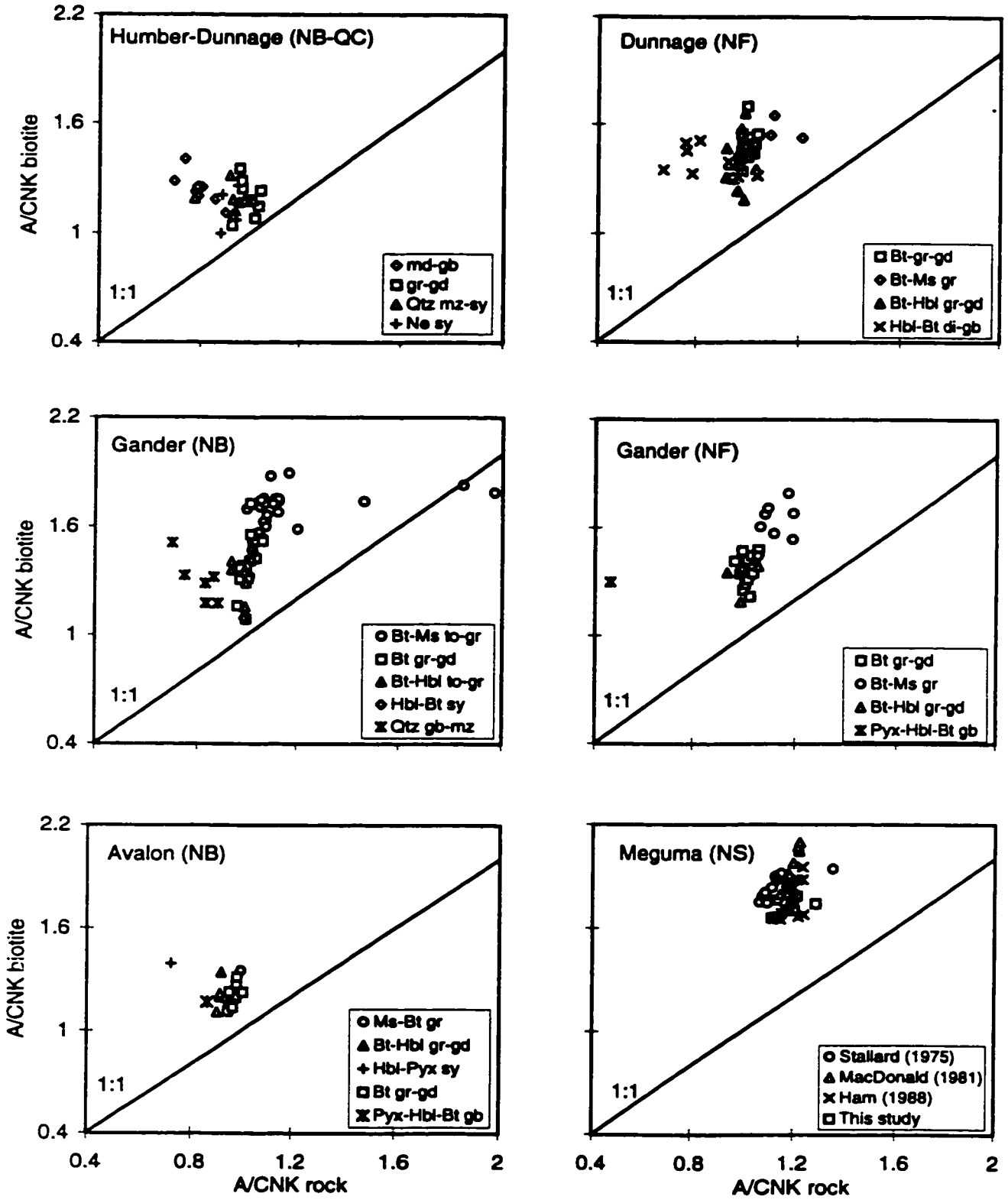

Figure 3 Peraluminosity of biotite versus that of its host rock for granitic rocks of the Canadian Appalachians.

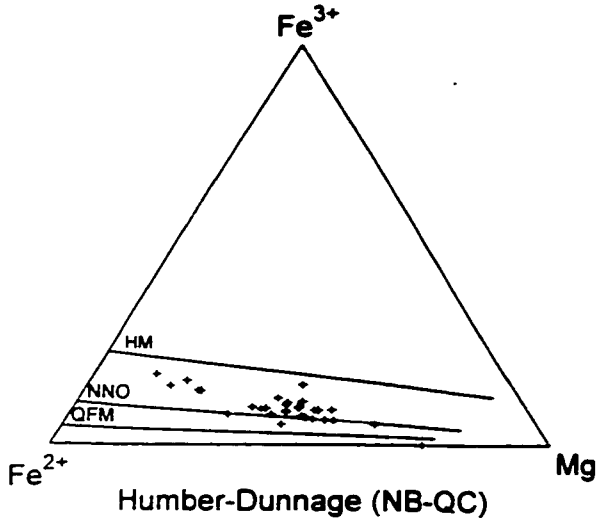

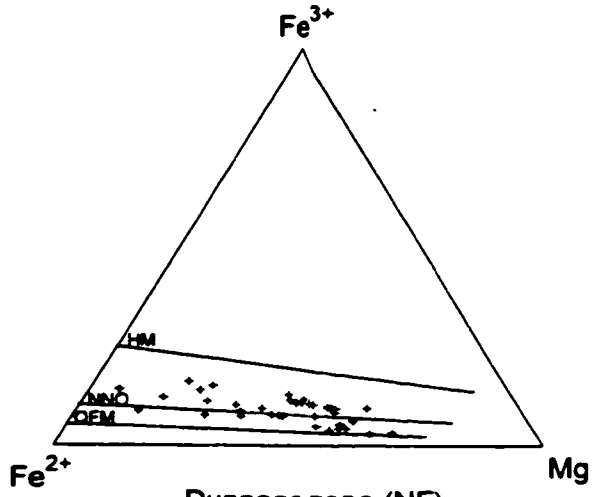

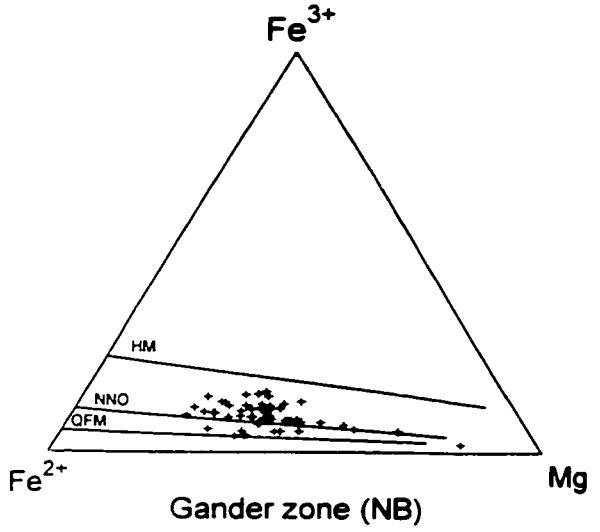

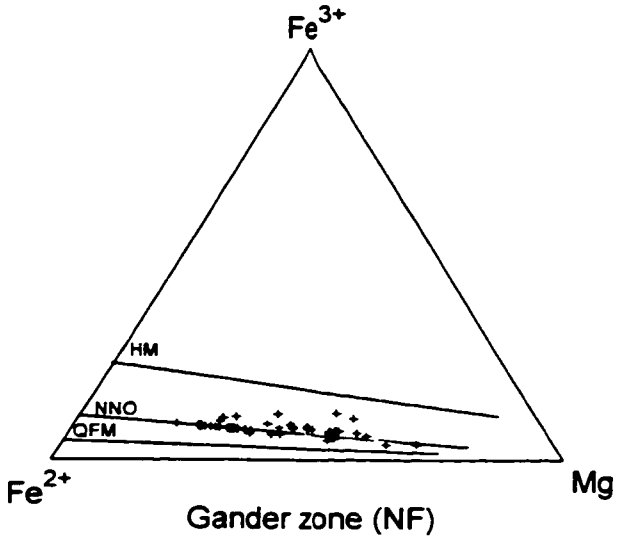

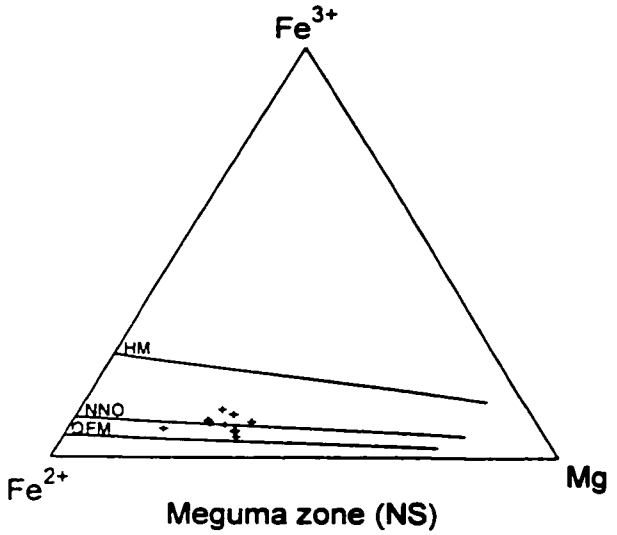

Figure 4 Composition of biotite from the Canadian Appalachian granites in the Fe^{3+} - Fe^{2+} - Mg ternary diagram of Wones and Eugster (1965). QFM=quartz-fayalite-magnetite, NNO=Ni-NiO and HM=hematite-magnetite buffers.

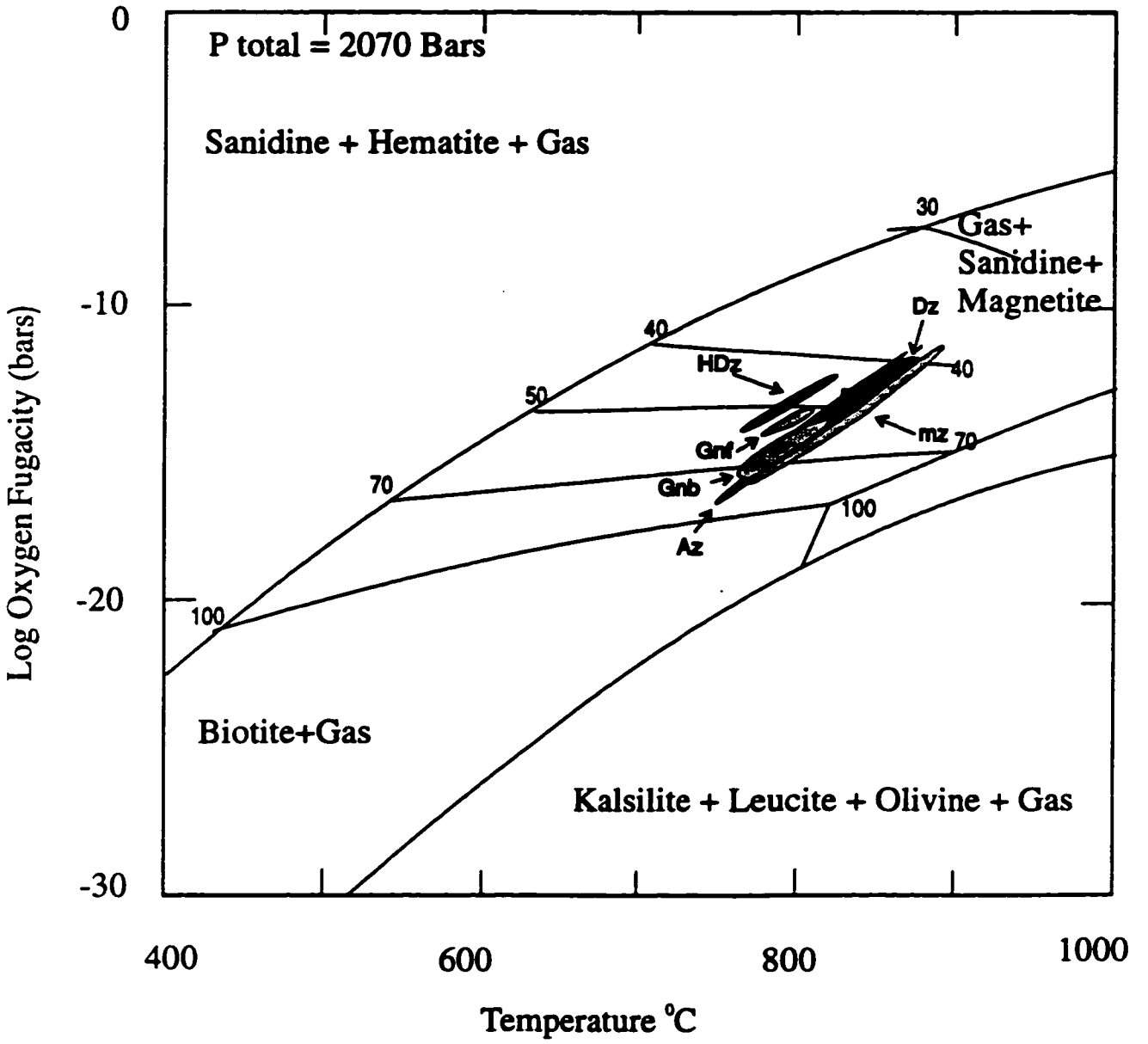

Figure 5 Log $f(O_2)$ - T diagram for the biotite + sanidine + magnetite + gas equilibrium at P total = 2070 bars (from Wones & Eugster 1965). Illustrated are Fe/(Fe+Mg) isopleths. Labeled patterns represent range of oxygen fugacity for biotite samples from Appalachian granites assuming an equilibrium temperature of 750-900 °C.

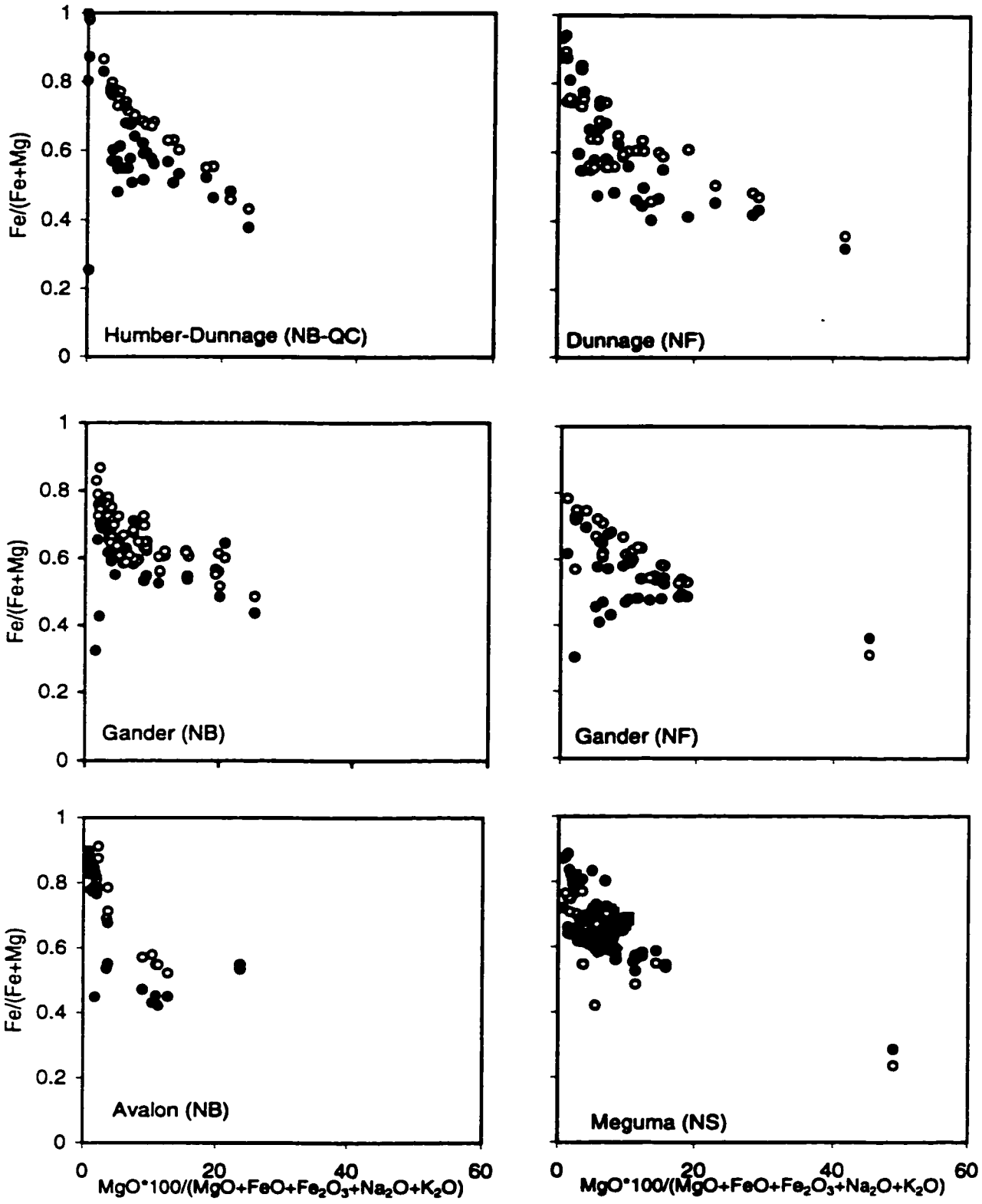

Figure 6 Plots of Fe/Fe+Mg for biotite and its host rock versus solidification index. Note that open symbols are biotite and closed ones are whole rock.

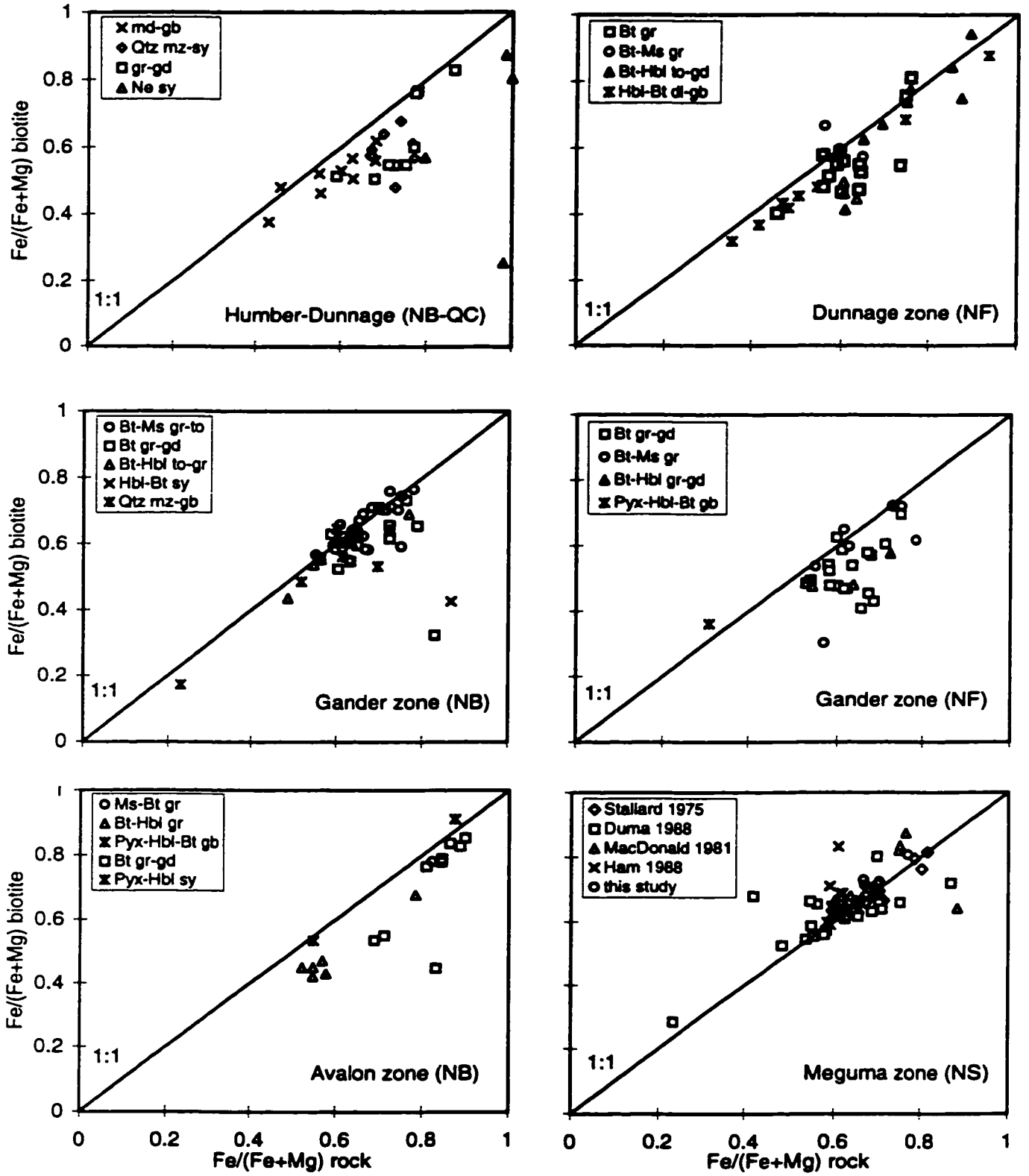

Figure 7 plots of biotite Fe/(Fe+Mg) versus that of its host rock from granitic rocks of the Canadian Appalachians.

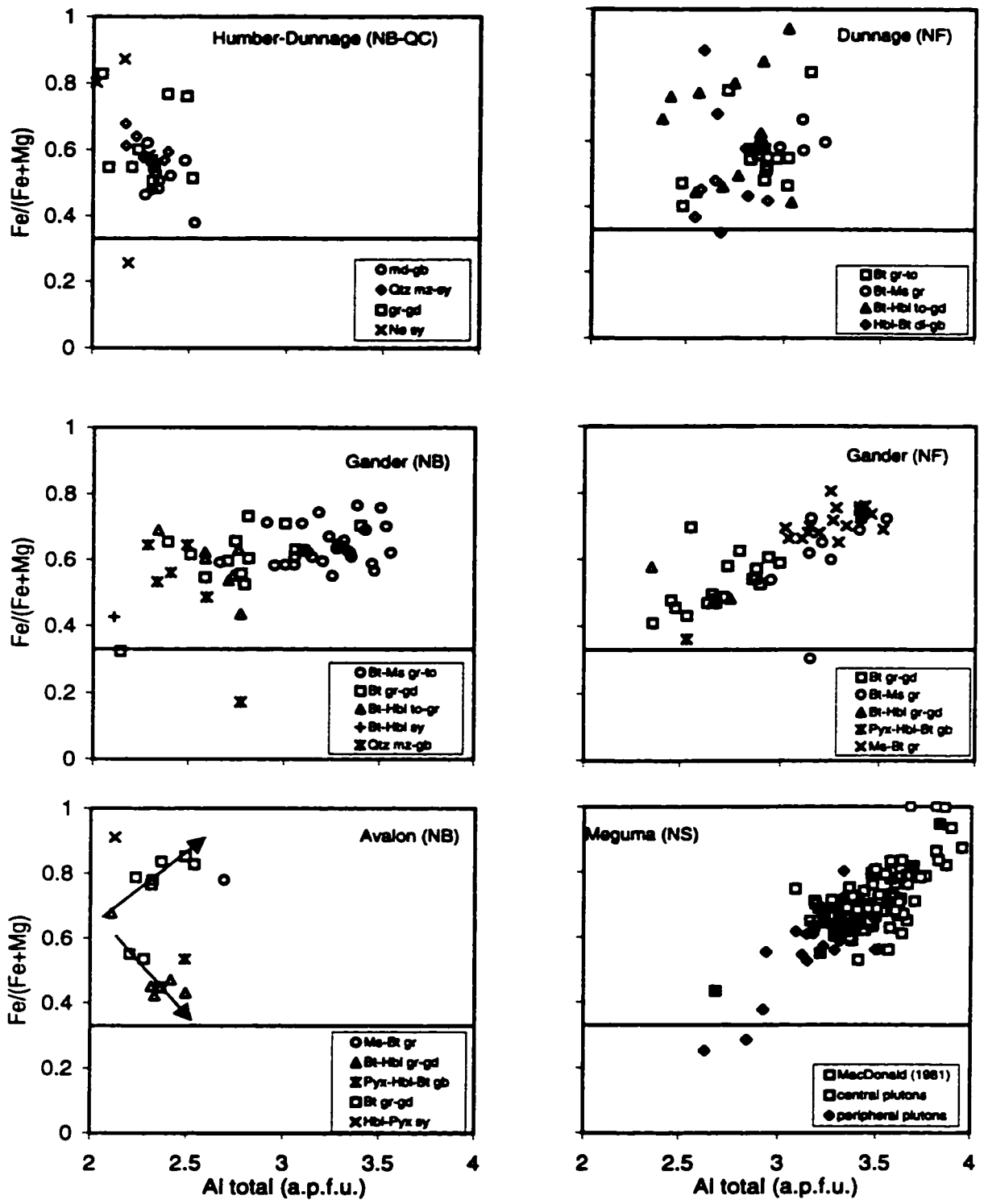

Figure 8 Biotite compositional trends from Canadian Appalachian granites in annite-eastonite-phlogopite-siderophyllite diagram. Fogo island samples are shown with solid symbols in the Dunnage (NF) plot.

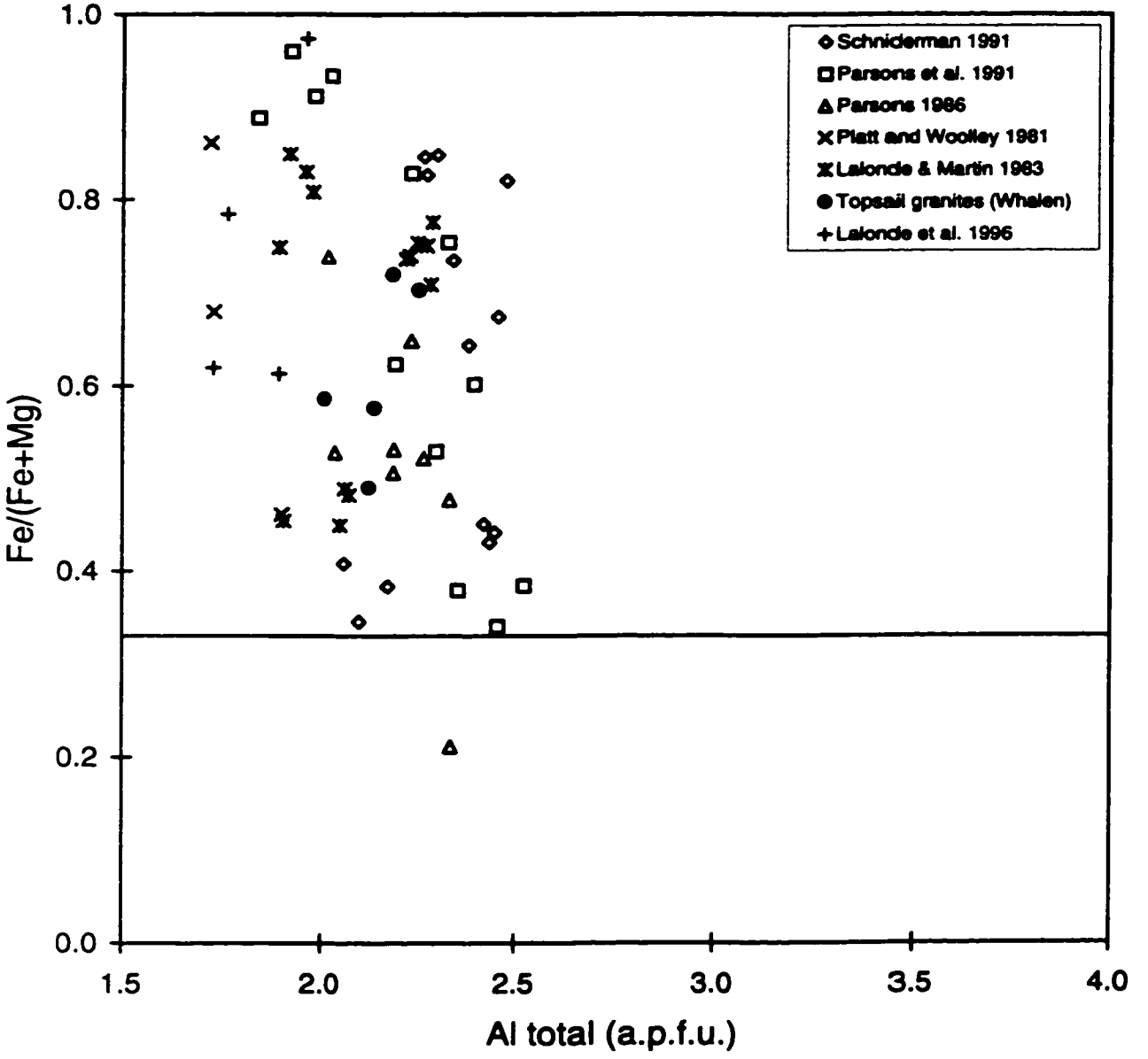

Figure 9 Biotite compositions from alkaline or A-type suites.

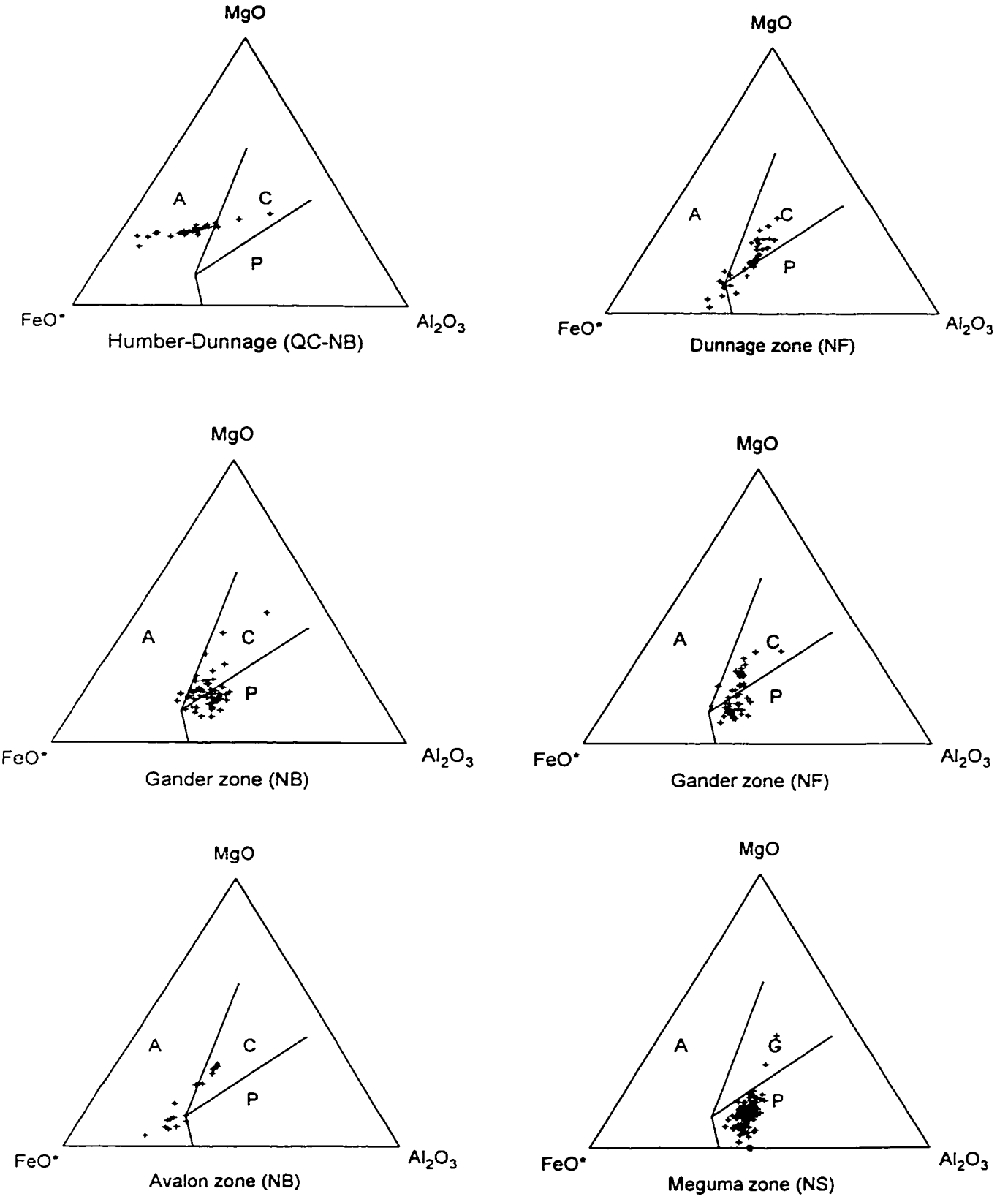

Figure 10 Biotite composition from Appalachian granites in the ternary discrimination diagram of Abdel-Rahman (1994), A=alkaline, C=calc-alkaline, P=peraluminous.
$FeO^* = [FeO + (Fe_2O_3 * 0.89981)]$.

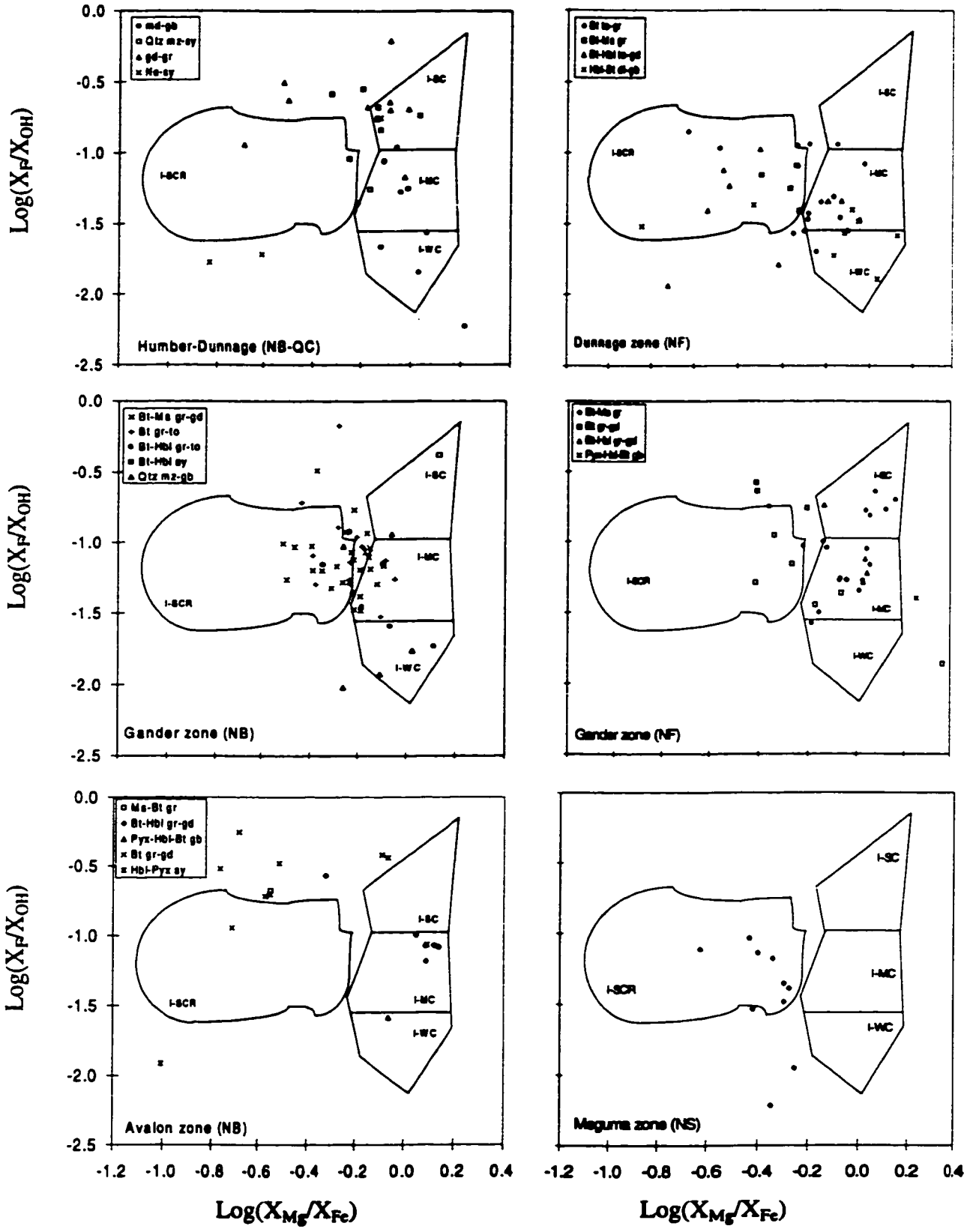

Figure 11 Biotite composition from Canadian Appalachian granites in the Ague and Brimhall (1988) diagram. I-WC, I-MC, I-SC and I-SCR are defined in the text.

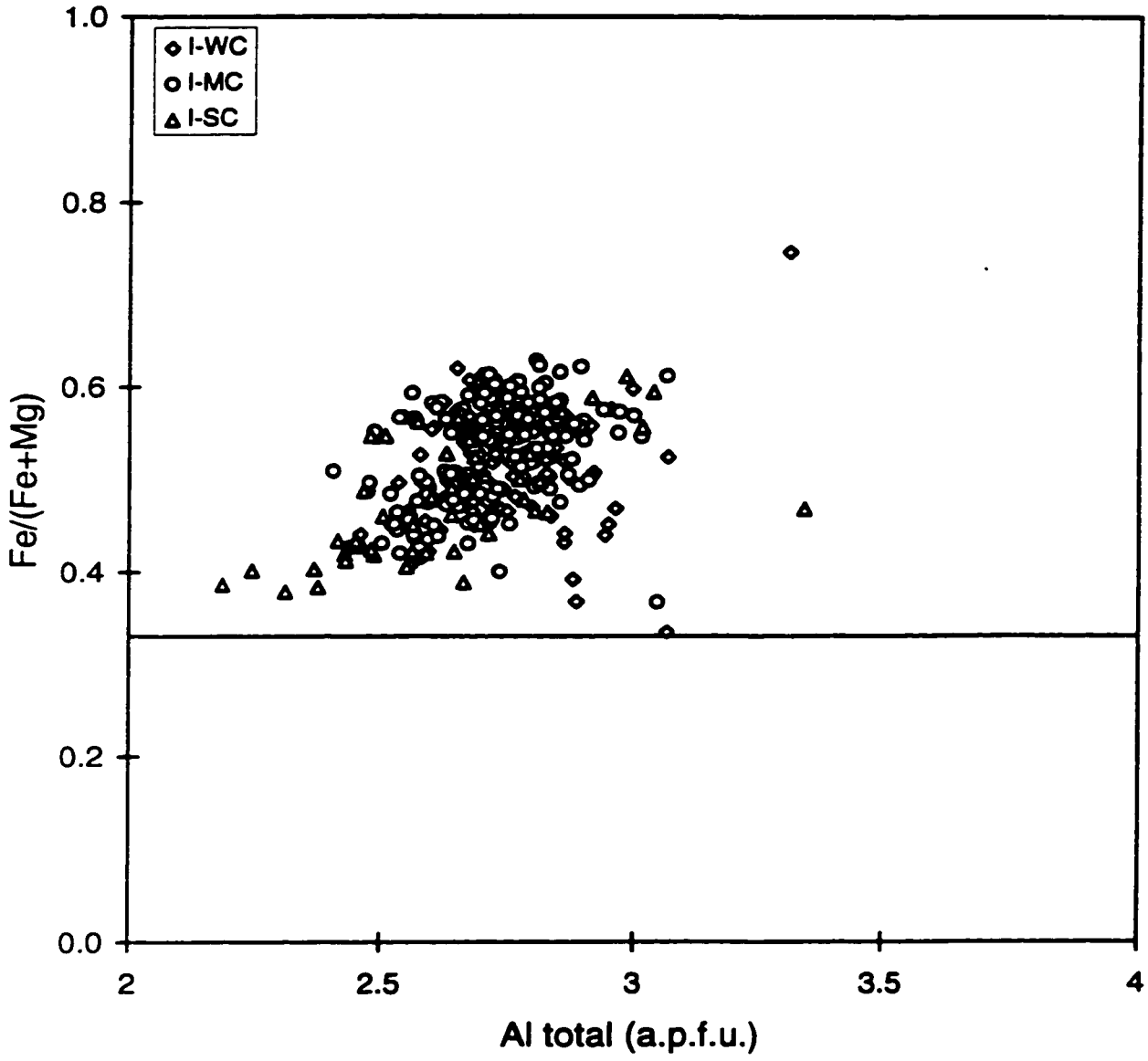

Figure 12 Composition of biotite from the granitic rocks of the California batholiths in the ASPE quadrilateral.

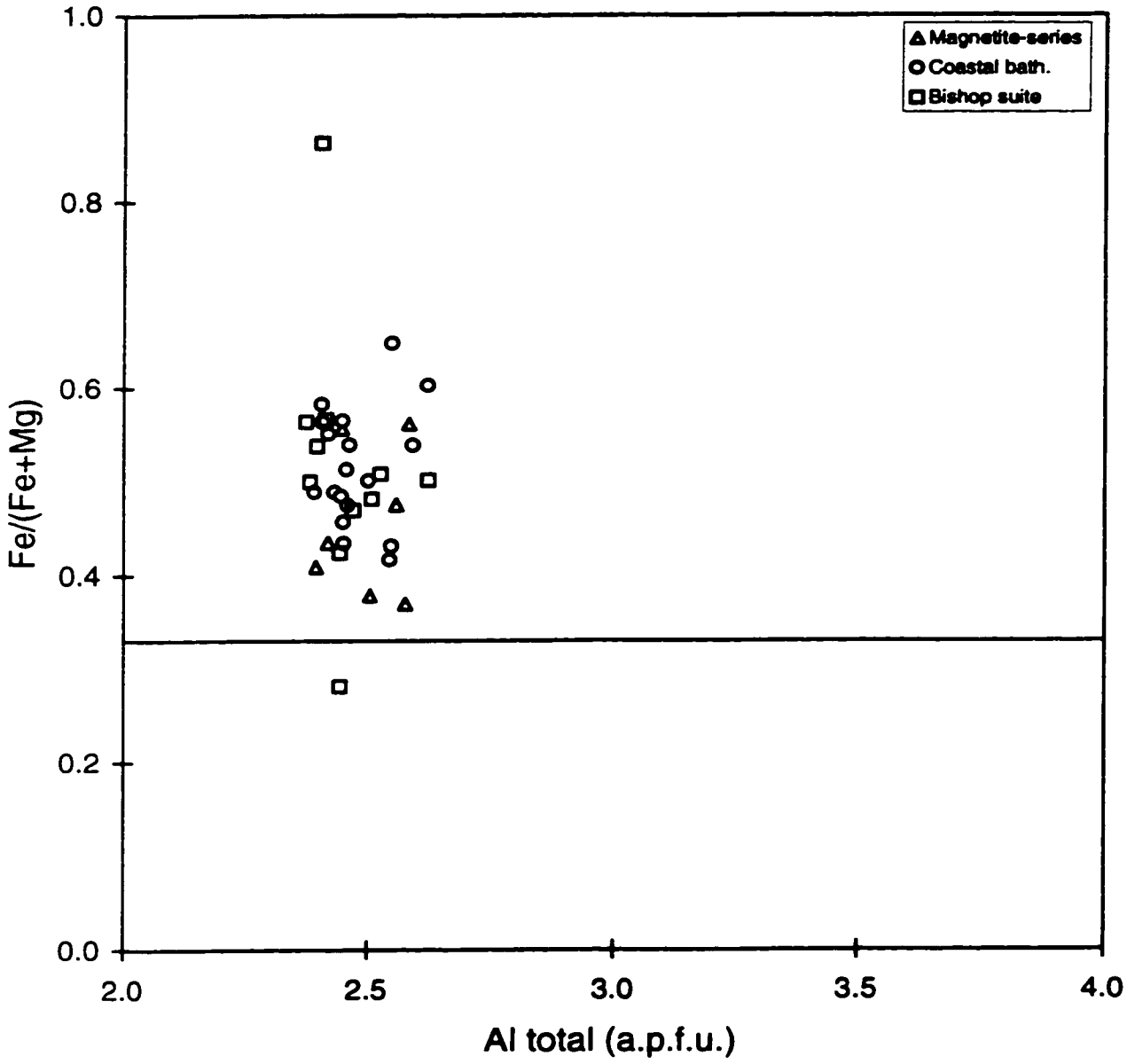

Figure 13 Composition of biotite from the Magnetite-series granites (Czamanske et al. 1981), Coastal batholith (Mason 1985) and Bishop granitic suite (Lalonde and Bernard, 1993), expressed in the ASPE quadrilateral.

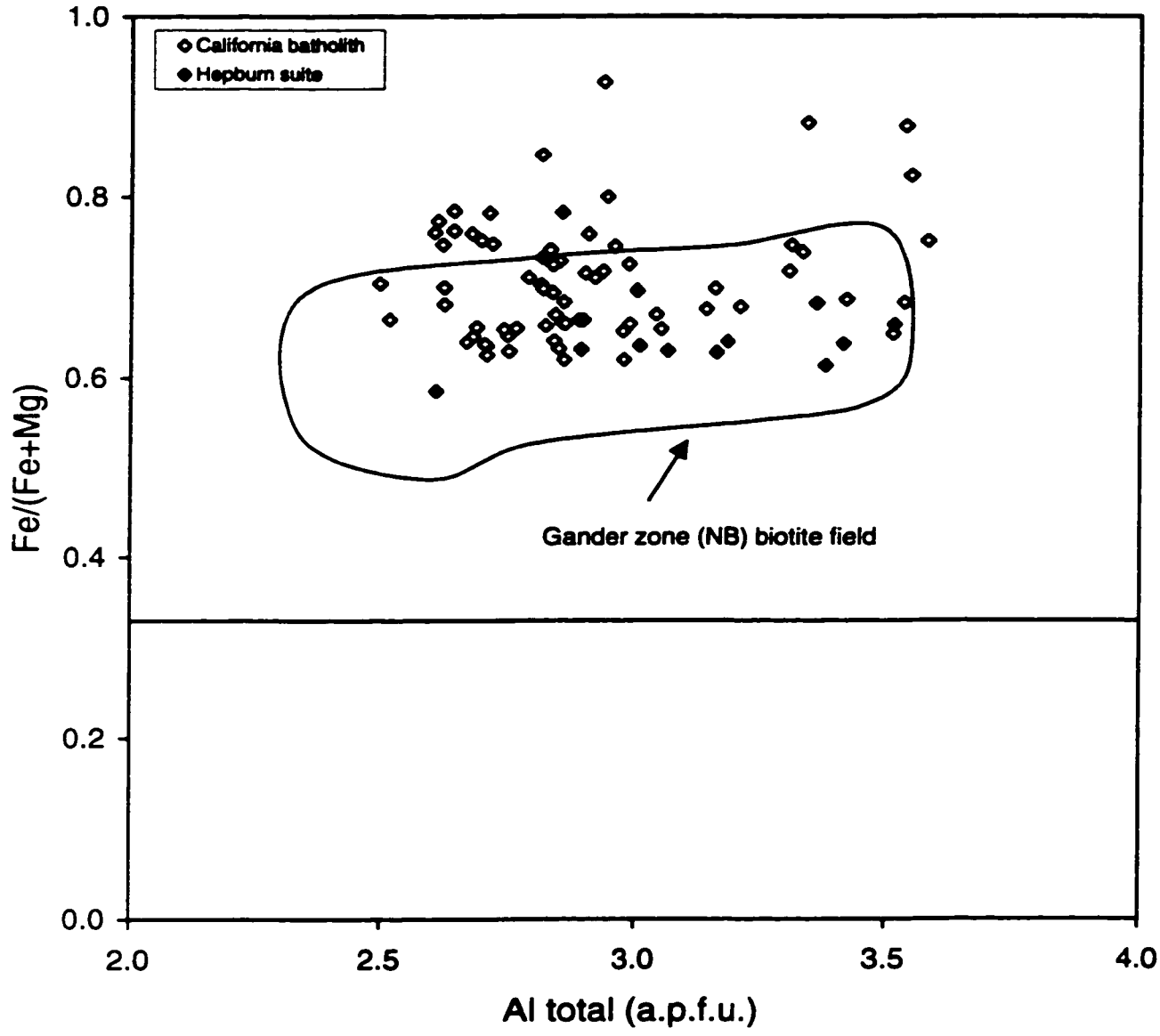

Figure 14 Composition of biotite from the granitic rocks of the California batholith (I-SCR type), Hepburn intrusive suites and Gander zone in New Brunswick, expressed in the ASPE quadrilateral.

CORRELATIONS BETWEEN OCTAHEDRAL - Fe^{2+} QUADRUPOLE SPLITTING DISTRIBUTIONS FROM MÖSSBAUER SPECTROSCOPY AND CHEMICAL PARAMETERS IN BIOTITE

Amir A.T. Shabani[1], Denis G. Rancourt[2], André E. Lalonde[1] and Patrick H. J. Mercier[2]

1) Ottawa-Carleton Geoscience Centre, Department of Earth Sciences,

University of Ottawa, Ottawa, Ontario, Canada, K1N 6N5

2) Department of Physics, University of Ottawa, Ottawa, Ontario, Canada, K1N 6N5

Abstract

Room temperature ^{57}Fe Mössbauer spectra of seventy one specimens of trioctahedral micas from the Paleozoic granitic rocks of the Canadian Appalachians, granitic rocks of the Hepburn and Bishop intrusive suites of the Early Proterozoic Wopmay orogen, Northwest Territories, Canada, and nepheline syenite of the Cretaceous Mont Saint-Hilaire alkaline suite, Quebec, Canada are described in terms of quadrupole splitting distribution (QSDs). We establish the possible range of Fe^{2+} QSDs in biotite and key limiting characteristics of the QSDs in all biotites.

We do not know why natural biotites have these types of QSDs, due to a lack of electronic structure calculations that link local distortion environments to quadrupole splitting values. Furthermore, several chemical parameters that are key crystal chemical parameters of the synthetic phlogopite-biotite-annite solid solution (e.g., Fe/(Fe+Mg), Fe^{3+}/Fe_{total}) do not correlate with any of the QSD features of natural biotites. We find the strongest single chemical parameter is Al_{total} , which is related to several crystal chemical features such as calculated average octahedral cation radius [R], tetrahedral rotation angle α and average octahedral flattening angle Ψ (degrees).

1. Introduction

Recently, in their studies on natural and synthetic trioctahedral micas by Mössbauer Spectroscopy, a number of researchers have tried to correlate Mössbauer parameters with chemical and physical parameters in order to interpret the crystal structural features of sheet silicates. Significant correlations exist between the Mössbauer parameters and chemical and physical parameters in synthetic trioctahedral micas (e.g., Ferrow 1987; Christie et al., 1993; Rancourt et al., 1994; Redhammer et al., 1995; Rancourt et al., 1996; Mercier et al., 1997; Redhammer 1998). On the other hand, such correlations seem to be minimal or absent in natural biotite (e.g., Bowen et al., 1969; Annersten, 1974, 1975; Heller-Kallai and Rozenson, 1981; Dyar, 1987). The lack of observed correlations in natural biotite may be due to: true competing influences on the hyperfine parameters from the more complex chemistry and greater variety of equilibration conditions in natural samples, or too small a sampling of biotite to be representative of the major variations that can occur and to allow isolation of the various influences, or improper spectral analysis methods that mask true variations (see below), or to some combination of these factors.

Recently, Rancourt et al. (Rancourt, 1989; Rancourt and Ping, 1991; Rancourt, 1994; Rancourt, 1994a; Rancourt et al., 1994; Rancourt et al., 1996) have developed Mössbauer spectroscopy data treatment and spectral analysis methods that allow true intrinsic Fe^{2+} quadrupole splitting distributions (QSDs) to be extracted from Mössbauer spectra for detailed comparative studies. They also showed that previous analyses in terms of Lorentzian

quadrupole doublets ascribed to specific crystallographic sites are incorrect. The QSDs are related to populations of local distortion environments and local chemical environments that cannot be obtained by other methods. So far, mainly synthetic trioctahedral micas (Christie et al., 1993; Rancourt et al., 1994; Rancourt et al., 1996; Mercier et al., 1997; Redhammer 1998) have been analysed by these methods. These studies have provided information concerning local crystal chemical effects that are related to the known compositions and crystal structures.

This paper represents the first attempt to describe the Mössbauer spectra of a large number of natural biotites in terms of QSDs and to search for possible correlations with chemical parameters. We find that several chemical parameters that are expected to be key crystal chemical parameters of the phlogopite-biotite-annite solid solution (e.g., Fe/(Fe+Mg), Fe^{3+}/Fe_{total}) do not correlate with any of the QSD features. The strongest single chemical indicator is Al_{total}, which is related to several crystal chemical features. We also established the possible range of QSDs in biotite and identified key limiting characteristics of the QSDs in all biotites.

2. Sample Selection, Characterization, and Description

Seventy one specimens of trioctahedral micas, mostly biotite, were included in this study. Fifty-four of these specimens are biotites that were separated from the Paleozoic granitic rocks of the Canadian Appalachians. The remaining seventeen micas have recently

been the object of extensive mineralogical and Mössbauer spectroscopy characterization (Lalonde and Bernard 1993; Lalonde et al., 1996, 1998). Thirteen of these specimens are biotites from granitic rocks of the Hepburn and Bishop intrusive suites of the Early Proterozoic Wopmay orogen, Northwest Territories, Canada (Lalonde and Bernard 1993; Lalonde et al., 1998). The other four mica specimens are from the Cretaceous Mont Saint-Hilaire alkaline suite, Québec, Canada (Lalonde et al., 1996). A brief description of biotite for each site is presented below.

2.1 Biotite from the Canadian Appalachian Granites

These biotites come from the plutonic rocks of the Canadian Appalachian orogen in the provinces of Newfoundland, New Brunswick, and Nova Scotia. Plutonic rocks in this area form about one quarter of the exposed rocks, occurring in all tectonostratigraphic zones. Most of the granitic plutonism in the orogen occurred during the Middle Ordovician to Early Devonian periods (Whalen, 1993).

Biotite is in general the main mafic mineral of the granitic rocks of the Canadian Appalachians. The mineral also occurs in the gabbroic and dioritic rocks of the orogen. A textural study of biotite grains displayed in polished thin sections indicates a remarkable variation in size, pleochroic color and textural relationships with other minerals.

In general, three groups of Appalachian rocks that contain biotite are recognized: mafic plutonic rocks, foliated granites, and massive granites. In mafic plutonic rocks biotite

is found as small ragged subhedral crystals, clustered with amphibole and pyroxene and opaque oxides. In these clusters, the mineral clearly rims and replaces pyroxene or amphibole and originated most likely by late deuteric hydration of these primary ferromagnesian silicates (Fig. 1a). This type of biotite which is secondary in origin, also occurs as the sole mafic mineral in felsic rocks which exhibit granophyric or micrographic texture. In the latter rocks biotite is found as clusters of fine grains or occasionally along microfractures within the felsic minerals (Fig. 1b). The granophyric or micrographic texture with turbid alkaline feldspar are interpreted as the product of late stage hydrothermal or deuteric fluid activity.

Biotite from foliated granites is, in turn, subdivided into two subgroups, corresponding to metamorphosed granites and non-metamorphosed granites. In metamorphosed granites, biotite is fine-grained (<1 mm across) and interpreted as the product of metamorphic recrystallization. In non-metamorphosed foliated granites, biotite flakes reach up to 5 mm across and show microscopic evidence of deformation (e.g., undulatory extinction, bending) and are interpreted as primary and magmatic in nature. Biotite from massive granites is mainly subhedral and reaches up to 4 mm across with no evidence of strain. The locations and host rock descriptions of the Appalachian biotite specimens are given in Appendix I.

2.2 Biotite from the Hepburn and Bishop Intrusive Suites

The Hepburn and Bishop intrusive suites are petrologically, geochemically and geochronologically two distinct plutonic suites within the Early Proterozoic Wopmay orogen, Northwest Territories, (Lalonde 1989; Lalonde and Bernard 1993).

Biotite from Hepburn and Bishop granitic rocks is texturally similar to biotite from granitic rocks of the Canadian Appalachians. In older foliated granites of the Hepburn suite, subhedral flakes of biotite up to 2 mm across are interstitial to the large megacrysts of feldspar and define the planar metamorphic fabric of the rock. In contrast, biotite in the Bishop suite and the younger massive units of the Hepburn suites are subhedral to euhedral reaching up to 4 mm across and show no evidence of strain. In both the Hepburn and Bishop suites, biotite is interpreted as being primary (Lalonde and Bernard 1993).

2.3 Micas from Mont Saint-Hilaire

Mont Saint-Hilaire, an alkaline intrusion of Cretaceous age, occurs approximately 30 km east of Montréal in the province of Québec. The Mössbauer data included in this project were taken from 3 specimens of biotite (Bt-b, -c, and -d) and one specimen of annite (Ann) from this intrusion (Lalonde et al., 1996).

Specimens Bt-b and -c occur as small euhedral to subhedral black crystals 0.5 to 1.5 cm across in granular micaceous rock associated with nepheline syenite. Specimen Bt-d

consists of small euhedral to subhedral black crystals typically 1 to 4 mm across that occur in a dark, micaceous granular rock associated with potassium feldspar and albite. Specimen Ann occurs in nepheline syenite as euhedral to subhedral crystals up to 6 cm across and 2 cm in thickness.

3. Experimental Methods

Mineral analyses were obtained by wavelength-despersive X-ray spectroscopy using the JEOL 8900 Superprobe of the McGill University Microprobe Laboratory. Typical beam operating conditions were 15 kV and 20 nA.

Transmission ^{57}Fe Mössbauer spectra of the seventy one samples were obtained at room temperature (RT=22°C) using an ^{57}Co rhodium-matrix source on a velocity range of ±4 mm/s with a constant acceleration mode transducer. Data was collected on 1024 channels, which covered twice the Doppler velocity range of ± 4 mm/s. Calibrations of spectra were obtained with a ^{57}Fe-enriched iron foil, both before and after each experiment. All positions are reported with respect to this calibration spectrum, i.e., with respect to the centre shift (CS) of metallic α-Fe at RT. All spectra were folded to give a flat background (BG).

Absorbers were prepared as follows. Whole-rock samples were crushed using both jaw crusher and pulverizer. The crushed samples were then sieved to retain the size fraction between 45 and 60 mesh (350-250 μm). All samples were washed with water or acetone to remove dust. Magnetite was removed with a strong permanent magnet and the mafic and

felsic grains were separated using a Frantz magnetic separator. Purification in some cases was achieved using heavy liquids (methylene Iodide, density = 3.33 g/cm^3). Final shaking on a tilted paper sheet and hand-picking were performed for all samples until the concentrates appeared at least 99% pure under the binocular microscope. However, impurities such as minute crystals of apatite, zircon and interleaved muscovite or chlorite in some of the specimens could not be avoided.

The amount of sample used in the absorbers varied between 70 to 130 mg and was determined by the method of Rancourt et al. (1993) to maximize the Mössbauer signal to noise ratio. The above mentioned amount of granulated mica corresponding to the ideal (or near-ideal) absorber thickness was then mixed with petroleum jelly in a 5 mm thick and 0.5 inch inside diameter holder. This method has been shown to give random orientation of the mica grains in the absorbers and allows one to impose equality in area of corresponding high and low-energy lines in site-specific doublets (Rancourt, 1994b).

The new Voigt-based model of arbitrary-shape QSDs of Rancourt and Ping (1991) was used to fit the spectra. This model assumes that the true underlying QSD for a given valence state and coordination number, i.e., for a given generalized site, is composed of a given number N of Gaussian components as can be justified on statistical grounds. Unique distributions are thereby obtained (Rancourt and Ping, 1991).

None of the spectra were thickness corrected. Thickness correction can be performed by a method which takes into account the spectral distortions that occur because of finite absorber thickness (Rancourt et al., 1993; Ping and Rancourt 1992; Rancourt 1989).

Previous studies (Rancourt et al., 1993; Ping and Rancourt 1992; Rancourt et al., 1992) have established that thickness effects are minimal for these types of absorbers with intrinsically broad lines and that systematic trends in QSDs with composition are not severely altered by thickness effects.

Finally, Rancourt et al. (1994) have shown the extreme sensitivity of extracted QSD shapes on the assumed Lorentzian width Γ. To avoid these problems we have imposed frozen Γ values of $\Gamma = 0.2$ mm/s in all our fits. This allows the QSDs from different samples to be compared directly and is consistent with neglecting thickness effects since the true exact value is $\Gamma = 0.197$ mm/s.

4. Mineral Chemistry Results

The chemical composition of each of the seventy-one specimens studied is presented in Appendix II along with its corresponding structural formula based on 20 oxygen atoms. H_2O was calculated based on stoichiometry (i.e. OH+F+Cl=4). FeO and Fe_2O_3 contents of each specimen were determined by imposing the Fe^{3+}/Fe^{2+} ratios determined by Mössbauer spectroscopy, assuming equal Mössbauer recoilless fractions for ferric and ferrous iron and negligible thickness effects. Chemical composition and structural formula of the micas from the Bishop, Hepburn and Mont Saint-Hilaire intrusive suites are also included in Appendix II.

4.1 Biotite from the Canadian Appalachian Granites

The compositions of these micas show that they are biotites in the sense of Deer et al. (1962) (i.e., Fe/(Fe+Mg) ≥ 0.33), except for two samples of phlogopite (nb-91 and nb-78), and that they are trioctahedral (5.34 < O-site < 5.90). The compositions are shown in the annite - siderophyllite - phlogopite - eastonite quadrilateral, commonly adopted to illustrate the composition of trioctahedral micas based on Al_{total} and Fe/(Fe+Mg) (Speer 1984), in Figure 2.

The biotite from the Canadian Appalachian granites display considerable compositional variations. However it can be clearly discriminated based on its origins. As described above, biotite in Appalachian mafic rocks is secondary and its compositions is inherited from the Mg-rich and Al-poor clinopyroxene or amphibole that it replaces. In all secondary Appalachian biotite specimens, except for nb-91, Al^{3+} is insufficient to fill the tetrahedral sites and Ti is required to complete the tetrahedral sites, hence, there is no octahedral Al^{3+}. Ti is preferred over Fe^{3+} to complete the tetrahedral sites, as seen in the Mössbauer spectra which show an absence of a shoulder at ~ +0.4 mm/s that would be attributed to the high-energy line of the quadrupole doublet of tetrahedral Fe^{3+} (Rancourt et al., 1992). In the rest of the Appalachian biotite specimens (45 samples), no compositional distinction can be recognized between primary and metamorphic biotite. They are all aluminum-rich (except for three samples), i.e., there is sufficient Al^{3+} to completely fill the

available tetrahedral sites and there is an excess of Al^{3+} carried over to octahedral sites (0.17 - 0.84 a.p.f.u.).

4.2 Biotite from the Hepburn and Bishop Intrusive Suites

The Hepburn and Bishop micas represent two compositionally-distinct suites. The most pronounced compositional characteristics of biotite in the Hepburn and Bishop intrusive suites is the differences in Al_{total}, Fe/(Fe+Mg) and Fe^{3+}/Fe_{total} values (Lalonde and Bernard, 1993). Biotite from the Hepburn suite has Al_{total} contents that are considerably higher than those from the Bishop suite. Consequently, in all Hepburn biotite specimens, Al^{3+} completely fills the available tetrahedral sites and an excess of Al^{3+} is accommodated in octahedral sites. However, in some of the biotite specimens from the Bishop suite, there is insufficient Al^{3+} to fill the tetrahedral sites and Ti is required to complete the tetrahedral sites. Here again the Mössbauer spectra show no evidence of any tetrahedral Fe^{3+}. Biotite in the Hepburn suite is more Fe-rich than biotite in the Bishop suite and Fe^{3+}/ Fe_{total} ratios observed in the biotite of the Hepburn suite are lower than those from the Bishop suite.

4.3 Micas from Mont Saint-Hilaire

All of the specimens from Mont Saint-Hilaire are Fe-rich with Fe/(Fe+Mg) between 0.613 and 0.974. Another striking feature of these micas is their high Mn contents, ranging

from 0.232 to 0.752 a.p.f.u. It is worth mentioning that Mn rarely exceeds 0.2 a.p.f.u. in biotite (Deer et al., 1962). They are all sub-aluminous, i.e., Al_{total} is less than 2 a.p.f.u. (Fig. 2). Hence, their tetrahedral Al contents are not sufficient to fill the tetrahedral sites and Fe^{3+} completes the tetrahedral sites. Mössbauer spectra show the presence of tetrahedral Fe^{3+} in all of the specimens (Lalonde et al. 1996). This feature (sub-aluminosity) of micas from Mont Saint-Hilaire is in contrast with our biotite from the Appalachian and the Bishop and Hepburn intrusive suites.

5. Mössbauer Spectroscopy Results

A selection of raw folded RT spectra of representative biotite specimens are shown in Figure 3. The solid line running through the data points is the fit result. The other solid lines show the separate contributions from octahedral Fe^{2+} and octahedral Fe^{3+}. In fitting all spectra, the octahedral Fe^{2+} contributions were assumed to be sums of three Gaussian components. The octahedral Fe^{3+} contributions were assumed to be composed of one or two Gaussian components depending on the structures of their spectra. Fitting parameters for the best fits of all spectra are given in Appendix III. Note that the width of the high-energy line of the octahedral Fe^{2+} doublet contribution is decreasing gradually from Figure 3a to Figure 3d, whereas, the average Fe^{2+} quadrupole splitting (QS) is increasing. Such features of spectra are reflected in their QSDs as will be discussed below.

We characterize a given QSD by: the average QS, <QS>; the QS value at which the probability density is the largest, QS_{peak}; the value, $P(\Delta_{peak})$, of the probability density at QS_{peak}; $QS_{L\text{-}edge}$ and $QS_{H\text{-}edge}$, the values of QS at half maximum of $P(\Delta)$ at the low and high edges of the QSD; $W_{QSD} = QS_{H\text{-}edge} - QS_{L\text{-}edge}$, the width of the QSD at half maximum of $P(\Delta)$; and the value of the standard deviation, σ_{QSD}, of the QSD. In addition, since our QSD extraction method (Rancourt and Ping, 1991) allows negative values of QS (for mathematical convenience) whereas only magnitudes of QS can be resolved physically in such analyses, care must be taken to properly define the standard deviation as:

$$\sigma^2_{QSD} = \int_{-\infty}^{+\infty} (|\Delta| - \langle |\Delta| \rangle)^2 P(\Delta) d\Delta \qquad (1)$$

$S_k = QS_{peak} - \langle QS \rangle$ is used as a measure of the skewness of the QSD: symmetric distributions have $S_k = 0$ and highly skewed distributions have large (positive or negative) values of S_k. We have also considered the true dimensionless statistical skewness, S_t, defined as:

$$S_t = \frac{1}{\sigma^3_{QSD}} \int_{-\infty}^{+\infty} (|\Delta| - \langle |\Delta| \rangle)^3 P(\Delta) d\Delta \qquad (2)$$

where $\langle |\Delta| \rangle = \langle QS \rangle$ is the average magnitude of the QS.

5.1 Octahedral - Fe^{2+} Quadrupole Splitting Distributions

We first explore in detail the relationships among the QSD parameters before examining possible relationships between chemical and Mössbauer parameters. Table 1

gives the characteristic parameters for the Fe^{2+} QSDs of all the samples. The $QS_{L\text{-}edge}$ versus $QS_{H\text{-}edge}$ for all the samples is shown in Figure 4 on the scale of equal range. This plot clearly shows that the $QS_{H\text{-}edge}$ is relatively insensitive to sample to sample variation, whereas $QS_{L\text{-}edge}$ has large sample to sample variations. This suggests that $QS_{L\text{-}edge}$ should be highly correlated with both W_{QSD} and $P(\Delta_{peak})$, as seen in Figures 5(a) and 5(b). Note that a width parameter such as W_{QSD} or σ_{QSD} should be inversely correlated to $P(\Delta_{peak})$ because, by definition, the probability density distribution, $P(\Delta)$, that is, the QSD, is normalized to 1. On the other hand, no correlation is found between $QS_{H\text{-}edge}$ and W_{QSD} or $P(\Delta_{peak})$.

We observe different characteristics in the behaviors of <QS> and QS_{peak}. <QS> correlates with $QS_{L\text{-}edge}$ (Fig. 6) and, hence, with the other parameters W_{QSD}, $P(\Delta_{peak})$ and S_k (Figs. 7a, b and c), whereas QS_{peak} does not correlate with any of these parameters.

The Mont Saint Hilaire micas do not follow the trends in most of the plots described above due to their distinct QSD characteristics.

We also observed that the standard deviation values for the majority of samples are almost the same (Fig. 8). Higher values ($\sigma_{QSD} > 0.4$ mm/s) of σ_{QSD} for some of the samples, mainly Hepburn and Bishop biotites, are due to relatively long flat low-QS tail of their QSDs which are probably due to thickness effects.

The measured characteristic features of the Fe^{2+} QSDs (Figs. 4-7) and the QSDs themselves (Fig. 9) suggest that the QSDs of all natural biotites and phlogopites fall within the continuum of QSD shapes that we have observed, ranging from skewed and broad distributions with lower $QS_{L\text{-}edge}$ and <QS> values to the least skewed and most narrow

distributions with highest $QS_{L\text{-}edge}$ and <QS> values. Figure 9 illustrates the continuous evolution of QSD shapes between the two extreme shapes that we have observed, using typical intermediate-shape QSDs. We believe we have thereby established the archetypal Fe^{2+} QSD shapes for natural biotites.

To a good first approximation, the continuum of QSD shapes is such that to a given <QS> corresponds: a given $QS_{L\text{-}edge}$ (Fig. 6), a given W_{QSD} (Fig. 7a), a given $P(QS_{peak})$ (Fig. 7b), and a given S_k (Fig. 7c), where the σ_{QSD} remains essentially constant (Fig. 8). This suggests that any one of these parameters (<QS>, $QS_{L\text{-}edge}$, W_{QSD}, $P(QS_{peak})$ or S_K) can be used as a single valid measure of the particular QSD of a given biotite sample. In other words, to the extent that the correlations illustrated in Figs. 6-7 are strong, the information content of a given QSD can be summarized in a single parameter.

Due to their unusual compositions, MSH micas have QSDs which are distinct from the rest of the micas and their QSDs are shown separately in Figure 10. One of the characteristic features of the MSH QSDs is their lower values of $QS_{H\text{-}edge}$ with respect to others.

5.2 Ferric Iron Contribution

Tetrahedral Fe^{3+} is seen only in Mont Saint-Hilaire micas where it has CS = 0.15 - 0.20 mm/s and <QS> = 0.34 - 0.47 mm/s (Lalonde et al. 1996). This assignment is consistent with the known tetrahedral Fe^{3+} parameters in true trioctahedral micas (Rancourt et

al. 1992; Rancourt 1993). The other Fe^{3+} contributions which are seen in all of our micas have CSs in the range of 0.24 - 0.53 mm/s and <QS> = 0.70 -1.10 mm/s that are consistent with those of octahedral Fe^{3+}.

Figure 11 shows a selection of typical Fe^{3+} QSDs of our trioctahedral micas. In Figure 11(a) the Fe^{3+} QSD is modeled by a single Gaussian component, whereas in Figure 11(b) the Fe^{3+} QSD has a structure that is modeled by two Gaussian components. The need for a second component arises because the particular shape of the Fe^{3+} QSD can not be adequately represented by only one component. Fe^{3+} QSDs in the latter case are characterized by a relatively narrow peak at QS ≈ 0.7 mm/s and a long high-QS tail extending to above 2 mm/s, whereas, in the former case, the Fe^{3+} QSDs have a broad shape with almost the same range of QSs at high values.

Defining the precise octahedral Fe^{3+} QSD shape needs further work due to unavoidable problems with both neighboring Fe^{2+} lines that have significant overlap and texture effects, which is beyond the scope of the present paper. Nevertheless, it appears that shapes such as the typical ones represented in Figure 11(b) are close to the true Fe^{3+} QSD shapes in biotites.

Finally, we observed the correlation between the measured Fe^{3+} QSD parameters and chemical and calculated physical parameters (defined below) is minimal or absent for our micas.

6. Comparison between Mineral Chemistry and Mössbauer Parameters

On the basis of the stoichiometric formulae (Appendix II) and ionic radii (Hazen and Burnham 1973; Shannon 1976), we calculated the average octahedral cation radius, [R], for each sample. [R] characterizes the overall crystal chemistry of the octahedral sheet and is relevent in terms of tetrahedral sheet to octahedral sheet lateral mismatch accommodation. In Figure 12, we illustrate the changes in <QS> as a function of [R] for all samples. The <QS> is seen to decrease with increasing [R], which is consistent with the results obtained by Redhammer (1998) for synthetic phlogopite-biotite-annite solid solutions. The high values of [R] for the MSH micas are due to the high Mn-content in the octahedral sheet.

The average octahedral cation radius, [R], is also a measure of the occupancies of smaller octahedral cations present in the octahedral sheet. We observed that among the smaller cations the individual fractions of Ti or Fe^{3+} in the octahedral sheet do not correlate with <QS> values, whereas Al^{3+} does, implying that the correlation of [R] with <QS> might be due to the fraction of octahedral Al^{3+} cations. As is shown in Figure 13, the Al_{total} of our samples correlates with <QS>. Al_{total} was used because octahedral Al^{3+} was absent in some of these samples. In addition, tetrahedral Al is also correlated to <QS>. There are also correlations between <QS> and some other chemical parameters [e.g. Fe+Mg, Fe+Mg+Mn, $(Al^{3+} + Fe^{3+})/(Fe^{2+} + Mg + Mn + Fe^{3+} + Al)$ and $(Al+Ti+Fe^{3+})/\Sigma$ oct. cations]. However, all of the latter correlations can be related to Al-content.

Recently, in their studies on synthetic iron-bearing trioctahedral micas, Ferrow (1987) and Redhammer (1995) examined the effect of the degree of calculated structural misfit (or octahedral-tetrahedral inter-sheet strain) on the quadrupole splitting of iron in different coordination and oxidation states. These studies show that there is a positive correlation between tetrahedral rotation angle α and <QS>. In the absence of lattice parameter data for our samples, we calculated theoretical tetrahedral rotation angles (α) and octahedral flattening angles (ψ) based on stoichiometry, and bond lengths (Weiss et al. 1992) using equations reported by Mercier et al. (1996; 1998). The calculated values of tetrahedral rotation angle α are higher than those in the reported range (0 - 9°) for synthetic annite-phlogopite (Redhammer 1995) and natural biotite (5.5 - 7.5°) (Brigatti and Davoli 1990), however, octahedral flattening ψ values are consistent with the commonly observed values ($59 \pm 1°$) for trioctahedral micas.

Figure 14 illustrates the positive correlation between our calculated tetrahedral rotation angle α and <QS>, which is consistent with results obtained by Ferrow (1987) and Redhammer (1995) for Fe-bearing trioctahedral micas. Similarly, calculated octahedral flattening ψ angles also correlate with <QS> (Fig. 15). As can be seen in Figures 14 and 15, Mont Saint-Hilaire micas have lower values of α and ψ, which can be related to their higher values of Mn^{2+} that cause expansions of the octahedral sheets which in turn compel the tetrahedral sheets to follow by taking in Fe^{3+}, the largest common cation in tetrahedral sites (Lalonde et al. 1996). A closer look at the trends in Figures 14 and 15 reveals their similarity to the Al - <QS> trend (Fig. 13), suggesting a dominant role of Al-content in the

determination of the α and ψ angles in our samples. That is, increasing aluminum in the octahedral sheet is expected to decrease the a and b cell parameters of the crystal, thereby producing larger tetrahedral rotation and octahedral flattening angles. This is also consistent with the result obtained by Redhammer (1998), indicating that tetrahedral rotation angles (α) and octahedral flattening angles (ψ) increase with increasing octahedral Al-content.

One way to explore the effect of a given chemical parameter or cation on the Mössbauer parameters of micas is to study synthetic micas with exactly defined compositions. For instance, in their study on the oxidation of synthetic trioctahedral micas, Christie et al. (1993) found a systematic trend in the evolution of the QSDs of annite-oxyannite samples. Similarly, the Fe^{2+} QSD and its characteristics from synthetic phlogopite-annite series display gradual trends with changing Fe/(Fe+Mg). In this series a definite trend is seen from broad distributions centered on small QS values to narrow distributions centered on large QS values as we go from annite toward phlogopite (Rancourt et al. 1994; Mercier et al. 1997; Redhammer 1998).

Although this is the case in synthetic micas, we found the two geologically and mineralogically important parameters, Fe^{3+}/Fe and Fe/(Fe+Mg), do not correlate with the Fe^{2+} QSD and its characteristics. In general, except for the correlations described above, we observed weak or absent correlations between the rest of the chemical parameters and the Fe^{2+} QSDs and their characteristics (<QS>, QS_{peak}, W_{QSD}, $QS_{H\text{-}edge}$, $QS_{L\text{-}edge}$ S_k and σ_{QSD}).

7. Relationship between Whole-rock Chemistry and Mössbauer Parameters

As described in earlier sections, our trioctahedral micas come from a wide variety of rock types. Due to their complex structure, micas can accommodate most of the common elements present in the rock, i.e., they reflect to some extent the composition of their host rocks. Also, we have shown above that the composition of biotite has direct effect on its QSD parameters. Now the question that might be raised is: does the host rock composition have a relation with the biotite QSD parameters or the QSD itself?

Our examination shows that chemical parameters of host rocks do not correlate with systematic variations of the QSD parameters of the biotite. In addition, it seems that other characteristics of the host rocks do not show relations with the QSDs. For instance, despite the differences in mineralogical and petrological characteristics of the Hepburn and the Bishop suites (Lalonde 1989; Lalonde and Bernard 1993), no significant systematic differences can be detected in the Fe^{2+} QSDs of their biotite. Similarly, we did not observe any systematic differences between the QSDs of biotite from metamorphosed granites and those from unmetamorphosed granites in the Appalachians.

Al-deficient biotite, being secondary in origin, from mafic plutonic rocks or deuterically altered felsic rocks is characterized by broad QSDs, however, such a QSD is not restricted to biotite from these types of rocks. There is biotite (being Al-deficient) from granitic rocks that has broad QSDs.

We also observed that QSDs of Appalachian biotite are indistinguishable from Hepburn and Bishop ones, although the geochemical and petrological characteristics of each suite of rocks are different from each other. Finally only small group of samples from the Mont Saint-Hilaire alkaline intrusion appear to be distinctive due to their distinct composition of mica and host rock with respect to the rest of our samples.

8. Discussion

According to Rancourt et al. (1994), each QS value in a QSD corresponds to a particular " local distortion environment " (LDE) that is populated by Fe^{2+} in an amount proportional to P(QS). In fact, there is not a unique one to one correspondance between a LDE and a particular QS value. Several different LDEs can lead to the same QS value. So each QS value corresponds, in general, to a set of LDEs, each LDE in the set having its own Fe^{2+} population, the sum of which is proportional to P(QS).

However, before drawing any conclusions from the results, we should mention that there is almost complete absence of theoretical calculations that link particular LDEs to their corresponding QS values. This major factor prevents us from achieving a detailed interpretation of the Fe^{2+} QSDs.

As shown above, the QSDs of all natural biotites fall within a continuum of QSD shapes, ranging from broad distributions with lower $QS_{L\text{-}edge}$ and <QS> values to the most narrow distributions with highest $QS_{L\text{-}edge}$ and <QS> values.

The next questions that arise are: why does natural biotite have these types of QSDs and what do these QSDs tell us about the characteristics of local distortion and local chemical environments in biotite? Does a single chemical parameter, such as Fe/(Fe+Mg), determine the QSD or which combination of crystal chemical parameters determines the QSD?

Definitive answers to the first question must await detailed electronic structure calculations, however, the QSD shapes themselves offer partial answers. For example, the stunning fact that there is a well defined $QS_{H\text{-}edge} = 2.80 \pm 0.05$ mm/s for all biotite specimens whereas $QS_{L\text{-}edge}$ has a broad range of ~ 2.0 - 2.6 mm/s (Fig. 4) suggests that $QS_{H\text{-}edge}$ corresponds to a maximum distortion environment that can occur in biotite. Also, the relation between W_{QSD} and $QS_{L\text{-}edge}$ (Fig. 5a) shows that larger widths of the QSDs arise from including small-QS contributions without going beyond the $QS_{H\text{-}edge}$ upper bound of ~ 2.85 mm/s.

As demonstrated above, Al_{total} is the strongest chemical parameter that correlates positively with <QS> which may imply that Al-content is the most important factor for the variations of the local environments in the octahedral sheet. This suggests that the average population of octahedral LDEs may have Al^{3+} in their nearest neighbour octahedral and tetrahedral sites. For instance, there is some distortion of the tetrahedral sheet to accommodate different sized cations (Si^{4+}, Al^{3+}, Ti^{4+}, and Fe^{3+}). These distortions are transmitted to the octahedral sheet through the shared apex oxygens. Among the tetrahedral cations, Al has a weak positive correlation with <QS> (Fig. 16), indicating its possible role in determining octahedral LDEs.

In connection with the Al-content and <QS> correlation, we collected published data regarding Mössbauer spectroscopy of natural biotite (Annersten 1974; Annersten 1975; Bancroft and Brown 1975; Bowen et al. 1969; Dyar and Burns 1986; Dyar 1987; Dyar 1990; Haggstrom et al. 1969; Hogg and Meads 1970; Hogg 1975; Ivanitskiy et al. 1977; Ivanitskiy et al. 1975a; Ivanitskiy et al. 1975b; Manapov and Sitdikov 1974; Rice and Williams 1969; Sanz et al. 1978 and Smith et al. 1980). Having calculated average quadrupole spillitings, we plotted these versus their Al_{total} contents (Fig. 17). As can be seen, no correlation can be detected, however, if plotted together with our samples, a positive weak correlation with <QS> is noted (Fig. 18). This may suggest that the strongest single chemical indicator of <QS> in natural biotite is Al-content, which is related to several crystal chemical features.

As explained above, QSDs are related to probe local environment populations, that is, to populations of crystallographic, chemical or local distortion environments and are interpreted as LDE population distributions. In this way, we may suggest that since the QSD of our secondary biotite specimens (except for nb-91, an Al-rich phlogopite) have broad distributions, they contain a wide variety of populated LDEs. These specimens, in addition to compositional effects, should probably have more defects and dislocations because they formed by the low temperature deuteric replacement of clinopyroxene or amphibole. Going from secondary to primary or metamorphic biotites, the QSDs become progressively narrower and less skewed, suggesting a decrease in the variety of local environments. The changes in the <QS> value, at which the average population LDE occurs, suggest that the degree of distortion gradually changes and might be due to progressive octahedral flattening

that occurs in going from secondary to primary biotite. The main factors related to sample composition that correlate with the distribution of LDEs seem to be the total number of neighbouring small octahedral Al and the number of adjacent tetrahedral sites that are occupied by Al.

9. Conclusions

Mössbauer spectra of a large number of natural biotite specimens was described in terms of QSDs which are related to population distributions of local distortion environments (LDEs). We also established the possible range of Fe^{2+} QSDs in biotite and the key limiting characteristics of the QSDs in all compositional variations of biotite. The measured characteristic features of Fe^{2+} QSDs and the QSDs themselves suggest that the QSDs of natural biotite and phlogopite fall within the continuum of QSD shapes.

We found that Fe/(Fe+Mg) and Fe^{3+}/Fe, which are the key crystal chemical parameters in the phlogopite-biotite-annite solid solution, do not correlate with any of the QSD features of natural biotite, whereas Al_{total}, which is related to several crystal chemical features, does. More detailed interpretation of the QSD shapes is primarily limited by the lack of electronic structure calculations linking LDEs to QS values.

Table 1 Fe^{2+} QSD characteristic parameters for all of our mica spectra.

Appalachians

sample	<QS>	QS_{peak}	$QS_{L\ edge}$	$QS_{H\ edge}$	S_K	S_t	σ_Δ	$P(\Delta_{peak})$	W_{QSD}
nb-214	2.5458	2.6769	2.5282	2.7918	0.1311	-0.8860	0.3139	2.2416	0.2636
pr5b	2.5174	2.6678	2.4963	2.8232	0.1504	-0.6893	0.3463	1.8622	0.3269
nb-146	2.4949	2.6718	2.4778	2.7743	0.1770	-0.8570	0.3393	2.1668	0.2966
nb-145	2.4728	2.6441	2.4687	2.7663	0.1713	-0.8177	0.3286	2.0385	0.2975
nb-30	2.4786	2.6942	2.4052	2.7837	0.2156	-0.7298	0.3561	1.9018	0.3786
br4	2.4515	2.6281	2.3932	2.7893	0.1766	-0.7167	0.3455	1.7299	0.3961
nf-28	2.4809	2.6103	2.3918	2.8187	0.1294	-0.7565	0.3269	1.7111	0.4268
ns-4	2.5127	2.6370	2.3867	2.8272	0.1243	-0.7031	0.3300	1.6680	0.4405
nb-122	2.4710	2.6531	2.3857	2.8097	0.1821	-0.7844	0.3421	1.7563	0.4240
nb-136	2.3992	2.6126	2.3732	2.7929	0.2134	-1.2512	0.4600	1.5781	0.4197
nb-162	2.4783	2.6768	2.3685	2.8007	0.1985	-0.6922	0.3312	1.8171	0.4322
nb-17	2.4519	2.6750	2.3593	2.7759	0.2231	-0.7189	0.3470	1.8519	0.4166
ed3	2.4527	2.6315	2.3538	2.7944	0.1788	-0.6866	0.3452	1.6788	0.4405
nb-173	2.4371	2.6072	2.3373	2.8231	0.1701	-0.7953	0.3359	1.5486	0.4859
ns-3	2.4360	2.6484	2.3292	2.7801	0.2124	-0.6382	0.3449	1.7267	0.4509
306-2	2.4399	2.6470	2.3269	2.7826	0.2071	-0.6700	0.3347	1.7392	0.4557
nb-8	2.4406	2.6616	2.3217	2.7980	0.2210	-0.6811	0.3557	1.6572	0.4763
nf-1	2.4289	2.5962	2.3176	2.8114	0.1673	-0.4737	0.3668	1.5031	0.4939
nb-29	2.4250	2.6394	2.3153	2.7671	0.2144	-0.7254	0.3455	1.7629	0.4518
nf-102	2.4390	2.6682	2.3138	2.7927	0.2293	-0.7190	0.3209	1.7573	0.4789
nb-227	2.4501	2.6432	2.3104	2.7901	0.1931	-0.6118	0.3599	1.6800	0.4797
nb-159	2.4567	2.6648	2.3101	2.8135	0.2081	-0.6517	0.3528	1.6371	0.5034
nb-38	2.4590	2.6509	2.3100	2.8046	0.1919	-0.6762	0.3595	1.7093	0.4946
nb-111	2.3644	2.5868	2.3081	2.7751	0.2224	-1.4158	0.4990	1.5189	0.4671
nb-169	2.4128	2.6313	2.3042	2.7503	0.2185	-0.6732	0.3432	1.7779	0.4461
slp	2.4207	2.5877	2.3007	2.7997	0.1670	-0.6417	0.3398	1.5213	0.4990
nf-23	2.4450	2.6732	2.2954	2.8135	0.2282	-0.6818	0.3623	1.5965	0.5181
nb-161	2.4333	2.6502	2.2926	2.7837	0.2170	-0.6669	0.3552	1.6595	0.4911
nf-106	2.4442	2.6546	2.2926	2.7946	0.2104	-0.7511	0.3395	1.6802	0.5020
nf-119	2.4514	2.5957	2.2872	2.8261	0.1443	-0.6417	0.3680	1.4471	0.5389
snf-19	2.4450	2.6716	2.2871	2.8029	0.2267	-0.7056	0.3472	1.6470	0.5158
nf-36	2.4426	2.6659	2.2720	2.8143	0.2233	-0.6560	0.3573	1.5514	0.5423
nb-13	2.4082	2.6282	2.2668	2.7731	0.2200	-0.6355	0.3635	1.5876	0.5063
snf-1	2.4228	2.6945	2.2623	2.8062	0.2717	-0.6316	0.3451	1.5332	0.5439
nb-125	2.4128	2.6553	2.2613	2.7708	0.2425	-0.7083	0.3513	1.6514	0.5094
pc2b	2.4041	2.6365	2.2596	2.7660	0.2324	-0.6109	0.3397	1.6319	0.5064
snf-2	2.4099	2.6177	2.2564	2.7731	0.2078	-0.8089	0.3254	1.6489	0.5168
nf-166	2.4222	2.6516	2.2545	2.7915	0.2294	-0.6728	0.3574	1.5715	0.5370
nwad	2.3947	2.6330	2.2509	2.7588	0.2383	-0.5979	0.3462	1.6354	0.5079
nb-166	2.4455	2.6064	2.2505	2.8058	0.1609	-0.5893	0.3473	1.4544	0.5553
nf-83	2.4243	2.6429	2.2503	2.7897	0.2186	-0.7055	0.3515	1.6169	0.5394
nb-91*	2.4267	2.6196	2.2450	2.7563	0.1929	-0.5984	0.3211	1.6958	0.5113
103b2	2.3903	2.6348	2.2433	2.7631	0.2445	-0.6403	0.3426	1.6034	0.5198
nf-29	2.4196	2.6174	2.2430	2.7731	0.1978	-0.6515	0.3489	1.6459	0.5300
nf-8	2.4234	2.6614	2.2405	2.7992	0.2380	-0.6000	0.3395	1.5594	0.5587
nb-89*	2.3630	2.6743	2.2299	2.7334	0.3113	-0.6073	0.3531	1.7369	0.5035
snf-25	2.4148	2.6771	2.2291	2.8014	0.2623	-0.5887	0.3417	1.5519	0.5723
nb-239*	2.3735	2.6695	2.1953	2.7749	0.2961	-0.6069	0.3593	1.5153	0.5795
snf-10	2.3579	2.6399	2.1490	2.7545	0.2820	-0.6248	0.3409	1.4776	0.6055
nb-92*	2.3517	2.5086	2.1018	2.7678	0.1569	-0.5097	0.3673	1.3043	0.6660

Table 1(Continued)

sample	<QS>	QS_{peak}	$QS_{L\ edge}$	$QS_{H\ edge}$	S_K	S_t	σ_Δ	P (Δ_{peak})	W_{QSD}
nb-99*	2.3324	2.6609	2.0973	2.7462	0.3285	-0.4556	0.3529	1.3763	0.6490
nb-88*	2.3378	2.6512	2.1235	2.7417	0.3134	-0.6081	0.3588	1.4147	0.6182
nb-58*	2.3291	2.6773	2.0737	2.7735	0.3482	-0.5391	0.3665	1.2834	0.6998
nb-78*	2.3095	2.5082	2.0660	2.7574	0.1987	-1.3824	0.4349	1.2893	0.6914
Hepburn and Bishop									
HL125	2.4645	2.6599	2.4278	2.7839	0.1954	-0.8231	0.3226	1.9602	0.3561
HL200	2.4235	2.6421	2.3610	2.8437	0.2186	-1.1070	0.5187	1.4561	0.4828
HL204	2.4448	2.6241	2.3149	2.8483	0.1793	-0.8582	0.4305	1.4035	0.5334
HL14	2.4120	2.5866	2.2572	2.8121	0.1747	-0.2950	0.3832	1.3887	0.5549
HL341	2.4206	2.5853	2.2881	2.8101	0.1647	-0.5468	0.4095	1.4185	0.5220
HS29	2.3712	2.5772	2.2168	2.8089	0.2060	-0.6796	0.4857	1.3121	0.5920
BL313	2.3872	2.6119	2.3384	2.8020	0.2247	-1.0911	0.4479	1.4895	0.4636
BL315	2.4252	2.6103	2.3011	2.8307	0.1851	-1.0695	0.4249	1.4345	0.5295
BL531	2.3792	2.5916	2.2840	2.7935	0.2123	-1.1133	0.4319	1.4588	0.5095
BZ53	2.3977	2.6596	2.2372	2.7791	0.2619	-0.6209	0.3533	1.5443	0.5419
BL255	2.3089	2.6007	2.0951	2.8273	0.2919	-0.9558	0.5689	1.1835	0.7322
BL246	2.3595	2.5462	2.1321	2.7901	0.1867	-0.9082	0.4051	1.3071	0.6580
HL243	2.4123	2.6866	2.2431	2.8022	0.2743	-0.6154	0.3694	1.4949	0.5591
Mont Saint-Hilaire									
Bt-b	2.3448	2.6370	2.5311	2.7215	0.2921	-0.8384	0.3231	2.2079	0.1904
Bt-c	2.3416	2.6168	2.4523	2.7292	0.2751	-1.4014	0.3823	2.1840	0.2769
Bt-d	2.4099	2.6127	2.4785	2.7231	0.2028	-1.3329	0.3239	2.0376	0.2446
Ann	2.3399	2.6035	2.4947	2.6937	0.2637	-1.6679	0.3957	2.4164	0.1990

* secondary biotite

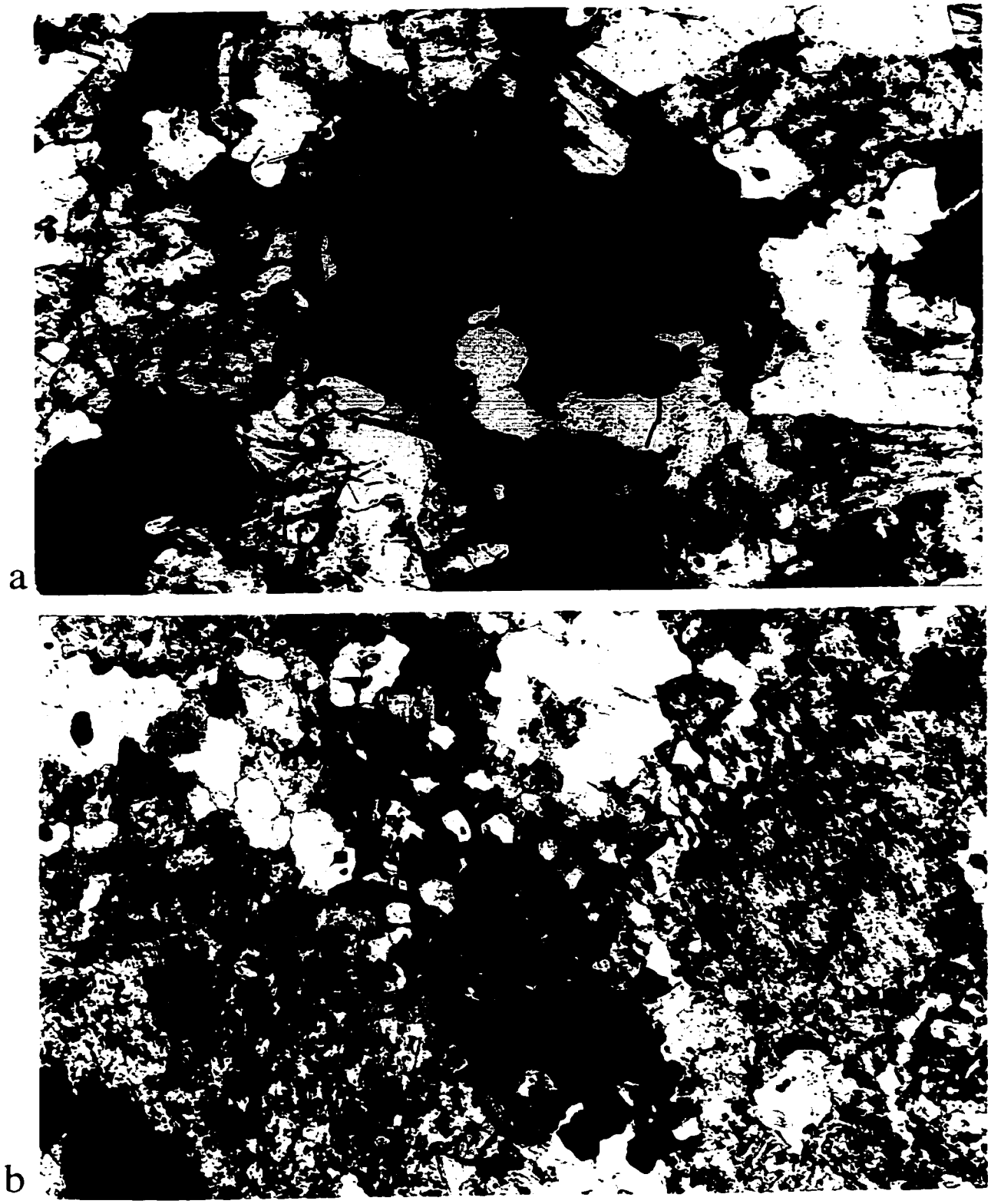

Figure 1 Photomicrographs of biotite: (a) in gabbro, where it replaces hornblende and, (b) in granophyric textured granite, as clusters of fine grains. Plane-polarized light; field of view: 2 mm.

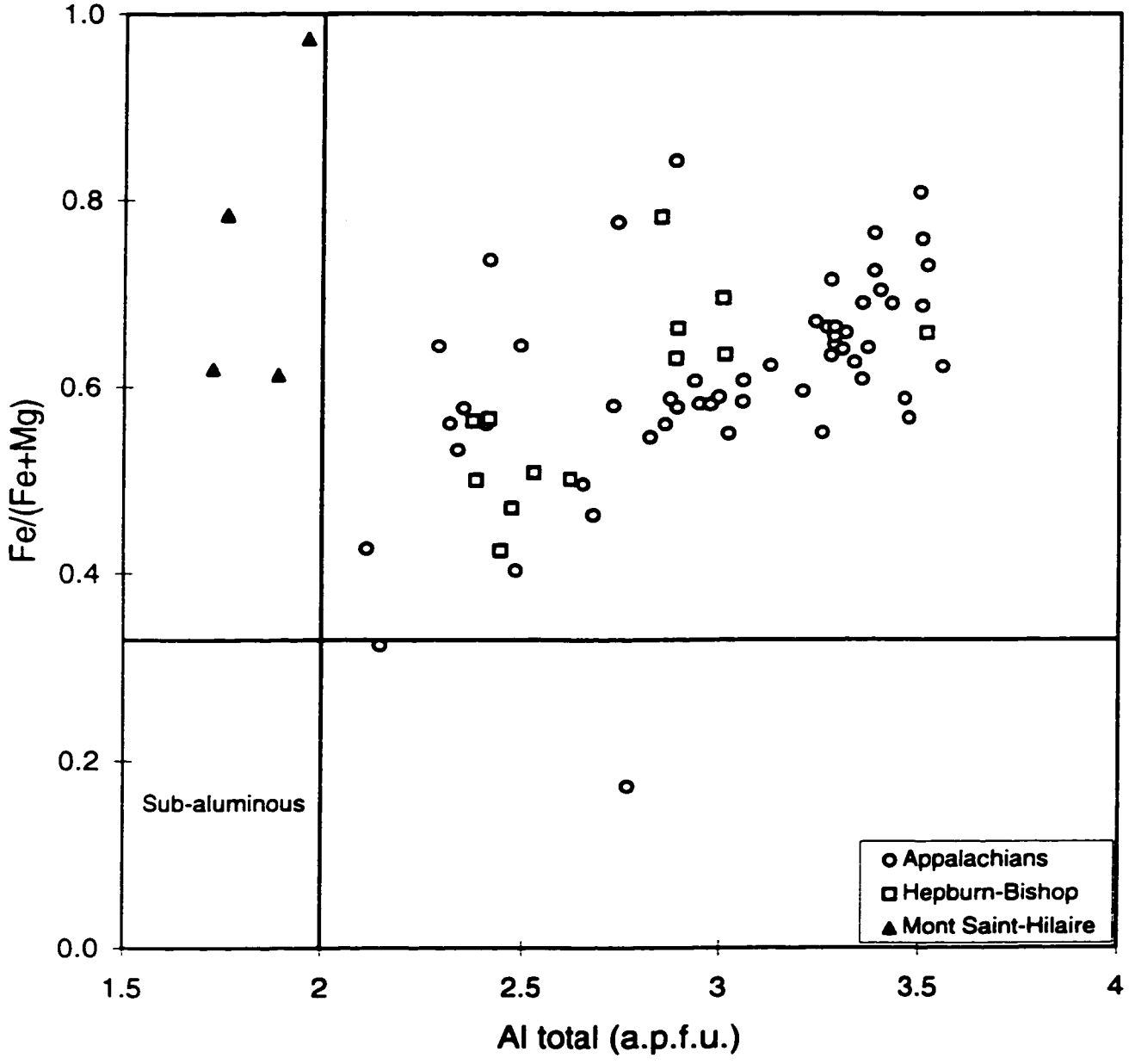

Figure 2 Composition of biotite from Appalachian, Hepburn-Bishop granitic suites and Mont Saint Hilaire alkaline suite in the annite-eastonite-phlogopite-siderophyllite diagram.

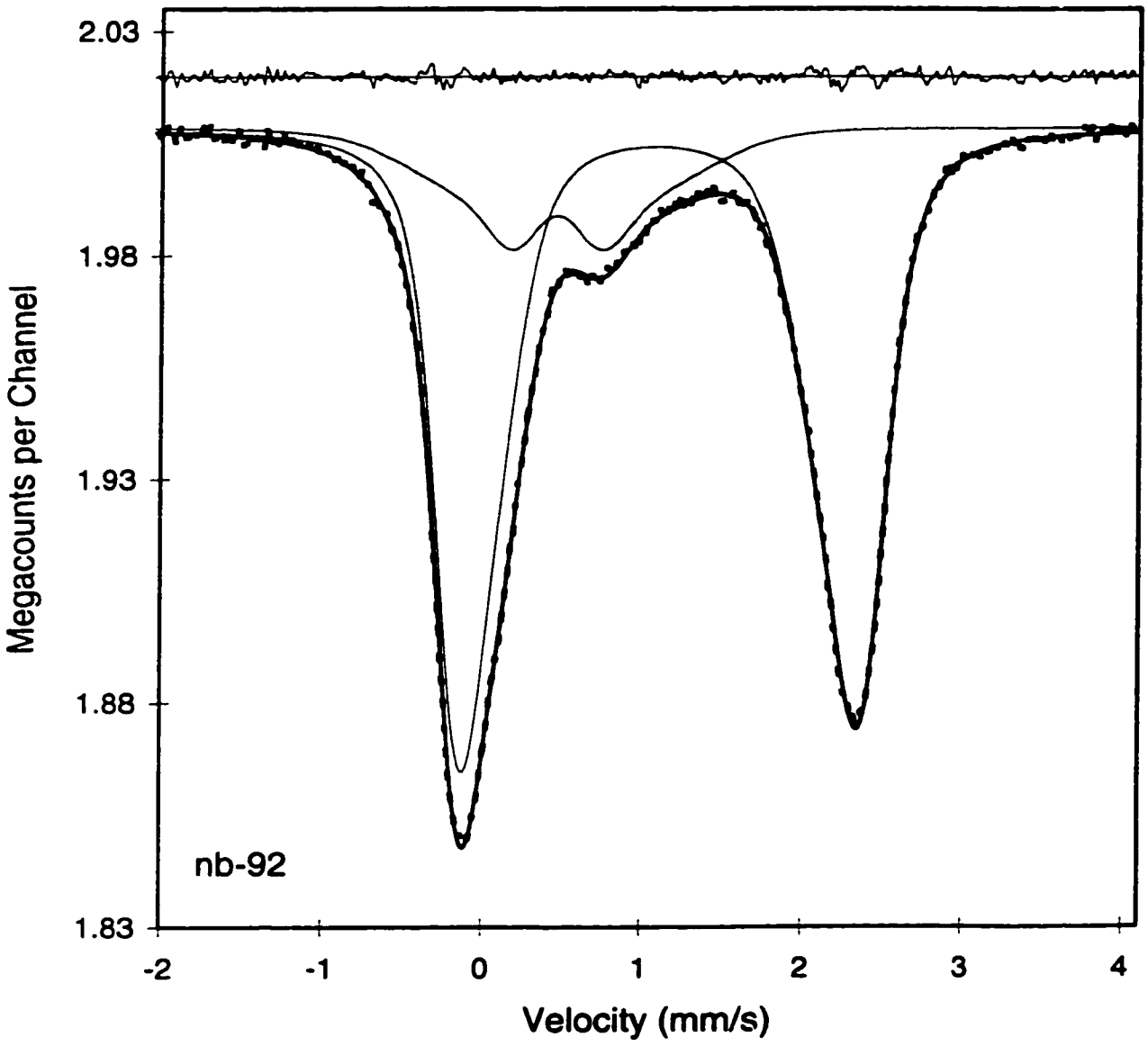

Figure 3(a-d) A selection of raw folded room temperature ^{57}Fe Mössbauer spectra of biotite. The solid line running through the data points is the fit results. The other solid lines show the separate contributions from octahedral Fe^{2+} and octahedral Fe^{3+}.

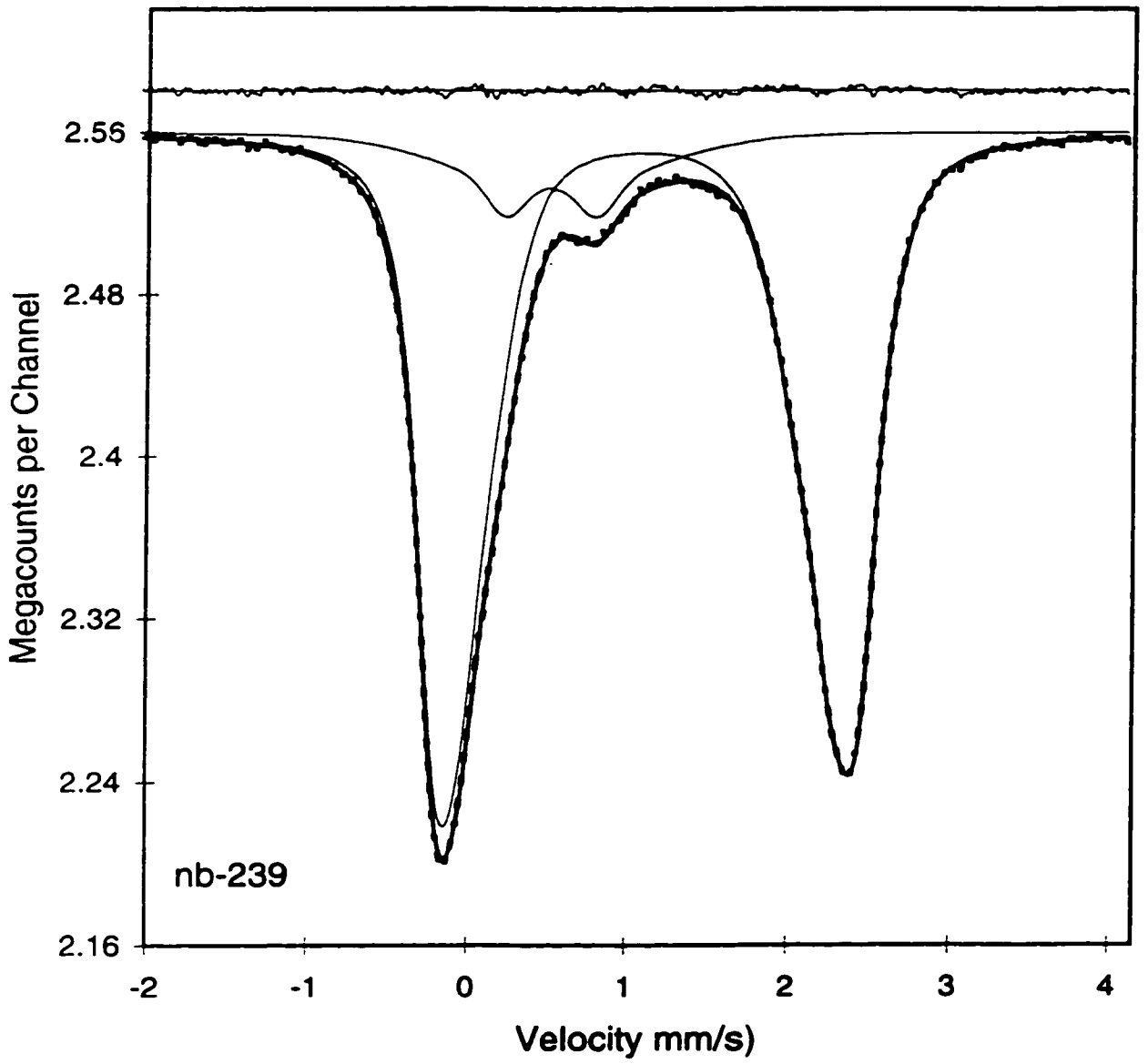
2.56
2.48
2.4
2.32
2.24
2.16
Megacounts per Channel
nb-239
-2
-1
0
1
2
3
4
Velocity mm/s)

Figure 3(b)

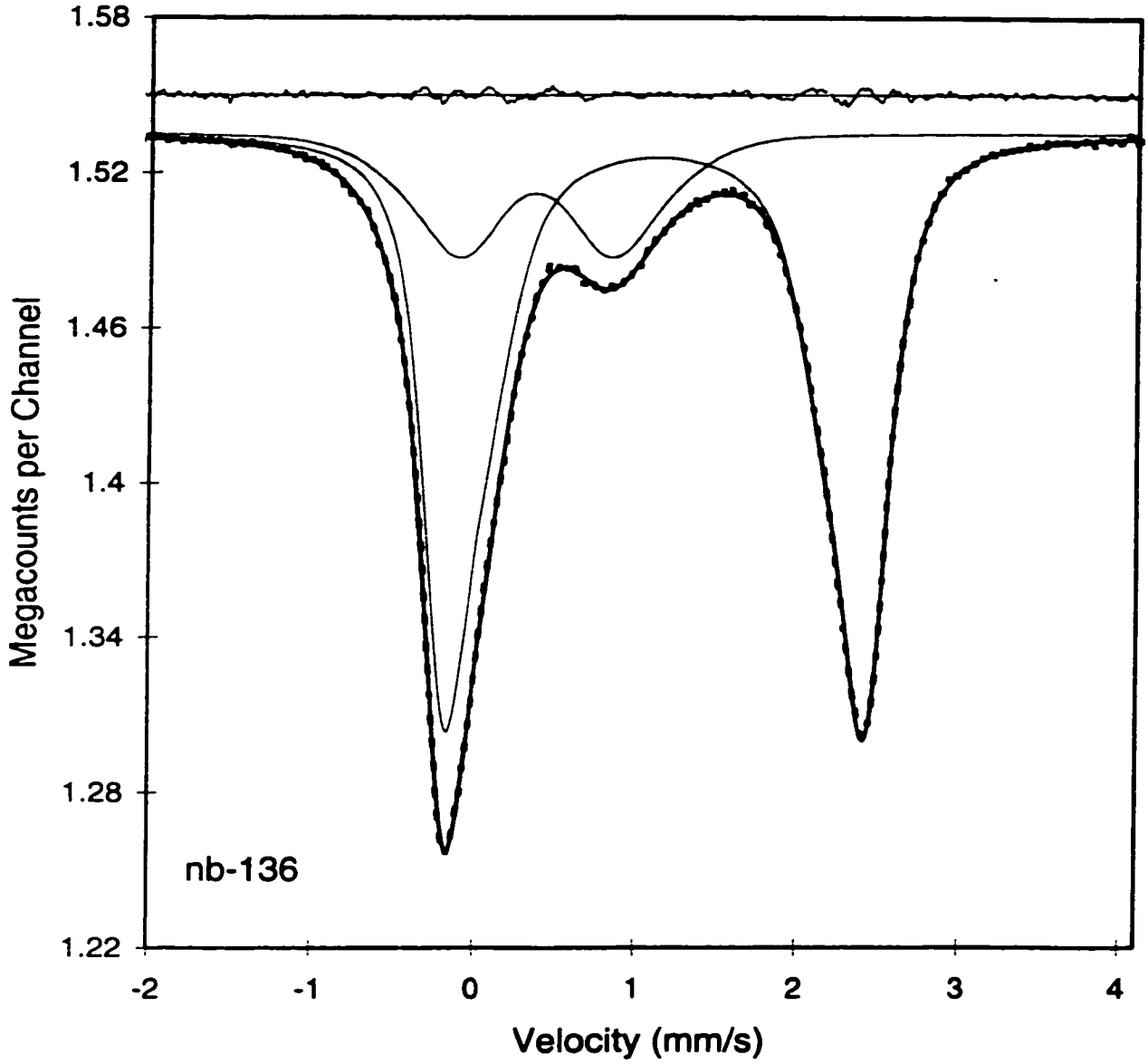
1.58
1.52
1.46
1.4
1.34
1.28
1.22
Megacounts per Channel
nb-136
-2
-1
0
1
2
3
4
Velocity (mm/s)

Figure 3(c)

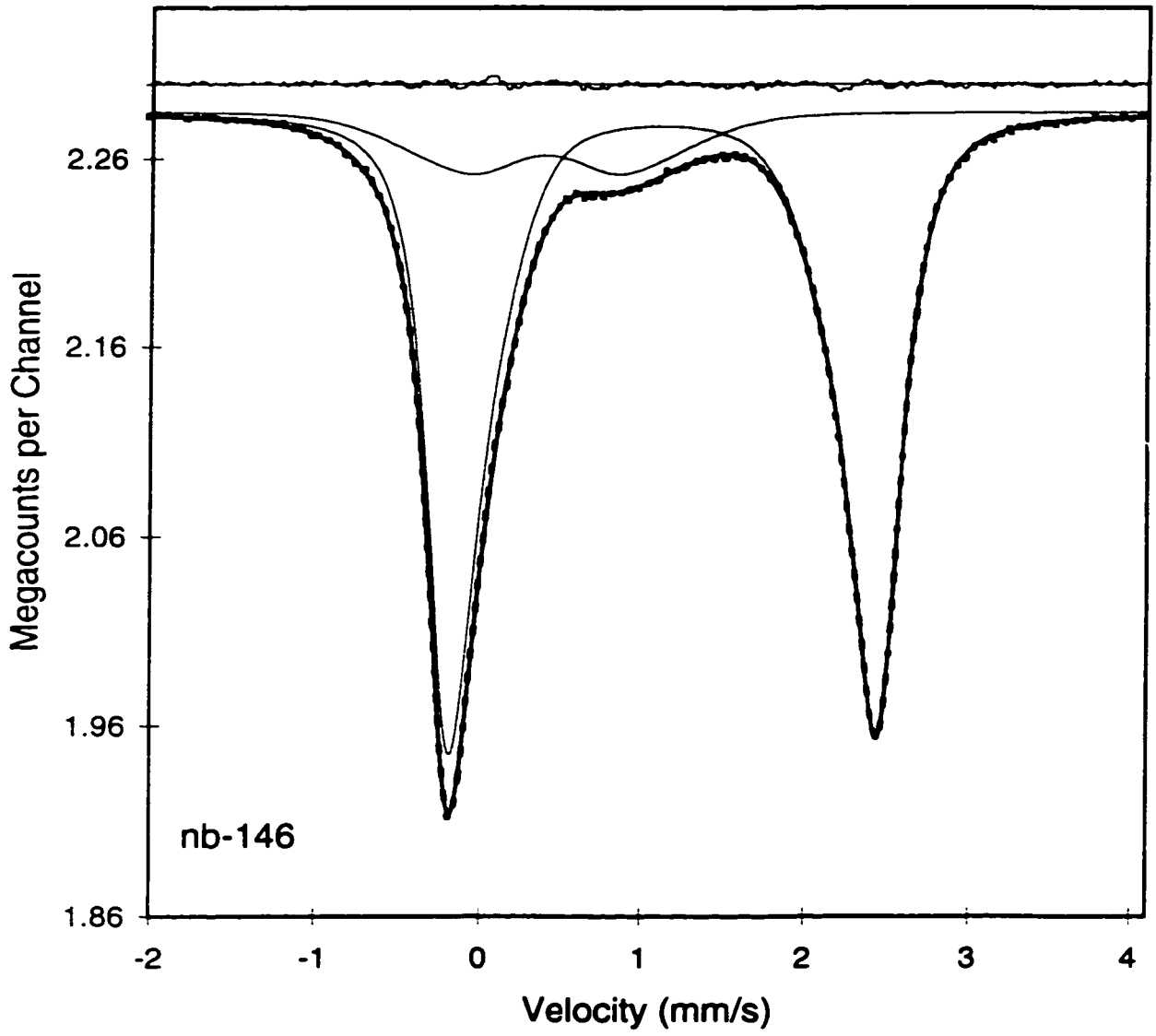
Megacounts per Channel
2.26
2.16
2.06
1.96
1.86
nb-146
-2
-1
0
1
2
3
4
Velocity (mm/s)

Figure 3(d).

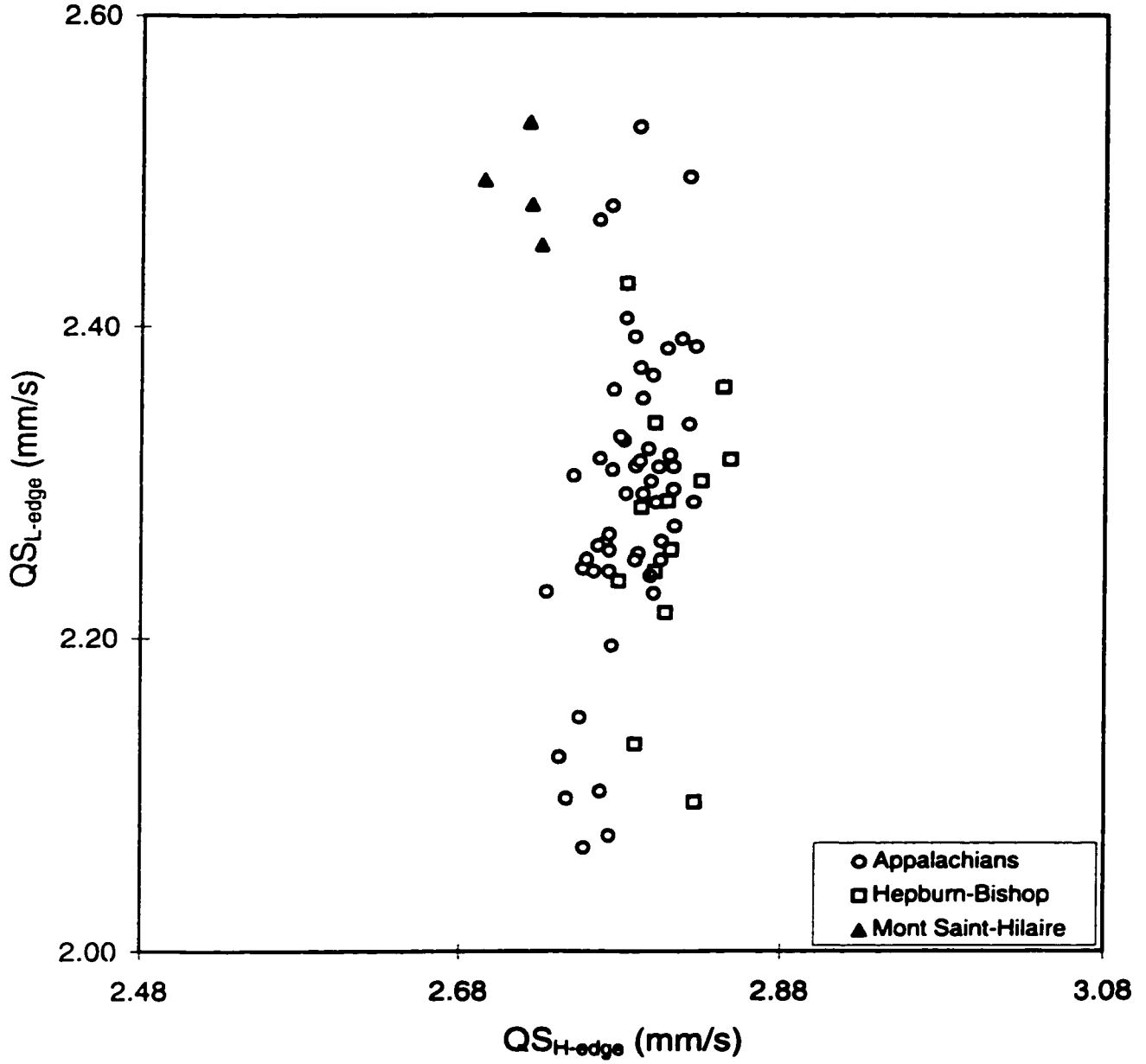

Figure 4 The relation between $QS_{H\text{-}edge}$ and $QS_{L\text{-}edge}$ of the Fe^{2+} QSDs for all of the investigated micas on scales of equal range.

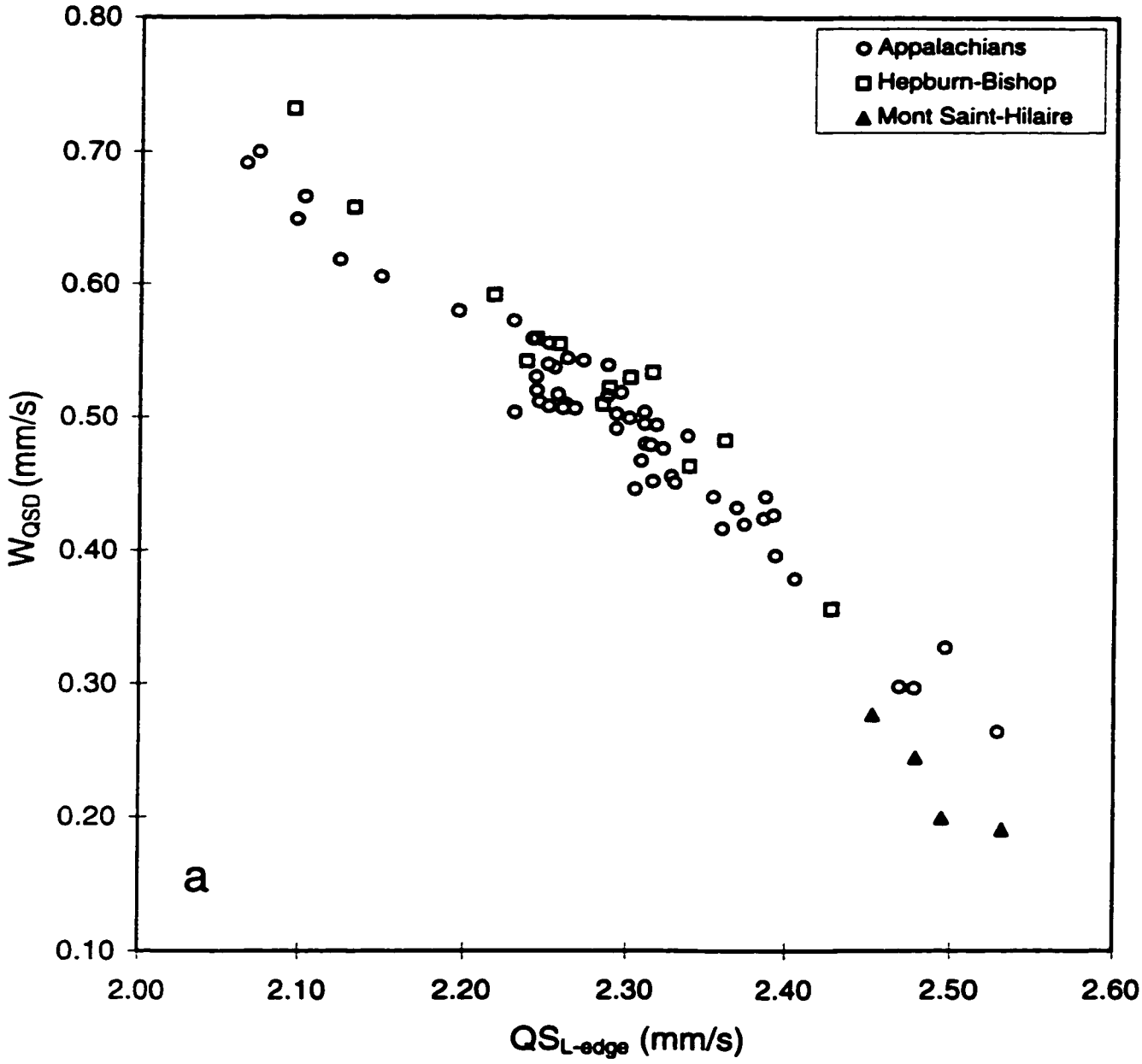

Figure 5 (a-b) The ralation between $QS_{L\text{-}edge}$ and (a) W_{QSD} and (b) $P(QS_{peak})$ of the Fe^{2+} QSDs for all the investigated micas.

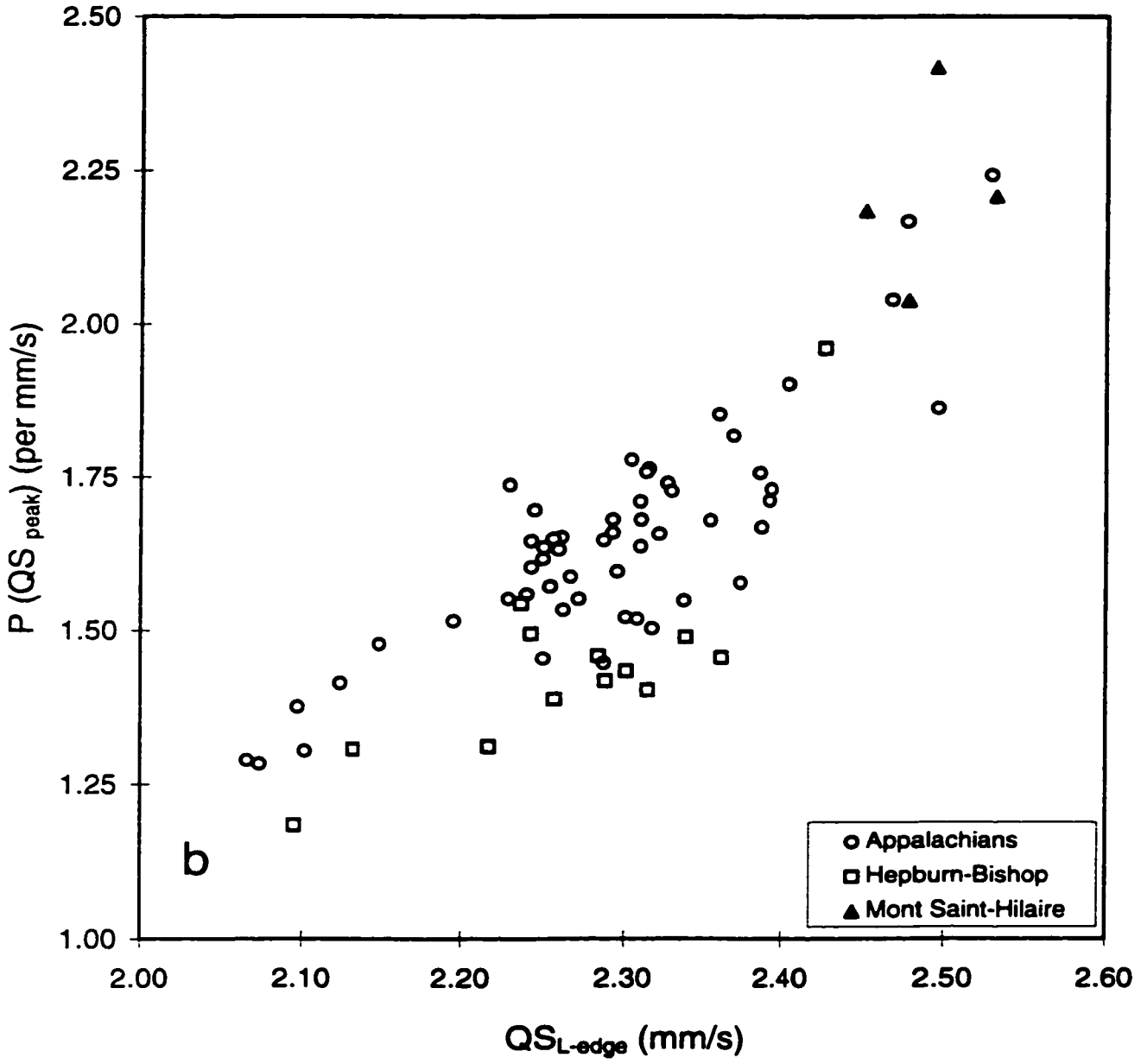
2.50
2.25
2.00
1.75
1.50
1.25
1.00
P (QS peak) (per mm/s)
2.00
2.10
2.20
2.30
2.40
2.50
2.60
QSL-edge (mm/s)
b
Appalachians
Hepburn-Bishop
Mont Saint-Hilaire

Figure 5 (b).

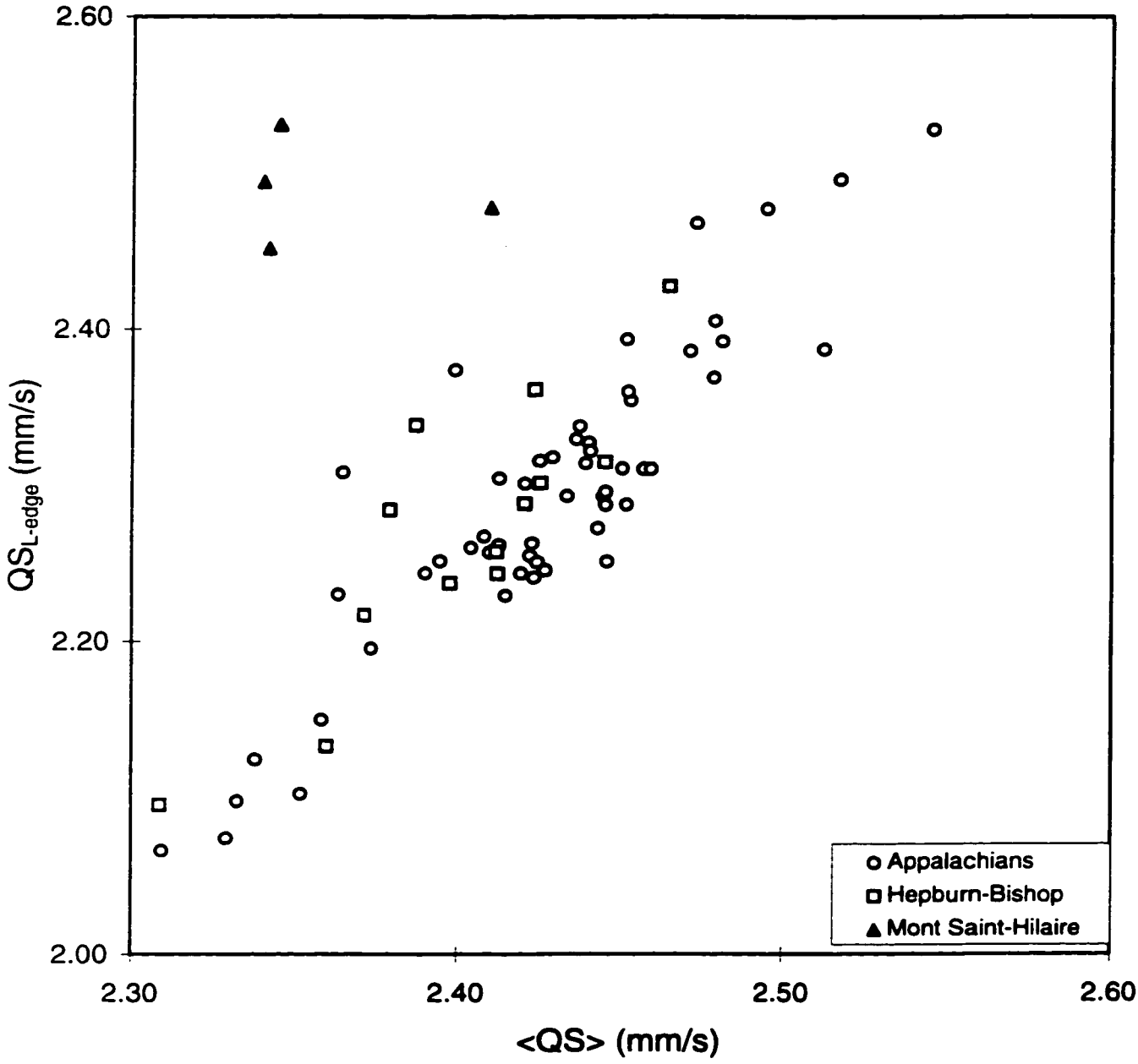

Figure 6 The relation between average quadrupole splitting, <QS>, and $QS_{L\text{-}edge}$ of the Fe^{2+} QSDs for the investigated micas.

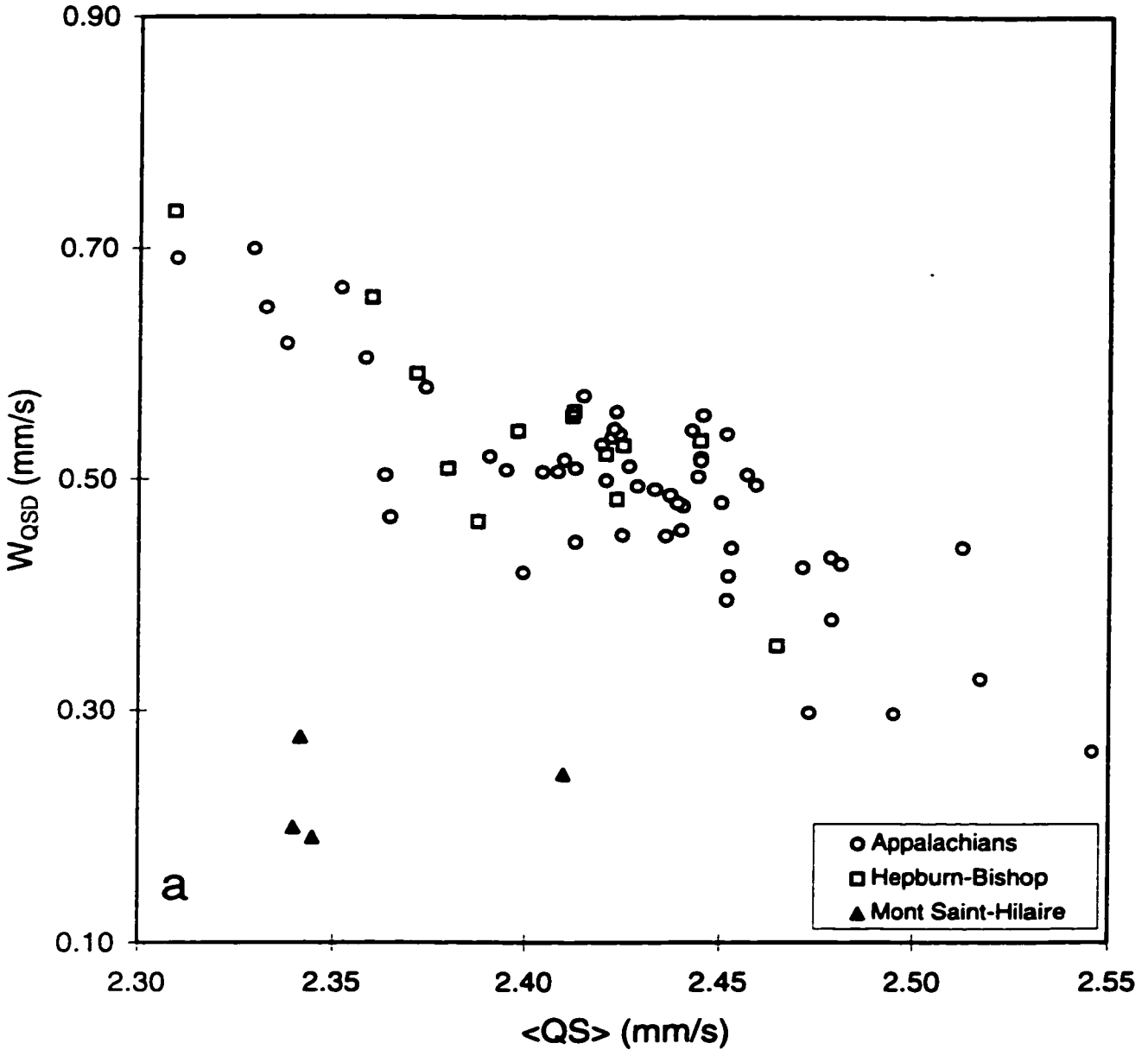

Figure 7 (a-c) The relation between average quadrupole splitting, <QS>, and (a) W_{QSD}, (b) $P(QS_{peak})$, and (c) skewness, S_k, of the Fe^{2+} QSDs for the investigated micas.

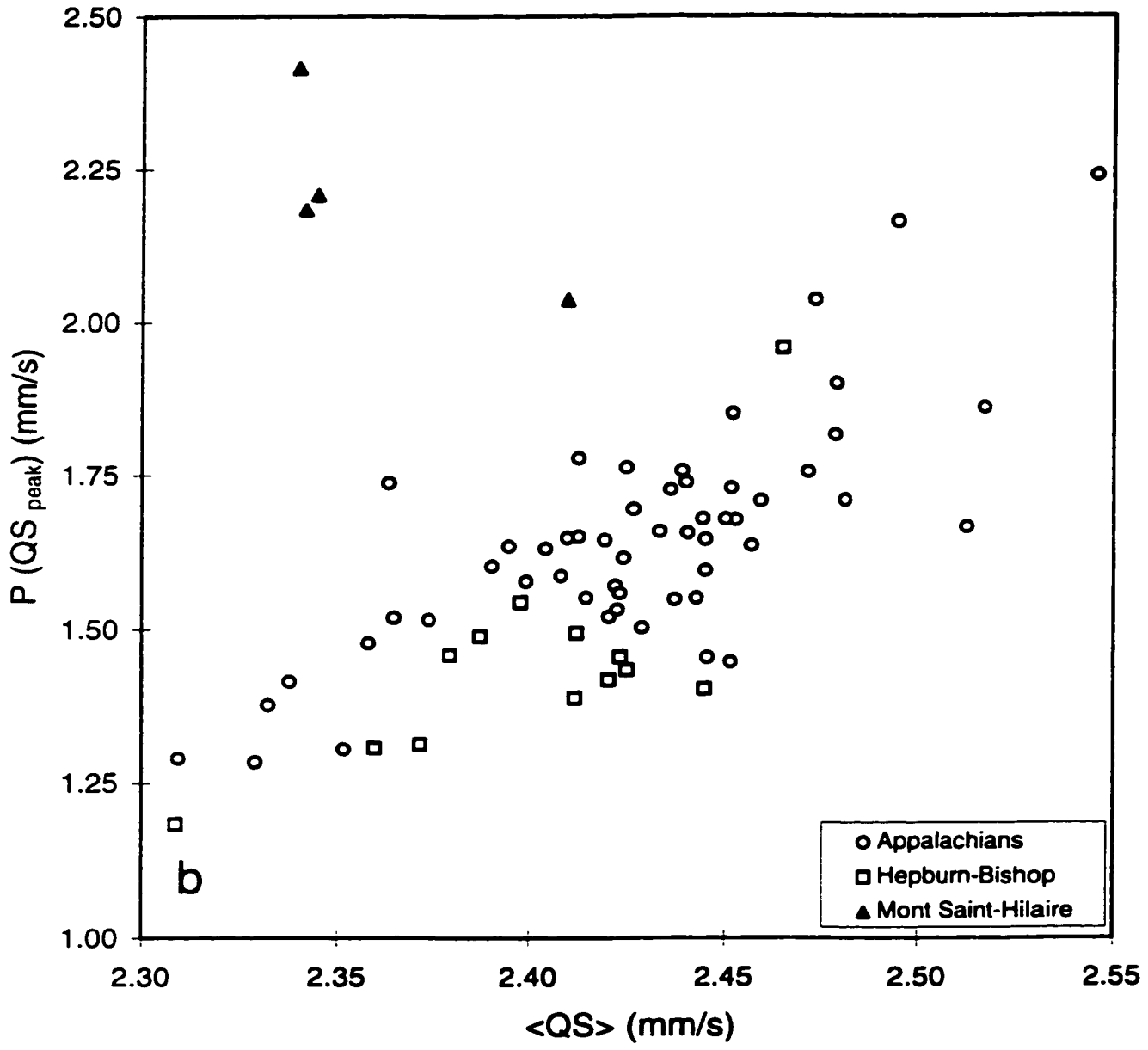
2.50
2.25
2.00
1.75
1.50
1.25
1.00
P (QS peak) (mm/s)
2.30
2.35
2.40
2.45
2.50
2.55
<QS> (mm/s)
b
Appalachians
Hepburn-Bishop
Mont Saint-Hilaire

Figure 7(b).

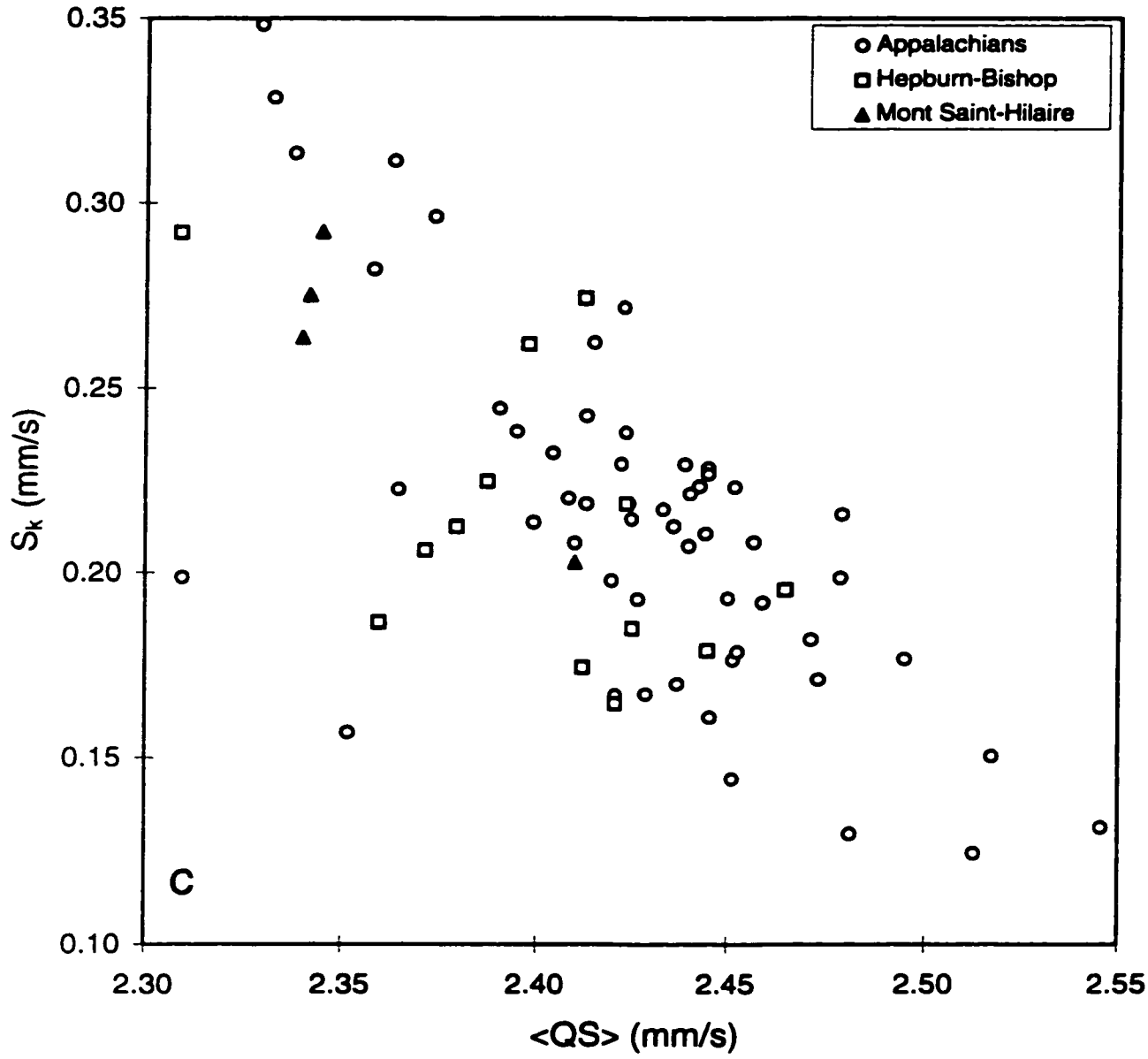
Appalachians
Hepburn-Bishop
Mont Saint-Hilaire
0.35
0.30
0.25
0.20
0.15
0.10
S_k (mm/s)
C
2.30
2.35
2.40
2.45
2.50
2.55
<QS> (mm/s)

Figure 7(c).

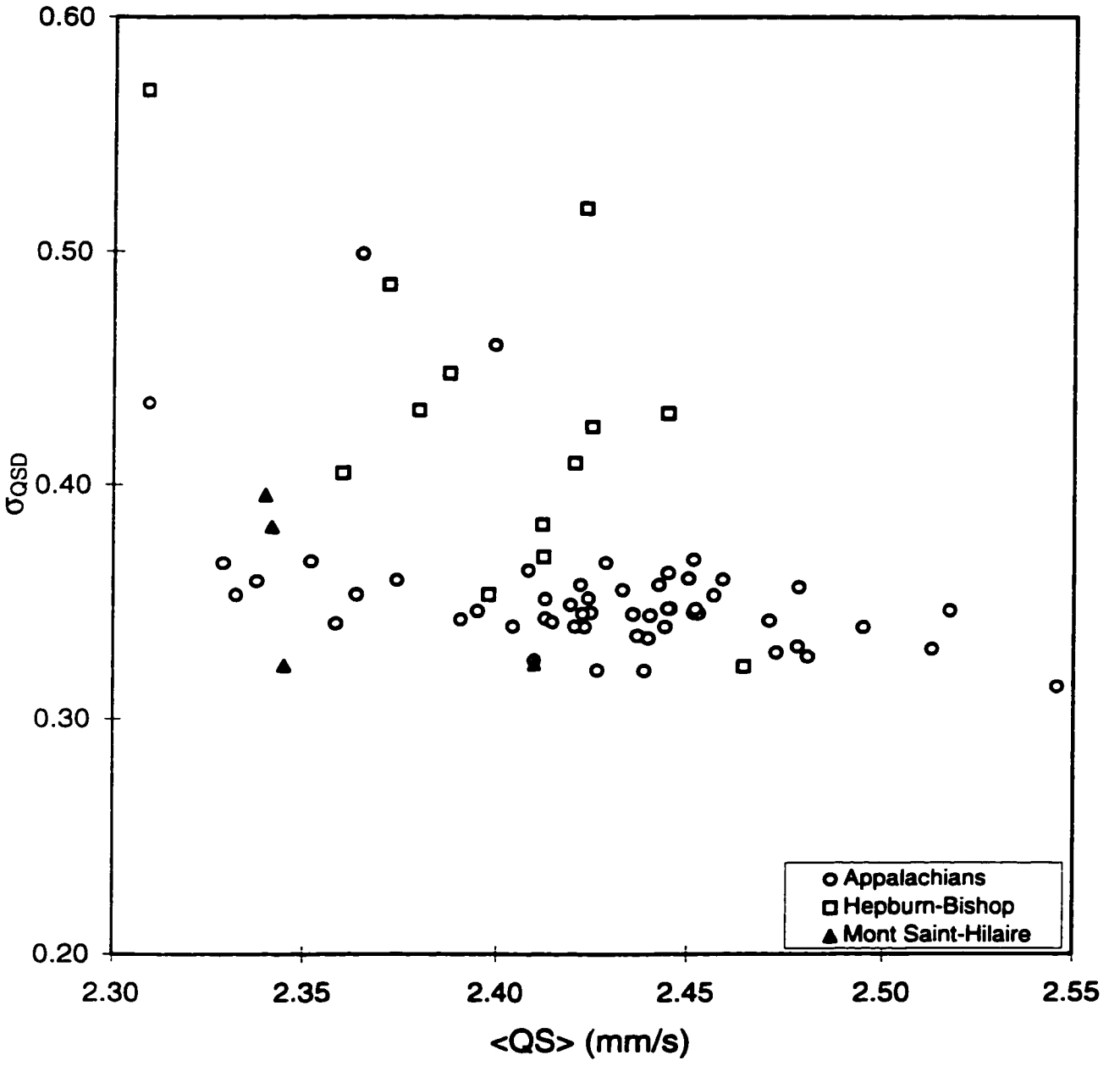

Figure (8) The relation between average quadrupole splitting, <QS>, and σ_{QSD} of the Fe^{2+} QSDs for the investigated micas. Note that the majority of QSDs have σ_{QSD} values in the range of 0.32-0.38 mm/s.

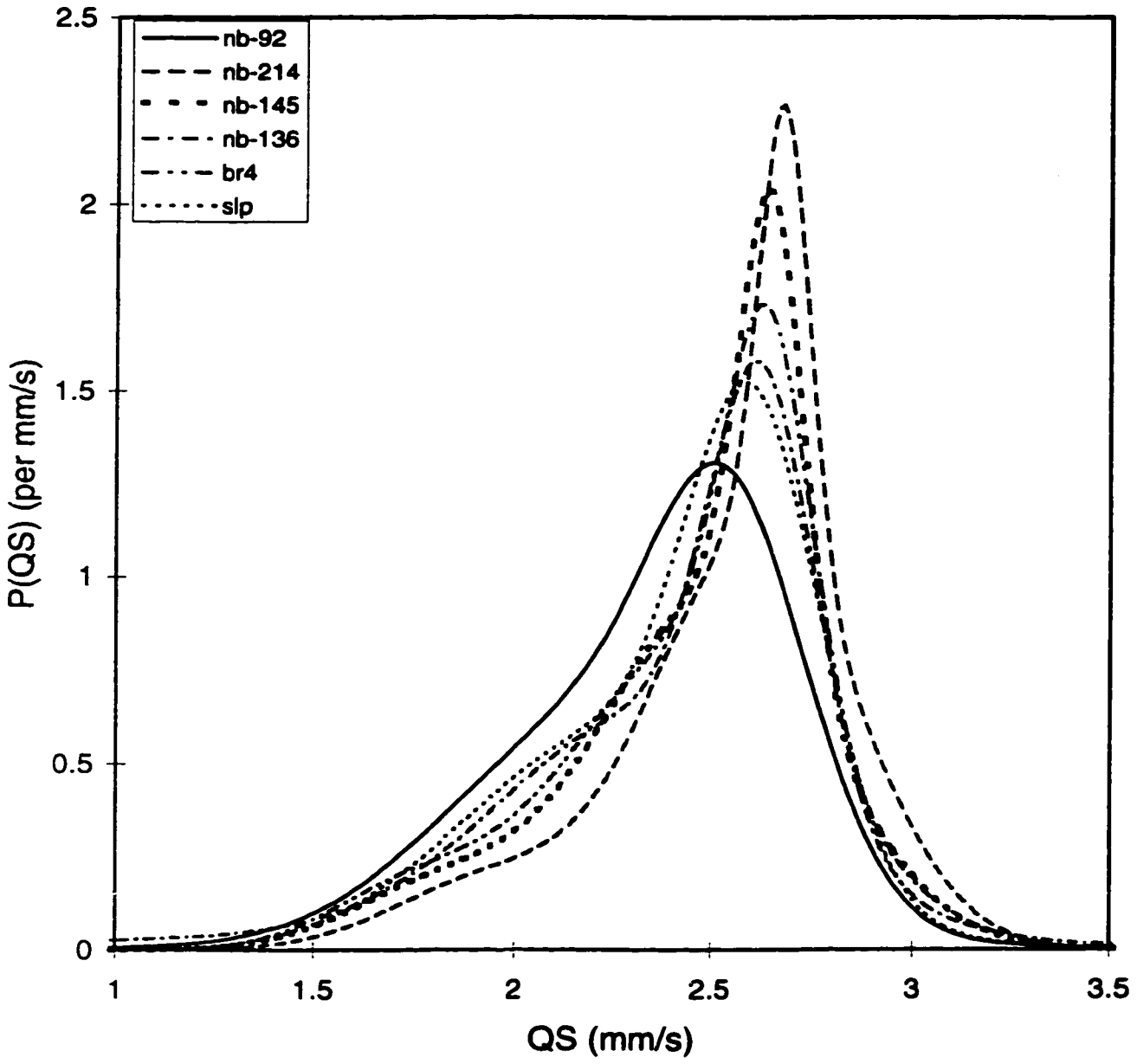

Figure 9 Continuous evolution of Fe^{2+} QSDs for biotite. The two extreme shapes with typical intermediate-shape are shown. The corresponding QSD parameters are given in Table 1.

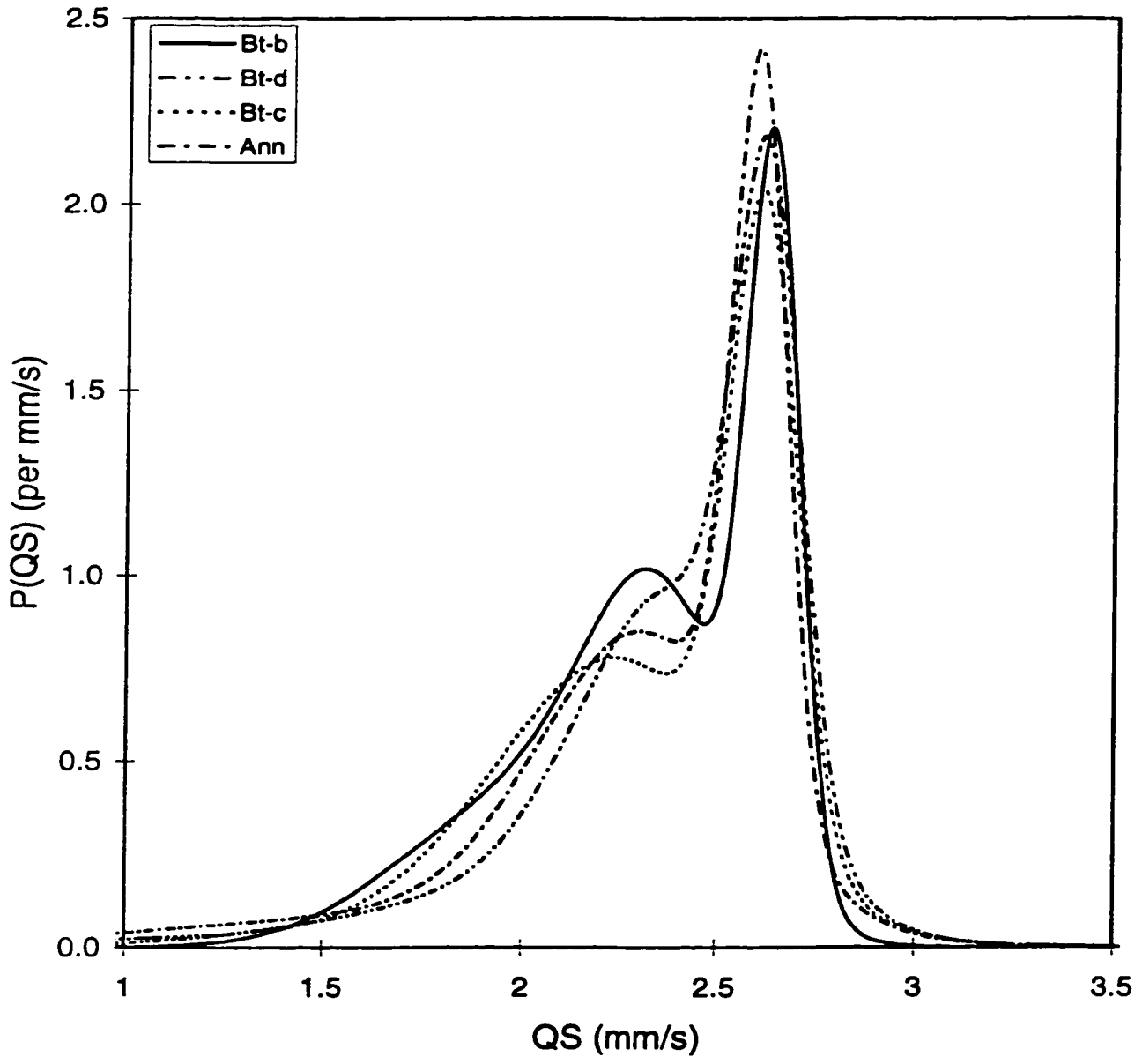

Figure 10 Fe^{2+} QSDs of Mont Saint-Hilaire micas. The corresponding QSD parameters are given in Table 1.

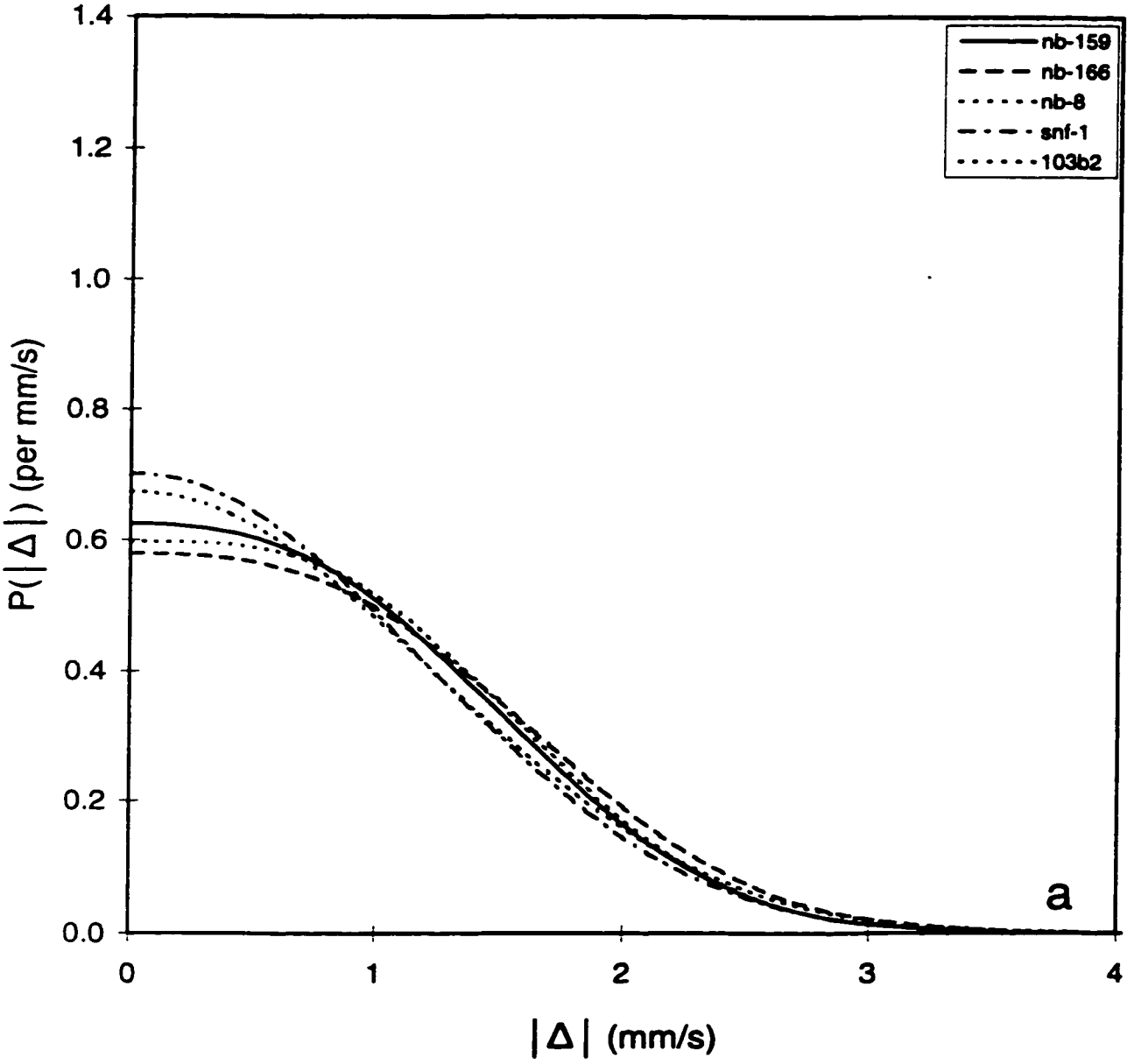

Figure 11(a-b) A selection of Fe^{3+} QSDs of biotite modeled by (a) a single Gaussian component and (b) two Gaussian components. Note that in both cases the QSDs have almost the same range of QSDs at high values.

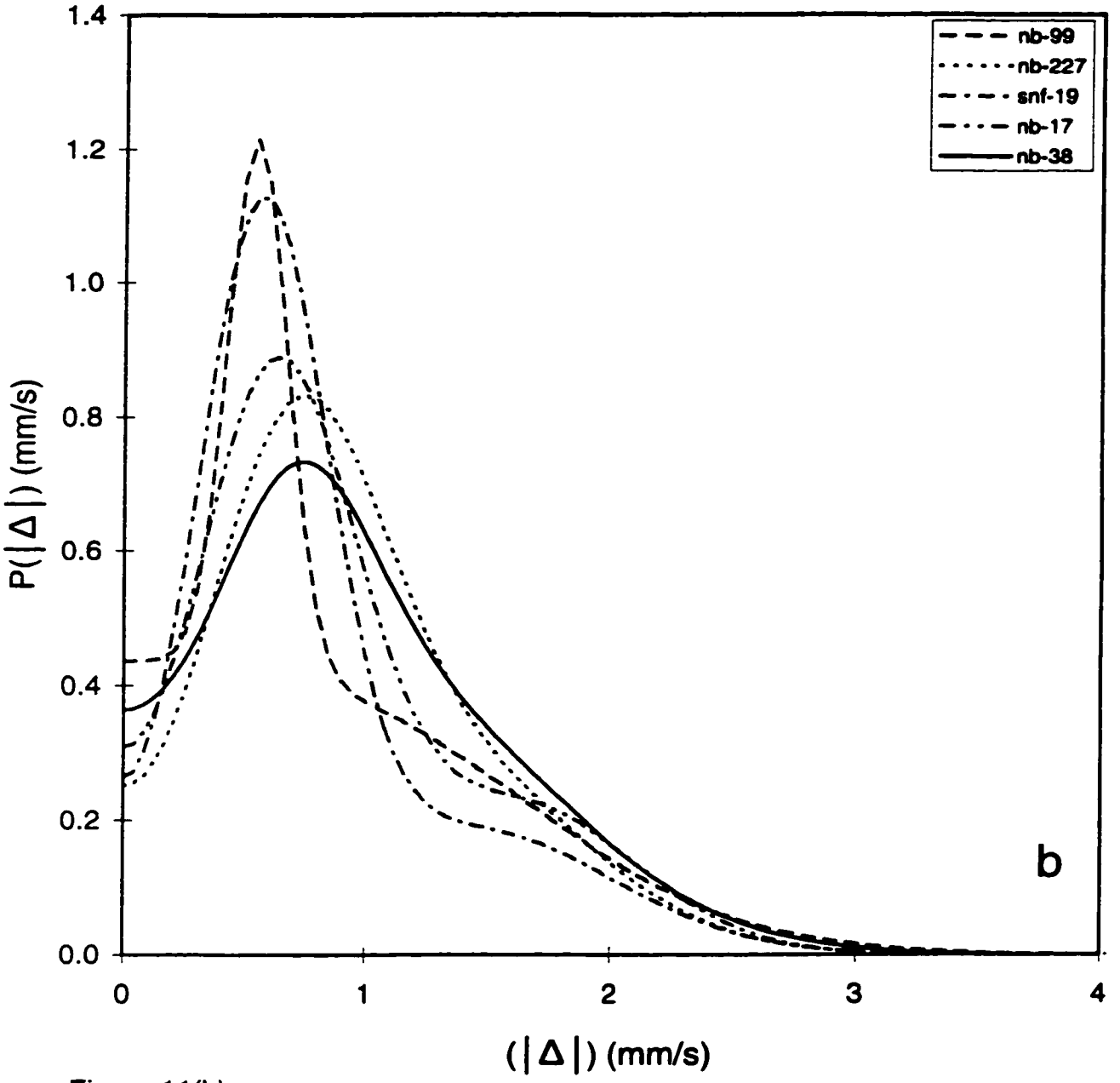
nb-99
nb-227
snf-19
nb-17
nb-38
b
P(|Δ|) (mm/s)
(|Δ|) (mm/s)
0.0
0.2
0.4
0.6
0.8
1.0
1.2
1.4
0
1
2
3
4

Figure 11(b).

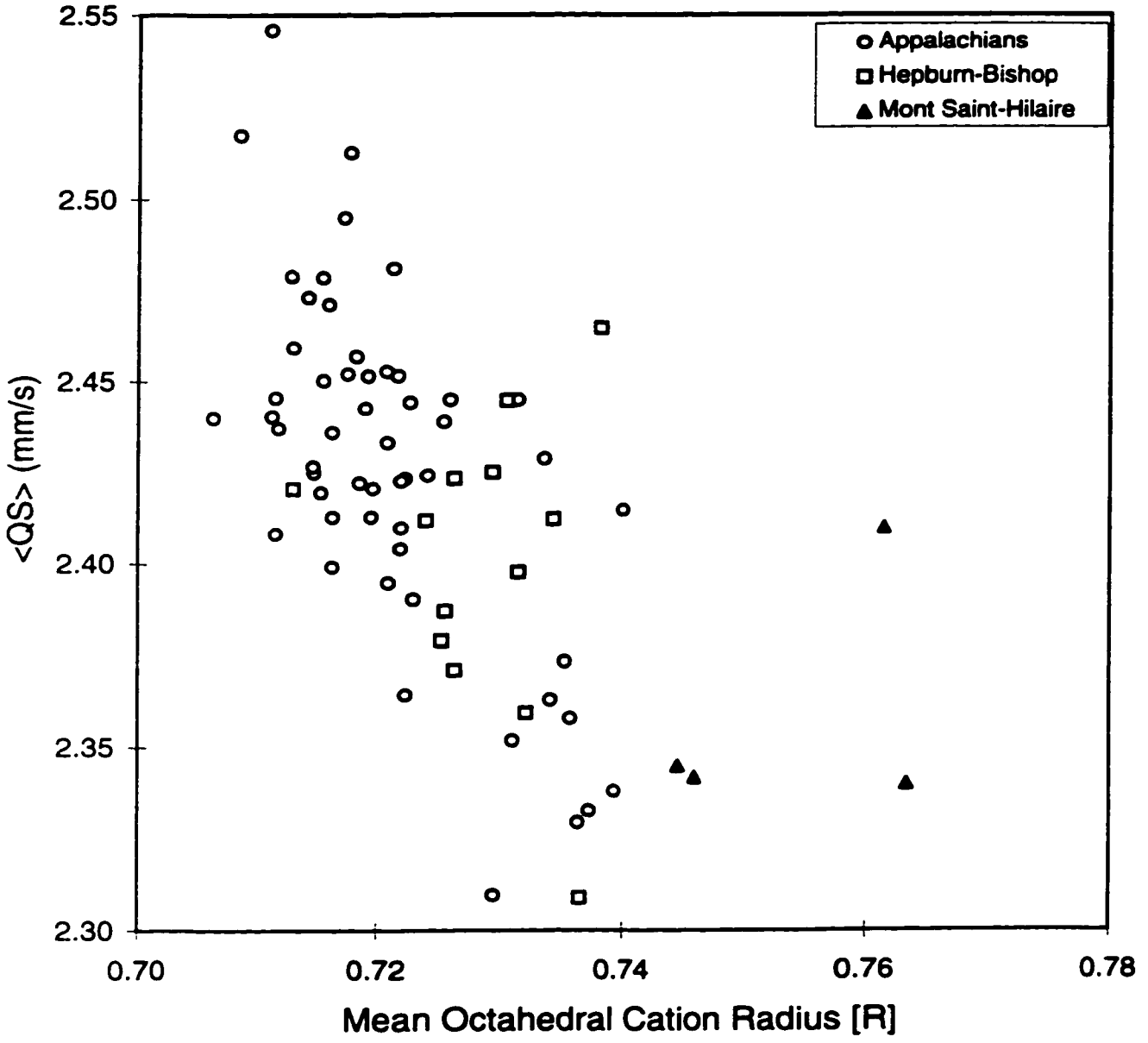

Figure 12 Changes in average quadrupole splitting, <QS>, as a function of the calculated average octahedral cation radius, [R], for the investigated micas.

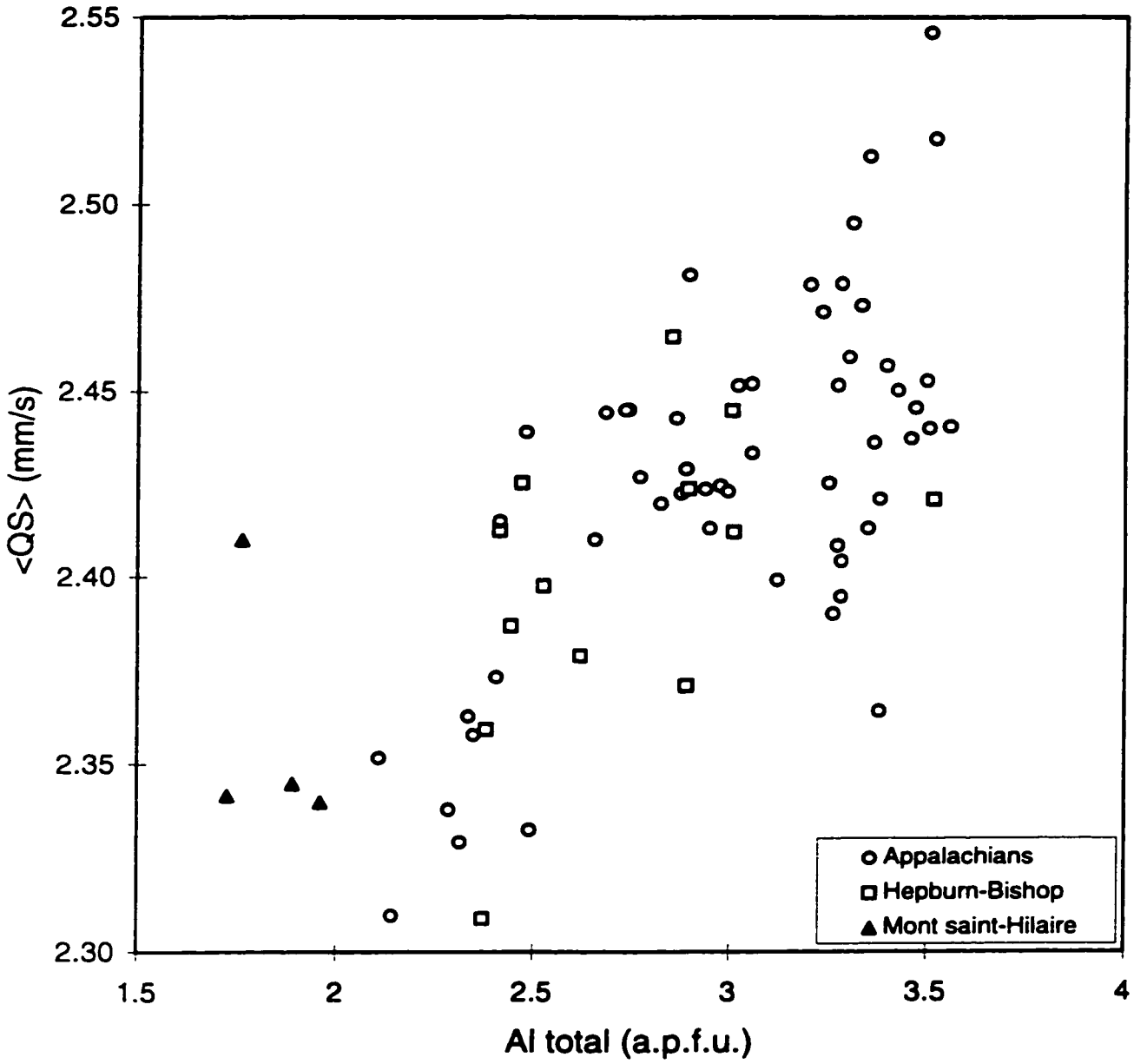

Figure 13 Changes in average quadrupole splitting, <QS>, as a function of the single compositional parameter Al_{total} (a.p.f.u.) for the investigated micas.

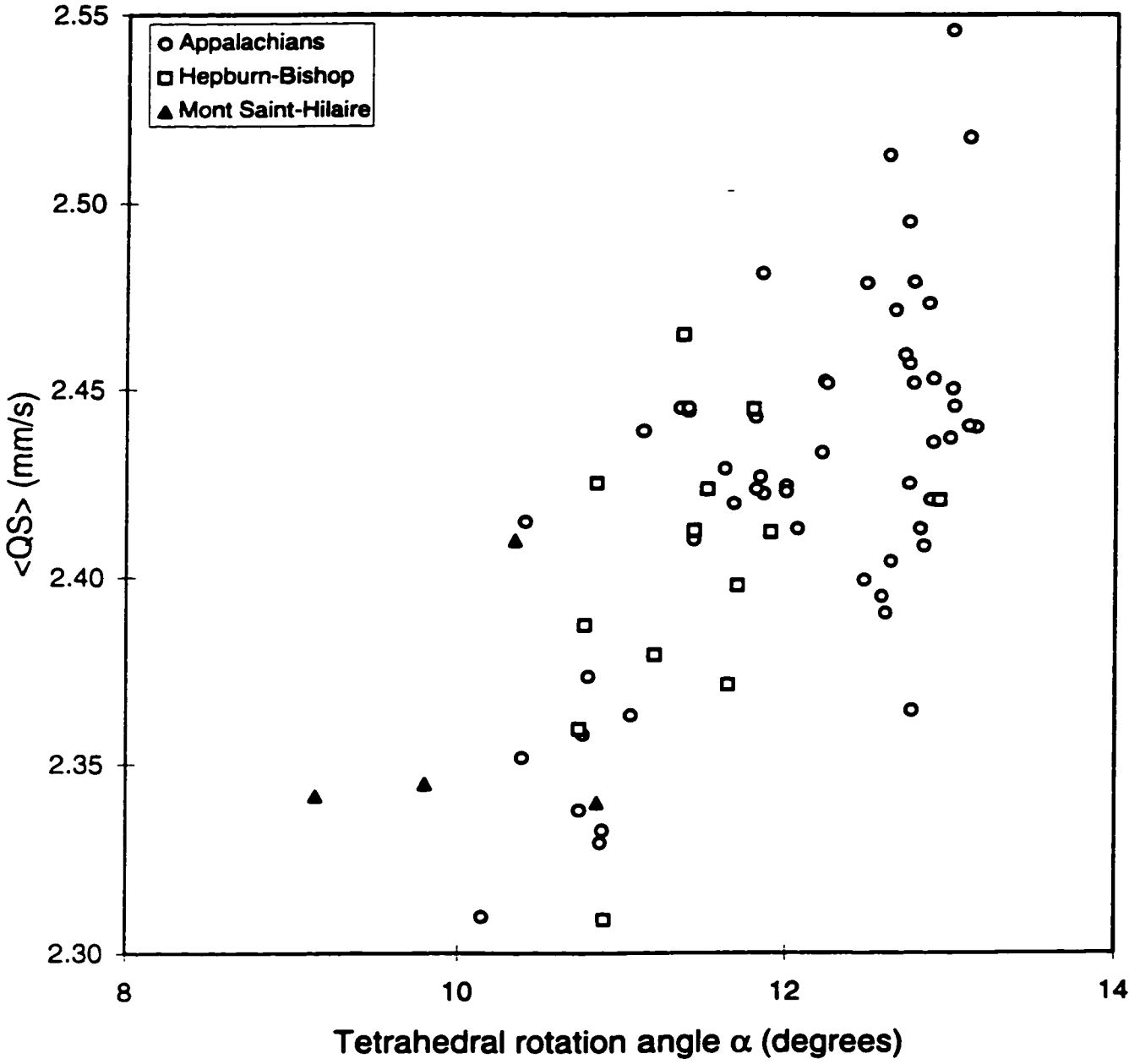

Figure 14 Changes in average quadrupole splitting, <QS>, as a function of the calculated tetrahedral rotation angle, α, (degrees), for the investigated micas.

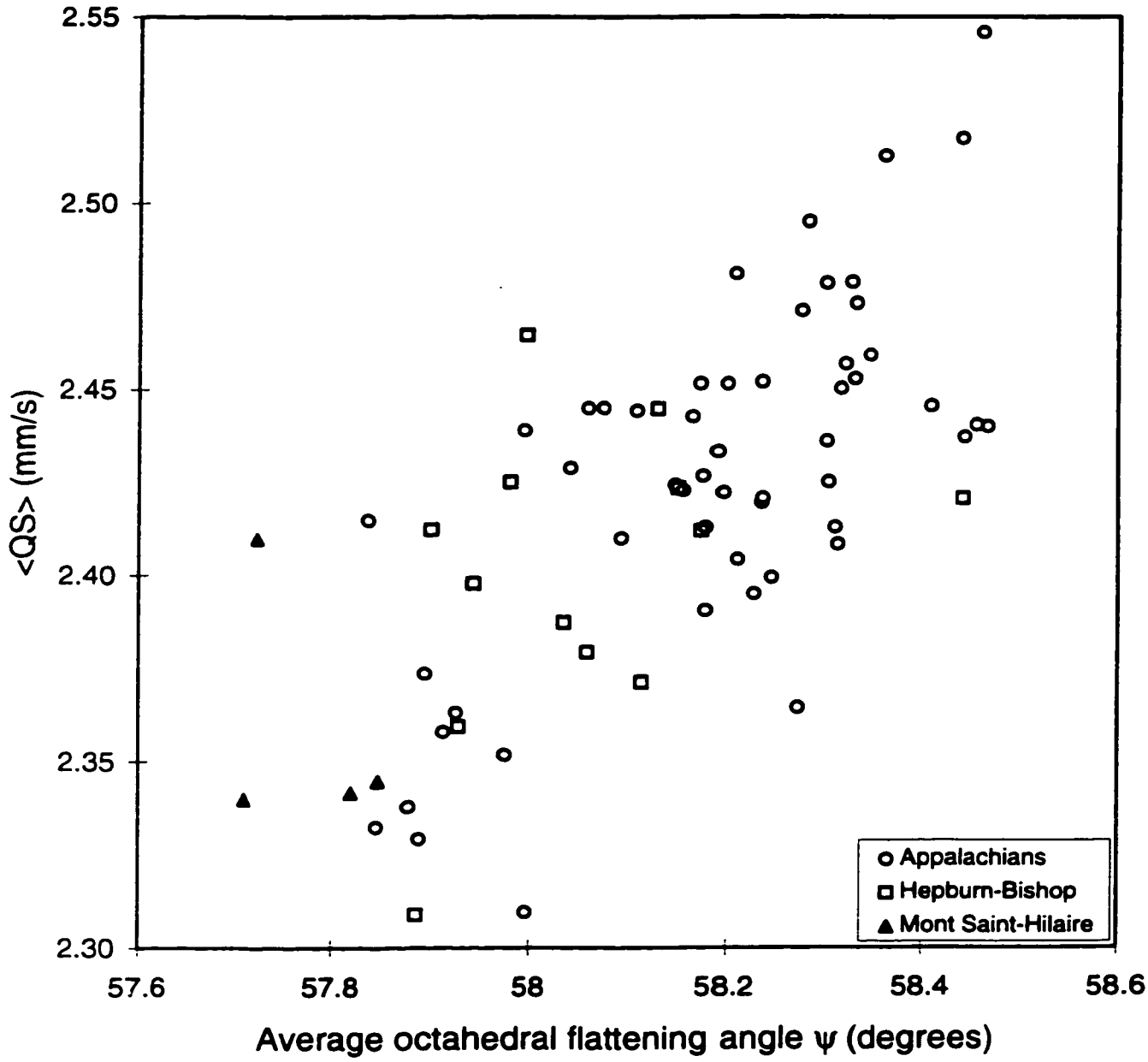

Figure 15 Changes in average quadrupole splitting, <QS>, as a function of the calculated flattening angle, ψ, for the investigated micas.

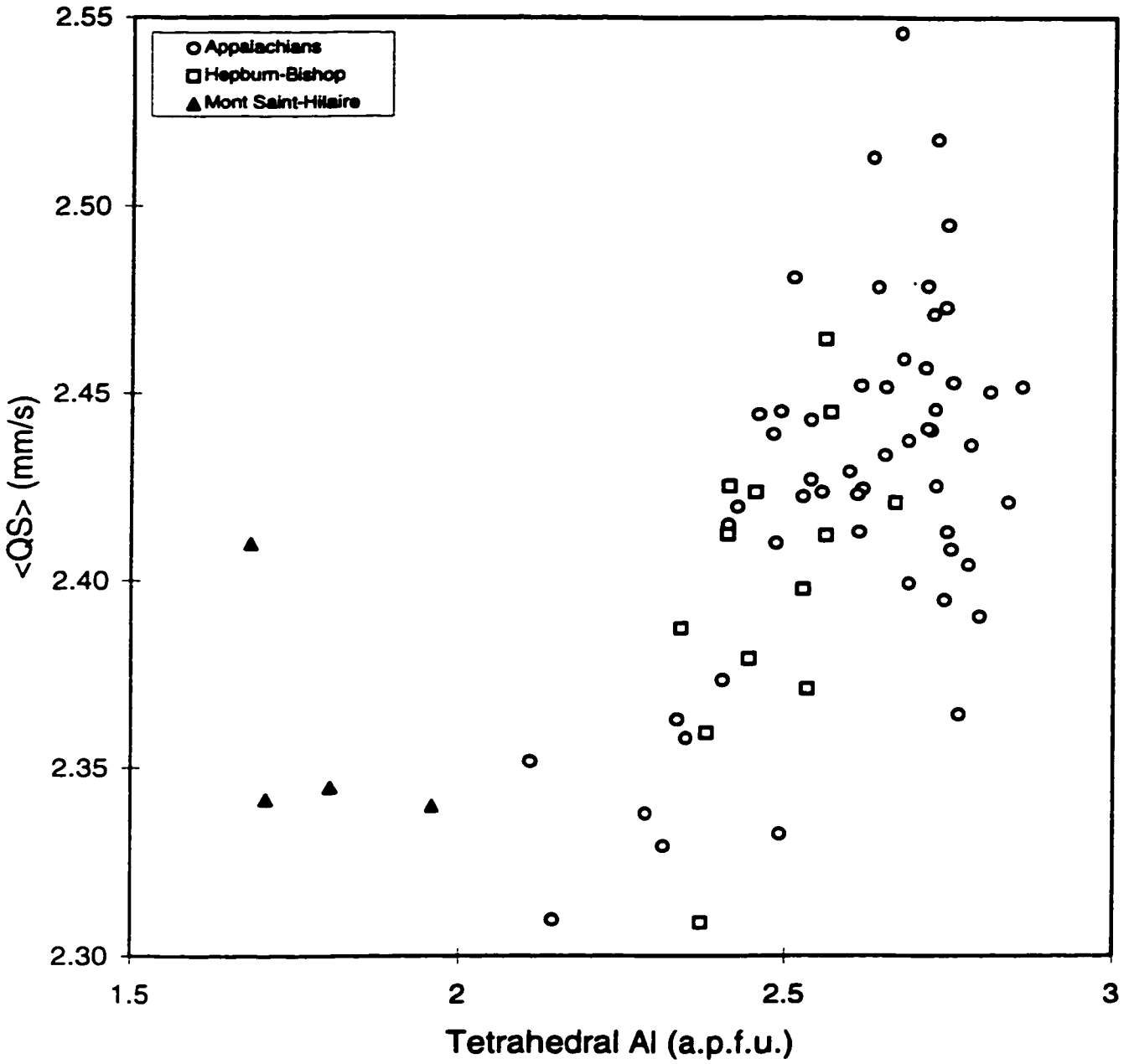

Figure 16 Changes in average quadrupole splitting, <QS>, as a function of the single compositional parameter tetrahedral Al (a.p.f.u.) for the investigated micas.

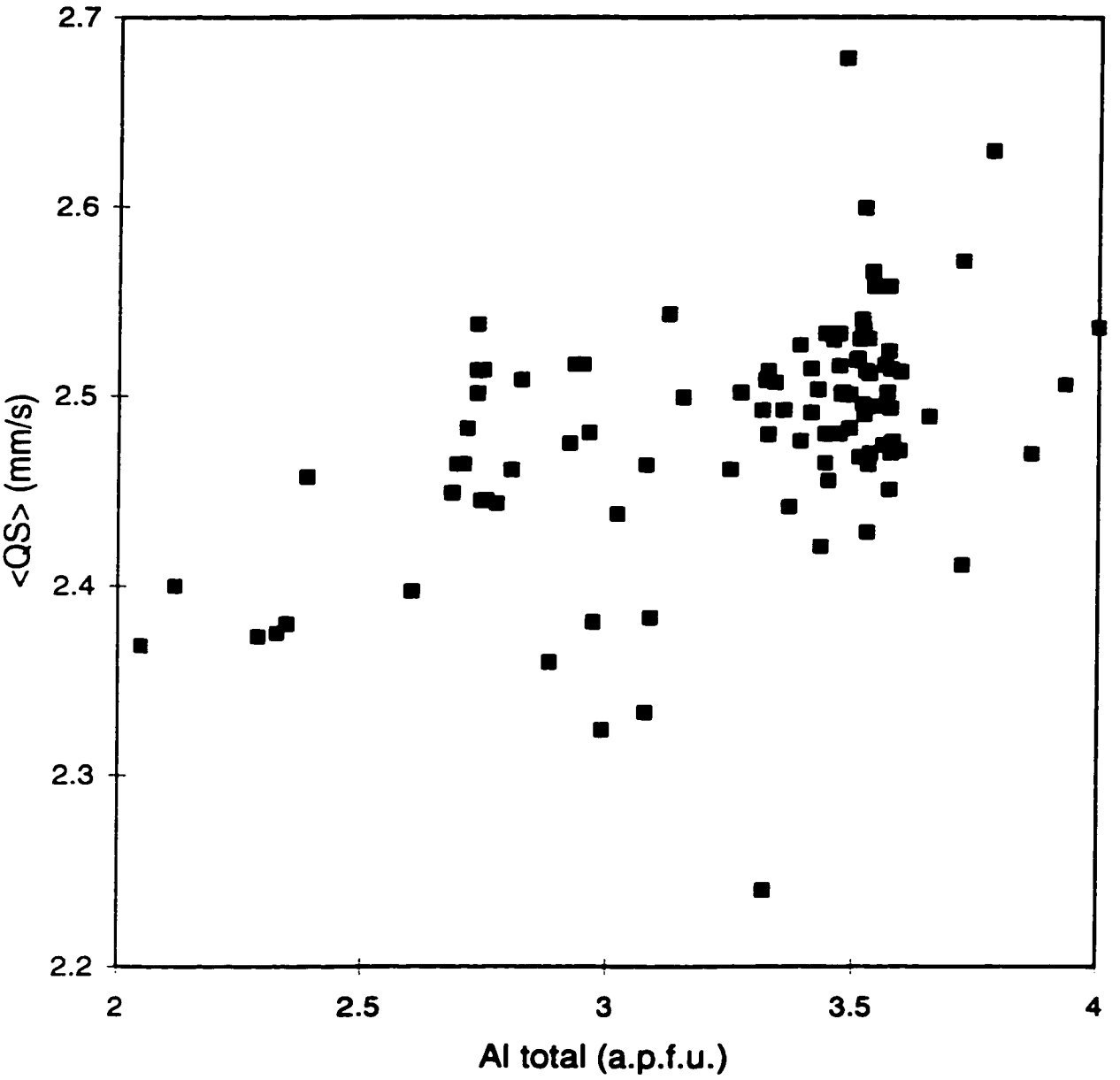

Figure 17 A plot of average quadrupole splitting, <QS>, versus the single compositional parameter Al_{total} (a.p.f.u.) from micas collected from published papers (references cited in the text).

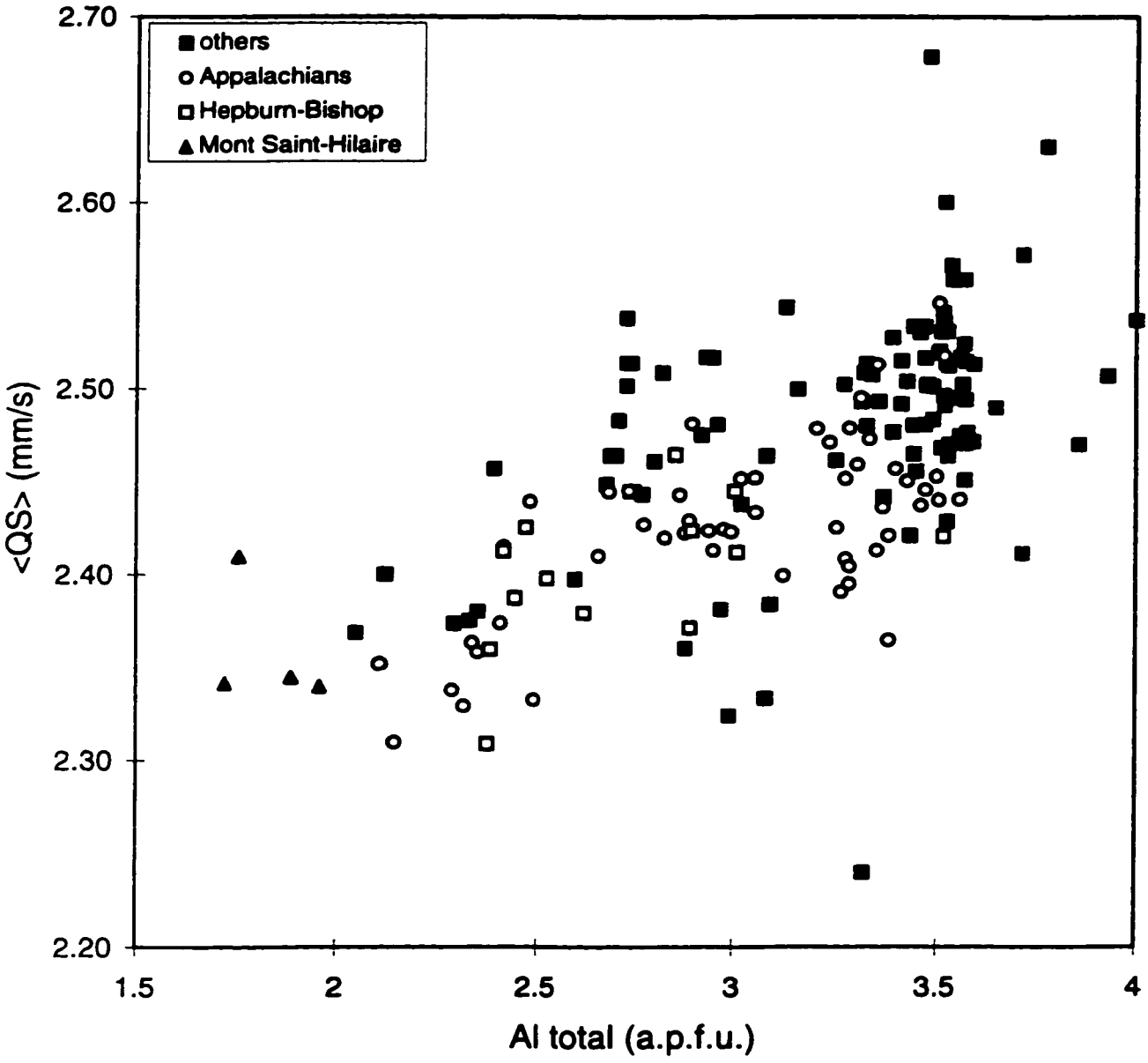

Figure 18 A plot of calculated average quadrupole splitting, <QS>, versus the single compositional parameter Al_{total} (a.p.f.u.) for the investigated micas along with the data from published papers (references cited in the text).

DETERMINATION OF CIS- AND TRANS- Fe^{2+} POPULATIONS IN $2M_1$ MUSCOVITE BY MÖSSBAUER SPECTROSCOPY

Amir A.T. Shabani[1], Denis G. Rancourt[2] and André E. Lalonde[1]

1) Ottawa-Carleton Geoscience Centre, Department of Earth Sciences, University of Ottawa, Ottawa, Ontario, Canada, K1N 6N5

2) Department of Physics, University of Ottawa, Ottawa, Ontario, Canada, K1N 6N5

* *Submitted to the Proceedings of the 11th International Clay Conference (to be published as a short paper in a special issue of the Canadian Journal of Soil Science).*

** *Published in the special issue of Hyperfine Interactions entitled "Mössbauer spectroscopy in Clay Science", edited by D. G. Rancourt, volume,117, (1998), pp. 117-129*

Abstract

Specimens of muscovite from Siluro-Devonian Appalachian granites of the Gander zone in New Brunswick were studied by ^{57}Fe Mössbauer spectroscopy, microprobe analysis and X-ray powder diffractometry. Chemical compositions, corresponding structural formulae and powder patterns indicate that they are dioctahedral true micas of $2M_1$ polytype. Mössbauer spectroscopy shows that this muscovite falls into two groups having distinct spectra, despite an absence of systematic differences in chemical compositions, X-ray patterns, unit-cell parameters, and Fe^{3+}/Fe ratios. In the first group, two distinct and well-resolved octahedral Fe^{2+} spectral contributions occur whereas, in the second group, a single but broader octahedral Fe^{2+} contribution occurs. All spectra from both groups have octahedral Fe^{3+} contributions. These observations are confirmed by quadrupole splitting distribution (QSD) analyses of the spectra. Spectra from the first group clearly show a bimodal distribution of quadrupole splittings for Fe^{2+}, with a dominant contribution at ~3.0 mm/s and a minor one at ~2.1 mm/s. In the second group, the spectra show a broad unimodal distribution of QSDs for Fe^{2+}. We attribute the 3.0 and 2.1 mm/s QSD components to Fe^{2+} in cis and trans octahedral sites, respectively. We argue that our assignment in the first group of samples is the only plausible one. Muscovite from the second group may have Fe^{2+} in both cis and trans sites but it cannot be resolved, as is usually the case, for example, with trioctahedral micas. In group one, cis/trans populations provide measures of the degree of cation order and of the density of vacancies on the cis sites. Simple models based on average unit-cell site

dimensions are found not to hold. Local effects seem to dominate, with Fe^{2+} showing no systematic preference for cis or trans sites.

1. Introduction

Attempts to determine cis and trans site populations have been a part of Mössbauer spectroscopy of the micas for the past three decades. A review of the literature on Mössbauer spectroscopy of micas reveals that most authors have fitted the octahedral Fe^{2+} contributions of their room temperature (RT) Mössbauer spectra with two Lorentzian line doublets and ascribed them to cis and trans octahedral sites. Moreover, using the spectral areas of the doublets, they have also attempted to determine octahedral Fe^{2+} cis and trans site populations (Dyar, 1987). Rancourt (1994), however, has recently shown that ascribing meaning to such Fe^{2+} doublets is not correct and cannot be used to even estimate cis/trans site populations, because cis and trans Fe^{2+} octahedral sites are in general not resolved as unique contributions in trioctahedral micas. A counter example is synthetic fluorannite where several distinct local environment contributions are resolved (Rancourt at al. 1996).

The purpose of the present paper is to show that a group of dioctahedral micas have spectra in which the octahedral Fe^{2+} contribution is resolved into two unique contributions attributable to cis and trans octahedral sites. Only such spectra, having true bimodal structure in both the measured absorption and the corresponding quadrupole splitting distribution (QSD), provide quantitative measures of the octahedral Fe^{2+} cis and trans site populations, the degree of cation order, and the density of vacancies on the cis sites.

Our examination of Mössbauer spectra of dioctahedral micas from the literature (e.g., Schmidt and Pietzsch, 1990; Pietzsch and Schmidt, 1990; Mackenzie at al. 1987; Finch at al.

1982; Goodman, 1976; Annersten and Halenius, 1976; Richardson, 1975; Hogg and Meads, 1970; and Bowen at al. 1969) indicates the existence of such a group of dioctahedral micas as the one described here. However, the presence of two distinct and well-resolved octahedral Fe^{2+} contributions was not recognized as a necessary condition for reliable quantification.

The present paper is the first study concerning the possibility and limits of quantitative determination of cis- and trans-Fe^{2+} populations in $2M_1$ muscovite. Its relevence stems from the fact that Mössbauer spectroscopy of most of the trioctahedral micas and some of the dioctahedral micas cannot resolve the octahedral Fe^{2+} cis and trans sites, due to overlapping of their broad contributions.

2. Experimental Methods and Sample Descriptions

This study is based on ten specimens of muscovites from Siluro-Devonian peraluminous granitic rocks of the Gander zone of the Canadian Appalachians in New Brunswick, (Whalen, 1993). The locations and host rock descriptions of the specimens are given in Table 1. A textural study of muscovite grains displayed in polished thin sections suggests that the mineral is mostly primary and magmatic in nature with minor amounts of secondary muscovite replacing K-feldspar. All muscovite crystals have about the same grain size and comprise about 3 to 6 percent of the rocks by volume. None of the muscovite specimens exhibit traces of deformation or pleochroic haloes.

Mineral analyses were obtained by wavelength-dispersive X-ray spectrometry using the JEOL 8900 Superprobe of the McGill University Microprobe Laboratory. Typical beam operating conditions were 15 kV and 20 nA. The chemical composition of each of the ten specimens studied is presented in Table 2 along with its respective structural formula based on 22 oxygen atoms. H_2O was calculated on the basis of stoichiometry (i.e. OH+F+Cl=4). FeO and Fe_2O_3 contents of each specimen were determined by imposing the Fe^{3+}/Fe ratios determined by Mössbauer spectroscopy (see below).

Unit-cell parameters were refined from X-ray powder diffraction patterns taken with a Phillips X'Pert PW 3510 X-ray diffractometer with Cu-Kα radiation using an IBM-PC version of the Appleman and Evans (1973) least-squares refinement program. The lattice parameters of representative specimens are given in Table 3. Also, XRD data are presented in the Appendix (pp. 272-282).

Chemical compositions, corresponding structural formulae and X-ray powder patterns indicate that all samples are dioctahedral true micas of $2M_1$ polytype.

Transmission ^{57}Fe Mössbauer spectra of 10 samples were obtained at RT (22°C) using a ^{57}Co rhodium matrix source on a velocity range of ±4 mm/s with a constant acceleration mode transducer. Data was collected on 1024 channels, which covered twice the Doppler velocity range of ±4 mm/s. Calibrations of spectra were obtained with a ^{57}Fe-enriched iron foil, both before and after each experiment. All positions are reported with respect to this calibration spectrum, i.e., with respect to the centre shift (CS) of metallic α-Fe at RT. Each spectrum was folded to give a flat background (BG).

Absorbers were prepared as follows: The grain size of the specimens lies in the range of 80 to 120 mesh (125-75 microns). Purification of each specimen was achieved by hand-picking under the binocular microscope. Specimens are estimated to be in excess of 99% pure. The amounts of samples used in the 0.5 inch diameter absorbers varied between 130 to 145 mg determined by the method of Rancourt et al. (1993) to maximize the signal to noise ratios. The above mentioned amount of granulated mica corresponding to the ideal (or near-ideal) absorber thickness was then mixed with petroleum jelly in a 5 mm thick and 0.5-inch inside diameter holder. This method gives a random orientation of mica grains in the absorbers and allows one to impose equality in area of corresponding high and low-energy lines in site-specific doublets (Rancourt, 1994a).

The new Voigt-based model of arbitrary-shape QSDs of Rancourt and Ping (1991) was used to fit the spectra. This model assumed that the true underlying QSD for a given valence state and coordination number, i.e., for a given site, is composed of a given number N of Gaussian components as can be justified on statistical grounds and used. Unique distributions are thereby obtained (Rancourt and Ping, 1991).

Rancourt et al. (1993) recently produced a graph that can be used to estimate thickness corrections to spectral areas of separate lines in a given observed spectrum. It gives a quantitative estimate of how individual lines in a spectrum are differently affected. Using this graph, we found that the ratio of observed area (A) over the thin-limit line area (A_{th}) corresponds to $A/A_{th} \approx 1$, as expected for truly thin absorbers. Hence, thickness corrections were not performed.

3. Results and Discussion

3.1 Bimodal or Unimodal QSDs

Mössbauer spectroscopy shows that our muscovite specimens fall into two groups having distinct spectra, despite an absence of systematic differences in chemical compositions and corresponding structural formulae, X-ray powder patterns, unit-cell parameters, and Fe^{3+}/Fe ratios (Tables 2, 3, 4). All RT spectra are shown in Fig.1.

In the first group two distinct and well-resolved octahedral Fe^{2+} spectral contributions occur whereas, in the second group, a single but broader octahedral Fe^{2+} contribution occurs. A representative spectrum from each group is shown with fitted model lineshapes in Figs. 2(a) and 2(b). In all spectra each of the octahedral Fe^{2+} and octahedral Fe^{3+} contributions were modeled by QSDs that were assumed to be sums of two Gaussian components. The reduced chi-squared values are in the range of x^2_{red} ~0.9-1.3.

Fitting parameters for the best fits of all spectra are given in Table 4. The quadrupole splitting (QS) and CS parameters of the Fe^{2+} sites in our samples (QS ≈ 2.0 - 3.0 and CS = 1.10 - 1.20 mm/s) are in reasonable agreement with previously reported values (QS_1=2.87-3.08, QS_2 = 2.14-2.28 and CS = 1.10 - 1.15 mm/s). The octahedral Fe^{3+} parameters of this study (QS = 0.73 - 0.81, and CS = 0.28 - 0.35 mm/s) are also consistent with reported values (QS = 0.66 - 0.73, and CS = 0.34 - 0.42 mm/s) (literature values are from Mackenzie at al. 1987).

The two distinct and well-resolved octahedral Fe^{2+} spectral contributions in the first group and a single but broader octahedral Fe^{2+} contribution in the second group are clearly seen in the high-energy lines of the Fe^{2+} doublets in the spectra themselves (Figs. 1 and 2). They are further confirmed by quadrupole splitting distribution (QSD) analyses of the spectra. The two groups of muscovite have characteristic QSDs shown in Figs. 3a and 3b. Spectra from the first group clearly show a bimodal distribution of quadrupole splittings for Fe^{2+} with a dominant contribution at ~3.0 mm/s and a minor one at ~2.1 mm/s, whereas, in the second group, the spectra show a broad asymmetrical unimodal distribution of QSDs for Fe^{2+}. We attribute the QSD contribution centered at ~3.0 mm/s with a Gaussian width $\sigma_{1\Delta}$ value of ~0.2 mm/s to cis-Fe^{2+} octahedral sites and the contribution centered at ~2.1 mm/s with a broader Gaussian width $\sigma_{2\Delta}$ value of ~0.3 mm/s to trans-Fe^{2+} octahedral sites. This assignment in the first group samples is the most plausible one. Muscovite from the second group may have Fe^{2+} in both cis and trans sites but it cannot be resolved, as is usually the case, for example, with trioctahedral micas (Rancourt et al. 1994).

A close look at Fig. 4 showing the total Fe^{2+} QSDs from both the first group (only maximum and minimum cis/trans Fe^{2+} ratios are shown) and the second group on the same scale, suggests that the Fe^{2+} QSDs from the second group can be interpreted as follows.

First of all, since the QSDs from both groups span the same range of values, from ~1.5 to ~3.5 mm/s, the second group samples probably also contain Fe^{2+} in both cis-type and trans-type local environments. The main difference in the QSDs of the two groups occurs at QS values (~2.5 mm/s) that fall between the characteristic QS values for cis and trans sites of

the first group samples. Here, contrary to first group samples, the second group samples have large probability densities (and corresponding site populations) for QS values in this intermediate range (QS ~2.5 mm/s).

This can only mean that in second group samples the Fe^{2+} local environments include sites that are not typical cis and trans sites. Whereas in first group samples the Fe^{2+} local environments can be classified as cis and trans sites (that have some local variability but not to the extent of being resolvable as cis or trans), in second group samples local distortions arising from local chemical and occupation disorder cause Fe^{2+} local environment variations that are as large as the difference between ideal cis and trans sites.

This strongly suggests that second group samples have higher degrees of disorder, possibly being further from ideal dioctahedral end-members. For this reason we looked for any other systematic difference between first and second group samples. We found no such differences. On the other hand, we must keep in mind that the reported QSDs specify only Fe^{2+} local environments and that Fe^{2+} is a minor cation in muscovite. It may be, therefore, that the observed first and second group Fe^{2+} QSD differences are due to differences in local spatial association between Fe^{2+} and other minor cations or between Fe^{2+} and local defects. So far we have not found evidence that might suggest a mechanism for the observed first and second group differences.

3.2 Cis/Trans Fe^{2+} Site Populations

Although we do not know the reason or reasons that our muscovite samples fall in two groups, having two different signatures, it is clear that the first group samples have spectra that are able to give reliable Fe^{2+} cis/trans populations. This allows one to quantitatively verify various proposed crystal chemical models of muscovite. In dioctahedral micas cis and trans sites are distinguishable by both size and symmetry. The octahedral cis sites are smaller and generally occupied by aluminum, whereas, octahedral trans sites are larger and generally vacant. The ratio of the number of small cis sites to larger trans sites is two to one. In view of the difference in size of the two octahedral sites, it has been suggested (Veitch and Radoslovich, 1963) that octahedral ordering should occur, with the small trivalent ions such as aluminum and ferric iron occupying the smaller site, and the larger divalent ions such as ferrous iron and magnesium occupying the larger site.

On the contrary, and in opposition to previous Mössbauer investigations (Hogg and Meads, 1970; Goodman, 1976), we find that Fe^{2+} does not preferentially go into the trans sites. Such a preference would give a cis to trans population ratio close to zero. Instead, assuming equal Mössbauer recoilless fractions for all Fe^{2+} sites, we find cis/trans ratios for first group samples in the range 1.4 - 3.4 (tables 4 and 5), with an average for all first group samples of 1.9.

Although there are large sample to sample variations, the latter ratios cluster around the theoretical value of 2.0 that corresponds to no Fe^{2+} preference for either cis or trans sites.

This suggests that local contributions completely override any site dimension considerations based on average unit-cell. This may be due to the fact that the Fe^{2+} cations are so much larger than the other cations, such that only large local distortions can allow them to be incorporated. Note that, in first group samples, we have only 1.85 - 2.70 % of cis sites and 1.60-2.62 % of trans sites being occupied by Fe^{2+}.

The situation is more complicated with second group samples but clearly (Figs. 3b and 4) any cis/trans population ratios that one could attempt to extract would be of order 1 rather than being close to zero, again contradicting the simple model based on average cell dimensions.

3.3 Site occupation inventory

Given that Fe^{3+} and Fe^{2+} and cis and trans Fe^{2+} are resolved in first group samples and given that the total Fe is obtained by microprobe analysis, we can completely quantify the Fe site occupancies. This assumes equal recoilless fractions for all Fe sites and valance states.

Whereas the usual interpretation of the microprobe data (Table 2) would suggest that all cis sites are filled and that the small octahedral site excesses of ~ 0.03 per formula unit are due to trans-site cations, we find that there are in fact more trans-site Fe^{2+} cations than can be accounted for by the calculated octahedral excesses.

This allows one to conclude two things: (i) most trans cations are probably Fe^{2+}, and (ii) the cis sites contain a minimum number of vacancies that can be calculated as the

difference between the trans- Fe^{2+} occupation and the microprobe octahedral excess. The results are reported in Table 5 where first group samples are found to have on average, at least 0.016 cis vacancies per formula unit. The sample to sample range is **at least** 0.18 to 1.26 % of cis sites that are vacancies.

Note that point (i) above is not inconsistent with our previous conclusion (section 3.2) that Fe^{2+} does not have a preference for cis or trans sites. Other octahedral cations presumably do have a strong preference for cis sites.

4. Conclusions

QSD analysis applied to muscovite provides clear criteria of when Fe^{2+} in cis and trans sites can or cannot be resolved. In cases where it can be resolved (i.e., where the QSD is bimodal rather than unimodal, with charactristic cis and trans centroids of ~ 3.0 and ~ 2.1 mm/s, respectively), the QSD analysis gives rise to accurate cis-Fe^{2+} and trans-Fe^{2+} site populations. In a group of eight muscovite samples, such site populations clearly show that Fe^{2+} does not have a systematic preference for the larger trans sites, as previously proposed. This non-preference and the large sample to sample differences suggest that local constraints play an overriding role, compared to average unit-cell dimension effects. The quantitative Fe^{2+} site populations also allow one to demonstrate the presence of cis vacancies and to calculate minimum numbers of such vacancies.

Table 1 Location of muscovite specimens and description of Siluro-Devonian granitic host rocks of the Gander zone in New Brunswick (from Whalen, 1993).

sample	geological unit	host rock description
Group I		
G1-127	North Dungarvan River pluton	medium-grained pink subporphyric k-feldspar biotite granite
G1-173	Nashwaak pluton	medium-grained equigranular white biotite-muscovite granodiorite
G1-122	North Pole Stream suite	fine- to medium-grained white biotite muscovite granodiorite
G1-214	Tower Hill pluton	medium-grained equigranular white muscovite-biotite granite
G1-162	Lost Lake	medium-grained equigranular foliated biotite-muscovite granite
G1-19	Pokiok batholith, Allandale pluton	medium-grained equigranular pink biotite-muscovite granite
G1-30	Pokiok batholith, Skiff Lake pluton	medium- to coarse-grained, equigranular muscovite-biotite granite
G1-13	Pokiok batholith, Skiff Lake pluton	banded fine- to medium-grained equigranular pink biotite-muscovite granite
Group II		
G2-29	Pokiok batholith, Skiff Lake pluton	coarse-grained seriate biotite-muscovite granite
G2-166	Beadle Mountain pluton	medium-grained grey biotite-muscovite granite

Table 2 Chemical compositions of group I and II muscovite and corresponding structural formulae based on 20 oxygen atoms and 4 (OH, F, Cl).

sample	G1-13	G1-19	G1-122	G1-127	G1-30	G1-173	G1-214	G1-162	G2-29	G2-166
# of analyses	5	4	4	3	6	4	4	5	7	4
SiO_2	45.59	44.79	46.12	45.31	45.05	46.03	45.93	45.98	45.04	45.24
TiO_2	0.85	0.71	0.63	0.58	0.82	0.13	0.81	1.23	0.42	0.66
Al_2O_3	33.83	33.33	33.69	35.32	31.94	35.28	35.25	33.95	32.94	34.94
FeO_{tot}	3.46	3.52	3.20	2.48	4.01	1.39	1.81	1.65	4.04	1.64
Fe_2O_3	2.86	2.52	2.23	1.59	3.20	0.58	0.60	0.66	3.14	0.75
FeO	0.87	1.23	1.17	1.04	1.11	0.86	1.26	1.05	1.19	0.95
MnO	0.01	0.04	0.04	0.03	0.03	0.02	0.03	0.02	0.04	0.01
MgO	0.73	0.85	0.88	0.63	0.89	0.73	0.64	0.84	0.94	0.63
CaO	0.00	0.00	0.00	0.01	0.01	0.00	0.01	0.01	0.02	0.00
Na_2O	0.49	0.64	0.43	0.72	0.51	0.54	0.50	0.43	0.56	0.68
K_2O	10.57	11.04	11.30	10.98	10.97	11.12	10.55	11.15	10.44	10.63
H_2O	4.41	4.23	4.36	4.34	4.31	4.41	4.23	4.39	4.32	4.44
F	0.12	0.43	0.19	0.26	0.27	0.19	0.31	0.18	0.27	0.12
Cl	0.00	0.00	0.01	0.00	0.00	0.00	0.00	0.00	0.00	0.00
O=F	-0.05	-0.18	-0.08	-0.11	-0.11	-0.08	-0.13	-0.07	-0.12	-0.05
O=Cl	0.00	0.00	0.00	0.00	0.00	0.00	0.00	0.00	0.00	0.00
total	100.28	99.64	100.98	100.70	99.00	99.80	100.00	99.81	99.22	98.99
Si IV	6.096	6.067	6.142	6.032	6.148	6.148	6.111	6.159	6.111	6.096
Al IV	1.904	1.933	1.858	1.968	1.852	1.852	1.889	1.841	1.889	1.904
T site #	8.000	8.000	8.000	8.000	8.000	8.000	8.000	8.000	8.000	8.000
Al VI	3.427	3.388	3.428	3.573	3.286	3.702	3.639	3.518	3.378	3.645
Ti VI	0.085	0.072	0.063	0.058	0.084	0.013	0.081	0.124	0.043	0.066
Fe^{+3}	0.287	0.257	0.224	0.159	0.329	0.058	0.060	0.066	0.320	0.076
Fe^{+2}	0.097	0.139	0.131	0.115	0.126	0.096	0.140	0.118	0.135	0.107
Mn	0.002	0.005	0.005	0.003	0.003	0.002	0.004	0.002	0.005	0.001
Mg	0.145	0.172	0.175	0.124	0.181	0.144	0.127	0.167	0.189	0.126
O site #	4.044	4.034	4.025	4.033	4.010	4.016	4.052	3.995	4.071	4.022
Ca	0.000	0.000	0.001	0.002	0.001	0.000	0.002	0.001	0.003	0.000
Na	0.127	0.167	0.110	0.185	0.136	0.139	0.130	0.112	0.149	0.177
K	1.803	1.908	1.920	1.864	1.910	1.895	1.790	1.906	1.807	1.827
A site #	1.931	2.075	2.030	2.051	2.047	2.035	1.922	2.019	1.958	2.004
O	20.000	20.000	20.000	20.000	20.000	20.000	20.117	19.999	20.000	20.000
OH	3.947	3.814	3.918	3.890	3.885	3.920	3.752	3.927	3.882	3.948
F	0.052	0.186	0.080	0.109	0.114	0.080	0.131	0.074	0.118	0.052
Cl	0.000	0.000	0.001	0.001	0.000	0.000	0.001	0.000	0.001	0.000
Charge	0.000	0.000	0.000	0.000	0.000	0.000	-0.117	0.001	0.000	0.000

Table 3. Cell refinements of representative specimens from group I and II muscovite.

sample	a (Å)	b (Å)	c (Å)	β (degrees)	cell vol. (Å^3)
G1-13	5.193(4)*	9.014(1)	20.01(2)	95.68(9)	935.7(1)
G1-173	5.189(2)	9.000(3)	20.068(7)	95.72(4)	932.5(4)
G1-19	5.200(1)	9.028(3)	20.059(5)	95.83(3)	936.9(4)
G1-127	5.190(6)	9.017(1)	20.03(2)	95.8(1)	932.3(2)
G2-29	5.189(3)	9.015(6)	20.07(2)	95.61(8)	934.2(9)
G2-166	5.188(2)	9.014(3)	20.077(6)	95.81(3)	934.1(4)

*Numbers in parantheses are standard errors and refer to the last digit.

Table 4. Mössbauer fitting parameters for $2M_1$ muscovite spectra[a]

Sample BG	Site	δ_0 (mm/s)	δ_1 (mm/s)	Δ (mm/s)	$\sigma\Delta$ (mm/s)	Fe^{+3}/Fe_{tot}	$Fe^{+2}c/t$	χ^2_{red}
G1-30	[3+]-1			1.1[f]	1.566			
	[3+]-2	0.345	0.0[f]	0.744	0.401			
	[2+]-I			3.012	0.206			
3775060	[2+]-2	1.174	-0.012	2.154	0.296	0.722	1.414	1.226
G1- 173	[3+]-1			1.1[f]	1.341			
	[3+]-2	0.297	0.0[f]	0.782	0.406			
	[2+]-1			3.01	0.192			
5037258	[2+]-2	1.174	-0.012	2.072	0.267	0.377	1.563	1.164
G1-162	[3+]-1			1.1[f]	1.197			
	[3+]-2	0.313	0.0[f]	0.811	0.329			
	[2+]-1			2.975	0.205			
3856816	[2+]-2	1.206	-0.023	2.118	0.302	0.36	1.594	1.14
G1-13	[3+]-1			1.1[f]	1.708			
	[3+]-2	0.349	0.0[f]	0.740	0.434			
	[2+]-1			3.027	0.195			
2346961	[2+]-2	1.108	0.008	2.104	0.236	0.750	1.678	0.982
G1-122	[3+]-1			1.1[f]	1.470			
	[3+]-2	0.343	0.0[f]	0.762	0.414			
	[2+]-1			3.015	0.188			
2659624	[2+]-2	1.167	-0.011	2.101	0.293	0.631	1.811	0.912
G1-127	[3+]-1			1.1[f]	1.449			
	[3+]-2	0.336	0.0[f]	0.757	0.407			
	[2+]-1			3.013	0.195			
4320052	[2+]-2	1.193	-0.018	2.126	0.306	0.580	1.845	1.198
G1-19	[3+]-1			1.1[f]	1.439			
	[3+]-2	0.355	0.0[f]	0.733	0.374			
	[2+]-1			3.023	0.193			
4564418	[2+]-2	1.203	-0.021	2.124	0.313	0.649	1.992	1.294
G1-214	[3+]-1			1.1[f]	1.421			
	[3+]-2	0.316	0.0[f]	0.760	0.410			
	[2+]-I			3.020	0.177			
3944602	[2+]-2	1.207	-0.022	2.073	0.327	0.302	3.366	1.218
G2-166	[3+]-I			1.1[f]	1.402			
	[3+]-2	0.283	0.0[f]	0.813	0.498			
	[2+]-I			2.905	0.260			
3626417	[2+]-2	1.108	0.012	2.183	0.335	0.416	ud[b]	1.130
G2-29	[3+]-I			1.1[f]	1.582			
	[3+]-2	0.350	0.0[f]	0.751	0.417			
	[2+]-1			2.989	0.245			
2172703	[2+]-2	1.124	0.004	2.315	0.354	0.703	ud[b]	1.082

[a] All fits impose a Lorentzian FWHM = 0.2 mm/s and symmetric elemental doublets (h-/h+=1).

[b] undeterminable.

[f] This parameter was frozen during fitting.

Table 5. Minimum calculated vacancies (per formula unit) in cis site of group I muscovite.

sample	Fe^{2+} cis/trans	Fe^{2+} trans[a]	Fe^{2+} cis[a]	cations in trans[b]	vacancy in cis[c]
G1-30	1.414	0.052	0.074	0.010	0.042
G1-173	1.563	0.038	0.059	0.016	0.022
G1-162	1.594	0.045	0.072	-0.005	0.051
G1-13	1.678	0.036	0.061	0.044	-0.008
G1-122	1.811	0.047	0.084	0.025	0.022
G1-127	1.845	0.041	0.075	0.033	0.007
G1-19	1.993	0.047	0.093	0.034	0.013
G1-214	3.366	0.032	0.108	0.052	-0.020

[a] per formula unit, based on 20 oxygens and 4(OH, F, Cl) anions.

[b] octahedral cis-excess from structural formula calculations (Table 2), per formula unit, based on 20 oxygens and 4(OH, F, Cl) anions.

[c] calculated minimum cis vacancies, from structural formula excess and Fe populations, per formula unit, based on 20 oxygens and 4(OH, F, Cl) anions, (negative values suggest absence of vacancies).

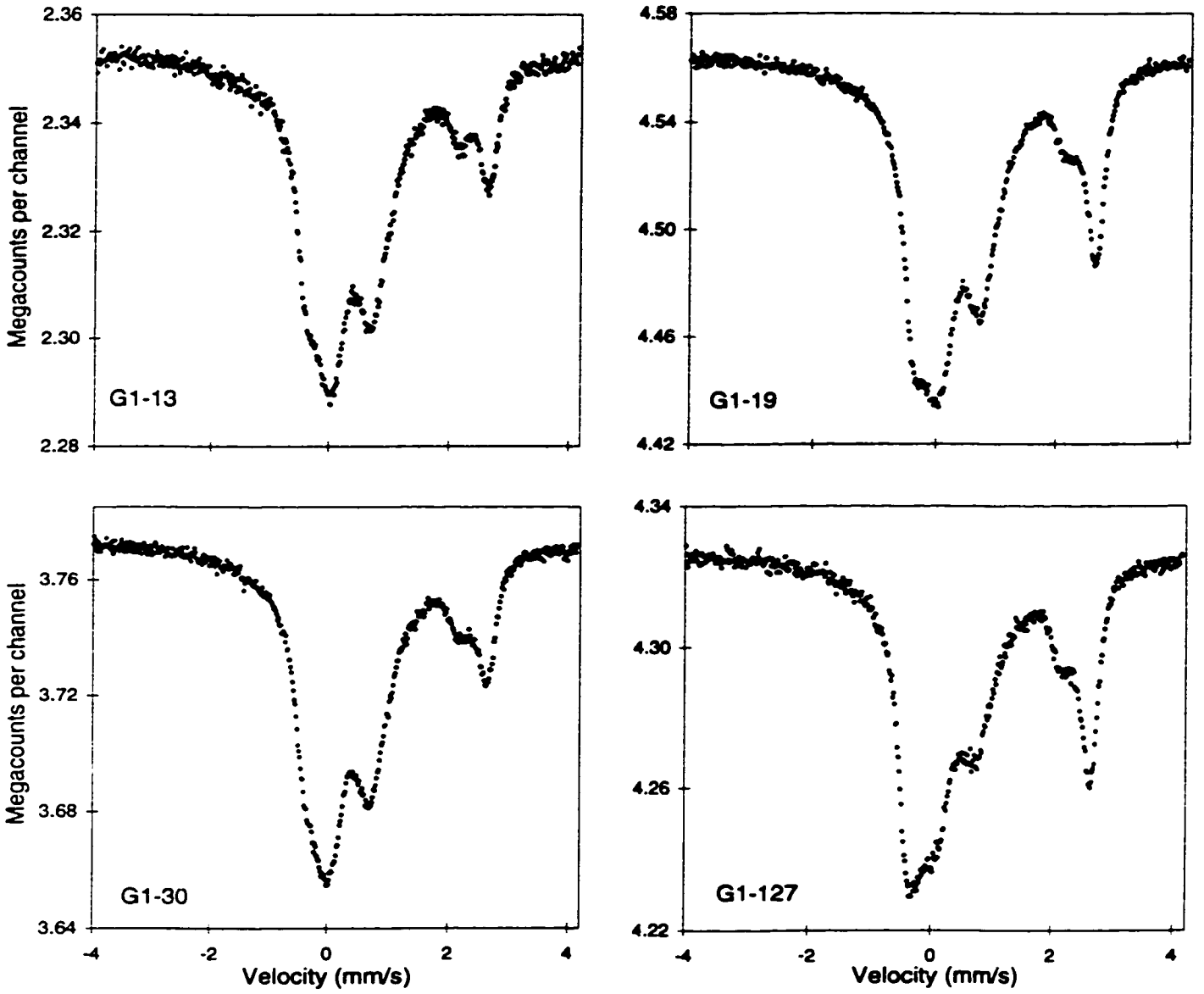

Fig. 1 Folded RT Mössbauer spectra of all muscovite specimens described in Table 1. G1 are the first group samples having well resolved cis and trans Fe^{2+} contributions whereas G2 are second group samples having unresolved cis and trans Fe^{2+} contributions.

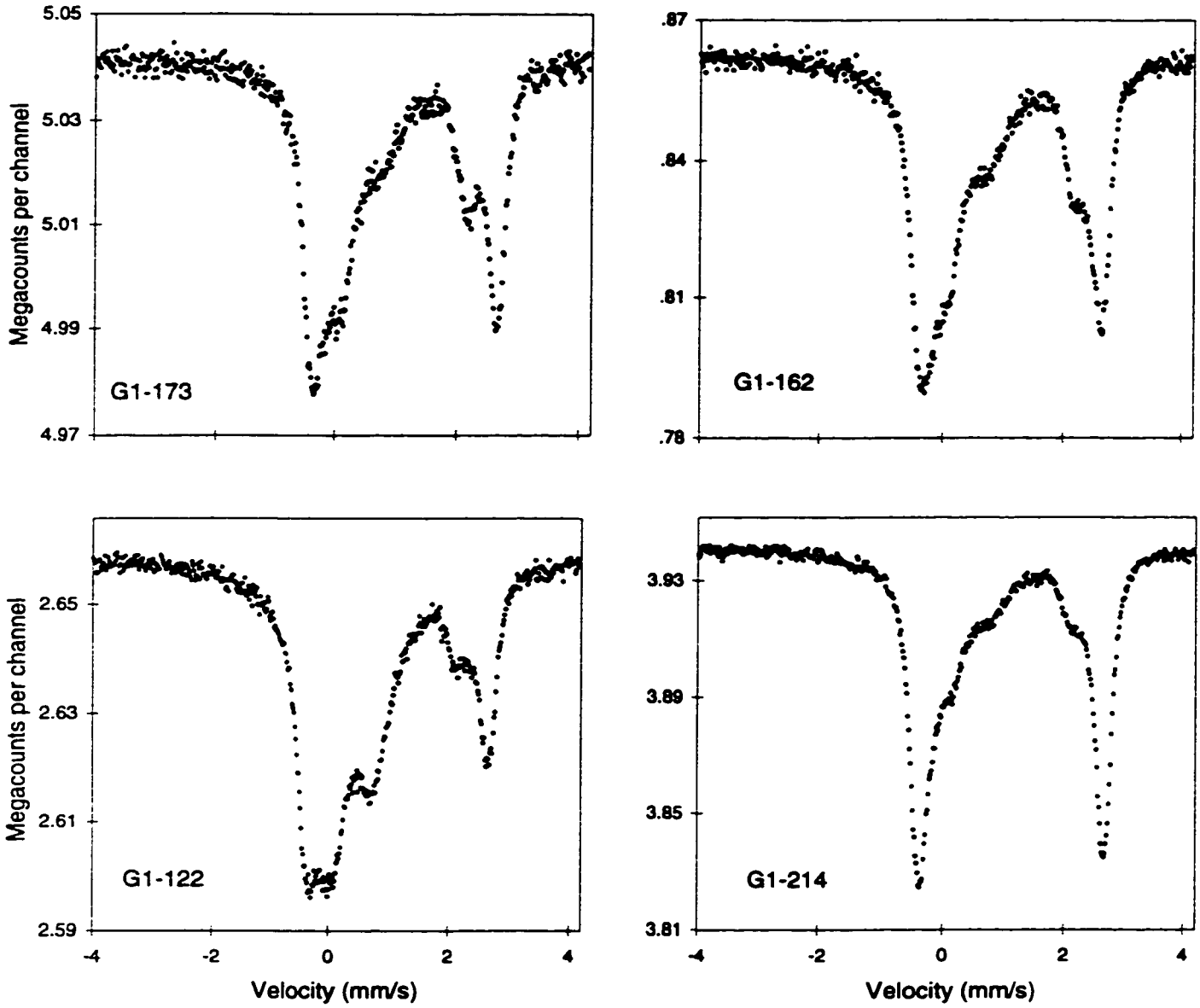

Group I

Continued Fig. 1

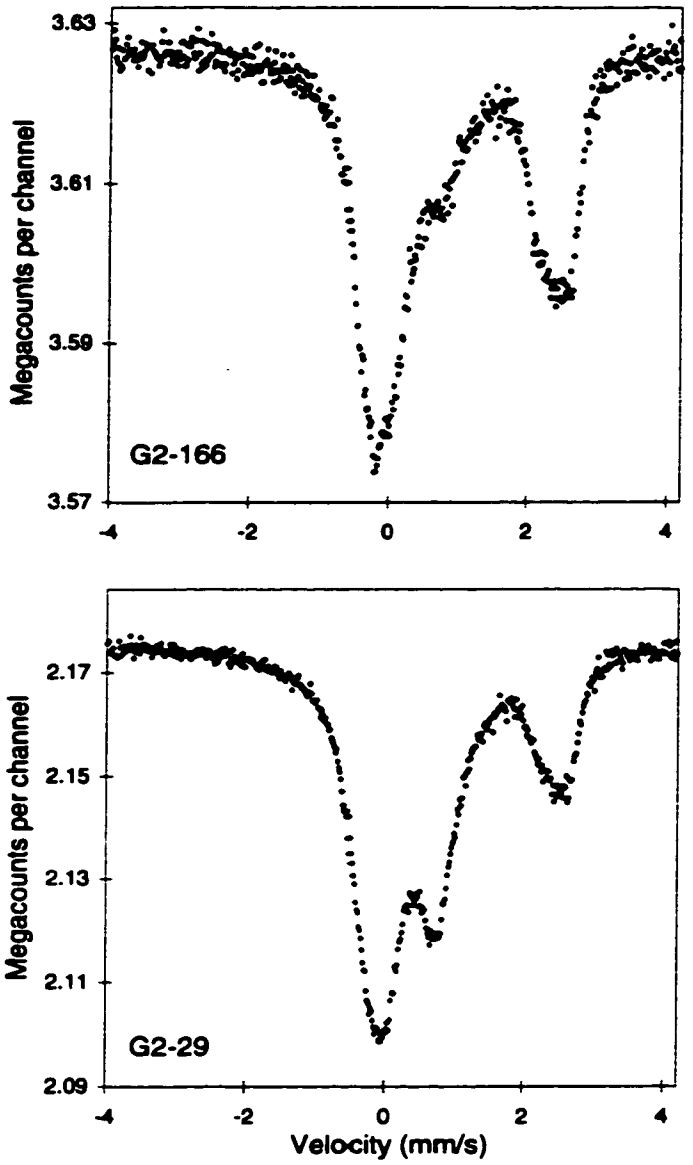

Group II

Continued Fig. 1

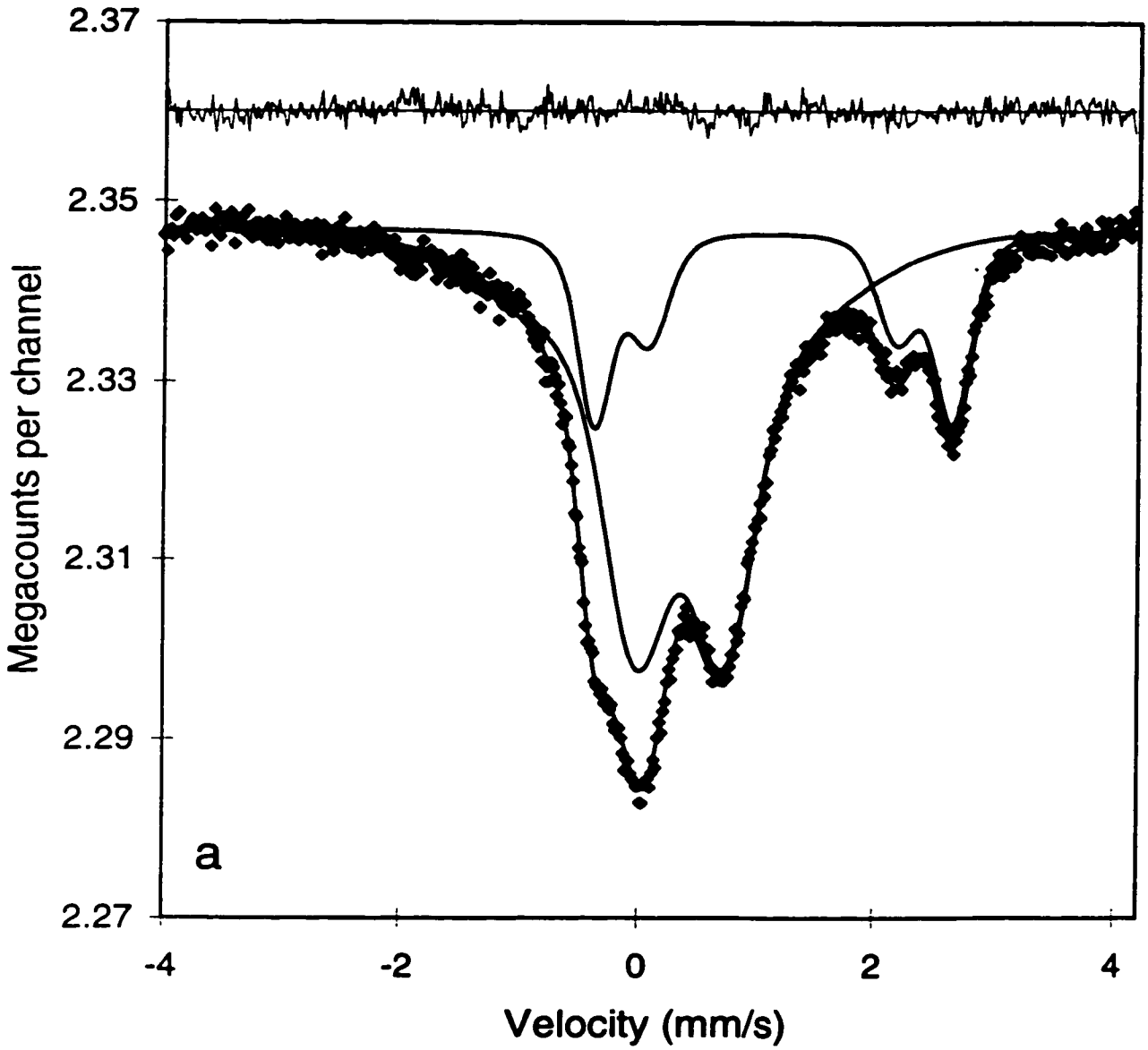

Figure 2 (a-b) Typical Voigt-based QSD fits of the RT Mössbauer spectra of samples G-13 (a) and G-29(b), representative of groups I and II. The solid line joining the data points of the spectrum is the fit result. Other solid line show the separate contributions from Fe^{3+} and Fe^{2+}. The difference spectra (or residuals) are shown with the same vertical scales as the respective spectra.

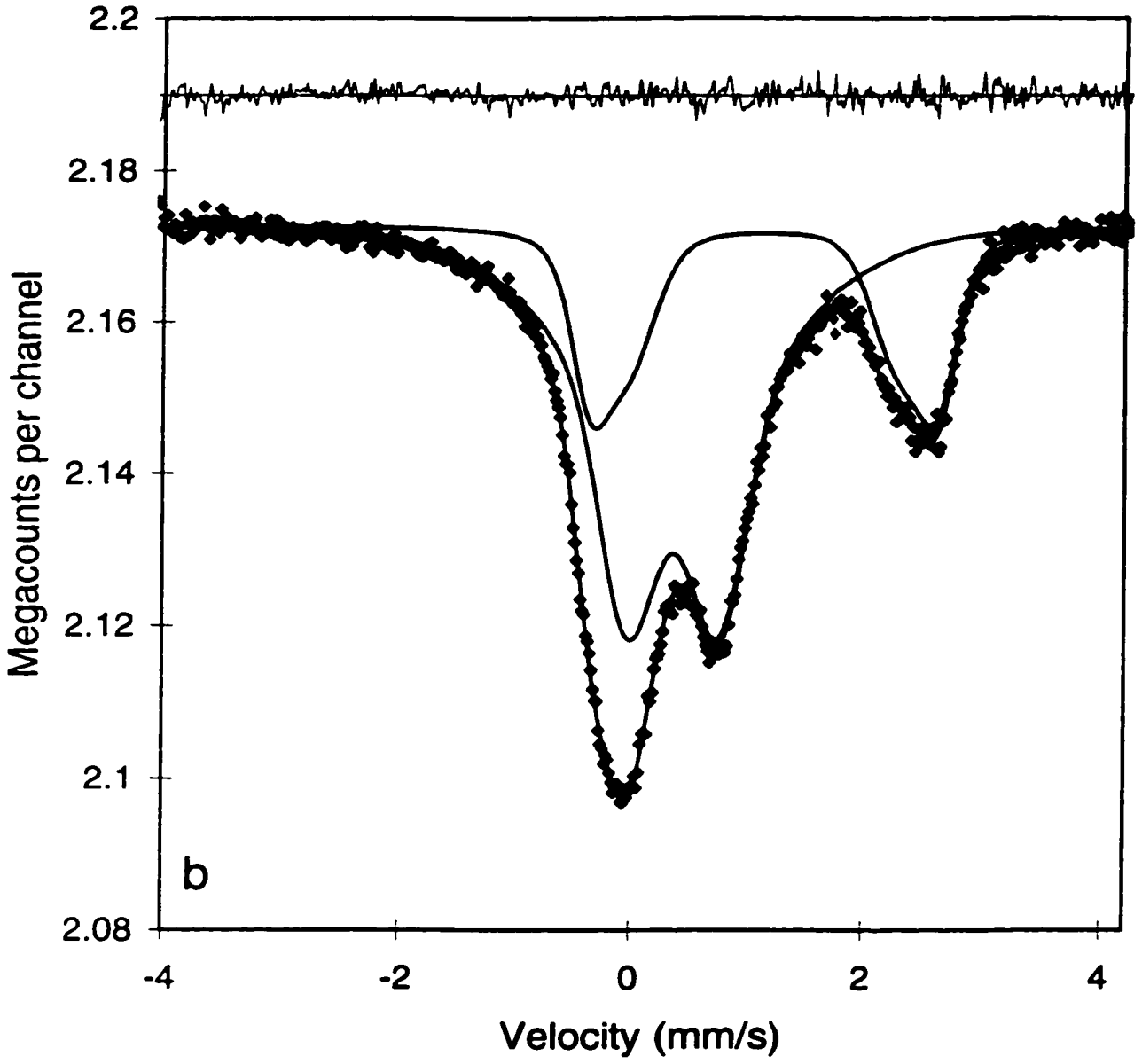
2.2
2.18
2.16
2.14
2.12
2.1
2.08
Megacounts per channel
b
-4
-2
0
2
4
Velocity (mm/s)

Figure 2(b).

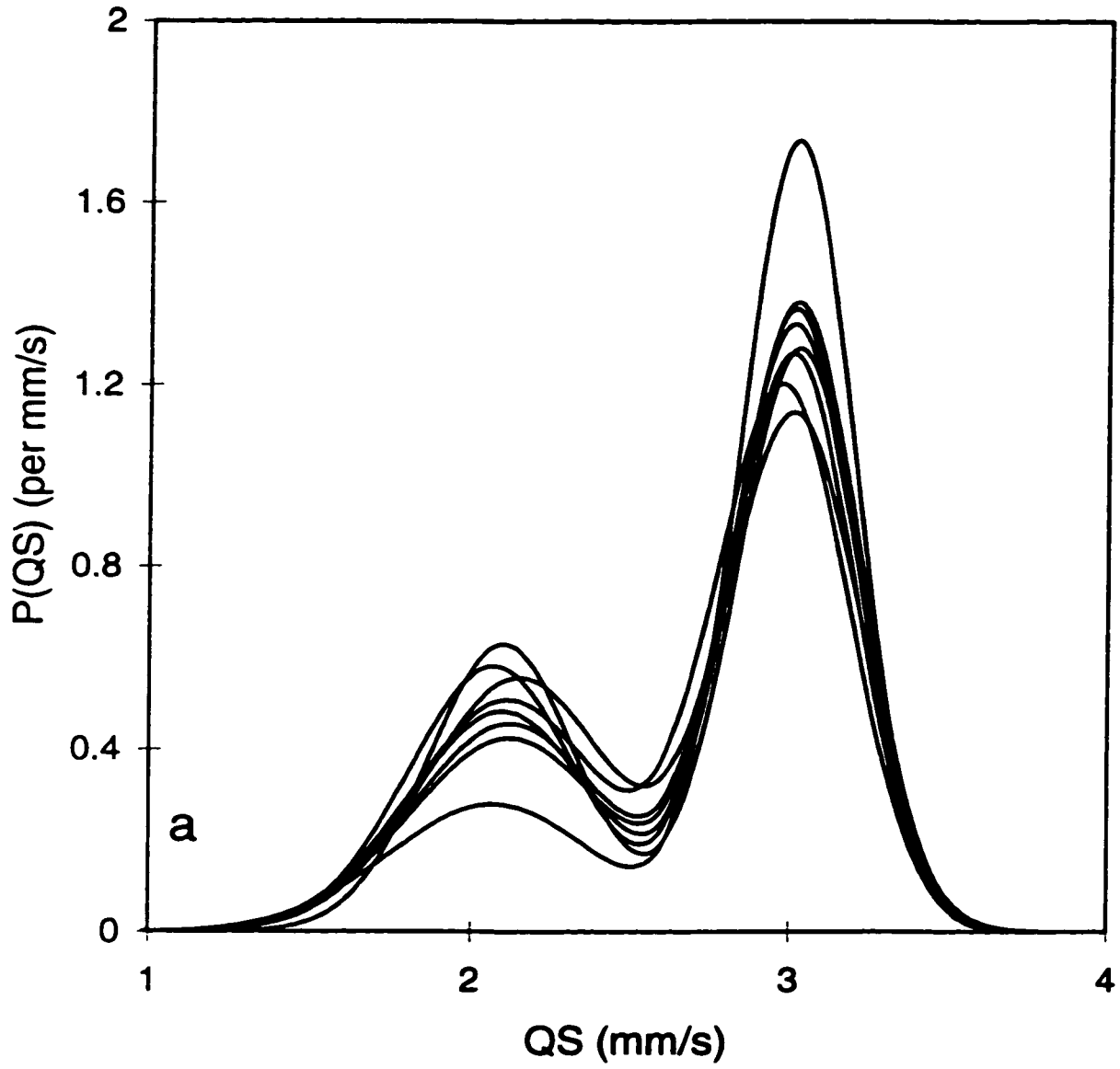

Figure 3 (a-b) Fe^{2+} QSDs from fits of the room temperature spectra of group I (a) and group II (b) muscovite specimens. The corresponding fit parameters are given in Table 4.

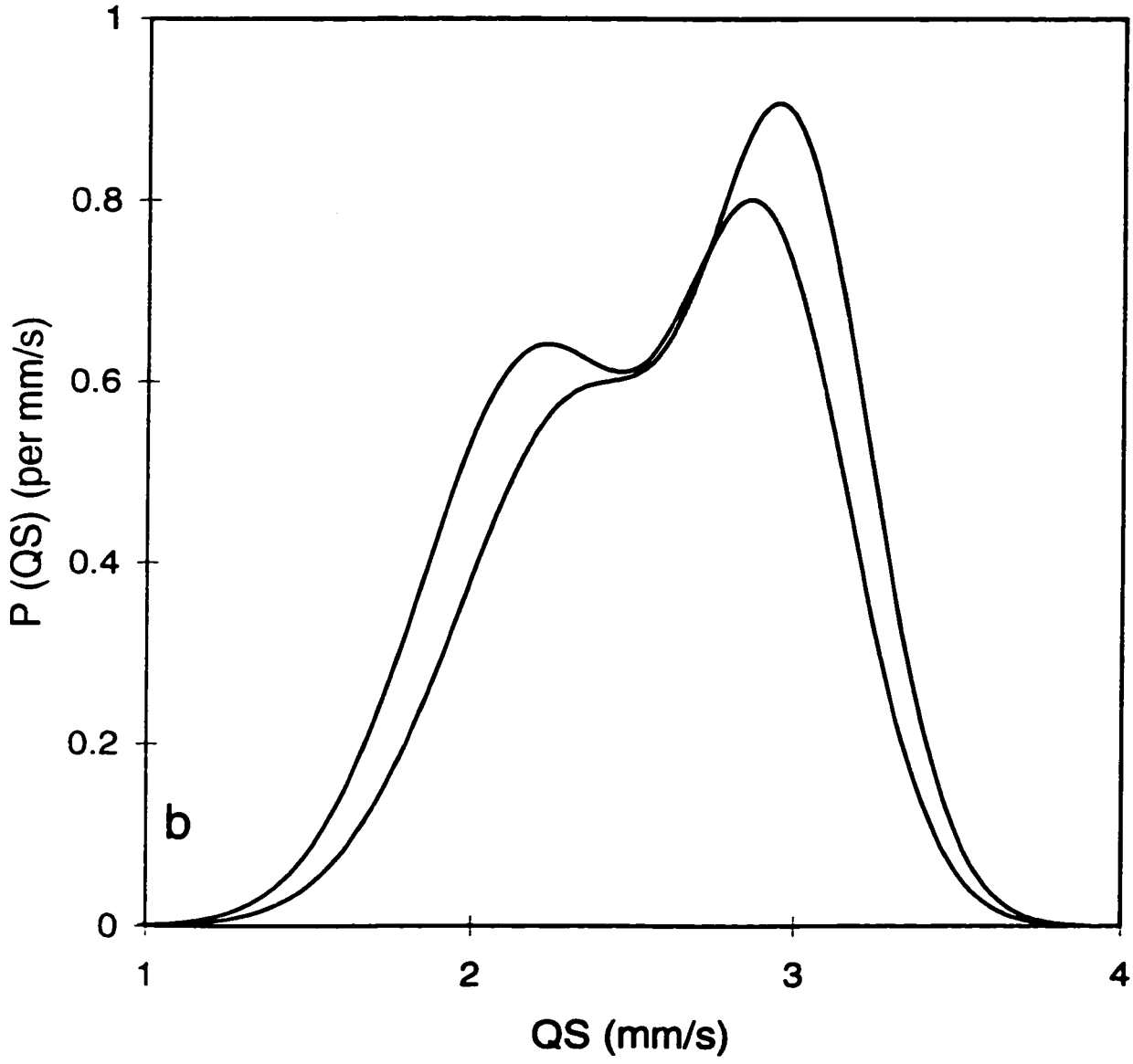

Figure 3(b).

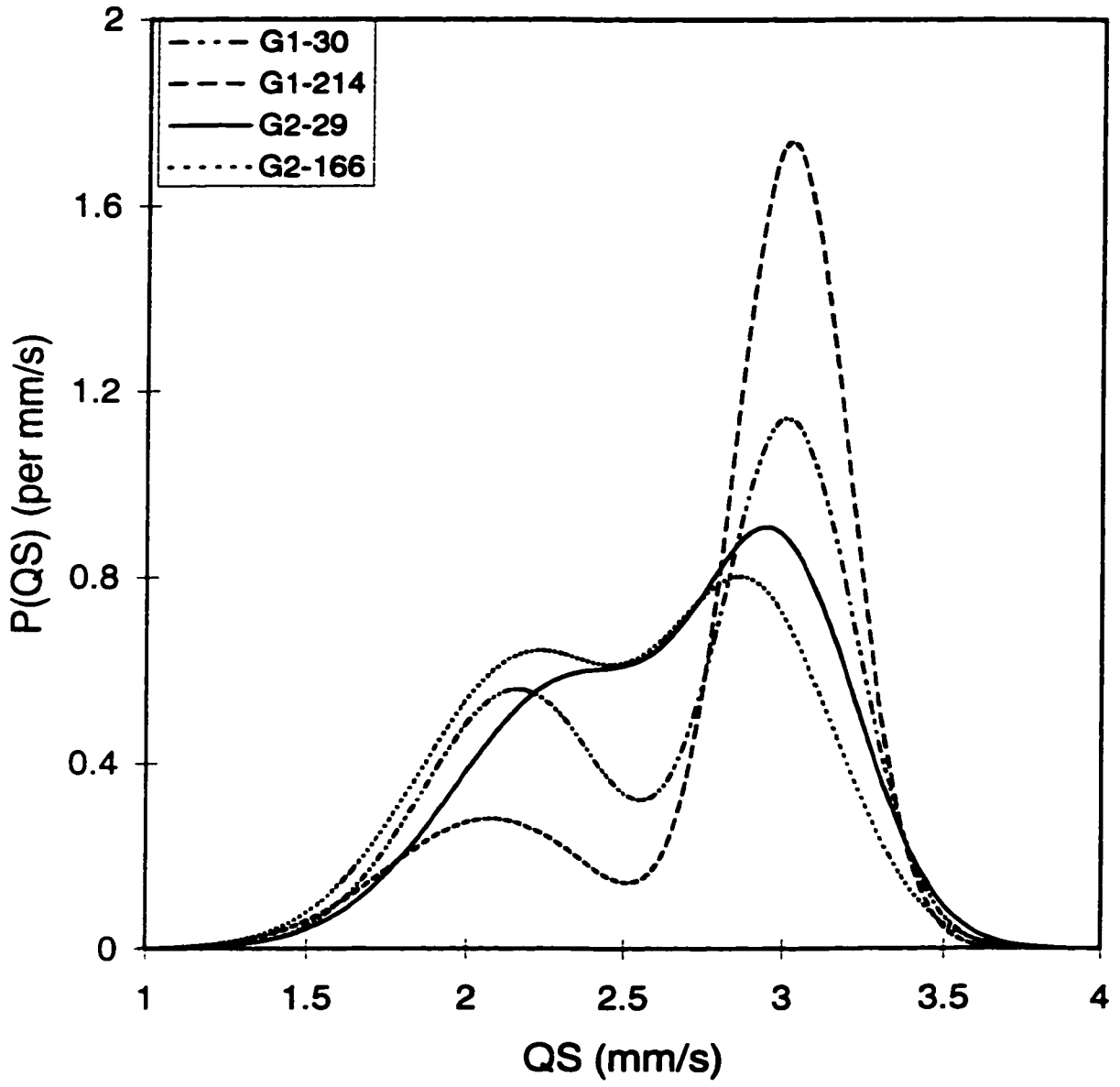

Figure 4 Comparison of representative Fe^{2+} QSDs from fits to the RT spectra of group I and group II muscovite (maximum and minimum range of cis/trans site ratios shown).

Conclusions and Suggestions for Future Research

The conclusions of this thesis, which consists of three individual manuscripts, are based on an investigation of a large number of specimens of micas from the Paleozoic granitic rocks of the Humber, Dunnage, Gander, Avalon and Meguma zones of the Canadian Appalachians by wavelength-dispersive X-ray microanalyses, X-ray powder diffractometry and ^{57}Fe Mössbauer spectroscopy.

In the first manuscript, the most pronounced biotite compositional variations observed in biotite from granitic rocks of the Canadian Appalachians are total Al-contents and Fe/(Fe+Mg) values. Both compositional variations are sensitive indicators of conditions that prevailed in the host magmas. For instance, biotite from A-type granites (Humber, Dunnage and Avalon zones in New Brunswick) is distinctly depleted in aluminium and enriched in total iron, consistent with the petrological and geochemical data. Biotite from granites derived from a mixture of supracrustal and mantle-derived source components (Gander zone), shows a pronounced trend of increasing total Al, confirming significant contributions from aluminous supracrustal material, either by assimilation or anatexis. Biotite from granite derived entirely from crustal material (Meguma zone), shows a remarkable increase in both total Al and Fe, approaching the siderophyllite end-member. These examples show that the composition of biotite can help to discriminate granites of different petrogenetic origins.

However, the major-element composition of biotite from these rocks is probably not a suitable indicator of tectonic origin since all granites of the Canadian Appalachians are

believed to result from lithospheric delamination. An alternative tectonic model has recently been proposed by van Staal et al. (1998) and this may cause us to re-evaluate our present interpretation.

Our results show that the major element composition of biotite can serve as one tool amongst others for the interpretation of tectonic origin (e.g., Lameyre and Bowden 1982, Pitcher 1983, Pearce et al. 1984, Batchelor and Bowden 1985, Maniar and Piccoli 1989) but that none of these methods are infallible and none should be employed in isolation. We therefore believe that biotite chemistry can be useful if coupled with other geochemical parameters, such as whole-rock composition, trace-element composition, isotopic data, field and other geological constraints.

In the second manuscript, the Mössbauer spectra of a large number of natural biotite specimens was described in terms of QSDs which are related to population distributions of local distortion environments (LDEs). We established the possible range of Fe^{2+} QSDs in biotite and key limiting characteristics of the QSDs in all biotites. The measured characteristic features of Fe^{2+} QSDs and the QSDs themselves suggest that spectra from all natural biotite and phlogopite fall within the continuum of QSD shapes.

We found that Fe/(Fe+Mg) and Fe^{3+}/Fe, which are the key crystal-chemical parameters in the synthetic phlogopite-biotite-annite solid solution, do not correlate with any of the QSD features of natural biotite, whereas Al_{total}, which is related to several crystal chemical features, does. A more detailed interpretation of the QSD shapes is limited primarily by the lack of electronic structure calculations linking LDEs to QS values.

In the third manuscript, QSD analysis applied to muscovite specimens provides clear criteria of when cis and trans sites can or cannot be resolved. In cases where they can be resolved (i.e., where the QSD is bimodal rather than unimodal, with charactristic cis and trans centroids of ~3.0 and ~2.1 mm/s, respectively), the QSD analysis gives rise to accurate cis-Fe^{2+} and trans-Fe^{2+} site populations. In a group of eight muscovite samples, such site populations clearly show that Fe^{2+} does not have a systematic preference for the larger trans sites, as previously proposed. This non-preference and the large sample to sample differences suggest that local constraints play an overriding role, compared to average-cell site dimension effects. The quantitative Fe^{2+} site populations also allow one to demonstrate the presence of cis vacancies and to calculate the minimum numbers of such vacancies.

This study has identified several possible areas of future research which could contribute to our understanding of the crystal structure and crystal chemistry of true micas. For instance, in the first manuscript of the thesis, in addition to documenting the major element chemistry of biotite, a study of trace elements in biotite could also provide a discriminating tool for identifying the nature or even tectonic environments of granites.

In the second manuscript, we described the octahedral Fe^{3+} QSDs of natural biotite specimens as a starting point that needs to be explored separately for future work. Also crystallographic data such as cell volume, average cell parameters and particularly powder X-ray diffraction linewidths and shapes when combined with Mössbauer spectroscopy and chemical data could contribute to a better understanding of QSDs.

In the third manuscript, a single crystal X-ray study of muscovite could provide information about the lattice structures of two group of muscovites identified by Mössbauer spectroscopy.

Note added in proof

After the submission of this thesis, we continued our study on the quadrupole splitting distributions of trioctahedral micas by performing powder X-ray diffractometry on a number of biotite specimens from the Appalachian granitic rocks to obtain crystallographic data such as cell volume, average cell parameters, powder X-ray diffraction linewidths and shapes for a better understanding of QSDs. In the majority (17 out of 20 specimens) of X-ray diffractograms of the biotite specimens studied so far, we recognized reflection peaks corresponding to chlorite, an alteration product interleaved with biotite. Quantitative determination of the chlorite contribution to the Fe^{2+} QSDs of biotite is now being investigated. So far we do not know the quantitative effect of the chlorite contribution to the QSD shapes and parameters.

References

Abdel-Rahman, A. M. (1994) Nature of biotites from alkaline, calc-alkaline, and peraluminous magmas. Journal of Petrology, 35, 525-541.

Ague, J. J., and Brimhall, G. H. (1988) Regional variations in bulk chemistry, mineralogy and the compositions of mafic and accessory minerals in the batholiths of California. Geological Society of America Bulletin, 100, 891-911.

Allan, B. (1980) Occurrence and origin of garnet in the South Mountain batholith, Nova Scotia. B.Sc. thesis, Dalhousie University, Nova Scotia, Canada.

Amonette, J. E., and Scott, A. D. (1991) Determination of ferrous iron in non-refractory silicate minerals-1. An improved semi-micro oxidimetric method. Chemical Geology, 92, 329-338.

Annersten, H. (1974) Mössbauer studies of natural biotites. American Mineralogist, 59, 143-151.

Annersten, H. (1975) Mössbauer study of iron in natural and synthetic biotites. Fortschritte der Mineralogie, 52, 583-590.

Annersten, H., and Halenius, U. (1976) Ion distribution in pink muscovite, a discussion. American Mineralogist, 61, 1045-1050.

Appleman, D. E., and Evans, H. T. Jr. (1973) Job 9214: indexing and least-squares refinement of powder diffraction data. United States Geological Survey, computer contribution 20.

Bailey, S. W. (1984) Micas, Reviews in Mineralogy, Mineralogical Society of America, volume 13, p. 574.

Bancroft, G. M., and Brown, J. R. (1975) A Mössbauer study of coexisting hornblendes and biotites: Quantitative Fe^{3+}/Fe^{2+} ratios. American Mineralogist, 60, 265-272.

Barrière, M., and Cotten, J. (1979) Biotites and associated minerals as markers of magmatic fractionation and deuteric equilibration in granites. Contributions to Mineralogy and Petrology, 70, 183-192.

Batchelor, R. A., and Bowden, P. (1985) Petrogenetic interpretation of granitoid rock series using multicationic parameters. Chemical Geology, 48, 43-55.

Bennett, V. W. (1990) Mineralogy and chemistry of biotite and muscovite from the granitoid rocks of the Bay D'Espoir area, Newfoundland. B.Sc. thesis, Memorial University, Newfoundland, Canada.

Bowen, L. H., Weed, S. B., and Stevens, J. G. (1969) Mössbauer study of micas and their potassium-depleted products, American Mineralogist, 54, 72-84.

Brigatti, M. F., and Davoli, P. (1990) Crystal structure refinements of 1M plutonic biotite. American Mineralogist, 75, 305-313.

Burkhard, D. J. M. (1993) Biotite crystallization temperatures and redox states in granitic rocks as indicators for tectonic setting. Geologie en Mijnbouw, 71, 337-349.

Chappell, B. W., and White, A. J. R. (1974) Two contrasting granite types. Pacific Geology, 8, 173-174.

Christie, I. A. D., Rancourt, D. G., Kodama, H., Murad, E., and Robert, J. L. (1993) Oxidation of synthetic annite mica characterized by ^{57}Fe Mössbauer spectroscopy: hydrogen de-intercalation and host layer valence state populations. In: Fisher, J. E., Bernier, P., Roth, S. and Solin, S. A. (eds.) Chemical physics of intercalation II, 387-391. Plenum, New York.

Clarke, D. B., and Muecke, G. K. (1985) Review of the petrochemistry and origin of the South Mountain batholith and associated plutons, Nova Scotia, Canada. In: High heat production (HHP) granites, hydrothermal circulation and ore genesis. Institute of Mineralogy and Metallurgy, London, 41-55.

Clarke, D. B., MacDonald, M. A. and Tate, M. C. (1997) Late Devonian mafic-felsic magmatism in Meguma zone, Nova Scotia. in: A. K. Sinha, J. B., Whalen, and J. Hogan (eds.), The Nature of Magmatism in the Appalachian Orogen, Geological Society of America, Memoir 191, 107-127.

Currie, K. L. (1995) Plutonic rocks, Chapter 8 in: Geology of the Appalachian-Caledonian orogen in Canada and Greenland, H. Williams (ed.). Geological Survey of Canada, Geology of Canada, no. 6, 629-680. (also Geological Society of America, The Geology of North America, v. F-1).

Currie, K. L., and Whalen, J. B. (1994) A note on the occurrence of beryl in the Port Mouton pluton, southwestern Nova Scotia. In: Current Research 1994-D; Geological Survey of Canada, 73-77.

Czamanske, G. K., Ishihara, S., and Atkin, S. A. (1981) Chemistry of rock-forming minerals of the Cretaceous-Paleocene batholith in southwestern Japan and implications for magma genesis. Journal of Geophysical Research, 86, No. B11, 10431-10469.

Debon, F., and Le Fort, P. (1982) A chemical-mineralogical classification of common plutonic rock associations. Transactions of the Royal Society of Edinburgh, Earth Sciences, 73, 135-149.

Deer, W. A., Howie, R. A., and Zussman, J. (1962) Rock-forming minerals. 3. Sheet Silicates. Longmans, London.

de Albuquerque, C. A. R. (1973) Geochemistry of biotites from granitic rocks, northern Portugal. Geochimica et Cosmochimica Acta, 37, 1779-1802.

De Pieri, R., and Jobstraibizer, P. G. (1977) On some biotites from Adamello massif, northern Italy. Neues Jahrbuch für Mineralogie Monatshefte, 1977, 15-24.

De Pieri, R. and Jobstraibizer, P. G. (1983) Crystal chemistry of biotites from dioritic to granodioritic rock-types of Adamello massif, northern Italy, Neues Jahrbuch für Mineralogie Abhandlungen, 148, 58-82.

Ding, Y. (1995) AFM minerals in the Halifax pluton, Nova Scotia, Canada. M.Sc. thesis, Dalhousie University, Halifax, Nova Scotia, Canada.

Dodge, F. C. W., Smith, V. C., and Mays, R. E. (1969) Biotites from granitic rocks of the central Sierra Nevada batholith, California. Journal of Petrology, 10, 250-271.

Douma, S. (1988) The mineralogy, petrology, and geochemistry of the Port Mouton pluton, Nova Scotia, Canada. M.Sc. thesis, Dalhousie University, Halifax, Nova Scotia, Canada.

Dunning, G. R., O' Brien, S. J., Colman-Sadd, S. P., Blackwood, R. F., Dickson, W. L., O'Neill, P., and Krogh, T. E. (1990) Silurian orogeny in the Newfoundland Appalachians. Journal of Geology, 98, 895-913.

Dyar, M. D., and Burns, R. G. (1986) Mössbauer spectral study of ferruginous one-layer trioctahedral micas. American Mineralogist. 71, 955-965.

Dyar, M. D. (1987) A review of Mössbauer data on trioctahedral micas: Evidence for tetrahedral Fe^{3+} and cation ordering. American Mineralogist, 72, 102-112.

Dyar, M. D. (1990) Mössbauer spectra of biotite from metapelites. American Mineralogist. 75, 656-666.

Ferrow, E. (1987) Mössbauer effect and X-ray diffraction studies of synthetic iron bearing trioctahedral micas. Physics and Chemistry of Minerals 14, 276-280.

Finch, J., Gainsford, A. R., and Tennant, W. C. (1982) Polarized optical absorption and ^{57}Fe Mössbauer study of pegmatitic muscovite, American Mineralogist, 67, 59-68.

Fyffe, L. R., and Fricker, A. (1987) Tectonostratigraphic terrane analysis of New Brunswick. Maritime Sediments and Atlantic Geology, 23, 113-122.

Goodman, B. A. (1976) The Mössbauer spectrum of a ferrian muscovite and its implications in the assignment of sites in dioctahedral micas, Mineralogical Magazine, 40, 513-517.

Haggstrom, L., Wappling, R., and Annersten, H. (1969) Mössbauer study of iron-rich biotites. Chemical Physics Letters, 4, 107-108.

Ham, L. J. (1988) The mineralogy, petrology, and geochemistry of the Halfway Cove-Queensport pluton, Nova Scotia, Canada. M.Sc. thesis, Dalhousie University, Halifax, Nova Scotia, Canada.

Haslam, H. W. (1968) The crystallization of intermediate and acid magmas at Ben Nevis, Scotland. Journal of Petrology, 9, 84-104.

Hazen, R. M., and Wones, D. R. (1972) The effect of cation substitution on the physical properties of trioctahedral micas. American Mineralogist, 57, 103-129.

Hazen, R. M., and Burnham, C. W. (1973) The crystal structure one-layer phlogopite and annite. American Mineralogist, 58, 889-900.

Hecht, L. (1994a) The chemical composition of biotite as an indicator of magmatic fractionation and metasomatism in Sn-Specialized granites of the Fichtelgebirge (NW Bohemian Massif, Germany). In: Metallogeny of collisional orogens, Proceedings of the IAGOD Erzgebirge Meeting, Geyer, june 4-6, 1993. (eds.) R. Seltmann et al. Prague, Czech Geological Survey, 1994, 295-300.

Hecht, L. (1994b) Biotites as petrogenetic indicators in Hercynian granites of the Fichtelgebirge (NW Bohemian Massif, Germany). In: Abstract of the 16th General Meeting of the International Mineralogical Association, STMP at University of Pisa, September 4-9, 1994, p.171.

Heller-Kallai, L., and Rozenson, I. (1981) The use of Mössbauer spectroscopy of iron in clay mineralogy. Physics and Chemistry of Minerals 7, 223-238.

Hill, J. D. (1991) Petrology, tectonic setting, and economic potential of Devonian peraluminous granitoid plutons in the Canso and Forest Hill areas, eastern Meguma terrane, Nova Scotia. Geological Survey of Canada, Bulletin 383.

Hogg, C. S., and Meads, R. E. (1970) The Mössbauer spectra of several micas and related minerals. Mineralogical Magazine, 37, 606-614.

Hogg, C. S. (1975) A Mössbauer study of thermal decomposition of biotites. Mineralogical Magazine, 40, 79-88.

Ishihara, S. (1977) The magnetite-series and ilmenite-series granitic rocks. Mining Geology, 27, 293-305.

Ishihara, S. (1981) The granitoid series and mineralization. Economic Geology, 75th Anniversary volume, 458-484.

Ivanitskiy, V. P., Kalinichenko, A. M., Matyash, I. V., and Ihanyak, T. P. (1975a) Mössbauer and PMR studies of oxidation and dehydroxylation in biotite. Geokhimiya, 12, 1864-1871.

Ivanitskiy, V. P., Matyash, I. V., and Rakovich, F. I. (1975b) Effects of irridation on the Mössbauer spectra of biotites. Geochemistry International, 12, 151-157, from Geokhimiya, 6, 850-856.

Ivanitskiy, V. P., Kalinichenko, A. M., Matyash, I. V., Kudelya, V. K., Zayats, A. P., and Shvets, D. I. (1977) On the influence of gamma-radiation upon processes of oxidation, dehydroxylation and magnetic properties of some alumosilicates (in Russian). Geokhimia, 8, 237-245.

Kabesh, M. L., and Refaat, A. M. (1972) The chemical composition of biotites as a guide to the petrogenesis of granitic rocks of Wadi El Mellaha, Northern Eastern Desert, Egypt. Neues Jahrbuch für Mineralogie Abhandlungen, 117, 85-95.

Kabesh, M. L., and Ragab, A. I. (1974) The chemistry of biotites as a guide to the evolution trends of El Atawi granitic rocks, Eastern Desert, Egypt. Neues Jahrbuch für Mineralogie Monatshefte, 1974, 307-316.

Kabesh, M. L., Aly, M. M., and Refaat, A. M. (1975) On the chemistry of biotites and variation of ferrous/ferric ratios in granitic rocks of Umm Naggat stock, Egypt. Neues Jahrbuch für Mineralogie Abhandlungen, 124, 47-60.

Kabesh, M. L., and Aly, M. M. (1980) The chemistry of biotites as a guide to the petrogenesis of some Precambrian granitic rocks, Yemen Arab Republic. Chemie Erde, 39, 313-324.

Keen, C. E., Keen, M. J., Nichols, B., Reid, I., Stockmal, G. S., Colman-Sadd, S. P., O'Brien, S. J., Miller, H., Quinlan, Q., Williams, H., and Wright, J. (1986) A deep seismic reflection profile across the northern Appalachians. Geology, 14, 141-145.

Kerr, A., Dickson, W. L., Colman-Sadd, S. P., Fryer, B. J. and Jenner, G. (1992) Paleozoic granites and orogenic evolution in the Newfoundland Appalachians: A new type area for Caledonian magmatism. Geological Association of Canada, Program with Abstracts. 17, A45.

Kerr, A., Dickson, W. L., Hayes, J. P., and Fryer, B. J. (1993) Devonian postorogenic granites on the southern margin of the Newfoundland Appalachians: A review of geology, geochemistry, petrogenesis and mineral potential, Newfoundland Department of Mines and Energy. Geological Survey Branch Report 93-1, 239-279.

Kerr, A., Jenner, G. A., and Fryer, B. J. (1995) Sm-Nd isotopic geochemistry of Precambrian to Paleozoic granites and the deep-crustal structure of the southeast margin of the Newfoundland Appalachians. Canadian Journal of Earth Sciences, 32, 224-245.

Kerr, A. (1997) Space-time-composition relationships amongst Appalachian-cycle plutonic suites in Newfoundland. in: A. K. Sinha, J. B., Whalen, and J. Hogan (eds.), The Nature of Magmatism in the Appalachian Orogen, Geological Society of America, Memoir 191, 193-220.

Konings, R. J. M., Boland, J. N., Vriend, S. P., and Jansen, J. B. H. (1988) Chemistry of biotites and muscovites in the Abas granite, northern Portugal. American Mineralogist, 73, 754-765.

Lalonde, A. E., and Martin, R. F. (1983) The Baie-des-Moutons syenitic complex, La Tabatière, Québec. II. The ferromagnesian minerals. Canadian Mineralogist, 21, 81-91.

Lalonde, A. E. (1989) Hepburn intrusive suite: peraluminous plutonism within a closing back-arc basin, Wopmay orogen, Canada. Geology, 17, 261-264.

Lalonde, A. E., and Bernard, P. (1993) Composition and color of biotite from granites: Two useful properties in the characterization of plutonic suites from the Hepburn internal zone of Wopmay orogen, Northwest Territories. Canadian Mineralogist, 31, 203-217.

Lalonde, A. E., Rancourt D. G., and Chao, G. Y. (1996) Fe-bearing triocatahedral micas from Mont Saint-Hilaire, Québec, Canada. Mineralogical Magazine 60, 447-460.

Lalonde, A. E., Rancourt D. G., and Ping, J. Y. (1998) Accuracy of ferric/ferrous determinations in phyllosilicates: A comparison of Mössbauer and wet-chemical methods. Special issue of Hyperfine Interaction entitled Mössbauer Spectroscopy in Clay Science, edited by D. G. Rancourt, 117, 175-204.

Lameyre, J., and Bowden, P. (1982) Plutonic rock series: Discrimination of various granitoid series and related rocks. Journal of Volcanology and Geothermal Research, 14, 169-186.

Logothetis, J. (1984) The mineralogy and geochemistry of metasomatized granitoid rocks from occurrences in the South Mountain batholith: New Ross area, southwestern Nova Scotia. M.Sc. thesis, Dalhousie University, Halifax, Nova Scotia. Canada.

MacDonald, M. A. (1981) The mineralogy, petrology, and geochemistry of the Musquodoboit batholith, Nova Scotia, Canada. M.Sc. thesis, Dalhousie University, Halifax, Nova Scotia, Canada.

McKenzie, C. B., and Clarke, D. B. (1974) Petrology of the South Mountain batholith, western Nova Scotia, M.Sc. thesis, Dalhousie University, Halifax, Nova Scotia, Canada.

Mackenzie, K. J. D., Brown, I. W. M., Cardile, C. M., and Meinhold, R. H. (1987) The thermal reactions of muscovite studied by high-resolution solid-state 29-Si and 27-Al NMR, Journal of Material Science, 22, 2645-2654.

Mahmood, A. (1983) Chemistry of biotites from a zoned granitic pluton in Morocco. Mineralogical Magazine, 47, 365-369.

Maillet, L. (1984) The origin and occurrence of cordierite in the South Mountain batholith, Nova Scotia. B.Sc. thesis, Dalhousie University, Nova Scotia, Canada.

Manapov, R. A., and Sitdikov, B. S. (1974) Mössbauer spectroscopic study of biotites of metamorphic rocks of the Tatar Arch Precambrian basement. Geochemistry International, 11, 976-980.

Maniar, P. D., and Piccoli, P. M. (1989) Tectonic discrimination of granitoids. Geological Society of America Bulletin, 101, 635-643.

Marillier, F., Keen, C. E., Stockmal, G. S., Quinlan, Q., Williams, H., Colman-Sadd, S. P., and O'Brien, S. J. (1989) Crustal structure and surface zonation of the Canadian Appalachians: implications of deep seismic reflection data. Canadian Journal of Earth Sciences, 26, 305-321.

Mason, G. H., (1985) The mineralogy and textures of the Coastal batholith, Peru. In: W. S. Pitcher et. al. (eds.), Magmatism at a plate edge, the Peruvian Andes, 156-166. Wiley, New York.

Mercier, P. H. J., Rancourt, D. G. and Berman, R. G. (1996) Aspect of the crystal chemistry of annite mica. in: Conference Proceedings vol. 50, ICAME-95, I. Ortalli (ed.) SIF, Bologna, 789-792.

Mercier, P. H. J., Rancourt, D. G., Berman, R. G., and Robert, J. L. (1997) Quadrupole splitting distributions from Mössbauer spectroscopy of synthetic Fe-Mg-micas on the phlogopite-annite-syderophyllite joins. The 11th International Clay Conference, 1997, Program with Abstaracts, A51.

Mercier, P. H. J., Rancourt, D. G., and Berman, R. G. (1998) Control of site populations, at synthesis, by inter-sheet differential thermal expansion in a 2:1 layer silicate. Proceedings of 11th International Clay Conference, 1997, Canadian Journal of Soil Science, in press.

Murakami, N. (1969) Two contrastive trends of evolution of biotite in granitic rocks. Journal of Japanese Association of Mineralogy, Petrology and Economic Geology, 62, 223-248.

Nachit, H., Razafimahefa, N., Stussi, J. M., and Carron, J. P. (1985) Composition chimique des biotites et typologie magmatique des granitoïdes. Comptes Rendus de l'Académie de Sciences de Paris, Série II, 301, 813-818.

Neiva, A. M. R. (1976) The geochemistry of biotites from granites of northern Portugal with special reference to their tin content. Mineralogical Magazine, 40, 453-466.

Neiva, A. M. R. (1981) Geochemistry of hybrid granitoid rocks and of their biotites from central northern Portugal and their petrogenesis. Lithos, 14, 149-163.

Parsons, I. (1981) The Klokken gabbro-syenite complex, south Greenland: quantitative interpretation of mineral chemistry. Journal of Petrology, 22, 233-260.

Parsons, I., Brown, W., and Jacquemin, H. (1986) Mineral chemistry and crystallization conditions of the Mboutou layered gabbro-syenite-granite complex, North Cameroon. Journal of Petrology, 27, 1305-1329.

Parsons, I., Mason, R. A., Becker, S. M., and Finch, A. A. (1991) Biotite equilibria and fluid circulation in the Klokken intrusion. Journal of Petrology, 32, 1299-1333.

Pearce, J. A., Harris, N. B. W., and Tindle, A. G. (1984) Trace element discrimination diagrams for the tectonic interpretation of granitic rocks. Journal of Petrology, 25, 956-983.

Peikert, E. W. (1963) Biotite variation as a guide to petrogenesis of granitic rocks in the Precambrian of northeastern Alberta. Journal of Petrology, 4, 432-459.

Phillips, G. N., Wall, V. J. and Clemens, J. D. (1981) Petrology of the Strathbogie batholith: a cordierite-bearing granite. Canadian Mineralogist, 19, 47-63.

Piasecki, M. A. J., Williams, H., and Colman-Sadd, S. P. (1990) Tectonic relationships along the Meelpaeg, Burgeo and Burlington LITHOPROBE transects in Newfoundland: in: Current Research, Newfoundland Department of Mines and Energy, Geological Survey Branch, Report 90-1, 327-339.

Pietzsch W. and Schmidt C. (1990) Mössbauer investigations of dioctahedral pegmatitic micas, Journal of Radioanalitical and Nuclear Chemistry Letters, 145, 1, 47-53.

Ping, J. Y., and Rancourt, D. G. (1992) Thickness effects with intrinsically broad absorption lines. Hyperfine Interactions, 71, 1433-1436.

Pitcher, W. S. (1983) Granite type and tectonic environment, In: Hsü, K. (editor) Mountain building processes. Academic Press, 19-40.

Quinlan, G. M., Hall, J., Williams, H., Wright, J., Colman-Sadd, S., O'brien, S. J., Stockmal, G. and Marillier, F. (1992) Onshore seismic reflection transects across the Newfoundland Appalachians. Canadian Journal of Earth Sciences, 29, 1865-1877.

Raeburn, S. P., Ilton, E. S., and Veblen, D. R. (1997a) Quantitative determination of the oxidation state of iron in biotite using X-ray photoelectron spectroscopy: I. Calibration. Geochimica et Cosmochimica Acta, 61, 4519-4530.

Raeburn, S. P., Ilton, E. S., and Veblen, D. R. (1997b) Quantitative determination of the oxidation state of iron in biotite using X-ray photoelectron spectroscopy: II. In situ analyses. Geochimica et Cosmochimica Acta, 61, 4531-4537.

Rancourt, D. G. (1989) Accurate site populations from Mössbauer spectroscopy. Nuclear Instruments and Methods in Physics Research, B44, 199-210.

Rancourt, D. G. and Ping, J. Y. (1991) Voigt-based methods for arbitrary-shape static hyperfine parameter distributions in Mössbauer spectroscopy, Nuclear Instruments and Methods in Physics Research, B53, 85-97.

Rancourt, D. G., Dang, M. Z., and Lalonde, A. E. (1992) Mössbauer spectroscopy of tetrahedral Fe^{3+} in trioctahedral micas. American Mineralogist, 77, 34-43.

Rancourt, D. G., McDonald, A. M., Lalonde, A. E., and Ping, J. Y. (1993) Mössbauer absorber thicknesses for accurate site populations in iron-bearing minerals. American Mineralogist, 78, 1-7.

Rancourt, D. G. (1994a) Mössbauer spectroscopy of minerals I, Inadequacy of Lorentzian-line doublets in fitting spectra arising from quadrupole splitting distributions. Physics and Chemistry of Minerals, 21, 244-249.

Rancourt, D. G. (1994) Mössbauer spectroscopy of minerals II, Problem of resolving cis and trans octahedral Fe^{2+} sites. Physics and Chemistry of Minerals, 21, 250-257.

Rancourt, D. G., Ping J. Y., and Berman R. G. (1994) Mössbauer spectroscopy of minerals III, Octahedral-site Fe^{2+} quadrupole splitting distributions in phlogopite-annite series. Physics and Chemistry of Minerals, 21, 258-267.

Rancourt, D. G., Ping, J. Y., Boukili, B., and Robert, J. L. (1996) Octahedral-site Fe^{2+} quadrupole splitting distributions from Mössbauer spectroscopy along the (OH, F)-annite join, Physics and Chemistry of Minerals, 23, 63-71.

Redhammer, G. J., Dachs, E., and Amthauer, G. (1995) Mössbauer spectroscopic and X-ray powder diffraction studies of synthetic micas on the join annite $KFe_3AlSi_3O_{10}(OH)_2$-phlogopite $KMg_3AlSi_3O_{10}(OH)_2$. Physics and Chemistry of Minerals, 22, 282-294.

Redhammer, G. J. (1998) Characterization of synthetic trioctahedral micas by Mössbauer spectroscopy. special issue of Hyperfine Interaction entitled Mössbauer Spectroscopy in Clay Science, edited by D. G. Rancourt.

Rice, C. M., and Williams, J. M. (1969) A Mössbauer study of biotite weathering. Mineralogical Magazine, 37, 210-215.

Richardson, S. M. (1975) A pink muscovite with reverse pleochroism from Archer's Post, Kenya, American Mineralogist, 60, 73-78.

Sanz, J., Meyers, J., Vielvoye, L., and Stone, W. E. E. (1978) The location and content of iron in natural biotites and phlogopites: A comparison of several methods. Clay Minerals, 13, 45-52.

Sapountzis, E. S. (1976) Biotites from the Sithonia igneous complex, North Greece. Neues Jahrbuch für Mineralogie Abhandlungen, 126, 327-341.

Schenk, P. E. (1971) Southeastern Atlantic Canada, northwestern Africa, and continental drift. Canadian Journal of Earth Sciences, 8, 1218-1251.

Schmidt, C. and Pietzsch, W. (1990) Iron distribution and geochemistry of pegmatitic dioctahedral $2M_1$ Micas, Chemie Erde, 50, 27-38.

Schneiderman, J. S. (1991) Petrology and mineral chemistry of the Ascutney Mountain igneous complex. American Mineralogist, 76, 218-229.

Shannon, R. D. (1976) Revised effective ionic radii and systematic studies of interatomic distances in halides and chalcogenides. Acta Crystalographica, A32, 751-767.

Smith, G., Howes, B., and Hazen, Z. (1980) Mössbauer and optical spectra of biotite: A case for Fe^{2+}-Fe^{3+} interactions. Physica Status Solidi (a), 57, K187-K192.

Speer, J. A. (1981) Petrology of cordierite- and almandine-bearing granitoid plutons of the southern Appalachian Piedmont, USA, Canadian Mineralogist, 19, 35-46.

Speer, J. A. (1984) Micas in igneous rocks. In: Micas, Bailey, S. W. (ed.), Mineralogical Society of America, Review in Mineralogy, 13, 299-356.

Speer, J. A. (1987) Evolution of magmatic AFM mineral assemblages in granitoid rocks: The hornblende + melt = biotite reaction in the Liberty Hill pluton, South Carolina, American Mineralogist, 72, 863-878.

Stallard, V. A. (1975) Geochemistry of biotites as a guide to the differentiation of the South Mountain batholith, Nova Scotia. B.Sc. thesis, Dalhousie University, Nova Scotia, Canada.

Stone, M., Klominský, J., and Rajpoot, G. S. (1997) Composition of trioctahedral micas in the Karlovy Vary pluton, Czech Republic and a comparison with those in the Cornubian batholith, SW England. Mineralogical Magazine, 61, 791-807.

Stucki, J., W. (1981) The quantitative assay of minerals for Fe^{2+} and Fe^{3+} using 1, 10-phenanthroline: II. A photochemical method. Soil Science Society of America Journal, 45, 638-641.

Stucki, J. W., and Anderson, W. L. (1981) The quantitative assay of minerals for Fe^{2+} and Fe^{3+} using 1, 10-phenanthroline: I. Sources of variability. Soil Science Society of America Journal, 45, 633-637.

Tate, M. C., and Clarke, D. B. (1996) The petrogenesis and regional tectonic significance of the Late Devonian mafic intrusions in Meguma zone, Nova Scotia. Canadian Journal of Earth Sciences, 32, 1883-1898.

Tate, M. C., and Clarke, D. B. (1997) Compositional diversity among Late Devonian peraluminous granitoid intrusions in Meguma zone of Nova Scotia, Canada. Lithos, 39, 179-194.

Van Staal, C. R., Murphy, J. B., Fyffe, L. R., Karabinos, P., Whalen, J. B. and Keppie, J. D. (1998) Is the Acadian a Laramide-style orogeny? The Geological Society of America, 33rd Annual Meeting, 30, number 1, 82.

Veitch, L. G., and Radoslovich, E. W. (1963) The cell dimensions and symmetry of layer-lattice silicates. III. Octahedral ordering. American Mineralogist, 48, 62-75.

Wallace, G. (1988) Petrogenesis of the McGerrigle plutonic complex: Mineralogical and oxygen isotopic constraints. M.Sc. thesis, McGill University, Montréal, Québec, Canada.

Weiss, Z., Rieder, M., and Chmielova, M. (1992) Deformation of coordination polyhedra and their sheets in phyllosilicates. European Journal of Mineralogy, 4, 665-682.

Whalen, J. B., Currie, K. L., and Chappell, B. W. (1987) A-type granites: Geochemical characteristics, discrimination and petrogenesis. Contributions to Mineralogy and Petrology, 95, 407-419.

Whalen, J. B., and Chappell, B. W. (1988) Opaque mineralogy and mafic mineral chemistry of I- and S-type granites of the Lachlan fold belt, Southeast Australia. American Mineralogist, 73, 281-296.

Whalen, J. B. (1993) Geology, petrography and geochemistry of Appalachian granites in New Brunswick and Gaspésie, Québec, Geological Survey of Canada, Bulletin 436.

Whalen, J. B., Jenner, G. A., Currie, K. L., Sandra, M. B., Longstaffe, F. J., and Hegner, E. (1994) Geochemical and isotopic characteristics of granitoids of the Avalon zone, Southern New Brunswick: Possible evidence for repeated delamination events. Journal of Geology, 102, 269-282.

Whalen, J. B., Jenner, G. A., Longstaffe, F. J., and Hegner, E. (1996) Nature and evolution of the eastern margin of Iapetus: geochemical and isotopic constraints from Siluro-Devonian granitoid plutons in the New Brunswick Appalachians, Canadian Journal of Earth Sciences, 33, 140-155.

Whalen, J. B., Jenner, G. A., Longstaffe, F. J., and Gariépy, C. (1997) Implications of granitoid geochemical and isotopic (Nd, O, Pb) data from the Cambro-Ordovician Notre Dame Arc for the evolution of the Central Mobile Belt, Newfoundland Appalachians. in: A.

K. Sinha, J. B., Whalen, and J. Hogan (eds.), The Nature of Magmatism in the Appalachian Orogen, Geological Society of America Memoir, 191, 367-395.

Williams, H. (1979) Appalachian orogen in Canada. Canadian Journal of Earth Sciences, 16, 792-807.

Williams, H., and Hatcher, R. D. (1983) Appalachian suspect terranes, in: Contributions to the tectonics and geophysics of the mountain chains (ed.) R. D. Hatcher, H. Williams, and I. Zietz, Geological Society of America Memoir, 158, 33-53.

Williams, H., Colman-Sadd, S. P. and Swinden, H. S. (1988) Tectonic-stratigraphic subdivisions of central Newfoundland, Geological Survey of Canada, Paper 88-1B, 91-98.

Williams, H., Dickson, W. L., Currie, K. L., Hayes, J. P., and Tuach, J. (1989) Preliminary report on classification of Newfoundland granitic rocks and their relations to tectonostratigraphic zones and lower crustal blocks. Geological Survey of Canada, Paper 89-1B, 47-53.

Wones, D. R., and Eugster, H. P. (1965) Stability of biotite: experiment, theory, and application. American Mineralogist, 50, 1228-1272.

Appendices for Manuscript 1

Appendix I of Manuscript 1

Locations and Descriptions of Rock Samples

Listed below in order of pluton code number ("Code") are locations of geochemical samples by NTS sheet ("Map"), easting ("East") and northing ("North"). Also given is a batholith or suite name, a pluton, phase or unit name, (Whalen, 1993) and a sample description. Unit letters (e.g. "Ogp") refer to map units on GSC Map 1751A (Geology of Northern Portion of the Central Plutonic Belt, New Brunswick, scale 1:100000, Geological Survey of Canada, 1990).

Key to abbreviations used in sample descriptions is after Whalen (1993):

vfg : very fine grained
fg : fine grained
mg : medium grained
cg : coarse grained
vcg : very coarse grained
eq : equigranular
porph : porphyritic
diss : disseminated
mass : massive
amygd:amygdaloidal
fol: foliated
incl : inclusion
metased : metasedimentary
pheno : phenocrysts
alt : alteration
miar: miarolitic
dk : dark
Hbl: hornblende
Bt : biotite
Chl : chlorite
Ep : epidote
Fld : feldspar
Kfs: K-feldspar
Ms: muscovite
Ne : nepheline
Ol : olivine
Pl : plagioclase
Pyx : pyroxene
Py : pyrite
Qtz : quartz

Humber-Dunnage (NB)

WX#	Code		Map	East	North	batholith/suite	Pluton, Phase or Unit	Sample Description
MG- 23	H	1	22H/4	8550	3205	McGerrigle	hybrid suite	cg eq Hbl-Bt-Pyx monzodiorite, grades to cg gabbro
MG- 29	H	1	22H/4	8430	3345	McGerrigle	hybrid suite	fg eq Bt-Pyx-Hbl monzonite, small mafic incl-rich
MG- 44	H	1	22A/13	8450	2980	McGerrigle	hybrid suite	cg red Hbl-Bt Qtz monzonite
MG- 28	H	1	22H/4	8610	3220	McGerrigle	granite suite	mg eq red Bt granite
MG- 60	H	1	22B/16	1910	2840	McGerrigle	granite suite	cg red seriate Bt-Hbl granite
MG- 46	H	1	22A/13	8310	2375	McGerrigle	granite suite	mg Pl porph Bt-Hbl granite
MG- 16	H	1	22H/4	8480	3350	McGerrigle	dyke suite	mg miaskitic ne syenite
MG- 94	H	1	22A/13	8180	3080	McGerrigle	dyke suite	fg grey feld porph alkine ne syenite dyke
NB- 58	D	3	21O/16	082	085	Charlo stocks	Benjamin River complex	mg-cg eq Pyx-Hbl-Bt leuco-gabbronorite
NB- 60	D	3	21O/16	078	076	Charlo stocks	Benjamin River complex	mg scarlet red Hbl-Bt granite
NB- 67	D	3	21O/16	012	997	Charlo stocks	Benjamin River complex	mg grey Hbl-Bt Qtz monzonite, fg mafic incl
NB- 52	D	5	21P/13	774	977		Anitouri Lake	mg-cg eq red Bt-Hbl granite
NB- 53	D	5	21P/13	774	977		Anitouri Lake	mg-cg eq red Bt granite
NB- 47	D	6	21P/12	834	864		Nicholas Denys	mg eq Bt granodiorite

Gander zone (NB)

NB- 97	G	3	21O/1	9036	3566	Ordovician suite	Meridian Brook (Ogm)	mg fol grey Bt-Ms granite
NB- 98	G	3	21O/1	9067	3546	Ordovician suite	Meridian Brook (Ogm)	mg fol reddish Bt granodiorite, small mafic incl
NB- 277	G	4	21O/2	6162	3400	Ordovician suite	Sweat Hill (Ogs)	vcg fol Fld porph Bt-Ms granite
NB- 280	G	5	21O/2	6477	2778	Ordovician suite	Serpentine River (Ogeb)	cg-vcg fol grey Bt-Ms granite
NB- 111	G	6	21O/1	9370	2305	Ordovician suite	Mullin Stream Lake (Ogu)	cg strongly fol grey Bt-Ms granodiorite
NB- 134	G	7	21J/15	630	012	Ordovician suite	Fox Ridge (Ogf)	cg fol scarlet Fld porph Bt-Ms granite
NB- 151	G	7	21J/10	564	732	Ordovician suite	Fox Ridge (Ogf)	vcg fol Fld porph (2-5 cm) Bt granodiorite
NB- 125	G	8	21J/15	843	026	Ordovician suite	South Renous River?	mg-cg strongly fol Bt-Ms granite
NB- 306	G	9a	21O/1	9145	1344	Ordovician suite	unnamed (Og)	cg eq Bt granite, banded portions
NB- 317	G	9b	21O/1	9235	0925	Ordovician suite	unnamed (Og)	fg strongly fol Bt granodiorite
NB- 175	G	9c	21J/15	880	039	Ordovician suite	unnamed (Og)	moderately fol pink Bt-Ms granite
NB- 44	G	11	21P/12	983	650		Papineau Falls	cg semi-porph (Kfs) Bt granite
NB- 45	G	11	21P/12	995	709		Papineau Falls	cg Kfs porph Bt granite
NB- 91	G	12	21O/7	8378	4329	Mt Elizabeth complex	Mafic suite (SEmd)	cg black Pyx-Hbl-ol-Bt gabbronorite
NB- 99	G	12	21O/7	855	475	Mt Elizabeth complex	Mafic suite (SEmd)	cg eq Hbl-Pyx-Bt gabbronorite, Plus Pl-Bt pegmatite
NB- 239	G	12	21O/7	8081	4916	Mt Elizabeth complex	Mafic suite (SEmd)	mg eq amph-Bt leuco-gabbro
NB- 88	G	12	21O/7	8277	4326	Mt Elizabeth complex	Alkaline suite (SEah)	mg amph-Bt Qtz monzonite, mafic and felsic zones
NB- 89	G	12	21O/7	8320	4367	Mt Elizabeth complex	Alkaline suite (SEaq)	mg grey amph-Bt Qtz monzodiorite, mafic incl-rich
NB- 92	G	12	21O/7	8328	4222	Mt Elizabeth complex	Alkaline suite (SEas)	mg red Bt-Hbl syenite
NB- 78	G	12	21O/7	8211	4250	Mt Elizabeth complex	Alkaline suite (SEag)?	fg pink Bt granite
NB- 115	G	13	21O/1	977	351		Miramichi (SM)	mg-cg slightly Kfs porph Bt granite
NB- 116	G	13	21O/1	974	355		Miramichi (SM)	mg pink Kfs porph (1-2 cm) Bt granite

WX#	Code		Map	East	North	batholith/suite	Pluton, Phase or Unit	Sample Description
NB- 326	G	13	21O/1	9965	3390		Miramichi (SM)	mg-cg pink seriate Bt-Ms granite
NB- 143	G	14	21J/15	879	049	North Pole Stream	Mafic suite (SNd)	mg grey Bt-Hbl Qtz diorite
NB- 123	G	14	21O/2	897	102	North Pole Stream	granite (SNg)	cg Kfs porph Bt granodiorite, metased incl
NB- 122	G	14	21O/2	778	177	North Pole Stream	granite (SNm)	fg-mg white Bt-Ms granodiorite, pegmatitic clots
NB- 145	G	14	21O/2	619	088	North Pole Stream	granite (SNm)	fg eq grey Bt-Ms granite
NB- 146	G	14	21O/2	613	091	North Pole Stream	granite (SNm)	mg eq grey Bt-Ms granite, weathered
NB- 136	G	14	21J/15	660	030	North Pole Stream	Squaw Lake	mg eq white Bt-Ms granite, rare Bt clots
NB- 144	G	15	21J/15	601	929	Redstone Mountain	granite (SRg)	mg red Bt-Hbl granite
NB- 152	G	15	21J/15	584	869	Redstone Mountain	granite (SRg)	mg eq Bt granite
NB- 155	G	16	21J/15	768	884		North Dungarvan River	mg-cg eq Bt-Hbl tonalite, minor metased incl
NB- 159	G	17	21J/10	604	752		Lost Lake	fg-mg eq Bt granodiorite
NB- 161	G	17	21J/11	468	750		Lost Lake	cg eq (larger Kfs) Bt-Ms granodiorite
NB- 162	G	17	21J/10	535	707		Lost Lake	mg eq fol Bt-Ms granite
NB- 294	G	18	21J/10	8138	7377	Burnthill Brook suite	Dungarvon	mg eq to porph Bt-Ms granodiorite
NB- 158	G	18	21J/10	658	769	Burnthill Brook suite	Burnthill	mg-cg Kfs-Pl porph Bt granite
NB- 166	G	19	21J/11	441	702		Beadle Mountain	mg grey Bt-Ms granite, metased and Qtz incl
NB- 168	G	20	21J/11	407	527		Juniper Barren	mg-cg eq pink Bt-Hbl granodiorite, rare incl
NB- 170	G	20	21J/11	390	531		Juniper Barren	mg eq pink Bt-Hbl granite, some Bt-rich incl
NB- 169	G	21	21J/11	409	529		Bogan Brook	fg grey Bt-Ms tonalite, metased incl-rich
NB- 173	G	22	21J/11	497	570		Nashwaak	mg eq white Bt-Ms granodiorite
NB- 227	G	22	21J/6	4887	4325		Nashwaak	cg eq pink Ms-Bt granite
NB- 1	G	23	21G/14	277	903	Pokiok batholith	Hartfield	cg slightly fol Bt granodiorite, rare fg mafic incl
NB- 7	G	23	21G/14	298	912	Pokiok batholith	Hartfield	cg eq Bt-Hbl tonalite
NB- 8	G	24	21G/13	962	688	Pokiok batholith	Skiff Lake	fg white Bt-Ms granite, Bt-rich incl
NB- 13	G	24	21G/13	092	671	Pokiok batholith	Skiff Lake	banded fg-mg eq pink Bt-Ms granite
NB- 29	G	24	21G/12	082	649	Pokiok batholith	Skiff Lake	cg seriate Bt-Ms granite
NB- 30	G	24	21G/12	034	640	Pokiok batholith	Skiff Lake	mg-cg eq Ms-Bt granite, chl veins
NB- 2	G	25	21G/14	313	898	Pokiok batholith	Hawkshaw	cg Kfs porph (2-3cm) Bt granite, fg igneous incl
NB- 17	G	25	21J/3	370	966	Pokiok batholith	Hawkshaw	mg grey Kfs porph Bt-Ms granite
NB- 19	G	26	21G/14	468	909	Pokiok batholith	Allandale	mg eq pink Ms-Bt granite, minor molybdenite
NB- 38	G	26	21G/14	344	799	Pokiok batholith	Allandale	mg-cg seriate Bt-Ms granite
NB- 214	G	28	21G/5	405	186		Tower Hill	mg eq white Ms-Bt granite
NB- 188	G	29	21G/7	641	304		Beech Hill	fg beige feld-Qtz-Bt porph granite
							Avalon zone (NB)	
NB- 206	A	1	21G/9	283	538	St George batholith	Hampstead	mg eq pink Bt-Hbl granite
NB- 207	A	1	21G/9	285	535	St George batholith	Hampstead	mg eq pink Bt-Hbl granodiorite
NB- 209	A	1	21G/9	295	518	St George batholith	Hampstead	mg eq pink Bt-Hbl granodiorite
NB- 211	A	2	21G/8	162	395	St George batholith	Welsford complex	fg-mg pink feld porph Hbl-Bt granite
NB- 223	A	2	21G/8	094	361	St George batholith	Welsford complex	mg-cg eq beige amph-Pyx syenite

WX#	Code		Map	East	North	batholith/suite	Pluton, Phase or Unit	Sample Description
NB- 197	A	3	21G/1	976	128	St George batholith	Mount Douglas	mg Kfs porph granite
NB- 198	A	3	21G/8	966	153	St George batholith	Mount Douglas	mg-cg seriate Bt granite, rapakivi feld
NB- 219	A	3	21G/8	067	376	St George batholith	Mount Douglas	cg seriate Bt granite
NB- 180	A	4	21G/2	744	075	St George batholith	Utopia	mg-cg eq beige Bt granite
NB- 184	A	4	21G/2	686	066	St George batholith	Utopia	cg eq beige Bt granite
NB- 185	A	4	21G/2	680	089	St George batholith	Utopia	cg eq cream Bt-Ms granite, rapakivi Fld
NB- 189	A	4	21G/2	617	089	St George batholith	Utopia	mg-cg eq pink Bt granite
NB- 195	A	5	21G/7	767	199	St George batholith	Magaguadavic	cg Kfs porph (2-5 cm) Bt-Hbl granodiorite
NB- 196	A	5	21G/7	748	264	St George batholith	Magaguadavic	vcg Kfs porph Bt-Hbl granite, rapakivi feld
NB- 199	A	5	21G/7	931	194	St George batholith	Magaguadavic	cg Kfs porph (2-4 cm) Bt granite
NB- 178	A	6	21G/3	436	033	St George batholith	Bocabec complex	mg-cg eq black Hbl-Bt-Pyx gabbronorite
NB- 176	A	6	21G/3	419	041	St George batholith	Bocabec complex	cg eq beige Bt granite
NB- 177	A	6	21G/3	439	038	St George batholith	Bocabec complex	cg eq beige Bt granite

Dunnage zone (NF)

Sample #	NTS name	zone	map	UTM zone	East	North	unit	sample description
NF-1	Little Grand Lake	NDZs	12A/12	21	4373	53842	Pierre's Pond plutonic suite	mass mg eq Bt-Hbl granite, cut by ep and pegmatitic veins
NF-5	Puddle Pond	DWZn	12A/5	21	4304	53691	Dashwoods - Ordovician plutonic suite	mass mg-cg eq Hbl diorite cut by pegmatitic veins
NF-8	King George IV	GZ	12A/4	21	4494	53178	Buck Lake granite	vcg pink Kfs porph (1-2 cm) Bt granite
NF-14	Cormack	NDZn	12H/6	21	5920	54655	Wild Cove Pond granite	fol mg white Kfs porph (0.5-2 cm) Bt granite
NF-18	Nippers Harbour	NDZn	2E/13	21	5799	55363	Dungarven granite	fol dark pink cg eq Bt granite
NF-23	Star Lake	NDZs	12A/11	21	4749	53778	Star Lake intrusive suite	cg eq dark pk Bt-Hbl hypersolvus granite
NF-26	Springdale	NDZn	12H/8	21	5691	54758	Mansfield Cove granodiorite	fol grey cg Qtz-eye (4-10 mm) Hbl-Bt tonalite
NF-28	Port aux Basques	DWZs	11O/11	21	3271	52826	Red Rocks granite	pale pink mg eq Bt granite
NF-29	Port aux Basques	DWZs	11O/11	21	3413	52728	Port aux Basque granite	strongly fol dark pink mg eq Bt granite
NF-36	Star Lake	NDZs	12A/11	21	4809	53779	Pierre's Pond plutonic suite	slightly fol pink fg-mg eq Bt granite
NF-38	Star Lake	NDZs	12A/11	21	4808	53800	Star Lake intrusive suite	mass pink cg eq Bt-Ms granite
NF-45	Rainy Lake	NDZn	12A/14	21	4969	54246	Hungry Mountain Complex	mg eq Hbl diorite, similar to NF-42 & 44
NF-49	Dawes Pond	NDZn	12H/1	21	5404	54347	Hungry Mountain Complex	cg-vcg Qtz-eye porph Hbl-Bt tonalite or granodiorite
NF-52	Star Lake	NDZs	12A/11	21	4734	53777	Pierre's Pond plutonic suite	fol grey cg Bt tonalite or granite
NF-75	Little Grand Lake	NDZs	12A/12	21	4462	53757	Pierre's Pond plutonic suite	white strongly fol cg Bt granodiorite or tonalite
NF-78	Little Grand Lake	NDZs	12A/12	21	4360	53729	Star Lake intrusive suite	white fg-mg eq Bt-Ms granite, some banding
NF-83	Little Grand Lake	NDZs	12A/12	21	4408	53754	Star Lake intrusive suite	white slightly fol mg-cg Bt-Ms granite
NF-85	Little Grand Lake	NDZs	12A/12	21	4406	53724	Dashwoods - early mafic intrusive	fol cg eq Hbl-Bt diorite or gabbro
NF-101	Sheffield Lake	NDZn	12H/7	21	5270	54562	Hungry Mountain complex	grey mg eq Hbl-Bt Qtz diorite
NF-102	The Topsails	NDZn	12H/2	21	5096	54464	Hinds Brook granite	grey and pink Kfld porph (0.3-2.5 cm) mg Bt granite
NF-106	Puddle Pond	DWZn	12A/5	21	4486	53585	Dashwoods - Ordovician plutonic suite	fol cg Bt-Hbl granodiorite or Qtz monzonite
NF-110	Puddle Pond	DWZn	12A/5	21	4525	53601	Dashwoods - younger granite suite	fol pink and grey mg eq Bt granite
NF-114	Puddle Pond	DWZn	12A/5	21	4382	53677	Dashwoods - Ordovician plutonic suite	fol banded cg Bt-Hbl tonalite or Qtz diorite
NF-119	Puddle Pond	DWZn	12A/5	21	4308	53674	Dashwoods - Ordovician plutonic suite	fol white cg Bt granodiorite
NF-128	Corner Brook	NDZs	12A/13	21	4520	54058	Glover Island pluton	fol cg white Kfs porph (0.5-1 cm) Bt granite
NF-131	Star Lake	NDZs	12A/11	21	4989	53933	Halfway Mountain pluton	mass mg Qtz-Fld porph (0.3-0.5 cm) Bt granite
NF-143	Star Lake	NDZs	12A/11	21	4726	53690	Caribou Lakes gneiss complex	mg-cg fol white Bt-Hbl granite to granodiorite, some banding and Kfs veins
NF-166	Port aux Basques	DWZs	11O/11	21	3336	52729	Grand Bay granodiorite suite	fg-mg grey Bt granodiorite
NF-171	Rose Blanche	GZ	11O/10	21	3713	52739	Rose Blanche granite	mg eq grey Bt-Ms granite
SNF-21	Fogo	NDZ	2 E/9	21	5497790	701590	Fogo Island gabbro	dark mg Hbl-Bt gabbro
SNF-22	Fogo	NDZ	2 E/9	21	5509830	711050	Fogo Island gabbro	dark mg Pyx-Bt gabbro
SNF-23	Fogo	NDZ	2 E/9	21	5510945	707275	Fogo Island granite	mass pink grey mg eq Hbl-Bt granodiorite
SNF-24	Fogo	NDZ	2 E/9	21	5508790	702710	Fogo Island granite	mass pink grey mg eq Hbl-Bt granodiorite
SNF-25	Fogo	NDZ	2 E/9	21	5503890	700455	Fogo Island granite	mass pale grey mg eq Hbl-Bt granodiorite

* based on geographic coordinates provided by global positioning system (GPS).

Gander zone (NF)

sample	zone	NTS map	UTM zone	East	North	pluton	sample description
AK-89-122*	GZ					Francois granite	pink mg Bt granite
AK-89-087	GZ	02F/04	22	309450	5438500	Deadman's Bay granite	cg mg porphyritic pink Kfs Bt granite
AK-89-134	AZ	11P/08	21	561120	5260610	Pass Island granite	mg pink Hbl-Bt granite
AK-91-414	GZ	02D/10	21	653050	5384430	Middle Ridge granite	mg foliated white Bt-Ms granite
AK-91-415*	GZ					Middle Ridge granite	mg cg creamy white Bt-Ms granite
AK-92-006	AZ	01M/15	21	685550	5293300	Ackley granite	mg cg grey Kfs megacrystic Bt-Hbl granite
AK-92-007	AZ	01M/16	21	688900	5296580	Ackley granite	grey mg pink Kfs megacrystic Bt granite
AK-92-043	GZ	02C/13	22	283150	5419900	Unnamed nebultic granite, Bonavista Bay	mg Bt-Ms granite
AK-92-054	GZ	02C/13	22	292260	5428900	Unnamed bi-ms granite, Bonavista Bay	fg mg foliated white Bt-Ms granite
Ak-92-061	GZ	02F/04	22	307400	5447800	Business Cove granite, Bonavista Bay	mg Bt-Ms granite
AK-92-187	GZ	02D/09	21	703680	5389400	Maccles lake granite	grey mg foliated pink Kfs megacrystic Bt granite
AK-92-108	AZ	01M/12	21	606670	5270200	Hr. Breton granite	mg cg pink leucocratic Bt granite
AK-92-131	GZ	01M/12	21	583450	5275720	Gaultois granite	grey mg cg foliated pink Kfs megacrystic Bt-Ms granite
AK-92-133	GZ	01M/12	21	582960	5273380	Gaultois granite	grey mg cg foliated pink Kfs megacrystic Hbl-Bt granodio
AK-92-166	GZ-DZ ?	11O/10	21	380750	5279200	Petites granite	mg pink Bt-Ms granite
AK-92-168A	GZ-DZ	11O/10	21	383110	5277720	La Poile granite	mg cg pink to grey Kfs megacrystic Bt-Hbl granodiorite
AK-92-170	GZ-DZ	11O/10	21	384300	5278660	La Poile granite	grey mg cg pink Kfs megacrystic Bt-Hbl granodiorite
AK-92-243	GZ	11O/09	21	406670	5279720	Otter Point granite	grey mg cg foliated pink Kfs megacrystic Bt-Hbl granodio
AK-92-291	GZ	11O/09	21	420810	5282600	Otter Point granite	mg foliated pink Kfs megacrystic Bt granite
Ak-92-292	GZ	11P/12	21	427080	5284280	Chetwynd granite	grey mg cg pink Kfs megacrystic Bt granite
SNF-1	GZ	12 A/4	21	5317798	449310	Burgeo granites	grey mg cg foliated Kfs megacrystic Bt granite
SNF-2**	GZ	11 P/12	21			Burgeo granites	mg cg pink Kfs megacrystic Bt granodiorite
SNF-3	GZ	11 P/12	21	5283890	452265	Burgeo granites	grey mg-cg foliated Kfs megacrystic Bt granite
SNF-4	GZ	11 P/12	21	5283890	452265	Burgeo granites	dark grey mg cg Kfs porphyry Bt granodiorite
SNF-5	GZ	11 P/13	21	5290545	450810	Burgeo granites	dark grey mg-cg Bt-Pyx gabbro
SNF-7	GZ	2 D/16	21	5412565	694620	Gander Lake granite	white cg Kfs megacrystic Bt-Hbl granite
SNF-8	GZ	2 D/9	21	5399155	709890	Lockers Bay granite	dark grey vcg foliated pink Kfs megacrystic Bt granite
SNF-10	GZ ?	1 M/15	21	5294810	686265	Ackley city granite	pale grey vcg pink Kfs megacrystic Bt-Hbl granodiorite
SNF-14	GZ	2 D/16	21	5405195	703890	Middle Brook granite	pale grey vcg pink Kfs megacrystic Bt granite
SNF-15	GZ	2 F/4	22	5437854	291915	Middle Brook granite	dark grey vcg foliated pink Kfs megacrystic Bt granite
SNF-16	GZ	2 F/4	22	5447505	305575	New Port granite	pink mg with minor Kfs phenocryst Bt-granite
SNF-17	GZ	2 F/4	22	5446325	311812	Cape Freel granite	vcg pink Kfs megacrystic Bt granite
SNF-18	GZ	2 F/4	22	5446325	311812	Cape Freel granite	fg mg dark green Bt-diorite cutting SNF-17
SNF-19	GZ	2 F/4	22	5449395	313645	Cape Freel granite	dark grey vcg foliated pink Kfs megacrystic Bt granite

* not available at the moment

** sampled from Burgeo wharf

Meguma zone (NS)

sample	UTM zone	NTS map	East	North	zone	batholith	pluton	unit*	sample description
pc2b	20	11 D/5	428010	4927390	MZ	South Mountain	Halifax	2b	mg-cg Bt monzogranite
ed3	20	11 D/12	431350	4929050	MZ	South Mountain	Halifax	3	mg-cg megacrystic Kfs Ms-Bt monzogranite
pr5b	20	11 D/12	438420	4930140	MZ	South Mountain	Halifax	5b	mg eq Bt-Ms monzogranite
br4	20	11 D/12	441495	4933840	MZ	South Mountain	Halifax	4	mg-cg megacrystic Kfs Bt-Ms monzogranite
103b2	20	11 D/12	447350	4942280	MZ	South Mountain	Halifax	b2	mg-cg grey Bt-monzogranite
306-2	20	11 D/5	450150	4926800	MZ	South Mountain	Halifax	4	fg-mg porphyritic Kfs Bt-Ms monzogranite
mwad	20	11 D/12	450180	4941175	MZ	South Mountain	Halifax	1	mg-cg grey Bt-granodiorite
slp**	20				MZ		Sherbrook Lake		mg eq grey Bt-Ms monzogranite
NS-3**	20				MZ		Port Mouton		mg eq moderately fol Bt-Ms granite
NS-4**	20				MZ		Port Mouton		fg-mg fol Bt-Ms granite

* According to MacDonald and Horne (1988), rocks of the Halifax pluton are divided into two sequences (A and B) on the basis of texture and field relationships and each sequence is subdivided into units

** coordinates not available.

Appendix II of the Manuscript 1

Electron Microprobe Analyses of Biotite

Tabulated below are electron microprobe analyses of biotite and their corresponding structural formulae (based on 20 oxygens) collected during this study as well as obtained from published or unpublished data in the literature. Major elements are in weight per cent oxides and analyses are listed by zones described in the text.

A/CNK: molar [$Al_2O_3/(CaO + Na_2O + K_2O)$].

"Determinations" denotes the number of analyses performed on the specimen.

sample	nb-58	mg-23	mg-24	mg-26	mg-29	mg-53	mg-6	mg-64
determinations	7	8	1	4	5	6	6	6
SiO_2	36.08	37.01	37.82	37.24	36.20	37.11	37.49	37.98
TiO_2	5.06	4.18	5.27	3.43	4.27	4.07	4.26	3.85
Al_2O_3	12.83	13.09	12.98	13.44	12.52	12.90	13.90	14.65
FeO_{total}	22.71	20.45	18.98	21.24	24.25	21.05	19.44	16.02
Fe_2O_3	2.30	2.90	2.80	3.10	3.90	3.20	2.80	2.40
FeO	20.64	17.84	16.46	18.45	20.74	18.17	16.92	13.86
MnO	0.12	0.25	0.18	0.14	0.49	0.22	8.16	0.14
MgO	9.99	11.19	12.33	10.92	8.35	10.40	11.75	14.81
CaO	0.01	0.01	0.03	0.01	0.02	0.01	0.02	0.01
Na_2O	0.26	0.12	0.10	0.11	0.07	0.07	0.13	0.79
K_2O	9.57	9.66	9.36	9.72	10.26	9.77	9.75	8.41
H_2O	3.42	3.63	3.81	3.64	3.61	3.41	3.68	3.98
F	0.64	0.43	0.22	0.41	0.34	0.79	0.12	0.05
Cl	0.56	0.35	0.22	0.32	0.27	0.48	0.42	0.17
O=F	-0.27	-0.18	-0.09	-0.17	-0.14	-0.33	-0.05	-0.02
O=Cl	-0.13	-0.08	-0.05	-0.07	-0.06	-0.11	-0.09	-0.04
total	101.09	100.40	101.44	100.69	100.83	100.16	109.25	101.04
^{iv}Si	5.53	5.62	5.62	5.65	5.60	5.67	5.35	5.56
^{iv}Al	2.32	2.34	2.27	2.35	2.28	2.32	2.34	2.44
^{iv}Ti	0.16	0.03	0.11	0.00	0.12	0.01	0.30	0.00
T site #	8.00	8.00	8.00	8.00	8.00	8.00	8.00	8.00
Al	0.00	0.00	0.00	0.05	0.00	0.00	0.00	0.09
Ti	0.42	0.44	0.48	0.39	0.38	0.46	0.15	0.42
Fe^{+3}	0.27	0.33	0.31	0.35	0.45	0.37	0.30	0.26
Fe^{+2}	2.64	2.27	2.05	2.34	2.68	2.32	2.02	1.70
Mn^{+2}	0.02	0.03	0.02	0.02	0.06	0.03	0.99	0.02
Mg	2.28	2.53	2.73	2.47	1.93	2.37	2.50	3.23
O site #	5.63	5.61	5.59	5.62	5.51	5.55	5.96	5.72
Ca	0.00	0.00	0.00	0.00	0.00	0.00	0.00	0.00
Na	0.08	0.04	0.03	0.03	0.02	0.02	0.04	0.22
K	1.87	1.87	1.77	1.88	2.03	1.90	1.78	1.57
A site #	1.95	1.91	1.81	1.91	2.05	1.93	1.82	1.80
O	20.00	20.00	20.00	20.00	20.00	20.00	20.00	20.00
OH	3.54	3.70	3.84	3.72	3.76	3.49	3.84	3.93
F	0.31	0.21	0.10	0.20	0.17	0.38	0.05	0.02
Cl	0.15	0.09	0.06	0.08	0.07	0.12	0.10	0.04
Charge	0.00	0.00	0.00	0.00	0.00	0.00	0.00	0.00
Fe_{total}	2.91	2.60	2.36	2.69	3.14	2.69	2.32	1.96
Al_{total}	2.32	2.34	2.27	2.40	2.28	2.32	2.34	2.53
Fe/(Fe+Mg)	0.56	0.51	0.46	0.52	0.62	0.53	0.48	0.38
A/CNK	1.19	1.23	1.25	1.25	1.11	1.20	1.29	1.41
Fe^{3+}/Fe_{total}	0.09	0.13	0.13	0.13	0.14	0.14	0.13	0.13
$Log(X_{Mg}/X_{Fe})$	-0.11	-0.01	0.06	-0.04	-0.21	-0.06	0.03	0.22
$Log(X_F/X_{OH})$	-1.06	-1.25	-1.57	-1.28	-1.35	-0.96	-1.85	-2.23

samples labelled mg- are from Wallace (1988)

sample	mg-90	nb-67	mg-8	mg-10	mg-40	mg-44	mg-52	mg-63
determinations	6	4	7	4	8	7	6	7
SiO_2	35.94	35.32	36.45	36.23	36.92	37.38	36.68	37.80
TiO_2	4.25	4.74	4.13	5.11	3.64	3.39	4.09	4.02
Al_2O_3	13.73	13.20	13.17	12.26	11.83	11.93	12.54	13.00
FeO_{total}	22.35	24.64	22.73	25.29	27.02	24.52	23.26	19.13
Fe_2O_3	3.60	3.56	3.80	4.20	3.40	4.10	4.50	3.90
FeO	19.11	21.44	19.31	21.51	23.96	20.83	19.21	15.62
MnO	0.49	0.23	0.39	0.40	0.47	0.25	0.34	0.24
MgO	9.58	9.48	9.69	7.98	7.19	8.74	9.62	11.62
CaO	0.01	0.16	0.00	0.04	0.01	0.01	0.02	0.01
Na_2O	0.06	0.17	0.10	0.04	0.09	0.07	0.12	0.06
K_2O	10.02	8.74	10.06	9.42	9.72	9.79	9.68	10.04
H_2O	3.71	3.58	3.32	3.42	2.93	2.90	3.18	3.25
F	0.17	0.42	1.04	0.67	1.64	1.75	1.20	1.28
Cl	0.34	0.30	0.21	0.38	0.33	0.42	0.46	0.33
O=F	-0.07	-0.18	-0.44	-0.28	-0.69	-0.74	-0.51	-0.54
O=Cl	-0.08	-0.07	-0.05	-0.09	-0.07	-0.09	-0.10	-0.07
total	100.86	101.10	101.19	101.29	101.37	100.73	101.03	100.56
^{iv}Si	5.50	5.42	5.56	5.58	5.74	5.77	5.61	5.69
^{iv}Al	2.48	2.39	2.37	2.22	2.17	2.17	2.26	2.31
^{iv}Ti	0.02	0.19	0.07	0.20	0.09	0.06	0.13	0.00
T site #	8.00	8.00	8.00	8.00	8.00	8.00	8.00	8.00
Al	0.00	0.00	0.00	0.00	0.00	0.00	0.00	0.00
Ti	0.47	0.36	0.41	0.40	0.33	0.33	0.35	0.45
Fe^{+3}	0.41	0.41	0.44	0.49	0.40	0.48	0.52	0.44
Fe^{+2}	2.45	2.75	2.47	2.77	3.11	2.69	2.46	1.97
Mn^{+2}	0.06	0.03	0.05	0.05	0.06	0.03	0.04	0.03
Mg	2.19	2.17	2.21	1.83	1.67	2.01	2.19	2.61
O site #	5.58	5.72	5.56	5.54	5.57	5.54	5.56	5.50
Ca	0.00	0.03	0.00	0.01	0.00	0.00	0.00	0.00
Na	0.02	0.05	0.03	0.01	0.03	0.02	0.04	0.02
K	1.96	1.71	1.96	1.85	1.93	1.93	1.89	1.93
A site #	1.98	1.79	1.99	1.87	1.96	1.95	1.93	1.95
O	20.00	20.00	20.00	20.00	20.00	20.00	20.00	20.00
OH	3.83	3.72	3.44	3.57	3.11	3.04	3.30	3.31
F	0.08	0.21	0.50	0.33	0.81	0.85	0.58	0.61
Cl	0.09	0.08	0.05	0.10	0.09	0.11	0.12	0.08
Charge	0.00	0.00	0.00	0.00	0.00	0.00	0.00	0.00
Fe_{total}	2.86	3.16	2.90	3.26	3.51	3.16	2.98	2.41
Al_{total}	2.48	2.39	2.37	2.22	2.17	2.17	2.26	2.31
Fe/(Fe+Mg)	0.57	0.59	0.57	0.64	0.68	0.61	0.58	0.48
A/CNK	1.25	1.32	1.19	1.19	1.11	1.11	1.17	1.18
Fe^{3+}/Fe_{total}	0.14	0.13	0.15	0.15	0.11	0.15	0.17	0.18
$Log(X_{Mg}/X_{Fe})$	-0.12	-0.16	-0.12	-0.25	-0.32	-0.20	-0.13	0.03
$Log(X_F/X_{OH})$	-1.67	-1.26	-0.84	-1.04	-0.59	-0.55	-0.75	-0.73

samples labelled mg- are from Wallace (1988)

sample	mg-66	nb-53	nb-52	nb-47	nb-60	mg-42	mg-46	mg-51
determinations	6	4	5	6	4	6	5	7
SiO_2	36.69	34.83	33.94	35.69	35.42	37.48	36.46	37.74
TiO_2	3.79	3.69	3.75	4.17	2.38	4.16	4.01	3.66
Al_2O_3	12.67	12.82	13.33	14.07	10.77	12.99	12.87	12.38
FeO_{total}	23.05	29.88	30.28	21.21	34.04	20.38	22.30	22.73
Fe_2O_3	4.70	5.98	6.06	4.01	6.81	3.90	4.30	4.30
FeO	18.82	24.50	24.83	17.61	27.91	16.87	18.43	18.86
MnO	0.27	0.78	0.80	0.21	0.19	0.37	0.20	0.39
MgO	9.54	5.06	5.33	11.24	3.95	11.15	10.35	10.50
CaO	0.00	0.04	0.04	0.01	0.08	0.01	0.02	0.02
Na_2O	0.10	0.18	0.17	0.11	0.12	0.09	0.15	0.09
K_2O	9.75	9.18	8.76	9.90	9.22	9.57	9.84	9.78
H_2O	3.13	2.77	2.95	3.62	2.90	3.17	3.13	3.06
F	1.41	1.87	1.50	0.52	0.72	1.39	1.36	1.52
Cl	0.29	0.32	0.32	0.17	1.65	0.39	0.39	0.42
O=F	-0.59	-0.79	-0.63	-0.22	-0.30	-0.59	-0.57	-0.64
O=Cl	-0.07	-0.07	-0.07	-0.04	-0.37	-0.09	-0.09	-0.09
total	100.50	101.16	101.08	101.07	101.45	100.86	100.85	101.99
^{iv}Si	5.63	5.50	5.37	5.41	5.70	5.65	5.57	5.69
^{iv}Al	2.29	2.38	2.48	2.51	2.04	2.31	2.32	2.20
^{iv}Ti	0.07	0.12	0.15	0.08	0.25	0.04	0.11	0.11
T site #	8.00	8.00	8.00	8.00	8.00	8.00	8.00	8.00
Al	0.00	0.00	0.00	0.00	0.00	0.00	0.00	0.00
Ti	0.36	0.32	0.30	0.40	0.04	0.44	0.35	0.31
Fe^{+3}	0.54	0.71	0.72	0.46	0.83	0.44	0.49	0.49
Fe^{+2}	2.42	3.23	3.28	2.23	3.76	2.13	2.35	2.38
Mn^{+2}	0.04	0.10	0.11	0.03	0.03	0.05	0.03	0.05
Mg	2.18	1.19	1.26	2.54	0.95	2.51	2.36	2.36
O site #	5.54	5.56	5.67	5.65	5.59	5.56	5.58	5.59
Ca	0.00	0.01	0.01	0.00	0.01	0.00	0.00	0.00
Na	0.03	0.05	0.05	0.03	0.04	0.03	0.04	0.03
K	1.91	1.85	1.77	1.92	1.89	1.84	1.92	1.88
A site #	1.94	1.91	1.83	1.95	1.95	1.87	1.97	1.91
O	20.00	20.00	20.00	20.00	20.00	20.00	20.00	20.00
OH	3.24	2.98	3.17	3.71	3.18	3.24	3.24	3.17
F	0.68	0.93	0.75	0.25	0.37	0.66	0.66	0.73
Cl	0.08	0.09	0.08	0.04	0.45	0.10	0.10	0.11
Charge	0.00	0.00	0.00	0.00	0.00	0.00	0.00	0.00
Fe_{total}	2.96	3.94	4.00	2.69	4.58	2.57	2.85	2.87
Al_{total}	2.29	2.38	2.48	2.51	2.04	2.31	2.32	2.20
Fe/(Fe+Mg)	0.58	0.77	0.76	0.51	0.83	0.51	0.55	0.55
A/CNK	1.18	1.25	1.35	1.29	1.04	1.23	1.18	1.15
Fe^{3+}/Fe_{total}	0.18	0.18	0.18	0.17	0.18	0.17	0.17	0.17
$Log(X_{Mg}/X_{Fe})$	-0.13	-0.52	-0.50	-0.02	-0.68	-0.01	-0.08	-0.08
$Log(X_F/X_{OH})$	-0.68	-0.50	-0.63	-1.17	-0.94	-0.69	-0.69	-0.64

samples labelled mg- are from Wallace (1988)

sample	mg-57	mg-83	mg-16	mg37-2	mg39-8	mg-94
determinations	5	8	5	2	4	4
SiO_2	38.67	37.44	37.39	38.00	41.88	35.67
TiO_2	3.52	3.64	2.71	1.77	2.56	3.74
Al_2O_3	11.71	12.48	12.82	10.78	12.58	11.50
FeO_{total}	22.30	24.28	22.28	27.57	9.10	30.37
Fe_2O_3	4.90	5.30	6.60	6.20	0.00	6.90
FeO	17.89	19.51	16.34	21.99	9.10	24.16
MnO	0.45	0.48	1.77	4.21	4.20	3.07
MgO	10.33	9.05	9.46	3.80	14.90	2.50
CaO	0.01	0.02	0.01	0.00	0.01	0.00
Na_2O	0.09	0.08	0.13	0.06	0.16	0.10
K_2O	9.84	9.60	9.18	9.88	9.34	9.75
H_2O	2.32	3.10	3.30	3.68	2.55	3.65
F	3.11	1.43	1.25	0.15	3.17	0.13
Cl	0.44	0.34	0.02	0.02	0.01	0.02
O=F	-1.31	-0.60	-0.53	-0.06	-1.33	-0.05
O=Cl	-0.10	-0.08	0.00	0.00	0.00	0.00
total	101.87	101.80	100.45	100.48	99.13	101.13
^{iv}Si	5.83	5.69	5.70	6.03	6.17	5.69
^{iv}Al	2.08	2.23	2.30	1.97	1.83	2.16
^{iv}Ti	0.09	0.08	0.00	0.00	0.00	0.15
T site #	8.00	8.00	8.00	8.00	8.00	8.00
Al	0.00	0.00	0.01	0.04	0.35	0.00
Ti	0.31	0.34	0.31	0.21	0.28	0.30
Fe^{+3}	0.56	0.61	0.76	0.74	0.00	0.83
Fe^{+2}	2.25	2.48	2.08	2.92	1.12	3.22
Mn^{+2}	0.06	0.06	0.23	0.57	0.52	0.41
Mg	2.32	2.05	2.15	0.90	3.27	0.59
O site #	5.49	5.53	5.54	5.37	5.55	5.36
Ca	0.00	0.00	0.00	0.00	0.00	0.00
Na	0.03	0.02	0.04	0.02	0.05	0.03
K	1.89	1.86	1.79	2.00	1.76	1.98
A site #	1.92	1.89	1.83	2.02	1.80	2.01
O	20.00	20.00	20.00	20.00	20.00	20.00
OH	2.41	3.23	3.39	3.92	2.52	3.93
F	1.48	0.69	0.60	0.08	1.48	0.07
Cl	0.11	0.09	0.01	0.01	0.00	0.01
Charge	0.00	0.00	0.00	0.00	0.00	0.00
Fe_{total}	2.81	3.08	2.84	3.66	1.12	4.05
Al_{total}	2.08	2.23	2.30	2.02	2.18	2.16
Fe/(Fe+Mg)	0.55	0.60	0.57	0.80	0.26	0.87
A/CNK	1.08	1.18	1.26	1.00	1.21	1.07
Fe^{3+}/Fe_{total}	0.20	0.20	0.27	0.20	0.00	0.20
$Log(X_{Mg}/X_{Fe})$	-0.08	-0.18	-0.12	-0.61	0.47	-0.83
$Log(X_F/X_{OH})$	-0.21	-0.67	-0.75	-1.72	-0.23	-1.78

samples labelled mg- are from Wallace (1988)

sample	nb-294	nb-111	nb-122	nb-125	nb-13	nb-134	nb-136	nb-145
determinations	5	5	3	6	4	3	6	4
SiO_2	35.25	33.97	34.53	35.67	34.78	35.18	34.64	34.51
TiO_2	1.92	2.74	2.82	2.90	3.13	2.48	2.79	2.48
Al_2O_3	19.68	18.62	17.97	16.56	18.42	16.82	17.27	18.58
FeO_{total}	22.84	27.27	24.12	22.21	22.47	22.84	22.75	22.76
Fe_2O_3	4.32	3.46	5.52	4.86	5.76	4.57	5.45	4.63
FeO	18.96	24.16	19.15	17.84	17.28	18.73	17.85	18.60
MnO	0.89	0.44	0.70	0.28	0.68	0.36	0.46	0.50
MgO	5.47	4.72	6.67	8.96	7.30	9.15	7.73	7.62
CaO	0.00	0.03	0.06	0.01	0.00	0.05	0.01	0.04
Na_2O	0.13	0.09	0.04	0.08	0.10	0.06	0.08	0.07
K_2O	10.16	9.70	9.55	10.28	10.25	10.11	10.06	9.77
H_2O	2.90	3.43	3.67	3.63	3.68	3.53	3.58	3.56
F	2.02	0.71	0.37	0.50	0.40	0.69	0.57	0.64
Cl	0.09	0.08	0.01	0.03	0.01	0.04	0.01	0.01
O=F	-0.85	-0.30	-0.16	-0.21	-0.17	-0.29	-0.24	-0.27
O=Cl	-0.02	-0.02	0.00	-0.01	0.00	-0.01	0.00	0.00
total	100.92	101.82	100.90	101.38	101.61	101.46	100.26	100.75
^{iv}Si	5.37	5.23	5.27	5.39	5.25	5.33	5.31	5.25
^{iv}Al	2.63	2.77	2.73	2.61	2.75	2.67	2.69	2.75
^{iv}Ti	0.00	0.00	0.00	0.00	0.00	0.00	0.00	0.00
T site #	8.00	8.00	8.00	8.00	8.00	8.00	8.00	8.00
Al	0.90	0.61	0.51	0.34	0.52	0.34	0.43	0.59
Ti	0.22	0.32	0.32	0.33	0.35	0.28	0.32	0.28
Fe^{+3}	0.49	0.40	0.63	0.55	0.65	0.52	0.63	0.53
Fe^{+2}	2.42	3.11	2.45	2.25	2.18	2.37	2.29	2.37
Mn^{+2}	0.11	0.06	0.09	0.04	0.09	0.05	0.06	0.06
Mg	1.24	1.08	1.52	2.02	1.64	2.07	1.77	1.73
O site #	5.39	5.59	5.52	5.53	5.43	5.63	5.50	5.56
Ca	0.00	0.00	0.01	0.00	0.00	0.01	0.00	0.01
Na	0.04	0.03	0.01	0.02	0.03	0.02	0.02	0.02
K	1.97	1.91	1.86	1.98	1.97	1.95	1.97	1.90
A site #	2.01	1.94	1.88	2.00	2.00	1.98	1.99	1.93
O	20.00	20.10	20.08	20.09	20.11	20.10	20.06	20.07
OH	3.00	3.53	3.74	3.66	3.70	3.56	3.66	3.62
F	0.98	0.35	0.18	0.24	0.19	0.33	0.28	0.31
Cl	0.02	0.02	0.00	0.01	0.00	0.01	0.00	0.00
Charge	0.00	-0.10	-0.08	-0.09	-0.11	-0.10	-0.06	-0.07
Fe_{total}	2.91	3.51	3.08	2.81	2.83	2.89	2.92	2.90
Al_{total}	3.53	3.38	3.23	2.95	3.27	3.00	3.12	3.33
Fe/(Fe+Mg)	0.70	0.76	0.67	0.58	0.63	0.58	0.62	0.63
A/CNK	1.75	1.74	1.71	1.47	1.64	1.51	1.57	1.73
Fe^{3+}/Fe_{total}	0.17	0.11	0.21	0.20	0.23	0.18	0.22	0.18
$Log(X_{Mg}/X_{Fe})$	-0.37	-0.51	-0.31	-0.14	-0.24	-0.15	-0.22	-0.22
$Log(X_F/X_{OH})$	-0.49	-1.01	-1.32	-1.19	-1.29	-1.03	-1.12	-1.07

sample	nb-146	nb-161	nb-162	nb-166	nb-169	nb-17	nb-173	nb-175
determinations	5	6	6	6	6	6	6	4
SiO_2	34.46	35.22	35.23	34.65	34.81	35.49	35.09	33.39
TiO_2	3.05	3.00	2.95	2.90	2.99	2.85	1.83	2.81
Al_2O_3	18.44	17.06	17.86	19.36	18.85	17.07	19.39	17.41
FeO_{total}	23.73	22.73	21.36	19.98	22.33	21.60	21.05	27.85
Fe_2O_3	3.88	3.92	3.30	1.75	2.79	4.27	3.05	5.57
FeO	20.24	19.21	18.40	18.40	19.82	17.76	18.31	22.84
MnO	0.54	0.42	0.43	0.21	0.27	0.48	0.55	0.40
MgO	6.91	8.28	8.16	8.59	8.08	8.65	8.30	5.39
CaO	0.02	0.01	0.01	0.00	0.01	0.02	0.00	0.03
Na_2O	0.08	0.07	0.06	0.22	0.23	0.06	0.08	0.07
K_2O	9.57	10.15	10.04	9.66	9.64	10.14	10.10	9.91
H_2O	3.61	3.74	3.59	3.74	3.73	3.56	3.62	3.44
F	0.52	0.26	0.64	0.40	0.33	0.68	0.60	0.69
Cl	0.02	0.01	0.01	0.01	0.03	0.01	0.01	0.10
O=F	-0.22	-0.11	-0.27	-0.17	-0.14	-0.29	-0.25	-0.29
O=Cl	0.00	0.00	0.00	0.00	-0.01	0.00	0.00	-0.02
total	101.12	101.23	100.41	99.74	101.44	100.73	100.68	101.73
^{iv}Si	5.25	5.35	5.36	5.27	5.25	5.39	5.31	5.18
^{iv}Al	2.75	2.65	2.64	2.73	2.75	2.61	2.69	2.82
^{iv}Ti	0.00	0.00	0.00	0.00	0.00	0.00	0.00	0.00
T site #	8.00	8.00	8.00	8.00	8.00	8.00	8.00	8.00
Al	0.56	0.40	0.56	0.74	0.60	0.44	0.77	0.35
Ti	0.35	0.34	0.34	0.33	0.34	0.33	0.21	0.33
Fe^{+3}	0.44	0.45	0.38	0.20	0.32	0.49	0.35	0.65
Fe^{+2}	2.58	2.44	2.34	2.34	2.50	2.25	2.32	2.96
Mn^{+2}	0.07	0.05	0.06	0.03	0.03	0.06	0.07	0.05
Mg	1.57	1.87	1.85	1.95	1.82	1.96	1.87	1.24
O site #	5.58	5.56	5.53	5.59	5.61	5.53	5.59	5.59
Ca	0.00	0.00	0.00	0.00	0.00	0.00	0.00	0.00
Na	0.02	0.02	0.02	0.07	0.07	0.02	0.02	0.02
K	1.86	1.97	1.95	1.87	1.85	1.96	1.95	1.96
A site #	1.89	1.99	1.97	1.94	1.93	1.98	1.98	1.98
O	20.08	20.08	20.05	20.01	20.08	20.07	20.06	20.00
OH	3.67	3.79	3.64	3.80	3.75	3.60	3.65	3.63
F	0.25	0.13	0.31	0.19	0.16	0.33	0.29	0.34
Cl	0.00	0.00	0.00	0.00	0.01	0.00	0.00	0.03
Charge	-0.08	-0.08	-0.05	-0.01	-0.08	-0.07	-0.06	0.00
Fe_{total}	3.02	2.89	2.72	2.54	2.82	2.74	2.66	3.61
Al_{total}	3.31	3.05	3.20	3.47	3.35	3.05	3.46	3.18
Fe/(Fe+Mg)	0.66	0.61	0.59	0.57	0.61	0.58	0.59	0.74
A/CNK	1.75	1.54	1.63	1.79	1.74	1.54	1.75	1.60
Fe^{3+}/Fe_{total}	0.15	0.15	0.14	0.08	0.11	0.18	0.13	0.18
$Log(X_{Mg}/X_{Fe})$	-0.28	-0.19	-0.17	-0.12	-0.19	-0.15	-0.15	-0.46
$Log(X_F/X_{OH})$	-1.17	-1.48	-1.07	-1.29	-1.38	-1.04	-1.10	-1.03

sample	nb-19	nb-214	nb-227	nb-277	nb-280	nb-29	nb-30	nb-326
determinations	3	6	6	5	5	7	5	6
SiO_2	34.47	34.65	33.94	35.13	36.19	34.57	34.37	34.36
TiO_2	2.74	2.65	3.06	1.47	1.50	2.01	2.70	2.86
Al_2O_3	18.49	19.35	19.02	17.02	16.07	18.10	18.13	17.44
FeO_{total}	21.55	24.98	24.56	26.76	27.16	20.63	22.66	22.98
Fe_2O_3	3.93	3.92	4.38	5.06	3.92	5.03	5.45	4.60
FeO	18.02	21.45	20.62	22.21	23.63	16.10	17.76	18.84
MnO	0.84	0.64	0.60	0.43	0.33	0.95	0.83	0.56
MgO	7.37	4.47	6.20	6.14	6.16	9.46	6.98	8.34
CaO	0.01	0.00	0.01	0.02	0.01	0.01	0.03	0.18
Na_2O	0.12	0.06	0.08	0.04	0.05	0.07	0.08	0.06
K_2O	9.97	9.42	9.12	9.83	10.18	9.44	9.54	9.11
H_2O	3.30	3.65	3.62	3.57	3.48	3.65	3.67	3.66
F	1.19	0.42	0.48	0.48	0.71	0.53	0.40	0.50
Cl	0.02	0.00	0.01	0.14	0.02	0.01	0.01	0.01
O=F	-0.50	-0.18	-0.20	-0.20	-0.30	-0.22	-0.17	-0.21
O=Cl	0.00	0.00	0.00	-0.03	-0.01	0.00	0.00	0.00
total	99.95	100.50	100.95	101.29	101.96	99.71	99.77	100.31
^{iv}Si	5.29	5.33	5.19	5.42	5.56	5.27	5.28	5.26
^{iv}Al	2.71	2.67	2.81	2.58	2.44	2.73	2.72	2.74
^{iv}Ti	0.00	0.00	0.00	0.00	0.00	0.00	0.00	0.00
T site #	8.00	8.00	8.00	8.00	8.00	8.00	8.00	8.00
Al	0.63	0.83	0.61	0.51	0.47	0.52	0.57	0.40
Ti	0.32	0.31	0.35	0.17	0.17	0.23	0.31	0.33
Fe^{+3}	0.45	0.45	0.50	0.59	0.45	0.58	0.63	0.53
Fe^{+2}	2.31	2.76	2.64	2.86	3.03	2.05	2.28	2.41
Mn^{+2}	0.11	0.08	0.08	0.06	0.04	0.12	0.11	0.07
Mg	1.68	1.02	1.41	1.41	1.41	2.15	1.60	1.90
O site #	5.50	5.46	5.59	5.60	5.58	5.65	5.50	5.65
Ca	0.00	0.00	0.00	0.00	0.00	0.00	0.00	0.03
Na	0.03	0.02	0.02	0.01	0.01	0.02	0.02	0.02
K	1.95	1.85	1.78	1.93	1.99	1.84	1.87	1.78
A site #	1.99	1.87	1.81	1.95	2.01	1.86	1.90	1.83
O	20.05	20.05	20.07	20.00	20.00	20.03	20.04	20.00
OH	3.37	3.74	3.69	3.73	3.65	3.71	3.76	3.76
F	0.58	0.20	0.23	0.23	0.34	0.25	0.20	0.24
Cl	0.00	0.00	0.00	0.04	0.01	0.00	0.00	0.00
Charge	-0.05	-0.05	-0.07	0.00	0.00	-0.03	-0.04	0.00
Fe_{total}	2.76	3.21	3.14	3.45	3.49	2.63	2.91	2.94
Al_{total}	3.34	3.50	3.43	3.09	2.91	3.25	3.28	3.15
Fe/(Fe+Mg)	0.62	0.76	0.69	0.71	0.71	0.55	0.65	0.61
A/CNK	1.68	1.88	1.89	1.58	1.44	1.75	1.73	1.70
Fe^{3+}/Fe_{total}	0.16	0.14	0.16	0.17	0.13	0.22	0.22	0.18
$Log(X_{Mg}/X_{Fe})$	-0.22	-0.50	-0.35	-0.39	-0.39	-0.09	-0.26	-0.19
$Log(X_F/X_{OH})$	-0.77	-1.26	-1.20	-1.20	-1.03	-1.16	-1.28	-1.19

sample	nb-38	nb-8	nb-97	nb-1	nb-116	nb-123	nb-151	nb-152
determinations	6	8	5	5	5	4	4	2
SiO_2	35.12	34.70	35.80	35.83	35.65	36.37	35.17	35.16
TiO_2	3.02	2.84	3.42	3.01	3.68	3.55	2.86	4.62
Al_2O_3	18.50	19.83	14.82	15.46	15.73	14.51	17.03	13.86
FeO_{total}	22.40	21.29	23.59	21.94	23.22	22.03	23.83	24.67
Fe_2O_3	3.96	1.40	3.41	3.17	3.35	3.18	3.44	3.56
FeO	18.84	20.03	20.52	19.08	20.20	19.17	20.73	21.47
MnO	0.54	0.26	0.17	0.47	0.62	0.34	0.37	0.38
MgO	7.06	7.27	9.17	9.75	8.55	10.26	7.82	8.65
CaO	0.01	0.01	0.08	0.02	0.00	0.02	0.03	0.01
Na_2O	0.15	0.21	0.04	0.07	0.11	0.08	0.07	0.20
K_2O	10.04	9.69	10.16	10.16	10.03	10.06	10.20	9.42
H_2O	3.46	3.78	3.36	3.78	3.53	3.62	3.66	3.41
F	0.87	0.27	0.84	0.24	0.72	0.58	0.43	0.79
Cl	0.03	0.03	0.39	0.01	0.02	0.03	0.01	0.13
O=F	-0.37	-0.11	-0.36	-0.10	-0.30	-0.24	-0.18	-0.33
O=Cl	-0.01	-0.01	-0.09	0.00	0.00	-0.01	0.00	-0.03
total	101.20	100.20	101.74	100.96	101.87	101.51	101.65	101.30
^{iv}Si	5.32	5.28	5.46	5.45	5.41	5.50	5.35	5.40
^{iv}Al	2.68	2.72	2.54	2.55	2.59	2.50	2.65	2.51
^{iv}Ti	0.00	0.00	0.00	0.00	0.00	0.00	0.00	0.09
T site #	8.00	8.00	8.00	8.00	8.00	8.00	8.00	8.00
Al	0.62	0.84	0.12	0.23	0.22	0.09	0.41	0.00
Ti	0.34	0.33	0.39	0.34	0.42	0.40	0.33	0.45
Fe^{+3}	0.45	0.16	0.39	0.36	0.38	0.36	0.39	0.41
Fe^{+2}	2.39	2.55	2.62	2.43	2.56	2.42	2.64	2.76
Mn^{+2}	0.07	0.03	0.02	0.06	0.08	0.04	0.05	0.05
Mg	1.59	1.65	2.08	2.21	1.93	2.31	1.77	1.98
O site #	5.47	5.56	5.62	5.63	5.59	5.63	5.59	5.65
Ca	0.00	0.00	0.01	0.00	0.00	0.00	0.00	0.00
Na	0.04	0.06	0.01	0.02	0.03	0.02	0.02	0.06
K	1.94	1.88	1.97	1.97	1.94	1.94	1.98	1.85
A site #	1.99	1.94	2.00	2.00	1.97	1.97	2.00	1.91
O	20.09	20.02	20.00	20.00	20.00	20.00	20.00	20.09
OH	3.49	3.84	3.49	3.88	3.65	3.72	3.79	3.49
F	0.42	0.13	0.41	0.12	0.34	0.28	0.21	0.39
Cl	0.01	0,01	0.10	0.00	0.00	0.01	0.00	0.03
Charge	-0.09	-0.02	0.00	0.00	0.00	0.00	0.00	-0.09
Fe_{total}	2.84	2.71	3.01	2.79	2.94	2.79	3.03	3.17
Al_{total}	3.30	3.56	2.66	2.77	2.81	2.59	3.06	2.51
Fe/(Fe+Mg)	0.64	0.62	0.59	0.56	0.60	0.55	0.63	0.62
A/CNK	1.66	1.83	1.32	1.39	1.42	1.31	1.52	1.31
Fe^{3+}/Fe_{total}	0.16	0.06	0.13	0.13	0.13	0.13	0.13	0.13
$Log(X_{Mg}/X_{Fe})$	-0.25	-0.22	-0.16	-0.10	-0.18	-0.08	-0.23	-0.20
$Log(X_F/X_{OH})$	-0.92	-1.47	-0.93	-1.52	-1.03	-1.13	-1.26	-0.96

sample	nb-158	nb-159	nb-188	nb-2	nb-306	nb-317	nb-45	nb-78
determinations	5	6	5	8	6	4	5	5
SiO_2	33.46	34.52	37.86	35.89	35.23	36.32	35.43	39.65
TiO_2	3.53	3.31	3.16	3.38	2.64	2.38	3.63	1.77
Al_2O_3	15.00	18.82	13.24	14.99	16.56	15.56	17.46	12.40
FeO_{total}	27.51	24.33	24.32	23.06	26.47	20.57	22.94	14.79
Fe_2O_3	3.97	2.00	3.51	3.33	3.82	2.97	3.31	2.73
FeO	23.93	22.53	21.15	20.06	23.03	17.90	19.96	12.33
MnO	0.63	0.33	0.77	0.38	0.28	0.40	0.64	0.27
MgO	5.66	5.76	7.22	8.78	6.08	10.46	7.60	17.33
CaO	0.01	0.04	0.21	0.02	0.01	0.02	0.00	0.01
Na_2O	0.10	0.13	0.14	0.09	0.06	0.03	0.13	0.12
K_2O	9.66	9.81	9.96	9.95	9.95	10.34	10.16	10.33
H_2O	3.10	3.65	2.23	3.53	3.51	3.71	3.61	1.94
F	1.26	0.39	3.26	0.67	0.61	0.43	0.57	4.28
Cl	0.13	0.07	0.28	0.02	0.12	0.01	0.04	0.11
O=F	-0.53	-0.16	-1.37	-0.28	-0.26	-0.18	-0.24	-1.80
O=Cl	-0.03	-0.02	-0.06	-0.01	-0.03	0.00	-0.01	-0.03
total	99.88	101.17	101.56	100.81	101.62	100.34	102.29	101.44
^{iv}Si	5.32	5.29	5.80	5.49	5.42	5.52	5.34	5.81
^{iv}Al	2.68	2.71	2.20	2.51	2.58	2.48	2.66	2.14
^{iv}Ti	0.00	0.00	0.00	0.00	0.00	0.00	0.00	0.04
T site #	8.00	8.00	8.00	8.00	8.00	8.00	8.00	8.00
Al	0.12	0.68	0.19	0.20	0.42	0.31	0.43	0.00
Ti	0.42	0.38	0.36	0.39	0.31	0.27	0.41	0.15
Fe^{+3}	0.48	0.23	0.40	0.38	0.44	0.34	0.38	0.30
Fe^{+2}	3.18	2.89	2.71	2.57	2.96	2.28	2.51	1.51
Mn^{+2}	0.09	0.04	0.10	0.05	0.04	0.05	0.08	0.03
Mg	1.34	1.31	1.65	2.00	1.40	2.37	1.71	3.79
O site #	5.63	5.54	5.41	5.59	5.56	5.63	5.52	5.79
Ca	0.00	0.01	0.03	0.00	0.00	0.00	0.00	0.00
Na	0.03	0.04	0.04	0.03	0.02	0.01	0.04	0.03
K	1.96	1.92	1.94	1.94	1.95	2.01	1.95	1.93
A site #	1.99	1.96	2.02	1.97	1.97	2.02	1.99	1.97
O	20.04	20.07	20.00	20.07	20.00	20.00	20.00	20.09
OH	3.29	3.72	2.35	3.60	3.67	3.79	3.72	1.90
F	0.63	0.19	1.58	0.33	0.30	0.21	0.27	1.99
Cl	0.03	0.02	0.07	0.01	0.03	0.00	0.01	0.03
Charge	-0.04	-0.07	0.00	-0.07	0.00	0.00	0.00	-0.09
Fe_{total}	3.65	3.12	3.11	2.95	3.41	2.62	2.89	1.81
Al_{total}	2.81	3.40	2.39	2.70	3.00	2.79	3.10	2.14
Fe/(Fe+Mg)	0.73	0.70	0.65	0.60	0.71	0.52	0.63	0.32
A/CNK	1.41	1.73	1.16	1.37	1.52	1.38	1.56	1.09
Fe^{3+}/Fe_{total}	0.13	0.07	0.13	0.13	0.13	0.13	0.13	0.17
$Log(X_{Mg}/X_{Fe})$	-0.44	-0.37	-0.28	-0.17	-0.39	-0.04	-0.23	0.32
$Log(X_F/X_{OH})$	-0.72	-1.30	-0.17	-1.04	-1.09	-1.26	-1.14	0.02

sample	nb-98	nb-115	nb-44	nb-144	nb-7	nb-155	nb-170	nb-168
determinations	4	5	4	4	4	5	5	4
SiO_2	36.49	35.72	35.18	35.39	35.96	36.60	35.50	36.14
TiO_2	2.02	3.46	3.95	4.66	2.62	3.11	4.30	3.71
Al_2O_3	15.28	15.12	15.21	12.86	15.13	15.78	14.40	14.46
FeO_{total}	25.73	21.16	23.66	27.27	21.87	17.76	24.64	23.71
Fe_2O_3	4.86	3.06	3.42	5.15	3.40	2.76	4.66	4.48
FeO	21.36	18.41	20.58	22.64	18.81	15.27	20.45	19.68
MnO	0.25	0.50	0.85	0.48	0.34	0.17	0.38	0.36
MgO	7.57	9.64	7.79	6.91	10.60	12.91	8.40	8.75
CaO	0.04	0.03	0.03	0.30	0.02	0.01	0.01	0.01
Na_2O	0.15	0.08	0.10	0.19	0.09	0.12	0.08	0.07
K_2O	10.00	10.10	9.67	9.48	10.10	10.16	9.71	10.26
H_2O	3.40	3.64	3.43	3.51	3.80	3.90	3.69	3.73
F	0.94	0.54	0.87	0.52	0.21	0.15	0.35	0.28
Cl	0.01	0.01	0.05	0.19	0.03	0.04	0.03	0.03
O=F	-0.40	-0.23	-0.37	-0.22	-0.09	-0.06	-0.15	-0.12
O=Cl	0.00	0.00	-0.01	-0.04	-0.01	-0.01	-0.01	-0.01
total	101.98	100.09	100.74	102.01	101.02	100.91	101.80	101.85
^{iv}Si	5.56	5.47	5.42	5.46	5.46	5.45	5.41	5.49
^{iv}Al	2.44	2.53	2.58	2.34	2.54	2.55	2.59	2.51
^{iv}Ti	0.00	0.00	0.00	0.20	0.00	0.00	0.01	0.00
T site #	8.00	8.00	8.00	8.00	8.00	8.00	8.00	8.00
Al	0.30	0.20	0.18	0.00	0.17	0.22	0.00	0.07
Ti	0.23	0.40	0.46	0.34	0.30	0.35	0.49	0.42
Fe^{+3}	0.56	0.35	0.40	0.60	0.39	0.31	0.53	0.51
Fe^{+2}	2.72	2.36	2.65	2.92	2.39	1.90	2.61	2.50
Mn^{+2}	0.03	0.06	0.11	0.06	0.04	0.02	0.05	0.05
Mg	1.72	2.20	1.79	1.59	2.40	2.87	1.91	1.98
O site #	5.56	5.58	5.58	5.52	5.69	5.67	5.58	5.54
Ca	0.01	0.01	0.01	0.05	0.00	0.00	0.00	0.00
Na	0.04	0.02	0.03	0.06	0.03	0.03	0.02	0.02
K	1.94	1.97	1.90	1.87	1.96	1.93	1.89	1.99
A site #	1.99	2.00	1.93	1.97	1.99	1.97	1.91	2.01
O	20.00	20.00	20.00	20.00	20.00	20.00	20.00	20.00
OH	3.54	3.73	3.56	3.69	3.89	3.92	3.82	3.86
F	0.46	0.26	0.43	0.26	0.10	0.07	0.17	0.14
Cl	0.00	0.00	0.01	0.05	0.01	0.01	0.01	0.01
Charge	0.00	0.00	0.00	0.00	0.00	0.00	0.00	0.00
Fe_{total}	3.28	2.71	3.05	3.52	2.78	2.21	3.14	3.01
Al_{total}	2.74	2.73	2.76	2.34	2.71	2.77	2.59	2.59
Fe/(Fe+Mg)	0.66	0.55	0.63	0.69	0.54	0.44	0.62	0.60
A/CNK	1.37	1.36	1.42	1.16	1.36	1.41	1.35	1.29
Fe^{3+}/Fe_{total}	0.17	0.13	0.13	0.17	0.14	0.14	0.17	0.17
$Log(X_{Mg}/X_{Fe})$	-0.28	-0.09	-0.23	-0.35	-0.06	0.11	-0.22	-0.18
$Log(X_F/X_{OH})$	-0.89	-1.15	-0.92	-1.16	-1.59	-1.73	-1.36	-1.45

sample	nb-92	nb-143	nb-239	nb-88	nb-89	nb-91	nb-99
determinations	7	4	6	6	6	4	7
SiO_2	38.72	36.16	36.83	36.16	36.33	38.46	35.12
TiO_2	3.15	3.91	4.48	4.55	4.32	2.73	5.57
Al_2O_3	12.05	14.58	13.60	12.63	13.08	16.57	13.61
FeO_{total}	18.70	19.63	23.26	26.18	22.21	7.80	24.73
Fe_2O_3	3.71	3.05	2.62	3.43	3.46	0.68	1.90
FeO	15.36	16.88	20.90	23.09	19.10	7.19	23.03
MnO	0.17	0.26	0.14	0.14	0.13	0.03	0.15
MgO	14.13	11.66	10.25	8.13	10.96	20.99	7.66
CaO	0.00	0.03	0.02	0.03	0.52	0.05	0.01
Na_2O	0.07	0.10	0.23	0.07	0.09	1.66	0.17
K_2O	10.07	10.00	9.39	9.79	9.26	7.53	9.17
H_2O	2.70	3.86	3.74	3.28	3.35	4.07	3.63
F	2.38	0.14	0.09	0.65	0.81	0.21	0.07
Cl	0.40	0.04	0.34	0.77	0.49	0.15	0.60
O=F	-1.00	-0.06	-0.04	-0.27	-0.34	-0.09	-0.03
O=Cl	-0.09	-0.01	-0.08	-0.17	-0.11	-0.03	-0.14
total	101.83	100.61	102.52	102.26	101.45	100.18	100.52
^{iv}Si	5.75	5.46	5.53	5.55	5.51	5.46	5.45
^{iv}Al	2.11	2.54	2.41	2.29	2.34	2.54	2.49
^{iv}Ti	0.14	0.00	0.06	0.16	0.16	0.00	0.05
T site #	8.00	8.00	8.00	8.00	8.00	8.00	8.00
Al	0.00	0.06	0.00	0.00	0.00	0.24	0.00
Ti	0.21	0.44	0.44	0.37	0.33	0.29	0.60
Fe^{+3}	0.41	0.35	0.30	0.40	0.39	0.07	0.22
Fe^{+2}	1.91	2.13	2.62	2.97	2.42	0.85	2.99
Mn^{+2}	0.02	0.03	0.02	0.02	0.02	0.00	0.02
Mg	3.13	2.63	2.29	1.86	2.48	4.44	1.77
O site #	5.68	5.64	5.68	5.61	5.64	5.90	5.60
Ca	0.00	0.00	0.00	0.00	0.08	0.01	0.00
Na	0.02	0.03	0.07	0.02	0.03	0.46	0.05
K	1.91	1.93	1.80	1.92	1.79	1.37	1.82
A site #	1.93	1.96	1.87	1.94	1.90	1.83	1.87
O	20.11	20.00	20.12	20.12	20.09	20.02	20.04
OH	2.68	3.92	3.75	3.36	3.39	3.85	3.76
F	1.11	0.07	0.04	0.32	0.39	0.09	0.04
Cl	0.10	0.01	0.09	0.20	0.13	0.04	0.16
Charge	-0.11	0.00	-0.12	-0.12	-0.09	-0.02	-0.04
Fe_{total}	2.32	2.48	2.92	3.36	2.81	0.93	3.21
Al_{total}	2.11	2.59	2.41	2.29	2.34	2.77	2.49
Fe/(Fe+Mg)	0.43	0.49	0.56	0.64	0.53	0.17	0.64
A/CNK	1.09	1.32	1.28	1.17	1.18	1.51	1.33
Fe^{3+}/Fe_{total}	0.18	0.14	0.10	0.12	0.14	0.08	0.07
$Log(X_{Mg}/X_{Fe})$	0.13	0.03	-0.10	-0.26	-0.06	0.68	-0.26
$Log(X_F/X_{OH})$	-0.38	-1.76	-1.92	-1.03	-0.94	-1.62	-2.02

sample	nf-112	nf-20	nf-28	nf-75	nf-102	nf-128	nf-131	nf-29
determinations	4	4	7	4	6	6	6	7
SiO_2	36.37	36.55	36.34	35.94	36.95	37.12	34.97	37.12
TiO_2	2.31	2.47	1.77	2.55	2.86	2.05	3.93	2.95
Al_2O_3	16.40	16.42	16.26	17.04	14.11	16.51	14.70	15.98
FeO_{total}	20.23	19.61	22.70	18.07	17.37	18.99	26.31	20.03
Fe_2O_3	4.50	4.36	5.02	4.02	4.55	4.22	5.85	4.76
FeO	16.18	15.69	18.18	14.45	13.28	15.19	21.05	15.75
MnO	0.61	0.56	0.45	0.31	0.42	0.50	1.82	0.62
MgO	10.22	10.38	9.31	11.62	14.44	11.43	4.79	9.34
CaO	0.00	0.01	0.02	0.01	0.05	0.02	0.01	0.04
Na_2O	0.07	0.04	0.08	0.15	0.09	0.07	0.09	0.07
K_2O	10.32	10.44	9.92	9.91	9.47	9.83	8.98	10.26
H_2O	3.86	3.78	3.48	3.82	3.65	3.77	3.31	3.51
F	0.17	0.36	0.83	0.28	0.65	0.39	0.76	0.86
Cl	0.03	0.02	0.02	0.03	0.05	0.00	0.38	0.01
O=F	-0.07	-0.15	-0.35	-0.12	-0.27	-0.16	-0.32	-0.36
O=Cl	-0.01	0.00	-0.01	-0.01	-0.01	0.00	-0.09	0.00
total	100.98	100.92	101.32	100.00	100.27	100.94	100.23	100.90
^{iv}Si	5.47	5.49	5.49	5.40	5.51	5.53	5.47	5.57
^{iv}Al	2.53	2.51	2.51	2.60	2.48	2.47	2.53	2.43
^{iv}Ti	0.00	0.00	0.00	0.00	0.01	0.00	0.00	0.00
T site #	8.00	8.00	8.00	8.00	8.00	8.00	8.00	8.00
Al	0.38	0.39	0.38	0.41	0.00	0.42	0.19	0.40
Ti	0.26	0.28	0.20	0.29	0.32	0.23	0.46	0.33
Fe^{+3}	0.51	0.49	0.57	0.45	0.51	0.47	0.69	0.54
Fe^{+2}	2.04	1.97	2.30	1.81	1.66	1.89	2.76	1.98
Mn^{+2}	0.08	0.07	0.06	0.04	0.05	0.06	0.24	0.08
Mg	2.29	2.32	2.10	2.60	3.21	2.54	1.12	2.09
O site #	5.56	5.53	5.61	5.61	5.75	5.61	5.45	5.41
Ca	0.00	0.00	0.00	0.00	0.01	0.00	0.00	0.01
Na	0.02	0.01	0.02	0.04	0.03	0.02	0.03	0.02
K	1.98	2.00	1.91	1.90	1.80	1.87	1.79	1.96
A site #	2.00	2.01	1.94	1.94	1.84	1.89	1.82	1.99
O	20.00	20.00	20.10	20.03	20.05	20.07	20.07	20.08
OH	3.91	3.82	3.50	3.83	3.63	3.74	3.46	3.51
F	0.08	0.17	0.40	0.13	0.31	0.18	0.37	0.41
Cl	0.01	0.00	0.01	0.01	0.01	0.00	0.10	0.00
Charge	0.00	0.00	-0.10	-0.03	-0.05	-0.07	-0.07	-0.08
Fe_{total}	2.55	2.46	2.87	2.27	2.17	2.36	3.44	2.51
Al_{total}	2.91	2.91	2.90	3.01	2.48	2.90	2.71	2.83
Fe/(Fe+Mg)	0.53	0.51	0.58	0.47	0.40	0.48	0.75	0.55
A/CNK	1.45	1.44	1.49	1.55	1.35	1.53	1.49	1.41
Fe^{3+}/Fe_{total}	0.20	0.20	0.20	0.20	0.24	0.20	0.20	0.21
$Log(X_{Mg}/X_{Fe})$	-0.05	-0.03	-0.14	0.06	0.17	0.03	-0.49	-0.08
$Log(X_F/X_{OH})$	-1.70	-1.34	-0.95	-1.46	-1.08	-1.31	-0.97	-0.94

sample	nf-36	nf-52	nf-110	nf-119	nf-14	nf-166	nf-18	nf-79
determinations	6	3	5	6	4	6	4	4
SiO_2	36.15	35.20	37.12	35.47	36.60	36.46	34.78	34.77
TiO_2	3.26	2.69	3.22	2.45	2.06	2.71	2.85	2.94
Al_2O_3	16.09	16.46	14.03	16.99	15.88	16.26	17.08	17.31
FeO_{total}	20.86	20.89	19.59	21.39	21.92	22.26	27.48	22.03
Fe_2O_3	4.48	4.64	4.35	4.80	4.87	5.43	6.11	3.18
FeO	16.83	16.71	15.67	17.07	17.54	17.37	21.98	19.16
MnO	0.61	0.55	0.51	0.51	0.75	0.55	0.84	0.30
MgO	9.20	9.66	12.21	9.84	9.02	8.78	3.62	9.24
CaO	0.00	0.03	0.05	0.03	0.00	0.03	0.01	0.01
Na_2O	0.09	0.09	0.05	0.09	0.05	0.06	0.06	0.10
K_2O	10.17	10.18	9.77	9.95	10.13	10.14	9.17	10.32
H_2O	3.79	3.72	3.44	3.74	3.59	3.78	3.30	3.72
F	0.23	0.29	0.83	0.27	0.61	0.22	0.99	0.31
Cl	0.00	0.10	0.33	0.10	0.00	0.01	0.05	0.08
O=F	-0.10	-0.12	-0.35	-0.11	-0.26	-0.09	-0.42	-0.13
O=Cl	0.00	-0.02	-0.07	-0.02	0.00	0.00	-0.01	-0.02
total	100.80	100.19	101.16	101.18	100.85	101.70	100.42	101.29
^{iv}Si	5.46	5.37	5.56	5.35	5.55	5.47	5.41	5.28
^{iv}Al	2.54	2.63	2.44	2.65	2.45	2.53	2.59	2.72
^{iv}Ti	0.00	0.00	0.00	0.00	0.00	0.00	0.00	0.00
T site #	8.00	8.00	8.00	8.00	8.00	8.00	8.00	8.00
Al	0.33	0.33	0.04	0.37	0.38	0.35	0.55	0.38
Ti	0.37	0.31	0.36	0.28	0.24	0.31	0.33	0.34
Fe^{+3}	0.51	0.53	0.49	0.55	0.56	0.61	0.72	0.36
Fe^{+2}	2.13	2.13	1.96	2.15	2.22	2.18	2.86	2.43
Mn^{+2}	0.08	0.07	0.06	0.07	0.10	0.07	0.11	0.04
Mg	2.07	2.20	2.73	2.21	2.04	1.97	0.84	2.09
O site #	5.49	5.57	5.64	5.62	5.53	5.49	5.41	5.64
Ca	0.00	0.00	0.01	0.01	0.00	0.00	0.00	0.00
Na	0.03	0.03	0.02	0.03	0.01	0.02	0.02	0.03
K	1.96	1.98	1.87	1.91	1.96	1.94	1.82	2.00
A site #	1.99	2.01	1.89	1.95	1.97	1.96	1.84	2.03
O	20.07	20.05	20.09	20.08	20.08	20.11	20.08	20.00
OH	3.82	3.79	3.44	3.76	3.63	3.79	3.43	3.83
F	0.11	0.14	0.39	0.13	0.29	0.10	0.49	0.15
Cl	0.00	0.03	0.08	0.03	0.00	0.00	0.01	0.02
Charge	-0.07	-0.05	-0.09	-0.08	-0.08	-0.11	-0.08	0.00
Fe_{total}	2.64	2.66	2.45	2.70	2.78	2.80	3.58	2.80
Al_{total}	2.87	2.96	2.48	3.02	2.84	2.88	3.13	3.10
Fe/(Fe+Mg)	0.56	0.55	0.47	0.55	0.58	0.59	0.81	0.57
A/CNK	1.44	1.47	1.30	1.55	1.44	1.46	1.70	1.53
Fe^{3+}/Fe_{total}	0.19	0.20	0.20	0.20	0.20	0.22	0.20	0.13
$Log(X_{Mg}/X_{Fe})$	-0.10	-0.08	0.05	-0.09	-0.13	-0.15	-0.63	-0.13
$Log(X_F/X_{OH})$	-1.55	-1.43	-0.94	-1.47	-1.09	-1.57	-0.85	-1.41

sample	nf-38	nf-78	nf-83	nf-1	nf-129	nf-143	nf-23	nf-106
determinations	3	3	6	6	3	4	6	6
SiO_2	34.25	33.76	35.26	34.33	31.66	36.30	35.46	37.38
TiO_2	2.64	2.23	2.82	3.12	2.03	3.15	2.47	2.66
Al_2O_3	16.88	17.59	16.54	15.58	15.50	15.59	15.00	15.38
FeO_{total}	24.00	22.82	22.20	30.51	35.10	19.68	29.19	18.80
Fe_2O_3	3.47	3.30	3.25	4.89	5.85	3.28	5.86	3.77
FeO	20.88	19.85	19.28	26.12	29.83	16.73	23.92	15.41
MnO	1.55	0.71	0.46	0.54	0.57	0.50	0.48	0.55
MgO	6.76	8.67	8.98	3.23	1.24	11.19	4.74	12.29
CaO	0.00	0.03	0.01	0.01	0.13	0.02	0.10	0.03
Na_2O	0.06	0.07	0.07	0.05	0.05	0.08	0.05	0.09
K_2O	10.01	9.70	10.13	9.69	8.32	9.96	9.82	10.10
H_2O	3.56	3.64	3.57	3.68	3.62	3.73	3.60	3.76
F	0.52	0.43	0.61	0.09	0.01	0.36	0.30	0.36
Cl	0.00	0.04	0.02	0.03	0.02	0.11	0.03	0.09
O=F	-0.22	-0.18	-0.26	-0.04	0.00	-0.15	-0.13	-0.15
O=Cl	0.00	-0.01	0.00	-0.01	-0.01	-0.03	-0.01	-0.02
total	100.36	99.83	100.72	101.31	98.82	100.83	101.70	101.67
^{iv}Si	5.32	5.23	5.38	5.40	5.23	5.46	5.51	5.54
^{iv}Al	2.68	2.77	2.62	2.60	2.77	2.54	2.49	2.46
^{iv}Ti	0.00	0.00	0.00	0.00	0.00	0.00	0.00	0.00
T site #	8.00	8.00	8.00	8.00	8.00	8.00	8.00	8.00
Al	0.42	0.44	0.36	0.29	0.25	0.23	0.25	0.23
Ti	0.31	0.26	0.32	0.37	0.25	0.36	0.29	0.30
Fe^{+3}	0.41	0.38	0.37	0.58	0.73	0.37	0.68	0.42
Fe^{+2}	2.71	2.57	2.46	3.44	4.12	2.11	3.11	1.91
Mn^{+2}	0.20	0.09	0.06	0.07	0.08	0.06	0.06	0.07
Mg	1.57	2.00	2.04	0.76	0.30	2.51	1.10	2.72
O site #	5.62	5.74	5.62	5.51	5.74	5.64	5.49	5.64
Ca	0.00	0.01	0.00	0.00	0.02	0.00	0.02	0.00
Na	0.02	0.02	0.02	0.02	0.02	0.02	0.01	0.02
K	1.98	1.91	1.97	1.95	1.75	1.91	1.95	1.91
A site #	2.00	1.94	1.99	1.96	1.79	1.94	1.98	1.94
O	20.05	20.02	20.06	20.09	20.00	20.06	20.11	20.10
OH	3.69	3.75	3.64	3.86	3.99	3.74	3.73	3.71
F	0.26	0.21	0.30	0.04	0.01	0.17	0.15	0.17
Cl	0.00	0.01	0.01	0.01	0.01	0.03	0.01	0.02
Charge	-0.05	-0.02	-0.06	-0.09	0.00	-0.06	-0.11	-0.10
Fe_{total}	3.12	2.95	2.83	4.02	4.85	2.48	3.79	2.33
Al_{total}	3.09	3.21	2.98	2.89	3.02	2.77	2.75	2.69
Fe/(Fe+Mg)	0.67	0.60	0.58	0.84	0.94	0.50	0.78	0.46
A/CNK	1.54	1.65	1.49	1.47	1.66	1.42	1.38	1.38
Fe^{3+}/Fe_{total}	0.13	0.13	0.13	0.14	0.15	0.15	0.18	0.18
$Log(X_{Mg}/X_{Fe})$	-0.30	-0.17	-0.14	-0.72	-1.20	0.01	-0.54	0.07
$Log(X_F/X_{OH})$	-1.16	-1.25	-1.09	-1.94	-2.90	-1.34	-1.41	-1.34

sample	nf-114	nf-26	nf-49	snf-23	snf-24	snf-25	nf-85	nf-5
determinations	5	4	4	5	3	6	2	4
SiO_2	37.03	35.59	35.64	36.38	35.31	36.31	36.30	35.93
TiO_2	1.79	3.07	4.74	3.01	4.46	4.56	2.14	2.13
Al_2O_3	17.38	16.00	14.33	14.05	12.97	13.34	16.43	15.71
FeO_{total}	16.48	23.80	18.15	28.30	26.48	28.44	17.03	18.02
Fe_2O_3	2.75	3.97	3.03	4.72	4.41	3.39	1.89	2.00
FeO	14.01	20.23	15.43	24.06	22.51	25.39	15.33	16.22
MnO	0.14	0.53	0.43	0.60	0.27	0.28	0.19	0.22
MgO	13.10	8.04	12.70	5.36	7.37	5.74	13.27	13.22
CaO	0.04	0.08	0.81	0.04	0.08	0.01	0.05	0.04
Na_2O	0.12	0.07	0.17	0.04	0.10	0.08	0.16	0.14
K_2O	9.94	9.68	8.48	9.45	9.81	9.84	9.70	9.41
H_2O	3.86	3.77	3.84	3.40	3.33	3.48	3.85	3.78
F	0.27	0.13	0.23	0.54	0.74	0.43	0.27	0.32
Cl	0.06	0.09	0.04	0.43	0.37	0.34	0.03	0.11
O=F	-0.12	-0.05	-0.10	-0.23	-0.31	-0.18	-0.11	-0.13
O=Cl	-0.01	-0.02	-0.01	-0.10	-0.08	-0.08	-0.01	-0.03
total	100.35	101.18	99.75	101.76	101.33	102.92	99.49	99.06
^{iv}Si	5.49	5.43	5.38	5.63	5.48	5.58	5.46	5.46
^{iv}Al	2.51	2.57	2.55	2.37	2.37	2.41	2.54	2.54
^{iv}Ti	0.00	0.00	0.07	0.00	0.15	0.01	0.00	0.00
T site #	8.00	8.00	8.00	8.00	8.00	8.00	8.00	8.00
Al	0.52	0.30	0.00	0.19	0.00	0.00	0.38	0.28
Ti	0.20	0.35	0.46	0.35	0.38	0.52	0.24	0.24
Fe^{+3}	0.31	0.46	0.34	0.55	0.52	0.39	0.21	0.23
Fe^{+2}	1.74	2.58	1.95	3.11	2.92	3.26	1.93	2.06
Mn^{+2}	0.02	0.07	0.05	0.08	0.04	0.04	0.02	0.03
Mg	2.89	1.83	2.86	1.24	1.70	1.31	2.98	3.00
O site #	5.68	5.59	5.67	5.52	5.55	5.52	5.77	5.83
Ca	0.01	0.01	0.13	0.01	0.01	0.00	0.01	0.01
Na	0.03	0.02	0.05	0.01	0.03	0.02	0.05	0.04
K	1.88	1.88	1.63	1.87	1.94	1.93	1.86	1.83
A site #	1.92	1.92	1.81	1.89	1.99	1.95	1.92	1.87
O	20.04	20.08	20.02	20.11	20.09	20.14	20.00	19.98
OH	3.82	3.84	3.86	3.51	3.44	3.56	3.87	3.83
F	0.13	0.06	0.11	0.27	0.37	0.21	0.13	0.15
Cl	0.01	0.02	0.01	0.11	0.10	0.09	0.01	0.03
Charge	-0.04	-0.08	-0.02	-0.11	-0.09	-0.14	0.00	0.02
Fe_{total}	2.04	3.03	2.29	3.66	3.44	3.65	2.14	2.29
Al_{total}	3.04	2.88	2.55	2.56	2.37	2.41	2.91	2.81
Fe/(Fe+Mg)	0.41	0.62	0.44	0.75	0.67	0.74	0.42	0.43
A/CNK	1.58	1.49	1.31	1.35	1.19	1.24	1.51	1.50
Fe^{3+}/Fe_{total}	0.15	0.15	0.15	0.15	0.15	0.11	0.10	0.10
$Log(X_{Mg}/X_{Fe})$	0.15	-0.22	0.10	-0.47	-0.30	-0.44	0.14	0.12
$Log(X_F/X_{OH})$	-1.47	-1.79	-1.55	-1.12	-0.97	-1.23	-1.48	-1.40

sample	nf-101	nf-45	snf-21	snf-22	nf-111	nf-4
determinations	6	4	3	6	5	4
SiO_2	34.73	35.16	34.01	36.81	36.03	36.25
TiO_2	3.60	4.58	3.85	3.58	4.14	4.91
Al_2O_3	14.53	14.27	13.69	15.39	14.79	14.43
FeO_{total}	26.80	18.37	32.88	13.79	18.83	15.29
Fe_2O_3	4.47	2.04	3.65	1.53	2.09	1.70
FeO	22.78	16.54	29.60	12.41	16.95	13.76
MnO	0.76	0.37	0.28	0.08	0.28	0.08
MgO	6.96	12.42	2.63	16.44	11.40	14.68
CaO	0.10	0.10	0.04	0.21	0.17	0.00
Na_2O	0.09	0.12	0.05	0.15	0.07	0.16
K_2O	9.33	9.56	9.44	9.19	10.03	9.62
H_2O	3.60	3.80	3.35	3.95	3.84	3.96
F	0.32	0.22	0.21	0.22	0.15	0.11
Cl	0.13	0.10	0.80	0.03	0.12	0.05
O=F	-0.14	-0.09	-0.09	-0.09	-0.06	-0.05
O=Cl	-0.03	-0.02	-0.18	-0.01	-0.03	-0.01
total	101.21	99.16	101.34	99.89	99.96	99.66
^{iv}Si	5.39	5.38	5.45	5.43	5.47	5.42
^{iv}Al	2.61	2.57	2.55	2.57	2.53	2.54
^{iv}Ti	0.00	0.04	0.00	0.00	0.00	0.03
T site #	8.00	8.00	8.00	8.00	8.00	8.00
Al	0.04	0.00	0.04	0.11	0.12	0.00
Ti	0.42	0.48	0.46	0.40	0.47	0.52
Fe^{+3}	0.52	0.24	0.44	0.17	0.24	0.19
Fe^{+2}	2.96	2.12	3.97	1.53	2.15	1.72
Mn^{+2}	0.10	0.05	0.04	0.01	0.04	0.01
Mg	1.61	2.83	0.63	3.61	2.58	3.27
O site #	5.65	5.72	5.59	5.83	5.60	5.72
Ca	0.02	0.02	0.01	0.03	0.03	0.00
Na	0.03	0.04	0.01	0.04	0.02	0.05
K	1.85	1.87	1.93	1.73	1.94	1.84
A site #	1.89	1.92	1.95	1.80	1.99	1.88
O	20.09	19.99	20.09	20.01	20.00	20.00
OH	3.72	3.88	3.59	3.88	3.90	3.94
F	0.16	0.11	0.11	0.10	0.07	0.05
Cl	0.03	0.03	0.22	0.01	0.03	0.01
Charge	-0.09	0.01	-0.09	-0.01	0.00	0.00
Fe_{total}	3.48	2.35	4.41	1.70	2.39	1.91
Al_{total}	2.66	2.57	2.59	2.68	2.65	2.54
Fe/(Fe+Mg)	0.68	0.45	0.88	0.32	0.48	0.37
A/CNK	1.40	1.33	1.32	1.46	1.31	1.35
Fe^{3+}/Fe_{total}	0.15	0.10	0.10	0.10	0.10	0.08
$Log(X_{Mg}/X_{Fe})$	-0.33	0.08	-0.85	0.33	0.03	0.23
$Log(X_F/X_{OH})$	-1.37	-1.57	-1.52	-1.58	-1.73	-1.89

sample	nf-8	snf-1	snf-14	snf-15	snf-16	snf-17	snf-19
determinations	6	6	5	3	6	3	5
SiO_2	36.02	35.59	36.77	35.95	38.03	35.46	36.18
TiO_2	3.89	3.72	4.25	3.06	2.90	2.98	3.31
Al_2O_3	16.49	16.77	13.89	16.13	14.15	16.03	15.25
FeO_{total}	22.19	21.70	19.59	20.80	18.44	22.11	22.04
Fe_2O_3	2.54	2.57	3.05	3.47	4.51	3.44	3.58
FeO	19.90	19.39	16.85	17.68	14.38	19.02	18.82
MnO	0.35	0.38	0.58	0.47	1.13	0.38	0.56
MgO	8.09	8.50	12.01	9.83	12.34	9.29	8.96
CaO	0.01	0.02	0.03	0.00	0.02	0.00	0.01
Na_2O	0.07	0.05	0.09	0.06	0.09	0.07	0.07
K_2O	10.21	10.37	10.05	10.37	9.99	10.36	10.17
H_2O	3.78	3.76	3.58	3.69	3.18	3.54	3.51
F	0.22	0.25	0.69	0.42	1.59	0.69	0.75
Cl	0.02	0.01	0.03	0.01	0.03	0.01	0.02
O=F	-0.09	-0.11	-0.29	-0.18	-0.67	-0.29	-0.32
O=Cl	-0.01	0.00	-0.01	0.00	-0.01	0.00	0.00
total	101.51	101.29	101.57	100.98	101.67	100.99	100.90
^{iv}Si	5.45	5.39	5.51	5.44	5.64	5.40	5.51
^{iv}Al	2.55	2.61	2.45	2.56	2.36	2.60	2.49
^{iv}Ti	0.00	0.00	0.00	0.00	0.00	0.00	0.00
T site #	8.00	8.00	8.00	8.00	8.00	8.00	8.00
Al	0.38	0.39	0.00	0.31	0.11	0.28	0.24
Ti	0.44	0.42	0.43	0.35	0.32	0.34	0.38
Fe^{+3}	0.29	0.29	0.34	0.39	0.50	0.39	0.41
Fe^{+2}	2.52	2.46	2.11	2.24	1.78	2.42	2.40
Mn^{+2}	0.05	0.05	0.07	0.06	0.14	0.05	0.07
Mg	1.82	1.92	2.68	2.22	2.73	2.11	2.03
O site #	5.50	5.53	5.64	5.57	5.59	5.60	5.54
Ca	0.00	0.00	0.00	0.00	0.00	0.00	0.00
Na	0.02	0.02	0.03	0.02	0.03	0.02	0.02
K	1.97	2.00	1.92	2.00	1.89	2.01	1.98
A site #	1.99	2.02	1.95	2.02	1.92	2.03	2.00
O	20.00	20.00	20.00	20.00	20.00	20.00	20.00
OH	3.89	3.88	3.67	3.80	3.25	3.67	3.63
F	0.10	0.12	0.33	0.20	0.74	0.33	0.36
Cl	0.01	0.00	0.01	0.00	0.01	0.00	0.01
Charge	0.00	0.00	0.00	0.00	0.00	0.00	0.00
Fe_{total}	2.81	2.75	2.45	2.63	2.29	2.82	2.81
Al_{total}	2.94	2.99	2.45	2.88	2.47	2.88	2.74
Fe/(Fe+Mg)	0.61	0.59	0.48	0.54	0.46	0.57	0.58
A/CNK	1.47	1.48	1.25	1.42	1.29	1.42	1.37
Fe^{3+}/Fe_{total}	0.10	0.11	0.12	0.15	0.22	0.14	0.15
$Log(X_{Mg}/X_{Fe})$	-0.19	-0.16	0.04	-0.07	0.08	-0.13	-0.14
$Log(X_F/X_{OH})$	-1.58	-1.50	-1.05	-1.27	-0.64	-1.04	-1.00

sample	snf-2	snf-3	snf-4	snf-8	snf-18	ak-89-087	ak-89-122
determinations	6	3	3	4	3	4	3
SiO_2	36.99	36.37	36.47	35.74	36.35	37.50	36.16
TiO_2	2.75	3.28	2.71	3.47	2.64	3.08	3.28
Al_2O_3	15.14	14.78	14.94	15.55	16.09	14.37	13.94
FeO_{total}	20.02	19.05	19.22	23.55	21.03	17.61	26.42
Fe_2O_3	5.09	2.33	2.14	3.66	3.27	2.94	4.40
FeO	15.43	16.96	17.30	20.25	18.08	14.97	22.46
MnO	0.42	0.51	0.56	0.44	0.30	0.43	0.78
MgO	11.44	12.07	11.69	7.89	10.04	13.01	6.43
CaO	0.02	0.02	0.01	0.56	0.01	0.01	0.03
Na_2O	0.12	0.08	0.07	0.05	0.08	0.07	0.05
K_2O	10.17	9.77	10.12	9.69	10.31	9.98	8.97
H_2O	3.75	3.38	3.34	3.50	3.69	3.38	3.22
F	0.36	1.12	1.19	0.71	0.44	1.23	1.23
Cl	0.01	0.04	0.02	0.05	0.02	0.02	0.08
O=F	-0.15	-0.47	-0.50	-0.30	-0.18	-0.52	-0.52
O=Cl	0.00	-0.01	-0.01	-0.01	0.00	-0.01	-0.02
total	101.57	100.23	100.07	101.28	101.16	100.46	100.50
^{iv}Si	5.52	5.50	5.54	5.45	5.48	5.61	5.61
^{iv}Al	2.48	2.50	2.46	2.55	2.52	2.39	2.39
^{iv}Ti	0.00	0.00	0.00	0.00	0.00	0.00	0.00
T site #	8.00	8.00	8.00	8.00	8.00	8.00	8.00
Al	0.17	0.14	0.22	0.25	0.34	0.14	0.17
Ti	0.31	0.37	0.31	0.40	0.30	0.35	0.38
Fe^{+3}	0.57	0.27	0.24	0.42	0.37	0.33	0.51
Fe^{+2}	1.92	2.15	2.20	2.58	2.28	1.87	2.92
Mn^{+2}	0.05	0.07	0.07	0.06	0.04	0.05	0.10
Mg	2.54	2.72	2.65	1.79	2.26	2.90	1.49
O site #	5.57	5.71	5.69	5.50	5.59	5.65	5.57
Ca	0.00	0.00	0.00	0.09	0.00	0.00	0.01
Na	0.04	0.02	0.02	0.02	0.02	0.02	0.01
K	1.93	1.89	1.96	1.89	1.98	1.91	1.78
A site #	1.97	1.91	1.99	1.99	2.01	1.93	1.80
O	20.00	20.00	20.00	20.00	20.00	20.00	20.00
OH	3.82	3.45	3.42	3.64	3.79	3.41	3.37
F	0.17	0.53	0.57	0.34	0.21	0.58	0.60
Cl	0.00	0.01	0.01	0.01	0.00	0.01	0.02
Charge	0.00	0.00	0.00	0.00	0.00	0.00	0.00
Fe_{total}	2.50	2.41	2.44	3.00	2.65	2.20	3.43
Al_{total}	2.66	2.64	2.68	2.80	2.86	2.53	2.55
Fe/(Fe+Mg)	0.50	0.47	0.48	0.63	0.54	0.43	0.70
A/CNK	1.35	1.38	1.35	1.34	1.42	1.31	1.42
Fe^{3+}/Fe_{total}	0.23	0.11	0.10	0.14	0.14	0.15	0.15
$Log(X_{Mg}/X_{Fe})$	0.01	0.05	0.04	-0.22	-0.07	0.12	-0.36
$Log(X_F/X_{OH})$	-1.35	-0.81	-0.78	-1.03	-1.26	-0.77	-0.75

sample	ak-92-087	ak-92-133	ak-92-291	ak-92-292	nf-171	snf-7	ak-91-414
determinations	4	3	5	4	4	4	4
SiO_2	36.58	37.02	36.12	38.15	35.54	35.80	35.40
TiO_2	2.63	2.73	2.32	3.00	3.14	2.49	2.49
Al_2O_3	16.31	15.29	14.92	13.39	17.88	19.86	18.86
FeO_{total}	19.95	19.08	19.24	16.96	22.72	22.29	23.29
Fe_2O_3	3.10	2.97	3.21	2.64	2.52	3.47	3.62
FeO	17.16	16.41	16.36	14.59	20.44	19.17	20.03
MnO	0.47	0.34	0.54	0.80	0.77	1.67	0.65
MgO	10.14	11.28	12.19	13.73	6.86	4.82	5.09
CaO	0.00	0.03	0.04	0.01	0.00	0.01	0.00
Na_2O	0.06	0.10	0.06	0.05	0.04	0.13	0.12
K_2O	10.32	10.25	9.96	10.05	9.79	10.02	10.18
H_2O	3.74	3.75	3.68	3.27	3.62	3.03	3.14
F	0.43	0.42	0.53	1.40	0.54	1.76	1.55
Cl	0.00	0.02	0.04	0.14	0.01	0.03	0.02
O=F	-0.18	-0.18	-0.22	-0.59	-0.23	-0.74	-0.65
O=Cl	0.00	-0.01	-0.01	-0.03	0.00	-0.01	0.00
total	100.75	100.43	99.72	100.60	100.95	101.53	100.48
^{iv}Si	5.51	5.58	5.50	5.70	5.41	5.41	5.43
^{iv}Al	2.49	2.42	2.50	2.30	2.59	2.59	2.57
^{iv}Ti	0.00	0.00	0.00	0.00	0.00	0.00	0.00
T site #	8.00	8.00	8.00	8.00	8.00	8.00	8.00
Al	0.41	0.29	0.18	0.06	0.62	0.95	0.84
Ti	0.30	0.31	0.27	0.34	0.36	0.28	0.29
Fe^{+3}	0.35	0.34	0.37	0.30	0.29	0.39	0.42
Fe^{+2}	2.16	2.07	2.08	1.82	2.60	2.42	2.57
Mn^{+2}	0.06	0.04	0.07	0.10	0.10	0.21	0.08
Mg	2.28	2.53	2.77	3.06	1.56	1.09	1.16
O site #	5.56	5.58	5.73	5.67	5.53	5.35	5.36
Ca	0.00	0.01	0.01	0.00	0.00	0.00	0.00
Na	0.02	0.03	0.02	0.01	0.01	0.04	0.04
K	1.98	1.97	1.93	1.91	1.90	1.93	1.99
A site #	2.00	2.01	1.96	1.93	1.91	1.97	2.03
O	20.00	20.00	20.00	20.00	20.00	20.00	20.00
OH	3.80	3.79	3.73	3.30	3.74	3.15	3.25
F	0.20	0.20	0.26	0.66	0.26	0.84	0.75
Cl	0.00	0.01	0.01	0.04	0.00	0.01	0.00
Charge	0.00	0.00	0.00	0.00	0.00	0.00	0.00
Fe_{total}	2.52	2.40	2.45	2.12	2.89	2.82	2.99
Al_{total}	2.90	2.71	2.68	2.36	3.21	3.54	3.41
Fe/(Fe+Mg)	0.52	0.49	0.47	0.41	0.65	0.72	0.72
A/CNK	1.45	1.35	1.36	1.22	1.68	1.79	1.68
Fe^{3+}/Fe_{total}	0.14	0.14	0.15	0.14	0.10	0.14	0.14
$Log(X_{Mg}/X_{Fe})$	-0.04	0.02	0.05	0.16	-0.27	-0.41	-0.41
$Log(X_F/X_{OH})$	-1.27	-1.28	-1.16	-0.70	-1.16	-0.57	-0.64

sample	ak-92-043	ak-92-054	ak-92-061	ak-92-131	ak-92-166	ak-91-415	snf-10
determinations	4	4	3	5	2	5	4
SiO_2	36.82	34.56	35.43	36.38	37.65	34.63	36.24
TiO_2	1.88	2.76	3.23	3.07	2.22	2.75	3.50
Al_2O_3	18.21	17.30	18.25	16.71	17.52	18.71	12.98
FeO_{total}	11.93	25.82	20.94	20.28	19.15	22.96	23.58
Fe_2O_3	1.59	3.73	3.03	3.15	3.83	2.81	4.14
FeO	10.50	22.46	18.22	17.44	15.70	20.44	19.86
MnO	1.06	0.64	0.44	0.46	1.84	0.76	0.52
MgO	15.39	5.55	7.89	9.78	6.65	5.86	9.69
CaO	0.01	0.00	0.00	0.02	0.05	0.00	0.02
Na_2O	0.07	0.08	0.14	0.09	0.05	0.05	0.09
K_2O	10.60	10.28	10.28	10.50	9.31	10.33	9.92
H_2O	4.01	3.63	3.78	3.77	3.37	3.48	3.21
F	0.12	0.40	0.29	0.35	1.23	0.82	1.26
Cl	0.03	0.01	0.02	0.01	0.02	0.01	0.07
O=F	-0.05	-0.17	-0.12	-0.15	-0.52	-0.35	-0.53
O=Cl	-0.01	0.00	0.00	0.00	-0.01	0.00	-0.01
total	100.24	101.24	100.87	101.59	98.93	100.31	100.97
^{iv}Si	5.40	5.34	5.36	5.45	5.73	5.34	5.56
^{iv}Al	2.60	2.66	2.64	2.55	2.27	2.66	2.35
^{iv}Ti	0.00	0.00	0.00	0.00	0.00	0.00	0.00
T site #	8.00	8.00	8.00	8.00	8.00	8.00	8.00
Al	0.55	0.50	0.61	0.40	0.87	0.74	0.00
Ti	0.21	0.32	0.37	0.35	0.25	0.32	0.32
Fe^{+3}	0.18	0.43	0.34	0.36	0.44	0.33	0.48
Fe^{+2}	1.29	2.90	2.30	2.18	2.00	2.63	2.55
Mn^{+2}	0.13	0.08	0.06	0.06	0.24	0.10	0.07
Mg	3.37	1.28	1.78	2.18	1.51	1.35	2.22
O site #	5.72	5.52	5.46	5.53	5.31	5.46	5.63
Ca	0.00	0.00	0.00	0.00	0.01	0.00	0.00
Na	0.02	0.02	0.04	0.03	0.01	0.02	0.03
K	1.98	2.03	1.98	2.01	1.81	2.03	1.94
A site #	2.01	2.05	2.02	2.04	1.83	2.05	1.97
O	20.00	20.00	20.00	20.00	20.00	20.00	20.00
OH	3.94	3.80	3.86	3.83	3.40	3.60	3.37
F	0.05	0.19	0.14	0.16	0.59	0.40	0.61
Cl	0.01	0.00	0.00	0.00	0.01	0.00	0.02
Charge	0.00	0.00	0.00	0.00	0.00	0.00	0.00
Fe_{total}	1.46	3.34	2.65	2.54	2.44	2.96	3.03
Al_{total}	3.15	3.15	3.25	2.95	3.14	3.40	2.35
Fe/(Fe+Mg)	0.30	0.72	0.60	0.54	0.62	0.69	0.58
A/CNK	1.57	1.54	1.61	1.45	1.71	1.66	1.19
Fe^{3+}/Fe_{total}	0.12	0.13	0.13	0.14	0.18	0.11	0.13
$Log(X_{Mg}/X_{Fe})$	0.36	-0.42	-0.17	-0.07	-0.21	-0.34	-0.14
$Log(X_F/X_{OH})$	-1.86	-1.29	-1.45	-1.37	-0.76	-0.95	-0.74

sample	ak-92-168	ak-92-170	ak-92-243	snf-5
determinations	3	4	4	6
SiO_2	36.71	37.03	37.22	37.36
TiO_2	2.39	1.91	2.05	4.17
Al_2O_3	15.00	15.04	15.55	14.53
FeO_{total}	19.53	19.72	19.27	14.99
Fe_2O_3	3.25	3.07	2.78	1.67
FeO	16.60	16.96	16.77	13.49
MnO	0.47	0.38	0.50	0.13
MgO	12.07	11.70	11.66	14.86
CaO	0.00	0.02	0.02	0.01
Na_2O	0.06	0.08	0.12	0.12
K_2O	9.90	10.13	10.19	10.16
H_2O	3.71	3.74	3.66	3.85
F	0.47	0.41	0.59	0.33
Cl	0.05	0.03	0.04	0.02
O=F	-0.20	-0.17	-0.25	-0.14
O=Cl	-0.01	-0.01	-0.01	0.00
total	100.48	100.32	100.89	100.55
^{iv}Si	5.54	5.60	5.59	5.53
^{iv}Al	2.46	2.40	2.41	2.47
^{iv}Ti	0.00	0.00	0.00	0.00
T site #	8.00	8.00	8.00	8.00
Al	0.20	0.28	0.33	0.06
Ti	0.27	0.22	0.23	0.46
Fe^{+3}	0.37	0.35	0.31	0.19
Fe^{+2}	2.09	2.14	2.10	1.67
Mn^{+2}	0.06	0.05	0.06	0.02
Mg	2.71	2.64	2.61	3.28
O site #	5.71	5.68	5.66	5.67
Ca	0.00	0.00	0.00	0.00
Na	0.02	0.02	0.04	0.03
K	1.90	1.95	1.95	1.92
A site #	1.92	1.98	1.99	1.95
O	20.00	20.00	20.00	20.00
OH	3.76	3.80	3.71	3.84
F	0.22	0.20	0.28	0.15
Cl	0.01	0.01	0.01	0.00
Charge	0.00	0.00	0.00	0.00
Fe_{total}	2.46	2.49	2.42	1.85
Al_{total}	2.67	2.68	2.75	2.53
Fe/(Fe+Mg)	0.48	0.49	0.48	0.36
A/CNK	1.39	1.35	1.38	1.30
Fe^{3+}/Fe_{total}	0.15	0.14	0.13	0.10
$Log(X_{Mg}/X_{Fe})$	0.04	0.02	0.03	0.25
$Log(X_F/X_{OH})$	-1.22	-1.29	-1.13	-1.40

Bennet (1990)

sample	170100	170140	170261	170041	170242	170122	170118
determinations	3	1	1	3	3	3	3
SiO_2	35.06	33.59	36.12	36.08	36.34	35.06	35.76
TiO_2	2.29	2.00	1.58	1.58	2.14	2.29	2.08
Al_2O_3	17.21	18.38	17.40	18.83	16.86	17.21	17.33
FeO_{total}	25.28	25.72	25.49	25.50	26.22	25.28	25.48
Fe_2O_3	3.09	3.14	3.12	3.12	3.20	3.09	3.12
FeO	22.50	22.89	22.68	22.70	23.33	22.50	22.68
MnO	0.62	0.66	0.61	1.02	0.55	0.62	0.36
MgO	6.66	5.48	6.18	4.85	6.48	6.66	7.29
CaO	0.01	0.00	0.00	0.01	0.00	0.01	0.00
Na_2O	0.14	0.11	0.50	0.10	0.16	0.14	0.11
K_2O	8.46	9.05	8.42	8.23	8.71	8.46	8.82
H_2O	3.86	3.83	3.87	3.88	3.86	3.86	3.87
F	0.00	0.00	0.00	0.00	0.00	0.00	0.00
Cl	0.00	0.00	0.00	0.00	0.00	0.00	0.00
O=F	0.00	0.00	0.00	0.00	0.00	0.00	0.00
O=Cl	0.00	0.00	0.00	0.00	0.00	0.00	0.00
total	99.90	99.13	100.48	100.39	101.62	99.90	101.41
^{iv}Si	5.42	5.28	5.54	5.52	5.53	5.42	5.44
^{iv}Al	2.58	2.72	2.46	2.48	2.47	2.58	2.56
^{iv}Ti	0.00	0.00	0.00	0.00	0.00	0.00	0.00
T site #	8.00	8.00	8.00	8.00	8.00	8.00	8.00
Al	0.56	0.68	0.68	0.92	0.55	0.56	0.54
Ti	0.27	0.24	0.18	0.18	0.24	0.27	0.24
Fe^{+3}	0.36	0.37	0.36	0.36	0.37	0.36	0.36
Fe^{+2}	2.91	3.01	2.91	2.90	2.97	2.91	2.88
Mn^{+2}	0.08	0.09	0.08	0.13	0.07	0.08	0.05
Mg	1.54	1.28	1.41	1.11	1.47	1.54	1.65
O site #	5.71	5.67	5.63	5.60	5.67	5.71	5.72
Ca	0.00	0.00	0.00	0.00	0.00	0.00	0.00
Na	0.04	0.03	0.15	0.03	0.05	0.04	0.03
K	1.67	1.81	1.65	1.61	1.69	1.67	1.71
A site #	1.71	1.85	1.80	1.64	1.74	1.71	1.74
O	20.02	19.99	20.04	20.04	20.09	20.02	20.08
OH	3.98	4.01	3.96	3.96	3.91	3.98	3.92
F	0.00	0.00	0.00	0.00	0.00	0.00	0.00
Cl	0.00	0.00	0.00	0.00	0.00	0.00	0.00
Charge	-0.02	0.01	-0.04	-0.04	-0.09	-0.02	-0.08
Fe_{total}	3.27	3.38	3.27	3.26	3.33	3.27	3.24
Al_{total}	3.14	3.40	3.15	3.40	3.02	3.14	3.11
Fe/(Fe+Mg)	0.68	0.72	0.70	0.75	0.69	0.68	0.66
A/CNK	1.83	1.84	1.75	2.07	1.74	1.83	1.78
Fe^{3+}/Fe_{total}	0.11	0.11	0.11	0.11	0.11	0.11	0.11

Bennet (1990)

sample	170517	170073	170157	170161	170189	170206	170144
determinations	2	3	3	2	3	3	2
SiO_2	34.24	34.41	34.49	36.00	34.88	35.02	35.54
TiO_2	1.30	2.37	2.06	1.30	1.43	1.59	1.73
Al_2O_3	19.25	17.51	17.38	18.37	19.22	18.04	18.60
FeO_{total}	24.84	25.85	27.92	24.28	27.39	28.07	25.54
Fe_2O_3	3.04	3.16	3.41	2.97	3.35	3.43	3.12
FeO	22.10	23.00	24.85	21.61	24.37	24.98	22.73
MnO	0.84	0.35	0.47	0.62	0.59	0.56	0.62
MgO	6.28	6.83	3.78	7.30	5.53	5.12	4.58
CaO	0.05	0.01	0.00	0.00	0.01	0.00	0.00
Na_2O	0.08	0.11	0.04	0.05	0.07	0.10	0.16
K_2O	8.26	8.68	8.08	8.64	8.32	8.50	8.35
H_2O	3.87	3.84	3.82	3.90	3.84	3.82	3.87
F	0.00	0.00	0.00	0.00	0.00	0.00	0.00
Cl	0.00	0.00	0.00	0.00	0.00	0.00	0.00
O=F	0.00	0.00	0.00	0.00	0.00	0.00	0.00
O=Cl	0.00	0.00	0.00	0.00	0.00	0.00	0.00
total	99.29	100.28	98.40	100.73	101.62	101.17	99.30
^{iv}Si	5.31	5.32	5.47	5.47	5.32	5.40	5.51
^{iv}Al	2.69	2.68	2.53	2.53	2.68	2.60	2.49
^{iv}Ti	0.00	0.00	0.00	0.00	0.00	0.00	0.00
T site #	8.00	8.00	8.00	8.00	8.00	8.00	8.00
Al	0.83	0.51	0.72	0.76	0.78	0.68	0.91
Ti	0.15	0.28	0.25	0.15	0.16	0.18	0.20
Fe^{+3}	0.35	0.37	0.41	0.34	0.38	0.40	0.36
Fe^{+2}	2.87	2.97	3.30	2.75	3.11	3.22	2.95
Mn^{+2}	0.11	0.05	0.06	0.08	0.08	0.07	0.08
Mg	1.45	1.58	0.89	1.65	1.26	1.18	1.06
O site #	5.76	5.75	5.63	5.72	5.77	5.73	5.56
Ca	0.01	0.00	0.00	0.00	0.00	0.00	0.00
Na	0.02	0.03	0.01	0.01	0.02	0.03	0.05
K	1.63	1.71	1.64	1.67	1.62	1.67	1.65
A site #	1.67	1.75	1.65	1.69	1.64	1.70	1.70
O	19.99	20.03	19.96	20.05	20.09	20.07	19.99
OH	4.01	3.97	4.04	3.95	3.91	3.93	4.01
F	0.00	0.00	0.00	0.00	0.00	0.00	0.00
Cl	0.00	0.00	0.00	0.00	0.00	0.00	0.00
Charge	0.01	-0.03	0.04	-0.05	-0.09	-0.07	0.01
Fe_{total}	3.22	3.34	3.70	3.09	3.49	3.62	3.31
Al_{total}	3.52	3.19	3.25	3.29	3.46	3.28	3.40
Fe/(Fe+Mg)	0.69	0.68	0.81	0.65	0.74	0.75	0.76
A/CNK	2.10	1.83	1.97	1.95	2.10	1.93	2.00
Fe^{3+}/Fe_{total}	0.11	0.11	0.11	0.11	0.11	0.11	0.11

Bennet (1990)

sample	170145	170001	170024	170123
determinations	3	3	3	3
SiO_2	36.15	35.65	35.43	35.29
TiO_2	1.85	1.95	1.81	1.97
Al_2O_3	18.88	18.55	18.09	16.81
FeO_{total}	24.97	25.13	26.64	26.31
Fe_2O_3	3.05	3.07	3.26	3.22
FeO	22.22	22.37	23.71	23.42
MnO	0.48	0.68	0.54	0.39
MgO	4.40	6.04	5.91	7.49
CaO	0.02	0.00	0.00	0.00
Na_2O	0.10	0.24	0.14	0.10
K_2O	8.47	8.46	8.34	8.41
H_2O	3.90	3.88	3.85	3.85
F	0.00	0.00	0.00	0.00
Cl	0.00	0.00	0.00	0.00
O=F	0.00	0.00	0.00	0.00
O=Cl	0.00	0.00	0.00	0.00
total	99.50	100.88	101.10	100.94
^{iv}Si	5.56	5.43	5.42	5.41
^{iv}Al	2.44	2.57	2.58	2.59
^{iv}Ti	0.00	0.00	0.00	0.00
T site #	8.00	8.00	8.00	8.00
Al	0.99	0.76	0.68	0.45
Ti	0.21	0.22	0.21	0.23
Fe^{+3}	0.35	0.35	0.37	0.37
Fe^{+2}	2.86	2.85	3.03	3.00
Mn^{+2}	0.06	0.09	0.07	0.05
Mg	1.01	1.37	1.35	1.71
O site #	5.49	5.65	5.72	5.82
Ca	0.00	0.00	0.00	0.00
Na	0.03	0.07	0.04	0.03
K	1.66	1.64	1.63	1.65
A site #	1.69	1.71	1.67	1.68
O	20.00	20.06	20.07	20.06
OH	4.00	3.94	3.93	3.94
F	0.00	0.00	0.00	0.00
Cl	0.00	0.00	0.00	0.00
Charge	0.00	-0.06	-0.07	-0.06
Fe_{total}	3.21	3.20	3.41	3.38
Al_{total}	3.42	3.33	3.26	3.04
Fe/(Fe+Mg)	0.76	0.70	0.72	0.66
A/CNK	2.02	1.94	1.95	1.81
Fe^{3+}/Fe_{total}	0.11	0.11	0.11	0.11

sample	nb-185	nb-195	nb-206	nb-207	nb-211	nb-196	nb-209
determinations	4	4	5	4	6	4	4
SiO_2	35.54	36.41	37.23	36.93	36.72	36.92	37.21
TiO_2	3.74	2.70	4.20	3.95	3.11	3.26	4.04
Al_2O_3	14.68	14.08	13.17	13.42	11.50	13.59	13.28
FeO_{total}	28.00	18.75	18.89	19.03	27.88	19.58	17.83
Fe_2O_3	4.05	3.75	3.99	4.02	5.58	3.05	3.37
FeO	24.36	15.38	15.30	15.41	22.86	16.84	14.80
MnO	0.69	0.52	0.33	0.30	0.28	0.53	0.30
MgO	4.43	13.91	12.90	13.05	7.47	12.30	13.71
CaO	0.01	0.18	0.03	0.01	0.04	0.01	0.00
Na_2O	0.10	0.10	0.10	0.10	0.16	0.05	0.14
K_2O	9.85	9.23	9.93	10.02	9.24	10.10	10.05
H_2O	3.02	3.62	3.58	3.66	2.83	3.56	3.63
F	1.39	0.66	0.65	0.52	1.67	0.77	0.64
Cl	0.28	0.03	0.17	0.09	0.53	0.04	0.15
O=F	-0.58	-0.28	-0.27	-0.22	-0.70	-0.32	-0.27
O=Cl	-0.06	-0.01	-0.04	-0.02	-0.12	-0.01	-0.03
total	101.52	100.30	101.29	101.26	101.20	100.68	101.00
^{iv}Si	5.54	5.48	5.56	5.52	5.72	5.58	5.56
^{iv}Al	2.46	2.50	2.32	2.37	2.11	2.42	2.34
^{iv}Ti	0.00	0.02	0.12	0.11	0.17	0.00	0.11
T site #	8.00	8.00	8.00	8.00	8.00	8.00	8.00
Al	0.23	0.00	0.00	0.00	0.00	0.00	0.00
Ti	0.44	0.28	0.35	0.33	0.19	0.37	0.34
Fe^{+3}	0.47	0.42	0.45	0.45	0.65	0.35	0.38
Fe^{+2}	3.17	1.93	1.91	1.93	2.98	2.13	1.85
Mn^{+2}	0.09	0.07	0.04	0.04	0.04	0.07	0.04
Mg	1.03	3.12	2.87	2.91	1.73	2.77	3.05
O site #	5.44	5.83	5.62	5.66	5.59	5.68	5.66
Ca	0.00	0.03	0.00	0.00	0.01	0.00	0.00
Na	0.03	0.03	0.03	0.03	0.05	0.01	0.04
K	1.96	1.77	1.89	1.91	1.83	1.95	1.91
A site #	1.99	1.83	1.93	1.94	1.89	1.96	1.95
O	20.00	20.00	20.00	20.00	20.00	20.00	20.00
OH	3.24	3.68	3.65	3.73	3.04	3.62	3.66
F	0.68	0.31	0.31	0.24	0.82	0.37	0.30
Cl	0.07	0.01	0.04	0.02	0.14	0.01	0.04
Charge	0.00	0.00	0.00	0.00	0.00	0.00	0.00
Fe_{total}	3.65	2.36	2.36	2.38	3.63	2.47	2.23
Al_{total}	2.70	2.50	2.32	2.37	2.11	2.42	2.34
Fe/(Fe+Mg)	0.78	0.43	0.45	0.45	0.68	0.47	0.42
A/CNK	1.35	1.34	1.20	1.22	1.11	1.23	1.20
Fe^{3+}/Fe_{total}	0.13	0.18	0.19	0.19	0.18	0.14	0.12
$Log(X_{Mg}/X_{Fe})$	-0.55	0.12	0.09	0.09	-0.32	0.05	0.14
$Log(X_F/X_{OH})$	-0.68	-1.07	-1.08	-1.18	-0.57	-1.00	-1.08

sample	nb-178	nb-176	nb-177	nb-180	nb-184	nb-189	nb-197
determinations	5	6	6	3	5	4	6
SiO_2	35.03	35.74	35.15	34.95	35.95	36.65	37.53
TiO_2	4.56	3.60	2.86	3.45	3.74	3.90	3.44
Al_2O_3	13.82	12.56	13.31	12.59	12.05	13.30	12.36
FeO_{total}	22.65	30.52	32.03	32.13	30.65	18.75	22.64
Fe_2O_3	2.52	4.41	4.63	4.64	4.43	3.96	4.78
FeO	20.39	26.55	27.87	27.95	26.66	15.19	18.34
MnO	0.14	0.60	0.98	0.70	0.63	0.29	0.71
MgO	11.07	4.85	3.10	3.52	4.61	12.96	10.37
CaO	0.30	0.01	0.00	0.00	0.00	0.06	0.00
Na_2O	0.11	0.11	0.13	0.07	0.04	0.14	0.09
K_2O	8.48	9.50	9.45	9.37	9.76	9.70	10.10
H_2O	3.76	2.96	2.67	3.20	3.00	3.59	2.73
F	0.21	1.28	1.77	0.79	1.26	0.66	2.29
Cl	0.07	0.56	0.59	0.39	0.41	0.10	0.12
O=F	-0.09	-0.54	-0.75	-0.33	-0.53	-0.28	-0.96
O=Cl	-0.02	-0.13	-0.13	-0.09	-0.09	-0.02	-0.03
total	100.36	102.10	101.67	101.22	101.96	100.23	101.90
^{iv}Si	5.36	5.61	5.59	5.58	5.66	5.53	5.68
^{iv}Al	2.49	2.32	2.41	2.37	2.24	2.37	2.20
^{iv}Ti	0.14	0.07	0.00	0.05	0.11	0.11	0.12
T site #	8.00	8.00	8.00	8.00	8.00	8.00	8.00
Al	0.00	0.00	0.09	0.00	0.00	0.00	0.00
Ti	0.38	0.36	0.34	0.36	0.33	0.34	0.27
Fe^{+3}	0.29	0.52	0.55	0.56	0.52	0.45	0.54
Fe^{+2}	2.61	3.48	3.71	3.73	3.51	1.92	2.32
Mn^{+2}	0.02	0.08	0.13	0.09	0.08	0.04	0.09
Mg	2.53	1.13	0.74	0.84	1.08	2.91	2.34
O site #	5.83	5.57	5.56	5.58	5.53	5.66	5.57
Ca	0.05	0.00	0.00	0.00	0.00	0.01	0.00
Na	0.03	0.03	0.04	0.02	0.01	0.04	0.03
K	1.66	1.90	1.92	1.91	1.96	1.87	1.95
A site #	1.74	1.94	1.96	1.93	1.97	1.92	1.98
O	20.00	20.00	20.00	20.00	20.00	20.00	20.00
OH	3.88	3.22	2.95	3.50	3.26	3.66	2.87
F	0.10	0.64	0.89	0.40	0.63	0.32	1.09
Cl	0.02	0.15	0.16	0.11	0.11	0.03	0.03
Charge	0.00	0.00	0.00	0.00	0.00	0.00	0.00
Fe_{total}	2.90	4.01	4.26	4.29	4.03	2.37	2.86
Al_{total}	2.49	2.32	2.50	2.37	2.24	2.37	2.20
Fe/(Fe+Mg)	0.53	0.78	0.85	0.84	0.79	0.45	0.55
A/CNK	1.40	1.20	1.27	1.23	1.13	1.23	1.11
Fe^{3+}/Fe_{total}	0.10	0.13	0.13	0.13	0.13	0.19	0.19
$Log(X_{Mg}/X_{Fe})$	-0.06	-0.55	-0.76	-0.71	-0.57	0.09	-0.09
$Log(X_F/X_{OH})$	-1.58	-0.70	-0.52	-0.94	-0.72	-1.06	-0.42

sample	nb-198	nb-199	nb-219	nb-223
determinations	3	4	4	3
SiO_2	37.07	36.08	36.41	33.71
TiO_2	3.39	3.78	3.24	2.88
Al_2O_3	12.75	12.56	13.76	10.99
FeO_{total}	22.13	29.19	29.68	37.31
Fe_2O_3	4.43	4.22	4.29	7.46
FeO	18.14	25.39	25.82	30.59
MnO	0.67	0.67	0.81	0.36
MgO	10.76	5.01	3.46	2.06
CaO	0.00	0.18	0.01	0.15
Na_2O	0.10	0.12	0.20	0.05
K_2O	10.00	9.70	9.34	8.35
H_2O	2.77	2.69	2.28	3.32
F	2.22	1.97	2.81	0.09
Cl	0.11	0.39	0.45	0.84
O=F	-0.93	-0.83	-1.18	-0.04
O=Cl	-0.02	-0.09	-0.10	-0.19
total	101.49	101.89	101.61	100.67
^{iv}Si	5.62	5.65	5.70	5.53
^{iv}Al	2.28	2.32	2.30	2.12
^{iv}Ti	0.10	0.04	0.00	0.35
T site #	8.00	8.00	8.00	8.00
Al	0.00	0.00	0.24	0.00
Ti	0.29	0.41	0.38	0.01
Fe^{+3}	0.51	0.50	0.51	0.92
Fe^{+2}	2.30	3.32	3.38	4.20
Mn^{+2}	0.09	0.09	0.11	0.05
Mg	2.43	1.17	0.81	0.50
O site #	5.61	5.49	5.43	5.68
Ca	0.00	0.03	0.00	0.03
Na	0.03	0.04	0.06	0.02
K	1.94	1.94	1.87	1.75
A site #	1.97	2.00	1.93	1.79
O	20.00	20.00	20.00	20.00
OH	2.91	2.92	2.49	3.72
F	1.06	0.98	1.39	0.04
Cl	0.03	0.10	0.12	0.23
Charge	0.00	0.00	0.00	0.00
Fe_{total}	2.81	3.82	3.89	5.12
Al_{total}	2.28	2.32	2.54	2.12
Fe/(Fe+Mg)	0.54	0.77	0.83	0.91
A/CNK	1.16	1.14	1.32	1.17
Fe^{3+}/Fe_{total}	0.18	0.13	0.13	0.18
$Log(X_{Mg}/X_{Fe})$	-0.06	-0.51	-0.68	-1.01
$Log(X_F/X_{OH})$	-0.44	-0.48	-0.25	-1.92

sample	ns-4	ns-3	306-2	pr5b	nwab	ed3	pc2b	103b2
determinations	5	4	5	3	4	3	5	4
SiO_2	34.91	34.32	34.72	34.60	34.87	34.38	34.83	35.00
TiO_2	2.20	3.07	3.43	3.81	3.79	2.97	3.57	3.86
Al_2O_3	18.50	18.79	19.57	19.61	18.48	19.47	18.59	18.63
FeO_{total}	23.95	23.16	22.38	23.28	23.65	27.52	24.62	24.86
Fe_2O_3	3.03	3.43	3.79	3.20	1.98	2.68	2.69	2.61
FeO	21.22	20.08	18.98	20.40	21.87	25.11	22.21	22.51
MnO	0.90	0.27	0.34	0.47	0.40	0.81	0.39	0.44
MgO	6.04	7.25	5.72	4.83	7.01	3.68	6.98	7.06
CaO	0.00	0.01	0.01	0.00	0.01	0.03	0.03	0.01
Na_2O	0.05	0.05	0.15	0.11	0.17	0.12	0.14	0.17
K_2O	9.79	10.23	10.10	10.23	9.98	9.83	10.08	10.09
H_2O	3.83	3.80	3.65	3.54	3.71	3.54	3.74	3.69
F	0.05	0.09	0.51	0.70	0.32	0.57	0.26	0.35
Cl	0.00	0.07	0.06	0.04	0.11	0.08	0.09	0.09
O=F	-0.02	-0.04	-0.22	-0.29	-0.13	-0.24	-0.11	-0.15
O=Cl	0.00	-0.02	-0.01	-0.01	-0.03	-0.02	-0.02	-0.02
total	100.50	101.39	100.80	101.24	102.54	103.01	103.45	104.36
^{iv}Si	5.37	5.22	5.28	5.27	5.26	5.24	5.22	5.20
^{iv}Al	2.63	2.78	2.72	2.73	2.74	2.76	2.78	2.80
^{iv}Ti	0.00	0.00	0.00	0.00	0.00	0.00	0.00	0.00
T site #	8.00	8.00	8.00	8.00	8.00	8.00	8.00	8.00
Al	0.72	0.58	0.78	0.79	0.54	0.74	0.50	0.46
Ti	0.25	0.35	0.39	0.44	0.43	0.34	0.40	0.43
Fe^{+3}	0.35	0.39	0.43	0.37	0.22	0.31	0.30	0.29
Fe^{+2}	2.73	2.55	2.41	2.60	2.76	3.20	2.78	2.80
Mn^{+2}	0.12	0.03	0.04	0.06	0.05	0.11	0.05	0.06
Mg	1.39	1.64	1.30	1.10	1.57	0.84	1.56	1.56
O site #	5.56	5.55	5.36	5.34	5.58	5.53	5.60	5.61
Ca	0.00	0.00	0.00	0.00	0.00	0.01	0.00	0.00
Na	0.02	0.02	0.05	0.03	0.05	0.04	0.04	0.05
K	1.92	1.98	1.96	1.99	1.92	1.91	1.93	1.91
A site #	1.94	2.00	2.01	2.02	1.97	1.95	1.97	1.96
O	20.04	20.08	20.00	20.00	20.09	20.11	20.12	20.15
OH	3.93	3.86	3.74	3.65	3.73	3.60	3.74	3.66
F	0.02	0.04	0.25	0.34	0.15	0.28	0.12	0.16
Cl	0.00	0.02	0.02	0.01	0.03	0.02	0.02	0.02
Charge	-0.04	-0.08	0.00	0.00	-0.09	-0.11	-0.12	-0.15
Fe_{total}	3.08	2.94	2.84	2.96	2.98	3.51	3.09	3.09
Al_{total}	3.35	3.37	3.51	3.52	3.28	3.50	3.28	3.26
Fe/(Fe+Mg)	0.69	0.64	0.69	0.73	0.65	0.81	0.66	0.66
A/CNK	1.73	1.68	1.75	1.74	1.66	1.79	1.66	1.66
Fe^{3+}/Fe_{total}	0.11	0.13	0.15	0.12	0.08	0.10	0.11	0.11
$Log(X_{Mg}/X_{Fe})$	-0.35	-0.25	-0.34	-0.43	-0.28	-0.62	-0.30	-0.30
$Log(X_F/X_{OH})$	-2.22	-1.95	-1.18	-1.03	-1.39	-1.12	-1.48	-1.35

sample	slp	br4
determinations	3	4
SiO_2	34.90	34.72
TiO_2	4.01	3.73
Al_2O_3	19.41	18.77
FeO_{total}	26.24	27.18
Fe_2O_3	3.43	4.92
FeO	23.16	22.75
MnO	0.44	0.37
MgO	5.61	6.09
CaO	0.00	0.00
Na_2O	0.13	0.18
K_2O	10.33	9.88
H_2O	3.75	3.60
F	0.23	0.55
Cl	0.05	0.04
O=F	-0.10	-0.23
O=Cl	-0.01	-0.01
total	105.35	105.37
^{iv}Si	5.16	5.14
^{iv}Al	2.84	2.86
^{iv}Ti	0.00	0.00
T site #	8.00	8.00
Al	0.54	0.41
Ti	0.45	0.41
Fe^{+3}	0.38	0.55
Fe^{+2}	2.86	2.81
Mn^{+2}	0.06	0.05
Mg	1.24	1.34
O site #	5.52	5.58
Ca	0.00	0.00
Na	0.04	0.05
K	1.95	1.87
A site #	1.99	1.92
O	20.18	20.17
OH	3.70	3.56
F	0.11	0.26
Cl	0.01	0.01
Charge	-0.18	-0.17
Fe_{total}	3.24	3.36
Al_{total}	3.38	3.27
Fe/(Fe+Mg)	0.72	0.71
A/CNK	1.70	1.71
Fe^{3+}/Fe_{total}	0.13	0.20
$Log(X_{Mg}/X_{Fe})$	-0.42	-0.40
$Log(X_F/X_{OH})$	-1.54	-1.14

Dumas (1988) Port Mouton pluton

sample	npm60	npm107	npm108	npm11	npm2	npm344	npm361	npm405
determinations	1	3	5	6	3	4	3	5
SiO_2	35.34	34.66	35.18	35.29	35.19	34.32	35.03	39.27
TiO_2	2.89	1.67	1.79	3.07	2.67	1.78	2.69	2.03
Al_2O_3	17.13	18.67	19.61	17.87	19.47	18.81	17.99	15.32
Fe_2O_3	0.00	0.02	0.02	0.02	0.03	0.02	0.02	0.03
FeO	21.38	23.64	20.28	20.63	19.09	23.18	23.07	10.83
MnO	0.75	0.54	0.27	0.49	0.48	0.73	0.67	0.14
MgO	7.72	5.57	8.85	8.68	8.41	6.42	6.67	18.13
CaO	0.04	0.01	0.01	0.00	0.07	0.00	0.01	0.02
Na_2O	0.00	0.04	0.14	0.04	0.17	0.00	0.03	0.50
K_2O	9.20	9.66	9.85	9.35	9.90	9.94	8.52	8.48
H_2O	3.85	3.80	3.94	3.91	3.93	3.83	3.85	4.11
F	0.00	0.00	0.00	0.00	0.00	0.00	0.00	0.00
Cl	0.00	0.00	0.00	0.00	0.00	0.00	0.00	0.00
O=F	0.00	0.00	0.00	0.00	0.00	0.00	0.00	0.00
O=Cl	0.00	0.00	0.00	0.00	0.00	0.00	0.00	0.00
total	98.30	98.29	99.93	99.35	99.42	99.03	98.54	98.86
^{iv}Si	5.50	5.46	5.35	5.41	5.37	5.37	5.46	5.73
^{iv}Al	2.50	2.54	2.65	2.59	2.63	2.63	2.54	2.27
^{iv}Ti	0.00	0.00	0.00	0.00	0.00	0.00	0.00	0.00
T site #	8.00	8.00	8.00	8.00	8.00	8.00	8.00	8.00
Al	0.65	0.93	0.87	0.64	0.86	0.84	0.76	0.36
Ti	0.34	0.20	0.21	0.35	0.31	0.21	0.31	0.22
Fe^{+3}	0.00	0.00	0.00	0.00	0.00	0.00	0.00	0.00
Fe^{+2}	2.78	3.12	2.58	2.65	2.43	3.04	3.01	1.32
Mn^{+2}	0.10	0.07	0.04	0.06	0.06	0.10	0.09	0.02
Mg	1.79	1.31	2.01	1.98	1.91	1.50	1.55	3.94
O site #	5.66	5.63	5.70	5.70	5.58	5.69	5.72	5.87
Ca	0.01	0.00	0.00	0.00	0.01	0.00	0.00	0.00
Na	0.00	0.01	0.04	0.01	0.05	0.00	0.01	0.14
K	1.83	1.94	1.91	1.83	1.93	1.99	1.69	1.58
A site #	1.83	1.96	1.95	1.84	1.99	1.99	1.70	1.72
O	20.00	20.00	20.00	20.00	20.00	20.00	20.00	20.00
OH	4.00	4.00	4.00	4.00	4.00	4.00	4.00	4.00
F	0.00	0.00	0.00	0.00	0.00	0.00	0.00	0.00
Cl	0.00	0.00	0.00	0.00	0.00	0.00	0.00	0.00
Charge	0.00	0.00	0.00	0.00	0.00	0.00	0.00	0.00
Fe_{total}	2.78	3.12	2.58	2.65	2.44	3.04	3.01	1.32
Al_{total}	3.14	3.47	3.52	3.23	3.50	3.47	3.30	2.63
Fe/(Fe+Mg)	0.61	0.70	0.56	0.57	0.56	0.67	0.66	0.25
A/CNK	1.71	1.77	1.80	1.75	1.75	1.75	1.94	1.53

Dumas (1988) Port Mouton pluton

sample	npm407	npm441	npm458	npm468	npm477	npm484	npm485	npm533
determinations	4	3	3	3	3	6	3	4
SiO_2	38.15	34.75	35.18	35.05	35.10	33.75	38.99	35.73
TiO_2	1.58	2.74	2.48	2.95	2.15	2.25	1.97	3.36
Al_2O_3	16.71	18.00	17.98	18.28	16.78	17.73	16.53	17.31
Fe_2O_3	0.05	0.04	0.04	0.02	0.01	0.02	0.02	0.02
FeO	14.91	22.71	22.17	22.31	22.74	27.84	11.60	19.75
MnO	0.27	0.66	0.60	0.68	0.58	0.43	0.16	0.45
MgO	13.87	6.63	6.55	5.69	7.94	3.86	16.38	9.26
CaO	0.00	0.00	0.03	0.01	0.00	0.00	0.00	0.00
Na_2O	0.18	0.06	0.06	0.08	0.00	0.03	0.10	0.03
K_2O	9.79	9.91	9.96	9.66	9.95	9.71	9.58	9.20
H_2O	4.03	3.85	3.84	3.84	3.84	3.76	4.10	3.92
F	0.00	0.00	0.00	0.00	0.00	0.00	0.00	0.00
Cl	0.00	0.00	0.00	0.00	0.00	0.00	0.00	0.00
O=F	0.00	0.00	0.00	0.00	0.00	0.00	0.00	0.00
O=Cl	0.00	0.00	0.00	0.00	0.00	0.00	0.00	0.00
total	99.53	99.34	98.91	98.57	99.09	99.37	99.44	99.01
^{iv}Si	5.67	5.41	5.48	5.47	5.48	5.39	5.69	5.47
^{iv}Al	2.33	2.59	2.52	2.53	2.52	2.61	2.31	2.53
^{iv}Ti	0.00	0.00	0.00	0.00	0.00	0.00	0.00	0.00
T site #	8.00	8.00	8.00	8.00	8.00	8.00	8.00	8.00
Al	0.60	0.71	0.78	0.84	0.57	0.72	0.54	0.59
Ti	0.18	0.32	0.29	0.35	0.25	0.27	0.22	0.39
Fe^{+3}	0.01	0.00	0.01	0.00	0.00	0.00	0.00	0.00
Fe^{+2}	1.85	2.96	2.89	2.91	2.97	3.72	1.42	2.53
Mn^{+2}	0.03	0.09	0.08	0.09	0.08	0.06	0.02	0.06
Mg	3.07	1.54	1.52	1.32	1.85	0.92	3.57	2.11
O site #	5.74	5.62	5.57	5.52	5.73	5.68	5.76	5.68
Ca	0.00	0.00	0.01	0.00	0.00	0.00	0.00	0.00
Na	0.05	0.02	0.02	0.03	0.00	0.01	0.03	0.01
K	1.86	1.97	1.98	1.93	1.98	1.98	1.79	1.80
A site #	1.91	1.99	2.00	1.95	1.98	1.98	1.81	1.81
O	20.01	20.00	20.01	20.00	20.00	20.00	20.00	20.00
OH	3.99	4.00	3.99	4.00	4.00	4.00	4.00	4.00
F	0.00	0.00	0.00	0.00	0.00	0.00	0.00	0.00
Cl	0.00	0.00	0.00	0.00	0.00	0.00	0.00	0.00
Charge	0.00	0.00	0.00	0.00	0.00	0.00	0.00	0.00
Fe_{total}	1.86	2.96	2.89	2.92	2.97	3.72	1.42	2.53
Al_{total}	2.93	3.30	3.30	3.37	3.09	3.33	2.84	3.12
Fe/(Fe+Mg)	0.38	0.66	0.66	0.69	0.62	0.80	0.28	0.54
A/CNK	1.53	1.66	1.64	1.72	1.56	1.68	1.57	1.73

Dumas (1988) Port Mouton pluton

sample	npm537	npm538	npm539	npm542	npm546	npm558	npm560	npm566
determinations	5	3	6	5	5	3	2	3
SiO_2	35.09	34.86	35.74	35.00	35.83	35.60	35.75	35.31
TiO_2	2.65	1.90	3.35	2.64	3.08	2.79	3.27	3.66
Al_2O_3	17.90	18.61	18.44	17.87	17.54	17.63	17.61	18.79
Fe_2O_3	0.03	0.06	0.06	0.02	0.04	2.81	0.03	0.04
FeO	22.61	23.19	19.60	23.08	18.97	17.50	21.63	21.65
MnO	0.77	0.72	0.56	0.51	0.47	0.34	0.76	0.46
MgO	7.17	6.58	8.68	6.08	9.64	9.06	7.80	7.08
CaO	0.00	0.00	0.00	0.01	0.00	0.01	0.00	0.00
Na_2O	0.00	0.03	0.05	0.03	0.06	3.56	0.05	0.04
K_2O	9.89	10.14	10.00	10.28	9.96	10.62	8.82	8.06
H_2O	3.88	3.86	3.96	3.84	3.93	3.92	3.91	3.91
F	0.00	0.00	0.00	0.00	0.00	0.00	0.00	0.00
Cl	0.00	0.00	0.00	0.00	0.00	0.00	0.00	0.00
O=F	0.00	0.00	0.00	0.00	0.00	0.00	0.00	0.00
O=Cl	0.00	0.00	0.00	0.00	0.00	0.00	0.00	0.00
total	100.01	99.96	100.44	99.35	99.51	110.65	99.61	98.99
^{iv}Si	5.42	5.41	5.41	5.46	5.46	5.04	5.48	5.41
^{iv}Al	2.58	2.59	2.59	2.54	2.54	2.94	2.52	2.59
^{iv}Ti	0.00	0.00	0.00	0.00	0.00	0.02	0.00	0.00
T site #	8.00	8.00	8.00	8.00	8.00	8.00	8.00	8.00
Al	0.68	0.81	0.70	0.75	0.61	0.00	0.66	0.80
Ti	0.31	0.22	0.38	0.31	0.35	0.28	0.38	0.42
Fe^{+3}	0.00	0.01	0.01	0.00	0.01	0.30	0.00	0.00
Fe^{+2}	2.92	3.01	2.48	3.01	2.42	2.07	2.77	2.77
Mn^{+2}	0.10	0.09	0.07	0.07	0.06	0.04	0.10	0.06
Mg	1.65	1.52	1.96	1.41	2.19	1.91	1.78	1.62
O site #	5.67	5.66	5.59	5.56	5.64	5.36	5.69	5.68
Ca	0.00	0.00	0.00	0.00	0.00	0.00	0.00	0.00
Na	0.00	0.01	0.02	0.01	0.02	0.98	0.01	0.01
K	1.95	2.01	1.93	2.05	1.94	1.92	1.72	1.57
A site #	1.95	2.02	1.95	2.06	1.95	2.90	1.74	1.59
O	20.00	20.01	20.01	20.00	20.01	20.30	20.00	20.00
OH	4.00	3.99	3.99	4.00	3.99	3.70	4.00	4.00
F	0.00	0.00	0.00	0.00	0.00	0.00	0.00	0.00
Cl	0.00	0.00	0.00	0.00	0.00	0.00	0.00	0.00
Charge	0.00	0.00	0.00	0.00	0.00	0.00	0.00	0.00
Fe_{total}	2.92	3.01	2.49	3.01	2.42	2.37	2.77	2.78
Al_{total}	3.26	3.40	3.29	3.29	3.15	2.94	3.18	3.39
Fe/(Fe+Mg)	0.64	0.66	0.56	0.68	0.53	0.55	0.61	0.63
A/CNK	1.67	1.69	1.69	1.60	1.61	1.02	1.83	2.14

Dumas (1988) Port Mouton pluton

sample	npm580	npm582	npm583	npm611	npm8a
determinations	5	3	4	6	4
SiO_2	35.20	35.29	34.61	34.97	34.53
TiO_2	2.36	2.54	2.78	2.27	2.15
Al_2O_3	18.24	18.29	18.18	18.76	17.96
Fe_2O_3	0.02	0.06	0.02	2.98	0.02
FeO	21.28	20.81	22.44	19.78	24.78
MnO	0.64	0.37	0.49	0.66	0.75
MgO	7.04	8.24	7.28	6.55	5.40
CaO	0.00	0.01	0.01	0.00	0.02
Na_2O	0.02	0.06	0.02	0.00	0.04
K_2O	10.32	9.75	9.58	10.33	9.93
H_2O	3.86	3.89	3.86	3.54	3.81
F	0.00	0.00	0.00	0.00	0.00
Cl	0.00	0.00	0.00	0.00	0.00
O=F	0.00	0.00	0.00	0.00	0.00
O=Cl	0.00	0.00	0.00	0.00	0.00
total	98.98	99.31	99.25	99.84	99.38
^{iv}Si	5.47	5.43	5.37	5.41	5.43
^{iv}Al	2.53	2.57	2.63	2.59	2.57
^{iv}Ti	0.00	0.00	0.00	0.00	0.00
T site #	8.00	8.00	8.00	8.00	8.00
Al	0.81	0.74	0.70	0.83	0.76
Ti	0.28	0.29	0.32	0.26	0.25
Fe^{+3}	0.00	0.01	0.00	0.35	0.00
Fe^{+2}	2.76	2.68	2.91	2.56	3.26
Mn^{+2}	0.08	0.05	0.06	0.09	0.10
Mg	1.63	1.89	1.68	1.51	1.27
O site #	5.56	5.66	5.69	5.60	5.64
Ca	0.00	0.00	0.00	0.00	0.00
Na	0.01	0.02	0.01	0.00	0.01
K	2.04	1.91	1.90	2.04	1.99
A site #	2.05	1.93	1.90	2.04	2.01
O	20.00	20.01	20.00	20.35	20.00
OH	4.00	3.99	4.00	3.65	4.00
F	0.00	0.00	0.00	0.00	0.00
Cl	0.00	0.00	0.00	0.00	0.00
Charge	0.00	0.00	0.00	0.00	0.00
Fe_{total}	2.77	2.68	2.92	2.91	3.26
Al_{total}	3.34	3.31	3.33	3.42	3.33
Fe/(Fe+Mg)	0.63	0.59	0.63	0.66	0.72
A/CNK	1.63	1.71	1.75	1.67	1.66

HAM (1988) Half-Cove-Qeens pluton

sample	nqp12	nqpo3	nqpo7	nqpo8	nqp10	nqp11	nqpl004
determinations	2	5	6	6	9	4	3
SiO_2	36.41	36.34	38.28	37.64	37.35	38.01	36.69
TiO_2	3.44	3.17	3.33	3.20	3.32	3.18	2.80
Al_2O_3	19.09	19.10	17.77	18.33	18.54	18.04	19.57
Fe_2O_3	0.06	0.04	0.04	0.04	0.04	0.04	0.03
FeO	19.91	21.13	19.89	20.74	21.65	20.47	22.30
MnO	0.64	0.41	0.77	0.35	0.47	0.64	0.48
MgO	7.80	6.75	6.03	6.57	5.55	6.24	4.88
CaO	0.00	0.00	0.11	0.04	0.06	0.12	0.00
Na_2O	0.00	0.00	0.00	0.00	0.00	0.00	0.00
K_2O	9.42	9.62	9.76	9.79	9.70	9.68	9.25
H_2O	3.99	3.96	3.97	3.98	3.96	3.98	3.93
F	0.00	0.00	0.00	0.00	0.00	0.00	0.00
Cl	0.00	0.00	0.00	0.00	0.00	0.00	0.00
O=F	0.00	0.00	0.00	0.00	0.00	0.00	0.00
O=Cl	0.00	0.00	0.00	0.00	0.00	0.00	0.00
total	100.76	100.52	99.94	100.67	100.66	100.39	99.93
^{iv}Si	5.46	5.50	5.78	5.66	5.65	5.73	5.59
^{iv}Al	2.54	2.50	2.22	2.34	2.35	2.27	2.41
^{iv}Ti	0.00	0.00	0.00	0.00	0.00	0.00	0.00
T site #	8.00	8.00	8.00	8.00	8.00	8.00	8.00
Al	0.84	0.90	0.95	0.91	0.95	0.93	1.10
Ti	0.39	0.36	0.38	0.36	0.38	0.36	0.32
Fe^{+3}	0.01	0.00	0.00	0.00	0.00	0.00	0.00
Fe^{+2}	2.50	2.67	2.51	2.61	2.74	2.58	2.84
Mn^{+2}	0.08	0.05	0.10	0.05	0.06	0.08	0.06
Mg	1.74	1.52	1.36	1.47	1.25	1.40	1.11
O site #	5.56	5.51	5.30	5.41	5.38	5.36	5.44
Ca	0.00	0.00	0.02	0.01	0.01	0.02	0.00
Na	0.00	0.00	0.00	0.00	0.00	0.00	0.00
K	1.80	1.86	1.88	1.88	1.87	1.86	1.80
A site #	1.80	1.86	1.90	1.88	1.88	1.88	1.80
O	20.01	20.00	20.00	20.00	20.00	20.00	20.00
OH	3.99	4.00	4.00	4.00	4.00	4.00	4.00
F	0.00	0.00	0.00	0.00	0.00	0.00	0.00
Cl	0.00	0.00	0.00	0.00	0.00	0.00	0.00
Charge	0.00	0.00	0.00	0.00	0.00	0.00	0.00
Fe_{total}	2.50	2.68	2.52	2.61	2.74	2.58	2.84
Al_{total}	3.38	3.40	3.16	3.25	3.30	3.20	3.51
Fe/(Fe+Mg)	0.59	0.64	0.65	0.64	0.69	0.65	0.72
A/CNK	1.87	1.83	1.65	1.72	1.75	1.69	1.95

HAM (1988) Half-Cove-Qeens pluton

sample	nqpl038	nqp01	nqp02	nhc01	nhc02	nhc06	nhcl014
determinations	8	9	10	3	6	5	5
SiO_2	36.05	36.93	36.28	38.09	35.94	37.18	35.68
TiO_2	3.22	2.97	3.20	2.72	3.27	3.32	1.21
Al_2O_3	19.03	18.44	19.04	18.81	19.97	18.97	20.63
Fe_2O_3	0.04	0.03	0.03	0.01	0.03	0.03	0.91
FeO	21.09	20.23	20.14	22.14	22.41	21.57	23.83
MnO	0.55	0.56	0.54	0.78	0.41	0.28	0.62
MgO	7.03	7.30	7.86	4.09	5.54	5.11	3.74
CaO	0.05	0.04	0.00	0.08	0.04	0.11	0.00
Na_2O	0.00	0.00	0.00	0.00	0.00	0.00	0.00
K_2O	9.28	9.60	9.51	9.55	9.41	9.38	9.05
H_2O	3.95	3.96	3.98	3.95	3.96	3.95	3.77
F	0.00	0.00	0.00	0.00	0.00	0.00	0.00
Cl	0.00	0.00	0.00	0.00	0.00	0.00	0.00
O=F	0.00	0.00	0.00	0.00	0.00	0.00	0.00
O=Cl	0.00	0.00	0.00	0.00	0.00	0.00	0.00
total	100.31	100.06	100.58	100.21	100.97	99.88	99.43
^{iv}Si	5.46	5.59	5.46	5.78	5.43	5.64	5.52
^{iv}Al	2.54	2.41	2.54	2.22	2.57	2.36	2.48
^{iv}Ti	0.00	0.00	0.00	0.00	0.00	0.00	0.00
T site #	8.00	8.00	8.00	8.00	8.00	8.00	8.00
Al	0.86	0.88	0.84	1.14	0.99	1.04	1.29
Ti	0.37	0.34	0.36	0.31	0.37	0.38	0.14
Fe^{+3}	0.00	0.00	0.00	0.00	0.00	0.00	0.11
Fe^{+2}	2.67	2.56	2.54	2.81	2.83	2.74	3.08
Mn^{+2}	0.07	0.07	0.07	0.10	0.05	0.04	0.08
Mg	1.59	1.65	1.76	0.92	1.25	1.16	0.86
O site #	5.57	5.50	5.57	5.29	5.50	5.35	5.56
Ca	0.01	0.01	0.00	0.01	0.01	0.02	0.00
Na	0.00	0.00	0.00	0.00	0.00	0.00	0.00
K	1.79	1.85	1.83	1.85	1.82	1.82	1.79
A site #	1.80	1.86	1.83	1.86	1.82	1.83	1.79
O	20.00	20.00	20.00	20.00	20.00	20.00	20.11
OH	4.00	4.00	4.00	4.00	4.00	4.00	3.89
F	0.00	0.00	0.00	0.00	0.00	0.00	0.00
Cl	0.00	0.00	0.00	0.00	0.00	0.00	0.00
Charge	0.00	0.00	0.00	0.00	0.00	0.00	0.00
Fe_{total}	2.68	2.56	2.54	2.81	2.84	2.74	3.19
Al_{total}	3.40	3.29	3.38	3.36	3.56	3.39	3.76
Fe/(Fe+Mg)	0.63	0.61	0.59	0.75	0.69	0.70	0.79
A/CNK	1.88	1.76	1.85	1.79	1.95	1.83	2.11

HAM (1988) Half-Cove-Qeens pluton

sample	nhcl036	nhc03	nh34	nop13	nqp14	nqp15	nqp16
determinations	8	8	6	10	5	6	4
SiO_2	35.85	35.89	35.94	36.12	38.42	36.89	36.47
TiO_2	2.64	3.04	2.68	3.11	3.28	2.81	2.77
Al_2O_3	19.47	19.53	19.16	18.86	17.87	19.79	19.19
Fe_2O_3	0.03	0.05	0.01	0.03	0.04	0.01	0.02
FeO	21.63	21.53	21.67	20.42	21.54	23.75	20.18
MnO	0.59	0.28	0.67	0.40	0.43	0.73	0.38
MgO	6.82	6.81	6.19	7.69	4.92	2.68	6.89
CaO	0.01	0.00	0.01	0.01	0.08	0.06	0.01
Na_2O	0.00	0.00	0.00	0.00	0.00	0.00	0.00
K_2O	9.37	9.61	9.41	9.58	9.76	9.27	9.41
H_2O	3.95	3.96	3.92	3.96	3.96	3.91	3.94
F	0.00	0.00	0.00	0.00	0.00	0.00	0.00
Cl	0.00	0.00	0.00	0.00	0.00	0.00	0.00
O=F	0.00	0.00	0.00	0.00	0.00	0.00	0.00
O=Cl	0.00	0.00	0.00	0.00	0.00	0.00	0.00
total	100.36	100.69	99.65	100.16	100.31	99.89	99.26
^{iv}Si	5.44	5.43	5.50	5.47	5.81	5.66	5.55
^{iv}Al	2.56	2.57	2.50	2.53	2.19	2.34	2.45
^{iv}Ti	0.00	0.00	0.00	0.00	0.00	0.00	0.00
T site #	8.00	8.00	8.00	8.00	8.00	8.00	8.00
Al	0.93	0.91	0.96	0.84	1.00	1.23	0.99
Ti	0.30	0.35	0.31	0.35	0.37	0.32	0.32
Fe^{+3}	0.00	0.01	0.00	0.00	0.00	0.00	0.00
Fe^{+2}	2.75	2.72	2.77	2.59	2.73	3.05	2.57
Mn^{+2}	0.08	0.04	0.09	0.05	0.06	0.09	0.05
Mg	1.54	1.53	1.41	1.74	1.11	0.61	1.56
O site #	5.60	5.56	5.54	5.57	5.27	5.31	5.49
Ca	0.00	0.00	0.00	0.00	0.01	0.01	0.00
Na	0.00	0.00	0.00	0.00	0.00	0.00	0.00
K	1.82	1.85	1.84	1.85	1.88	1.81	1.83
A site #	1.82	1.85	1.84	1.85	1.90	1.82	1.83
O	20.00	20.01	20.00	20.00	20.00	20.00	20.00
OH	4.00	3.99	4.00	4.00	4.00	4.00	4.00
F	0.00	0.00	0.00	0.00	0.00	0.00	0.00
Cl	0.00	0.00	0.00	0.00	0.00	0.00	0.00
Charge	0.00	0.00	0.00	0.00	0.00	0.00	0.00
Fe_{total}	2.75	2.73	2.78	2.59	2.73	3.05	2.57
Al_{total}	3.49	3.48	3.46	3.37	3.19	3.58	3.44
Fe/(Fe+Mg)	0.64	0.64	0.66	0.60	0.71	0.83	0.62
A/CNK	1.92	1.88	1.88	1.82	1.67	1.95	1.88

HAM (1988) Half-Cove-Qeens pluton		
sample	nqp18	nqp20
determinations	10	7
SiO_2	36.75	38.23
TiO_2	3.06	3.31
Al_2O_3	18.73	18.05
Fe_2O_3	0.02	0.02
FeO	20.31	21.21
MnO	0.33	0.45
MgO	7.07	5.45
CaO	0.00	0.08
Na_2O	0.00	0.00
K_2O	9.72	9.80
H_2O	3.96	3.98
F	0.00	0.00
Cl	0.00	0.00
O=F	0.00	0.00
O=Cl	0.00	0.00
total	99.95	100.58
^{iv}Si	5.57	5.76
^{iv}Al	2.43	2.24
^{iv}Ti	0.00	0.00
T site #	8.00	8.00
Al	0.91	0.97
Ti	0.35	0.38
Fe^{+3}	0.00	0.00
Fe^{+2}	2.57	2.67
Mn^{+2}	0.04	0.06
Mg	1.60	1.23
O site #	5.47	5.30
Ca	0.00	0.01
Na	0.00	0.00
K	1.88	1.88
A site #	1.88	1.90
O	20.00	20.00
OH	4.00	4.00
F	0.00	0.00
Cl	0.00	0.00
Charge	0.00	0.00
Fe_{total}	2.58	2.68
Al_{total}	3.34	3.21
Fe/(Fe+Mg)	0.62	0.69
A/CNK	1.78	1.68

MacDonald (1981) Mousquodubite batholith				
m-097	m-103	m-010	m-022	m-096
35.82	35.27	34.91	35.36	35.94
2.97	3.51	3.60	3.15	2.77
19.42	19.17	18.99	20.25	20.41
0.00	0.00	0.00	0.00	0.00
20.65	20.43	20.75	19.89	22.23
0.68	0.41	0.39	0.23	0.39
6.71	6.41	6.31	5.97	6.24
0.02	0.02	0.02	0.05	0.03
0.24	0.17	0.19	0.21	0.15
9.57	9.57	9.45	9.36	9.26
3.94	3.94	3.93	3.97	3.94
0.00	0.00	0.00	0.00	0.00
0.00	0.00	0.00	0.00	0.00
0.00	0.00	0.00	0.00	0.00
0.00	0.00	0.00	0.00	0.00
100.02	98.90	98.54	98.44	101.36
5.45	5.43	5.40	5.43	5.40
2.55	2.57	2.60	2.57	2.60
0.00	0.00	0.00	0.00	0.00
8.00	8.00	8.00	8.00	8.00
0.93	0.90	0.87	1.10	1.01
0.34	0.41	0.42	0.36	0.31
0.00	0.00	0.00	0.00	0.00
2.63	2.63	2.69	2.56	2.79
0.09	0.05	0.05	0.03	0.05
1.52	1.47	1.46	1.37	1.40
5.50	5.46	5.48	5.41	5.57
0.00	0.00	0.00	0.01	0.00
0.07	0.05	0.06	0.06	0.04
1.86	1.88	1.87	1.83	1.77
1.93	1.93	1.93	1.91	1.82
20.00	20.00	20.00	20.00	20.00
4.00	4.00	4.00	4.00	4.00
0.00	0.00	0.00	0.00	0.00
0.00	0.00	0.00	0.00	0.00
0.00	0.00	0.00	0.00	0.00
2.63	2.63	2.69	2.56	2.79
3.48	3.48	3.46	3.67	3.61
0.63	0.64	0.65	0.65	0.67
1.80	1.80	1.80	1.92	1.98

MacDonald (1981) Mousquodubite batholith

sample determinations	m-044	m-109	m-101	m-102	m-104	m-076
SiO_2	35.47	35.25	35.06	34.67	35.00	34.82
TiO_2	3.49	3.49	2.82	2.54	1.73	2.25
Al_2O_3	19.89	19.43	21.09	20.65	21.39	20.82
Fe_2O_3	0.00	0.00	0.00	0.00	0.00	0.00
FeO	21.80	21.11	22.53	23.91	24.36	26.57
MnO	0.22	0.43	0.78	0.41	0.68	0.13
MgO	5.74	5.58	2.74	2.63	1.96	2.34
CaO	0.02	0.01	0.03	0.02	0.04	0.05
Na_2O	0.16	0.12	0.17	0.22	0.24	0.24
K_2O	9.36	9.32	9.22	8.85	9.00	8.59
H_2O	3.93	3.94	3.92	3.90	3.89	3.87
F	0.00	0.00	0.00	0.00	0.00	0.00
Cl	0.00	0.00	0.00	0.00	0.00	0.00
O=F	0.00	0.00	0.00	0.00	0.00	0.00
O=Cl	0.00	0.00	0.00	0.00	0.00	0.00
total	100.08	98.68	98.36	97.80	98.29	99.68
^{iv}Si	5.40	5.44	5.46	5.46	5.49	5.42
^{iv}Al	2.60	2.56	2.54	2.54	2.51	2.58
^{iv}Ti	0.00	0.00	0.00	0.00	0.00	0.00
T site #	8.00	8.00	8.00	8.00	8.00	8.00
Al	0.97	0.98	1.33	1.29	1.44	1.23
Ti	0.40	0.41	0.33	0.30	0.20	0.26
Fe^{+3}	0.00	0.00	0.00	0.00	0.00	0.00
Fe^{+2}	2.78	2.73	2.93	3.15	3.19	3.46
Mn^{+2}	0.03	0.06	0.10	0.05	0.09	0.02
Mg	1.30	1.28	0.64	0.62	0.46	0.54
O site #	5.48	5.45	5.33	5.40	5.39	5.51
Ca	0.00	0.00	0.01	0.00	0.01	0.01
Na	0.05	0.04	0.05	0.07	0.07	0.07
K	1.82	1.84	1.83	1.78	1.80	1.70
A site #	1.87	1.87	1.89	1.85	1.88	1.79
O	20.00	20.00	20.00	20.00	20.00	20.00
OH	4.00	4.00	4.00	4.00	4.00	4.00
F	0.00	0.00	0.00	0.00	0.00	0.00
Cl	0.00	0.00	0.00	0.00	0.00	0.00
Charge	0.00	0.00	0.00	0.00	0.00	0.00
Fe_{total}	2.78	2.73	2.93	3.15	3.19	3.46
Al_{total}	3.57	3.54	3.87	3.83	3.95	3.82
Fe/(Fe+Mg)	0.68	0.68	0.82	0.84	0.87	0.86
A/CNK	1.91	1.89	2.04	2.07	2.09	2.13

ALLAN (1981) South Mountain batholith

sample	as	ec	eda	edm	kl	mu	ng
determination	3	3	2	9	3	10	10
SiO_2	33.55	34.95	34.72	35.73	33.63	35.06	37.46
TiO_2	2.45	2.86	4.56	3.33	2.56	2.63	2.33
Al_2O_3	19.88	20.34	19.65	20.04	20.00	18.64	20.45
Fe_2O_3	0.00	0.00	0.00	0.00	0.00	0.00	0.00
FeO	26.13	24.49	27.16	26.39	21.69	24.49	20.93
MnO	0.50	0.27	0.35	0.50	0.38	0.27	0.20
MgO	6.85	6.42	3.75	3.86	7.75	7.18	6.95
CaO	0.00	0.00	0.00	0.00	0.00	0.00	0.00
Na_2O	0.12	0.03	0.17	0.12	0.13	0.00	0.03
K_2O	8.12	9.29	9.48	9.51	9.22	9.25	8.95
H_2O	3.86	3.89	3.83	3.85	3.91	3.88	3.99
F	0.00	0.00	0.00	0.00	0.00	0.00	0.00
Cl	0.00	0.00	0.00	0.00	0.00	0.00	0.00
O=F	0.00	0.00	0.00	0.00	0.00	0.00	0.00
O=Cl	0.00	0.00	0.00	0.00	0.00	0.00	0.00
total	101.46	102.54	103.67	103.33	99.27	101.40	101.29
^{iv}Si	5.14	5.25	5.24	5.37	5.19	5.34	5.56
^{iv}Al	2.86	2.75	2.76	2.63	2.81	2.66	2.44
^{iv}Ti	0.00	0.00	0.00	0.00	0.00	0.00	0.00
T site #	8.00	8.00	8.00	8.00	8.00	8.00	8.00
Al	0.72	0.85	0.73	0.92	0.83	0.69	1.13
Ti	0.28	0.32	0.52	0.38	0.30	0.30	0.26
Fe^{+3}	0.00	0.00	0.00	0.00	0.00	0.00	0.00
Fe^{+2}	3.35	3.08	3.43	3.32	2.80	3.12	2.60
Mn^{+2}	0.06	0.03	0.04	0.06	0.05	0.03	0.03
Mg	1.56	1.44	0.84	0.87	1.78	1.63	1.54
O site #	5.98	5.73	5.56	5.55	5.76	5.78	5.55
Ca	0.00	0.00	0.00	0.00	0.00	0.00	0.00
Na	0.04	0.01	0.05	0.03	0.04	0.00	0.01
K	1.59	1.78	1.82	1.82	1.82	1.80	1.69
A site #	1.62	1.79	1.87	1.86	1.85	1.80	1.70
O	20.00	20.00	20.00	20.00	20.00	20.00	20.00
OH	4.00	4.00	4.00	4.00	4.00	4.00	4.00
F	0.00	0.00	0.00	0.00	0.00	0.00	0.00
Cl	0.00	0.00	0.00	0.00	0.00	0.00	0.00
Charge	0.00	0.00	0.00	0.00	0.00	0.00	0.00
Fe_{total}	3.35	3.08	3.43	3.32	2.80	3.12	2.60
Al_{total}	3.59	3.60	3.49	3.55	3.64	3.35	3.57
Fe/(Fe+Mg)	0.68	0.68	0.80	0.79	0.61	0.66	0.63
A/CNK	2.21	2.01	1.86	1.91	1.96	1.86	2.10

Maillet (1984) South Mountain batholith

sample determinations	I83-151	I83-152	I83-65	80-83	16.9	I83-121	I83-122
SiO_2	34.87	35.11	35.57	35.51	35.68	36.19	35.23
TiO_2	3.60	3.36	3.32	3.14	4.03	3.03	3.05
Al_2O_3	20.09	20.02	20.02	19.10	19.08	20.41	20.59
Fe_2O_3	0.00	0.00	0.00	0.00	0.00	0.09	0.00
FeO	20.97	21.98	18.53	22.40	22.82	22.31	23.48
MnO	0.08	0.17	0.19	0.23	0.14	0.34	0.53
MgO	5.83	5.58	8.15	5.73	5.93	4.94	3.64
CaO	0.00	0.00	0.00	0.00	0.00	0.00	0.00
Na_2O	0.08	0.08	0.14	0.04	0.00	0.00	0.00
K_2O	9.55	9.55	9.44	9.49	9.59	9.81	9.33
H_2O	3.94	3.93	3.99	3.92	3.91	3.96	3.90
F	0.00	0.00	0.00	0.00	0.00	0.00	0.00
Cl	0.00	0.00	0.00	0.00	0.00	0.00	0.00
O=F	0.00	0.00	0.00	0.00	0.00	0.00	0.00
O=Cl	0.00	0.00	0.00	0.00	0.00	0.00	0.00
total	99.01	99.83	99.35	99.56	101.18	101.08	99.75
^{iv}Si	5.36	5.37	5.38	5.46	5.40	5.47	5.42
^{iv}Al	2.64	2.63	2.62	2.54	2.60	2.53	2.58
^{iv}Ti	0.00	0.00	0.00	0.00	0.00	0.00	0.00
T site #	8.00	8.00	8.00	8.00	8.00	8.00	8.00
Al	1.00	0.99	0.95	0.92	0.81	1.10	1.16
Ti	0.42	0.39	0.38	0.36	0.46	0.34	0.35
Fe^{+3}	0.00	0.00	0.00	0.00	0.00	0.01	0.00
Fe^{+2}	2.70	2.81	2.34	2.88	2.89	2.82	3.02
Mn^{+2}	0.01	0.02	0.02	0.03	0.02	0.04	0.07
Mg	1.34	1.27	1.84	1.31	1.34	1.11	0.84
O site #	5.46	5.49	5.53	5.51	5.51	5.43	5.44
Ca	0.00	0.00	0.00	0.00	0.00	0.00	0.00
Na	0.02	0.02	0.04	0.01	0.00	0.00	0.00
K	1.87	1.86	1.82	1.86	1.85	1.89	1.83
A site #	1.90	1.89	1.86	1.87	1.85	1.89	1.83
O	20.00	20.00	20.00	20.00	20.00	20.01	20.00
OH	4.00	4.00	4.00	4.00	4.00	3.99	4.00
F	0.00	0.00	0.00	0.00	0.00	0.00	0.00
Cl	0.00	0.00	0.00	0.00	0.00	0.00	0.00
Charge	0.00	0.00	0.00	0.00	0.00	0.00	0.00
Fe_{total}	2.70	2.81	2.34	2.88	2.89	2.83	3.02
Al_{total}	3.64	3.61	3.57	3.46	3.40	3.63	3.74
Fe/(Fe+Mg)	0.67	0.69	0.56	0.69	0.68	0.72	0.78
A/CNK	1.92	1.91	1.92	1.85	1.84	1.92	2.04

Maillet (1984) South Mountain batholith

sample determinations	l83-123	l83-80	l83-81	l83-152b	d15-304	d15-439	d15-560
SiO_2	35.49	36.63	35.59	35.76	35.72	35.35	36.33
TiO_2	3.22	3.04	2.85	4.04	2.47	2.44	2.00
Al_2O_3	20.48	20.67	20.59	19.27	20.49	19.96	20.17
Fe_2O_3	0.00	0.00	0.00	0.00	0.00	0.03	0.00
FeO	22.76	22.50	23.51	21.46	22.01	22.82	20.68
MnO	0.35	0.81	0.54	0.26	0.21	0.24	0.30
MgO	0.01	0.00	0.03	0.00	5.03	5.30	5.68
CaO	0.01	0.00	0.03	0.00	0.00	0.00	0.00
Na_2O	0.11	0.03	0.00	0.00	0.02	0.14	0.11
K_2O	9.31	10.15	9.71	9.25	9.53	9.17	9.42
H_2O	3.90	3.99	3.91	3.94	3.94	3.89	3.97
F	0.00	0.00	0.00	0.00	0.00	0.00	0.00
Cl	0.00	0.00	0.00	0.00	0.00	0.00	0.00
O=F	0.00	0.00	0.00	0.00	0.00	0.00	0.00
O=Cl	0.00	0.00	0.00	0.00	0.00	0.00	0.00
total	95.64	97.82	96.76	93.98	99.42	99.34	98.66
^{iv}Si	5.68	5.74	5.66	5.80	5.47	5.44	5.57
^{iv}Al	2.32	2.26	2.34	2.20	2.53	2.56	2.43
^{iv}Ti	0.00	0.00	0.00	0.00	0.00	0.00	0.00
T site #	8.00	8.00	8.00	8.00	8.00	8.00	8.00
Al	1.55	1.56	1.52	1.48	1.17	1.07	1.22
Ti	0.39	0.36	0.34	0.49	0.28	0.28	0.23
Fe^{+3}	0.00	0.00	0.00	0.00	0.00	0.00	0.00
Fe^{+2}	3.05	2.95	3.13	2.91	2.82	2.94	2.65
Mn^{+2}	0.05	0.11	0.07	0.04	0.03	0.03	0.04
Mg	0.00	0.00	0.01	0.00	1.15	1.22	1.30
O site #	5.03	4.97	5.07	4.91	5.46	5.54	5.44
Ca	0.00	0.00	0.01	0.00	0.00	0.00	0.00
Na	0.03	0.01	0.00	0.00	0.01	0.04	0.03
K	1.90	2.03	1.97	1.91	1.86	1.80	1.84
A site #	1.94	2.04	1.98	1.91	1.87	1.84	1.88
O	19.84	19.83	19.85	19.74	20.00	20.00	20.00
OH	4.16	4.17	4.15	4.26	4.00	4.00	4.00
F	0.00	0.00	0.00	0.00	0.00	0.00	0.00
Cl	0.00	0.00	0.00	0.00	0.00	0.00	0.00
Charge	0.16	0.17	0.15	0.26	0.00	0.00	0.00
Fe_{total}	3.05	2.95	3.13	2.91	2.82	2.94	2.65
Al_{total}	3.86	3.82	3.86	3.68	3.71	3.62	3.65
Fe/(Fe+Mg)	1.00	1.00	1.00	1.00	0.71	0.71	0.67
A/CNK	1.99	1.87	1.95	1.92	1.98	1.97	1.94

Ding (1995) South Mountain batholith

sample	349-1	92-hp-l	333-2	333-7	333-8	333-6	103-2
determinations	30	14	10	7	2	30	29
SiO_2	35.55	33.92	35.09	34.54	34.95	34.65	35.92
TiO_2	2.95	3.68	3.67	3.41	3.57	3.90	4.03
Al_2O_3	18.97	18.05	18.32	18.86	19.42	18.65	19.04
Fe_2O_3	0.00	0.00	0.00	0.00	0.00	0.00	0.00
FeO	18.04	20.19	20.87	21.51	22.08	22.05	22.42
MnO	0.45	0.36	0.44	0.44	0.16	0.37	0.56
MgO	8.99	6.90	6.82	5.79	6.31	5.93	4.37
CaO	0.00	0.00	0.00	0.00	0.00	0.00	0.00
Na_2O	0.27	0.30	0.29	0.36	0.44	0.32	0.33
K_2O	9.48	9.14	9.15	9.20	9.14	8.86	9.27
H_2O	3.99	3.93	3.93	3.92	3.92	3.92	3.92
F	0.00	0.00	0.00	0.00	0.00	0.00	0.00
Cl	0.00	0.00	0.00	0.00	0.00	0.00	0.00
O=F	0.00	0.00	0.00	0.00	0.00	0.00	0.00
O=Cl	0.00	0.00	0.00	0.00	0.00	0.00	0.00
total	98.69	96.47	98.58	98.03	99.99	98.65	99.86
^{iv}Si	5.42	5.37	5.43	5.40	5.34	5.38	5.51
^{iv}Al	2.58	2.63	2.57	2.60	2.66	2.62	2.49
^{iv}Ti	0.00	0.00	0.00	0.00	0.00	0.00	0.00
T site #	8.00	8.00	8.00	8.00	8.00	8.00	8.00
Al	0.83	0.74	0.77	0.87	0.84	0.79	0.95
Ti	0.34	0.44	0.43	0.40	0.41	0.46	0.46
Fe^{+3}	0.00	0.00	0.00	0.00	0.00	0.00	0.00
Fe^{+2}	2.30	2.67	2.70	2.81	2.82	2.86	2.87
Mn^{+2}	0.06	0.05	0.06	0.06	0.02	0.05	0.07
Mg	2.04	1.63	1.57	1.35	1.44	1.37	1.00
O site #	5.57	5.53	5.53	5.49	5.54	5.53	5.35
Ca	0.00	0.00	0.00	0.00	0.00	0.00	0.00
Na	0.08	0.09	0.09	0.11	0.13	0.10	0.10
K	1.84	1.85	1.81	1.83	1.78	1.75	1.81
A site #	1.92	1.94	1.89	1.94	1.91	1.85	1.91
O	20.00	20.00	20.00	20.00	20.00	20.00	20.00
OH	4.00	4.00	4.00	4.00	4.00	4.00	4.00
F	0.00	0.00	0.00	0.00	0.00	0.00	0.00
Cl	0.00	0.00	0.00	0.00	0.00	0.00	0.00
Charge	0.00	0.00	0.00	0.00	0.00	0.00	0.00
Fe_{total}	2.30	2.67	2.70	2.81	2.82	2.86	2.87
Al_{total}	3.41	3.37	3.34	3.47	3.50	3.41	3.44
Fe/(Fe+Mg)	0.53	0.62	0.63	0.68	0.66	0.68	0.74
A/CNK	1.77	1.74	1.76	1.79	1.83	1.84	1.80

Ding (1995) South Mountain batholith				Clarke (1995)			
sample	213-4	103-a5-e	103-a5	3127	3127	8018	8027
determinations	30	49	40	7	2	5	2
SiO_2	35.86	34.98	33.49	34.47	35.33	35.06	34.24
TiO_2	3.51	3.40	2.90	3.27	0.40	2.82	1.67
Al_2O_3	19.22	20.27	19.35	19.51	21.77	19.14	20.79
Fe_2O_3	0.00	0.00	0.00	0.00	0.00	0.00	0.00
FeO	22.94	25.65	24.53	23.80	22.87	22.65	26.72
MnO	0.85	0.39	0.64	0.93	0.99	0.24	0.63
MgO	4.05	3.94	4.26	2.64	3.14	5.04	1.04
CaO	0.00	0.00	0.00	0.00	0.01	0.00	0.01
Na_2O	0.30	0.36	0.35	0.30	0.35	0.22	0.27
K_2O	9.21	9.07	9.32	9.12	9.32	9.41	9.20
H_2O	3.91	3.87	3.85	3.51	3.43	3.73	3.46
F	0.00	0.00	0.00	0.68	0.92	0.71	0.73
Cl	0.00	0.00	0.00	0.07	0.08	0.07	0.03
O=F	0.00	0.00	0.00	-0.29	-0.39	-0.30	-0.31
O=Cl	0.00	0.00	0.00	-0.02	-0.02	-0.02	-0.01
total	99.85	101.93	98.69	98.00	98.20	98.78	98.48
^{iv}Si	5.51	5.32	5.29	5.45	5.52	5.47	5.45
^{iv}Al	2.49	2.68	2.71	2.55	2.48	2.53	2.55
^{iv}Ti	0.00	0.00	0.00	0.00	0.00	0.00	0.00
T site #	8.00	8.00	8.00	8.00	8.00	8.00	8.00
Al	1.00	0.95	0.89	1.09	1.54	0.99	1.34
Ti	0.41	0.39	0.34	0.39	0.05	0.33	0.20
Fe^{+3}	0.00	0.00	0.00	0.00	0.00	0.00	0.00
Fe^{+2}	2.95	3.26	3.24	3.15	2.99	2.95	3.55
Mn^{+2}	0.11	0.05	0.09	0.12	0.13	0.03	0.08
Mg	0.93	0.89	1.00	0.62	0.73	1.17	0.25
O site #	5.39	5.54	5.57	5.37	5.44	5.47	5.43
Ca	0.00	0.00	0.00	0.00	0.00	0.00	0.00
Na	0.09	0.11	0.11	0.09	0.11	0.07	0.08
K	1.81	1.76	1.88	1.84	1.86	1.87	1.87
A site #	1.90	1.87	1.99	1.93	1.97	1.94	1.95
O	20.00	20.00	20.00	19.93	19.95	19.75	19.95
OH	4.00	4.00	4.00	3.71	3.58	3.88	3.67
F	0.00	0.00	0.00	0.34	0.45	0.35	0.37
Cl	0.00	0.00	0.00	0.02	0.02	0.02	0.01
Charge	0.00	0.00	0.00	0.07	0.05	0.25	0.05
Fe_{total}	2.95	3.26	3.24	3.15	2.99	2.95	3.55
Al_{total}	3.48	3.63	3.60	3.64	4.01	3.52	3.90
Fe/(Fe+Mg)	0.76	0.79	0.76	0.83	0.80	0.72	0.94
A/CNK	1.84	1.95	1.81	1.88	2.04	1.81	1.99

Stallard (1975) South Mountain batholith

sample	m72-176	m72-50	m72-49	m72-161	m72-137	m72-124	m72-31
determinations							
SiO_2	35.00	34.19	34.88	35.40	34.06	34.16	34.61
TiO_2	3.44	2.88	3.01	2.84	4.31	3.78	4.11
Al_2O_3	19.14	19.14	19.11	19.85	18.50	18.37	18.13
Fe_{total}	23.11	23.23	22.68	23.38	22.65	23.42	23.28
Fe_2O_3	9.12	5.86	3.24	6.62	1.74	2.36	2.98
FeO	14.90	17.96	19.76	17.42	21.08	21.30	20.60
MnO	0.26	0.42	0.69	0.35	0.35	0.42	0.65
MgO	5.06	6.09	6.68	5.59	6.55	6.56	6.39
CaO	0.00	0.02	0.00	0.04	0.02	0.00	0.00
Na_2O	0.17	0.00	0.09	0.13	0.00	0.17	0.07
K_2O	9.45	9.29	9.45	9.47	9.29	9.38	9.40
H_2O	3.97	3.91	3.95	4.00	3.89	3.90	3.93
F	0.00	0.00	0.00	0.00	0.00	0.00	0.00
Cl	0.00	0.00	0.00	0.00	0.00	0.00	0.00
O=F	0.00	0.00	0.00	0.00	0.00	0.00	0.00
O=Cl	0.00	0.00	0.00	0.00	0.00	0.00	0.00
total	100.51	99.76	100.86	101.71	99.79	100.40	100.87
^{iv}Si	5.28	5.24	5.30	5.30	5.24	5.25	5.28
^{iv}Al	2.72	2.76	2.70	2.70	2.76	2.75	2.72
^{iv}Ti	0.00	0.00	0.00	0.00	0.00	0.00	0.00
T site #	8.00	8.00	8.00	8.00	8.00	8.00	8.00
Al	0.69	0.70	0.71	0.80	0.60	0.57	0.54
Ti	0.39	0.33	0.34	0.32	0.50	0.44	0.47
Fe^{+3}	1.04	0.68	0.37	0.75	0.20	0.27	0.34
Fe^{+2}	1.88	2.30	2.51	2.18	2.71	2.74	2.63
Mn^{+2}	0.03	0.05	0.09	0.04	0.05	0.05	0.08
Mg	1.14	1.39	1.51	1.25	1.50	1.50	1.45
O site #	5.17	5.45	5.54	5.33	5.56	5.57	5.52
Ca	0.00	0.00	0.00	0.01	0.00	0.00	0.00
Na	0.05	0.00	0.03	0.04	0.00	0.05	0.02
K	1.82	1.82	1.83	1.81	1.82	1.84	1.83
A site #	1.87	1.82	1.86	1.85	1.83	1.89	1.85
O	20.00	20.00	20.00	20.01	20.01	20.00	20.00
OH	4.00	4.00	4.00	3.99	3.99	4.00	4.00
F	0.00	0.00	0.00	0.00	0.00	0.00	0.00
Cl	0.00	0.00	0.00	0.00	0.00	0.00	0.00
Charge	0.00	0.00	0.00	-0.01	-0.01	0.00	0.00
Fe_{total}	2.92	2.98	2.88	2.92	2.92	3.01	2.97
Al_{total}	3.41	3.46	3.42	3.50	3.36	3.33	3.26
Fe/(Fe+Mg)	0.72	0.68	0.66	0.70	0.66	0.67	0.67
A/CNK	1.82	1.90	1.84	1.88	1.83	1.76	1.76
Fe^{3+}/Fe_{total}	0.36	0.23	0.13	0.25	0.07	0.09	0.12

Stallard (1975) South Mountain batholith

sample determinations	m72-39	m72-54e	m72-192	m72-60	m72-72	m72-127	m72-64
SiO_2	35.16	34.66	33.74	35.64	34.50	34.27	33.96
TiO_2	4.17	4.04	4.34	4.63	4.54	4.61	4.05
Al_2O_3	18.35	18.41	18.13	17.92	17.84	18.75	18.25
Fe_{total}	22.87	23.45	23.23	23.59	23.01	22.72	24.14
Fe_2O_3	1.54	3.73	3.72	3.53	0.56	0.06	0.00
FeO	21.48	20.09	19.88	20.41	22.51	22.66	24.14
MnO	0.45	0.44	0.48	0.37	0.39	0.49	0.41
MgO	6.42	5.99	5.71	5.63	6.05	5.89	6.22
CaO	0.02	0.00	0.01	0.02	0.05	0.03	0.00
Na_2O	0.02	0.15	0.12	0.03	0.00	0.00	0.15
K_2O	9.51	9.49	9.40	9.20	9.05	9.03	9.53
H_2O	3.94	3.93	3.87	3.97	3.87	3.88	3.88
F	0.00	0.00	0.00	0.00	0.00	0.00	0.00
Cl	0.00	0.00	0.00	0.00	0.00	0.00	0.00
O=F	0.00	0.00	0.00	0.00	0.00	0.00	0.00
O=Cl	0.00	0.00	0.00	0.00	0.00	0.00	0.00
total	101.06	100.93	99.40	101.35	99.36	99.68	100.59
^{iv}Si	5.34	5.28	5.23	5.39	5.35	5.29	5.25
^{iv}Al	2.66	2.72	2.77	2.61	2.65	2.71	2.75
^{iv}Ti	0.00	0.00	0.00	0.00	0.00	0.00	0.00
T site #	8.00	8.00	8.00	8.00	8.00	8.00	8.00
Al	0.63	0.58	0.54	0.58	0.60	0.70	0.58
Ti	0.48	0.46	0.51	0.53	0.53	0.53	0.47
Fe^{+3}	0.18	0.43	0.43	0.40	0.07	0.01	0.00
Fe^{+2}	2.73	2.56	2.58	2.58	2.92	2.92	3.12
Mn^{+2}	0.06	0.06	0.06	0.05	0.05	0.06	0.05
Mg	1.45	1.36	1.32	1.27	1.40	1.35	1.43
O site #	5.52	5.45	5.44	5.40	5.56	5.58	5.65
Ca	0.00	0.00	0.00	0.00	0.01	0.00	0.00
Na	0.01	0.04	0.04	0.01	0.00	0.00	0.04
K	1.84	1.84	1.86	1.77	1.79	1.78	1.88
A site #	1.85	1.89	1.90	1.79	1.80	1.78	1.92
O	20.01	20.01	20.00	20.00	20.00	20.01	20.00
OH	3.99	3.99	4.00	4.00	4.00	3.99	4.00
F	0.00	0.00	0.00	0.00	0.00	0.00	0.00
Cl	0.00	0.00	0.00	0.00	0.00	0.00	0.00
Charge	-0.01	-0.01	0.00	0.00	0.00	0.00	0.00
Fe_{total}	2.91	2.99	3.01	2.98	2.98	2.93	3.12
Al_{total}	3.29	3.30	3.31	3.19	3.26	3.41	3.33
Fe/(Fe+Mg)	0.67	0.69	0.70	0.70	0.68	0.68	0.69
A/CNK	1.77	1.75	1.74	1.78	1.80	1.91	1.73
Fe^{3+}/Fe_{total}	0.06	0.14	0.14	0.13	0.02	0.00	0.00

Stallard (1975) South Mountain batholith

sample	m72-121	m72-91	m72-82	m72-165	m72-433	m72-102	m72-153
determinations							
SiO_2	34.66	34.61	33.60	33.78	34.89	34.50	34.76
TiO_2	2.11	3.78	3.71	2.66	2.67	3.35	3.10
Al_2O_3	20.48	16.99	18.53	20.07	19.69	19.44	19.71
Fe_{total}	24.38	25.95	23.99	26.49	23.30	25.48	23.89
Fe_2O_3	7.57	5.79	0.02	11.10	0.00	8.90	0.00
FeO	17.57	20.74	23.97	16.50	23.30	17.47	23.89
MnO	0.24	0.52	0.36	0.57	0.43	0.37	0.32
MgO	4.24	4.90	5.71	3.64	5.00	3.66	4.91
CaO	0.06	0.08	0.00	0.04	0.01	0.01	0.05
Na_2O	0.14	0.10	0.12	0.12	0.07	0.14	0.16
K_2O	9.56	9.40	9.53	9.25	9.36	9.31	9.22
H_2O	3.94	3.89	3.83	3.96	3.87	3.95	3.89
F	0.00	0.00	0.00	0.00	0.00	0.00	0.00
Cl	0.00	0.00	0.00	0.00	0.00	0.00	0.00
O=F	0.00	0.00	0.00	0.00	0.00	0.00	0.00
O=Cl	0.00	0.00	0.00	0.00	0.00	0.00	0.00
total	100.57	100.80	99.38	101.69	99.29	101.10	100.01
^{iv}Si	5.27	5.33	5.26	5.11	5.41	5.24	5.36
^{iv}Al	2.73	2.67	2.74	2.89	2.59	2.76	2.64
^{iv}Ti	0.00	0.00	0.00	0.00	0.00	0.00	0.00
T site #	8.00	8.00	8.00	8.00	8.00	8.00	8.00
Al	0.94	0.42	0.67	0.69	1.00	0.72	0.94
Ti	0.24	0.44	0.44	0.30	0.31	0.38	0.36
Fe^{+3}	0.87	0.67	0.00	1.26	0.00	1.02	0.00
Fe^{+2}	2.23	2.67	3.14	2.09	3.02	2.22	3.08
Mn^{+2}	0.03	0.07	0.05	0.07	0.06	0.05	0.04
Mg	0.96	1.13	1.33	0.82	1.16	0.83	1.13
O site #	5.27	5.40	5.63	5.24	5.55	5.21	5.55
Ca	0.01	0.01	0.00	0.01	0.00	0.00	0.01
Na	0.04	0.03	0.04	0.04	0.02	0.04	0.05
K	1.85	1.85	1.90	1.79	1.85	1.80	1.81
A site #	1.90	1.89	1.94	1.83	1.87	1.85	1.87
O	20.01	20.00	20.00	20.00	20.00	20.00	20.00
OH	3.99	4.00	4.00	4.00	4.00	4.00	4.00
F	0.00	0.00	0.00	0.00	0.00	0.00	0.00
Cl	0.00	0.00	0.00	0.00	0.00	0.00	0.00
Charge	-0.01	0.00	0.00	0.00	0.00	0.00	0.00
Fe_{total}	3.10	3.34	3.14	3.35	3.02	3.23	3.08
Al_{total}	3.67	3.09	3.42	3.58	3.60	3.48	3.58
Fe/(Fe+Mg)	0.76	0.75	0.70	0.80	0.72	0.80	0.73
A/CNK	1.92	1.62	1.76	1.95	1.92	1.88	1.91
Fe^{3+}/Fe_{total}	0.28	0.20	0.00	0.38	0.00	0.31	0.00

Stallard (1975) South Mountain batholith

sample	m72-143	m72-187	m72-160
determinations			
SiO_2	34.79	34.11	34.07
TiO_2	2.75	2.71	2.67
Al_2O_3	20.35	19.42	20.18
Fe_{total}	24.87	25.75	25.28
Fe_2O_3	3.77	0.06	3.85
FeO	21.48	25.70	21.82
MnO	0.40	0.51	0.92
MgO	3.69	4.09	3.19
CaO	0.02	0.03	0.01
Na_2O	0.18	0.10	0.13
K_2O	9.36	9.30	9.39
H_2O	3.92	3.83	3.87
F	0.00	0.00	0.00
Cl	0.00	0.00	0.00
O=F	0.00	0.00	0.00
O=Cl	0.00	0.00	0.00
total	100.71	99.86	100.10
^{iv}Si	5.32	5.33	5.28
^{iv}Al	2.68	2.67	2.72
^{iv}Ti	0.00	0.00	0.00
T site #	8.00	8.00	8.00
Al	0.98	0.91	0.96
Ti	0.32	0.32	0.31
Fe^{+3}	0.43	0.01	0.45
Fe^{+2}	2.75	3.36	2.83
Mn^{+2}	0.05	0.07	0.12
Mg	0.84	0.95	0.74
O site #	5.37	5.61	5.40
Ca	0.00	0.01	0.00
Na	0.05	0.03	0.04
K	1.83	1.85	1.85
A site #	1.88	1.89	1.90
O	20.00	20.01	20.00
OH	4.00	3.99	4.00
F	0.00	0.00	0.00
Cl	0.00	0.00	0.00
Charge	0.00	0.00	0.00
Fe_{total}	3.18	3.37	3.27
Al_{total}	3.67	3.58	3.68
Fe/(Fe+Mg)	0.79	0.78	0.82
A/CNK	1.94	1.89	1.94
Fe^{3+}/Fe_{total}	0.14	0.00	0.14

Appendix III of Manuscript 1

Whole-rock Geochemical Data

Tabulated below are all the major element and trace element data collected during this study or unpublished data provided by researchers. Major elements are in weight per cent oxides. Trace elements are in part per million.

Whole-rock analyses of specimens from Gander zone of Newfoundland.

sample	snf-1	snf-10	snf-14	snf-15	snf-16	snf-17	snf-18	snf-19	snf-2
SiO_2	68.05	69.57	68.62	61.29	71.58	67.75	61.36	65.94	60.14
TiO_2	0.61	0.60	0.54	0.97	0.35	0.64	0.77	0.88	1.11
Al_2O_3	15.09	14.18	13.91	16.63	13.95	14.90	17.80	14.77	16.04
Fe2O3	0.36	1.39	1.17	2.06	0.79	0.91	1.82	1.50	2.47
FeO	3.10	1.75	1.94	3.60	1.28	2.46	3.13	3.16	3.77
MnO	0.07	0.06	0.07	0.13	0.07	0.07	0.07	0.12	0.14
MgO	1.23	0.65	1.20	2.22	0.55	0.88	1.55	1.26	2.88
CaO	2.65	2.00	2.46	4.16	1.85	2.03	4.63	2.55	3.86
Na_2O	3.03	3.30	2.65	2.92	3.34	2.86	3.69	2.96	3.03
K_2O	4.15	4.90	4.74	3.76	4.65	5.49	2.87	4.79	3.95
P_2O_5	0.21	0.17	0.17	0.37	0.08	0.18	0.35	0.26	0.36
LOI	0.5	0.2	1.0	0.9	0.4	0.9	1.1	0.8	1.1
total	99.55	99.19	98.83	99.65	99.18	99.54	99.73	99.62	99.56
V	52	38	48	115	34	51	58	77	130
Cr	21	28	38	39	2	18	12	33	85
Co	7	3	6	13	4	4	8	8	17
Ni	17	7	16	18	6	11	5	14	38
Zn	104	73	59	104	47	68	107	84	147
Rb	173	166	224	184	276	231	144	237	203
Sr	184	157	180	270	181	149	484	157	316
Y	23	48	30	44	19	29	17	48	35
Zr	293	309	194	368	151	309	283	450	376
Nb	21	25	18	26	17	20	16	32	24
Ba	697	668	559	893	435	862	538	669	744
La	30	65	52	22	31	34	29	44	73
Ce	79	87	88	66	63	79	82	90	75
Nd	37	38	44	36	22	36	36	53	42
Pb	21	7	21	3	15	21	10	19	7
Th	10	10	22	2	32	8	5	8	12
U	2	1	4	b.d.	7	1	4	1	3

b.d.= below detection limit

Whole-rock analyses of specimens from Gander zone of Newfoundland.

sample	snf-21	snf-22	snf-23	snf-24	snf-25	snf-3	snf-4	snf-5	snf-7	snf-8
SiO_2	76.55	49.42	75.98	72.16	71.31	72.35	60.35	49.00	74.24	66.88
TiO_2	0.11	0.79	0.15	0.30	0.45	0.34	0.92	1.45	0.16	0.71
Al_2O_3	12.25	17.99	12.07	13.34	13.33	13.58	17.97	11.17	13.64	15.10
Fe2O3	0.00	3.25	0.18	0.35	0.46	0.80	1.74	3.21	0.25	1.50
FeO	1.74	5.31	1.31	2.23	3.18	1.23	3.61	6.15	0.95	2.30
MnO	0.02	0.14	0.03	0.05	0.07	0.06	0.15	0.17	0.09	0.08
MgO	0.07	8.33	0.12	0.64	0.68	0.67	2.08	11.26	0.22	0.84
CaO	0.91	10.34	0.82	1.95	2.32	1.51	4.68	10.39	0.64	2.06
Na_2O	2.91	2.66	3.73	3.67	4.19	2.99	4.29	1.21	3.38	3.29
K_2O	4.96	0.42	3.75	3.65	2.55	5.06	2.24	2.99	4.54	5.60
P_2O_5	0.01	0.11	0.02	0.05	0.07	0.11	0.31	0.24	0.14	0.24
LOI	0.2	1.3	0.4	0.5	0.4	0.3	0.6	1.4	0.6	0.4
total	99.54	100.78	98.90	99.31	99.58	99.31	99.52	99.65	99.04	99.45
V	b.d.	122	8	27	29	27	107	280	11	48
Cr	18	256	5	13	35	8	39	622	2	23
Co	b.d.	45	b.d.	5	4	3	11	53	1	5
Ni	2	93	12	8	9	11	19	131	6	9
Zn	27	65	181	56	81	48	192	152	56	66
Rb	146	9	154	140	93	231	217	195	485	231
Sr	90	547	59	103	150	130	256	207	50	134
Y	36	11	39	54	51	25	48	16	23	39
Zr	113	43	158	176	412	176	336	103	76	352
Nb	8	1	11	14	23	18	37	9	25	24
Ba	609	129	434	354	717	370	488	1012	151	637
La	65	b.d.	22	37	49	19	42	30	23	54
Ce	126	29	52	77	60	55	76	33	65	143
Nd	49	11	22	35	34	30	41	26	22	53
Pb	b.d.	b.d.	87	3	5	28	8	b.d.	15	19
Th	20	3	16	20	7	25	8	10	17	6
U	4	b.d.	3	4	1	2	b.d.	b.d.	9	b.d.

b.d.= below detection limit

Whole-rock analyses from Gander zone of Newfoundland (supplied by A. Kerr).

sample	ak-89-087	ak-89-122	ak-91-414	ak-92-043	ak-92-054	ak-92-061	ak-92-087	ak-92-131
SiO_2	69.25	76.05	73.50	75.35	72.49	66.95	60.05	57.49
TiO_2	0.63	0.23	0.14	0.07	0.13	0.59	1.02	1.01
Al_2O_3	14.05	12.65	14.89	13.20	13.78	14.63	17.21	17.74
Fe_2O_3	0.88	0.68	0.11	0.31	0.11	0.60	1.74	0.93
FeO	2.69	0.91	0.90	0.17	0.99	3.53	3.89	4.66
MnO	0.09	0.03	0.05	0.02	0.02	0.09	0.12	0.13
MgO	0.91	0.29	0.21	0.19	0.23	1.36	2.21	2.53
CaO	2.01	2.26	0.68	0.78	0.47	2.21	4.21	2.46
Na_2O	3.22	4.55	3.63	2.82	2.80	3.32	3.31	2.70
K_2O	4.53	1.41	4.88	5.33	5.65	3.95	3.33	7.31
P_2O_5	0.20	0.04	0.31	0.13	0.38	0.53	0.32	0.72
LOI	0.7	0.8	0.8	0.5	0.9	1.0	1.3	1.3
total	99.16	99.88	100.07	98.86	97.90	98.79	98.74	98.99
Li	60	b.d.	118.2	6.5	26.6	188.5	191.1	126.4
Be	7.1	2.2	8.5	0.4	4.1	2.5	5.9	1.6
F	802	86	1088	33	463	953	1183	1166
V	55	b.d.	10	6	3	68	117	116
Cr	12	2	2	2	2	26	33	44
Ni	5	1	2	2	1	14	16	24
Cu	11	12	11	1	3	17	27	24
Zn	59	18	56	7	46	77	83	94
Ga	22	b.d.	24	11	22	23	27	26
Rb	259	27	325	120	282	211	184	278
Sr	129	b.d.	36	108	48	190	315	236
Y	34	b.d.	8	2	14	26	26	45
Zr	336	136	70	15	46	374	369	229
Nb	22	b.d.	13	1	22	18	19	11
Ba	693	b.d.	159	277	176	612	1324	1724
La	35	b.d.	18	5	11	53	37	28
Ce	80	b.d.	44	9	30	113	78	65
Pb	25	5	18	17	33	26	14	25
Th	15	b.d.	10	2	7	21	5	5
U	9.9	b.d.	6.2	0.3	3.8	4.3	2.8	2.9

b.d.= below detection limit

Whole-rock analyses from Gander zone of Newfoundland (supplied by A. Kerr).

sample	ak-92-133	ak-92-166	ak-92-168	ak-92-170	ak-92-243	ak-92-291	ak-92-292
SiO_2	60.14	75.19	64.80	62.64	65.77	68.46	73.15
TiO_2	1.22	0.08	0.69	1.00	1.05	0.67	0.40
Al_2O_3	15.36	13.14	15.95	14.88	14.68	14.77	13.40
Fe_2O_3	1.43	0.29	1.17	1.66	1.80	1.36	0.86
FeO	4.69	0.32	2.59	3.60	3.03	2.13	1.24
MnO	0.13	0.03	0.08	0.11	0.09	0.06	0.06
MgO	2.98	0.09	1.72	2.56	1.49	1.18	0.60
CaO	3.28	0.50	2.75	3.64	3.12	2.63	1.51
Na_2O	2.56	3.97	3.38	3.29	3.28	3.34	3.50
K_2O	4.31	4.24	4.21	3.59	3.46	4.27	4.24
P_2O_5	0.42	0.02	0.27	0.33	0.31	0.21	0.11
LOI	2.5	0.4	1.0	1.1	1.0	0.7	0.5
total	99.02	98.28	98.56	98.42	99.03	99.80	99.59
Li	116.7	59.4	50.9	64.6	26.7	22.6	51.4
Be	3.9	6.6	4.1	3.9	2.2	2.5	3.1
F	996	95	907	905	759	663	721
V	136	4	75	114	100	74	32
Cr	71	1	28	55	10	9	4
Ni	35	5	20	27	11	10	4
Cu	28	5	12	26	18	14	8
Zn	86	15	61	82	72	54	40
Ga	25	24	21	27	22	20	24
Rb	190	414	152	141	117	118	226
Sr	288	22	567	439	265	228	112
Y	38	22	26	30	63	28	46
Zr	405	58	268	287	438	300	174
Nb	19	51	16	22	22	9	21
Ba	1011	40	991	726	924	930	410
La	66	8	51	65	66	56	40
Ce	143	20	117	152	157	110	100
Pb	10	31	26	26	13	9	19
Th	18	27	13	21	20	13	26
U	3.3	15.3	3.1	4.6	3.3	1.8	4.3

b.d.= below detection limit

Whole-rock analyses of specimens from Meguma zone of Nova Scotia.

sample	nwad	pc2b	306-2	103b2	slp	br4	pr5b	eds
SiO_2	67.49	68.07	72.28	69.14	70.00	70.62	72.22	73.75
TiO_2	0.63	0.56	0.28	0.52	0.54	0.37	0.28	0.20
Al_2O_3	15.09	14.95	14.16	14.47	14.09	14.41	13.81	13.04
Fe_2O_3	4.47	4.18	2.02	3.77	4.03	2.65	2.26	2.26
MnO	0.09	0.08	0.05	0.07	0.08	0.07	0.04	0.08
MgO	1.21	1.09	0.45	1.02	0.86	0.66	0.57	0.34
CaO	2.25	1.85	0.81	1.97	1.38	0.73	0.63	0.71
Na_2O	3.14	3.17	3.09	3.11	3.04	3.02	3.00	3.03
K_2O	3.79	4.16	4.88	3.94	4.09	5.26	4.30	4.13
P_2O_5	0.21	0.21	0.26	0.19	0.22	0.25	0.30	0.17
total	98.52	98.48	98.38	98.38	98.48	98.18	97.52	97.80
V	49	44	13	39	38	25	17	15
Cr	32	24	10	25	22	19	15	16
Co	7	7	b.d.	5	7	3	2	1
Ni	7	5	b.d.	5	6	2	2	1
Zn	64	98	35	60	70	45	107	72
Rb	167	184	269	173	173	248	321	292
Sr	175	158	90	157	127	116	68	35
Y	36	32	17	37	34	19	17	26
Zr	216	216	122	209	206	127	109	93
Nb	14	14	13	14	14	12	14	10
Ba	586	552	428	610	522	619	299	89
La	40	34	23	40	42	24	25	10
Ce	75	92	44	73	80	41	56	47
Nd	31	42	19	32	34	20	23	20
Pb	9	30	13	8	10	11	14	16
Th	10	11	12	11	9	10	13	7
U	4	2	8	7	3	4	10	6
Ga	20	21	20	20	21	19	21	21

b.d.= below detection limit

Appendix IV of Manuscript 1

Mössbauer Spectra of Biotite

Following are folded RT Mössbauer spectra of biotite collected during this study.

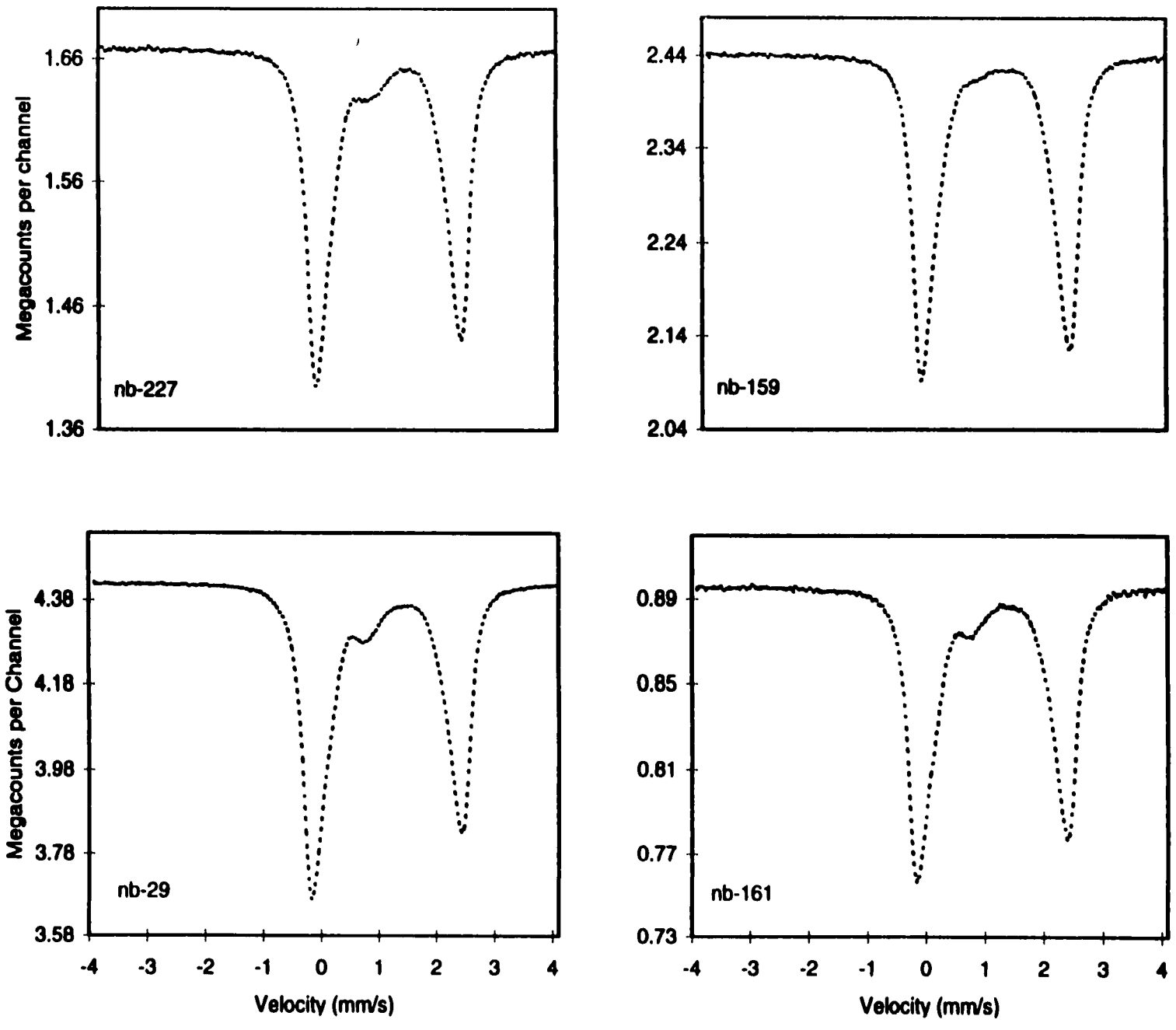
Megacounts per channel
1.66
1.56
1.46
1.36
nb-227
2.44
2.34
2.24
2.14
2.04
nb-159
Megacounts per Channel
4.38
4.18
3.98
3.78
3.58
nb-29
0.89
0.85
0.81
0.77
0.73
nb-161
-4
-3
-2
-1
0
1
2
3
4
Velocity (mm/s)
Velocity (mm/s)

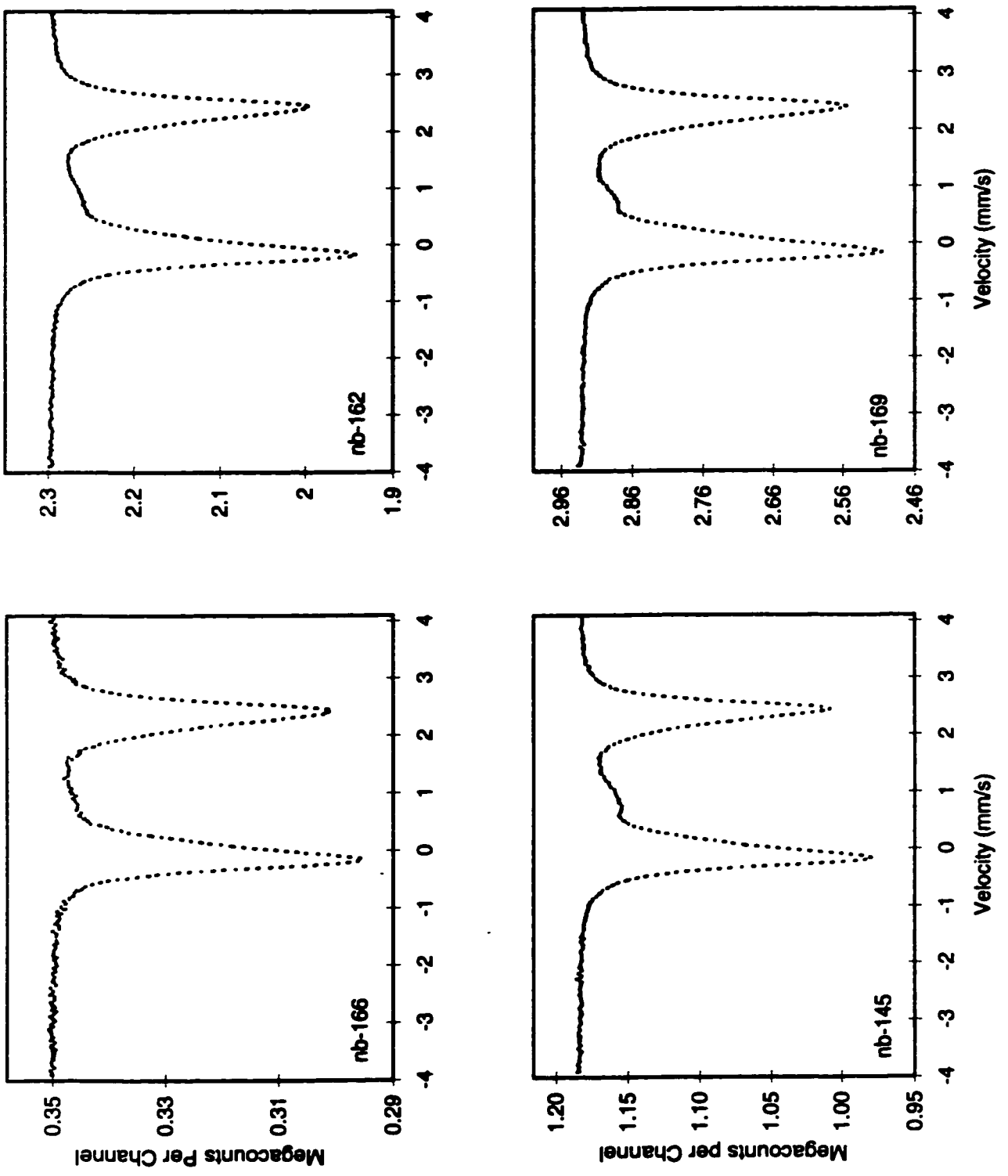
nb-166
nb-162
nb-145
nb-169
Megacounts Per Channel
Megacounts per Channel
Velocity (mm/s)
Velocity (mm/s)

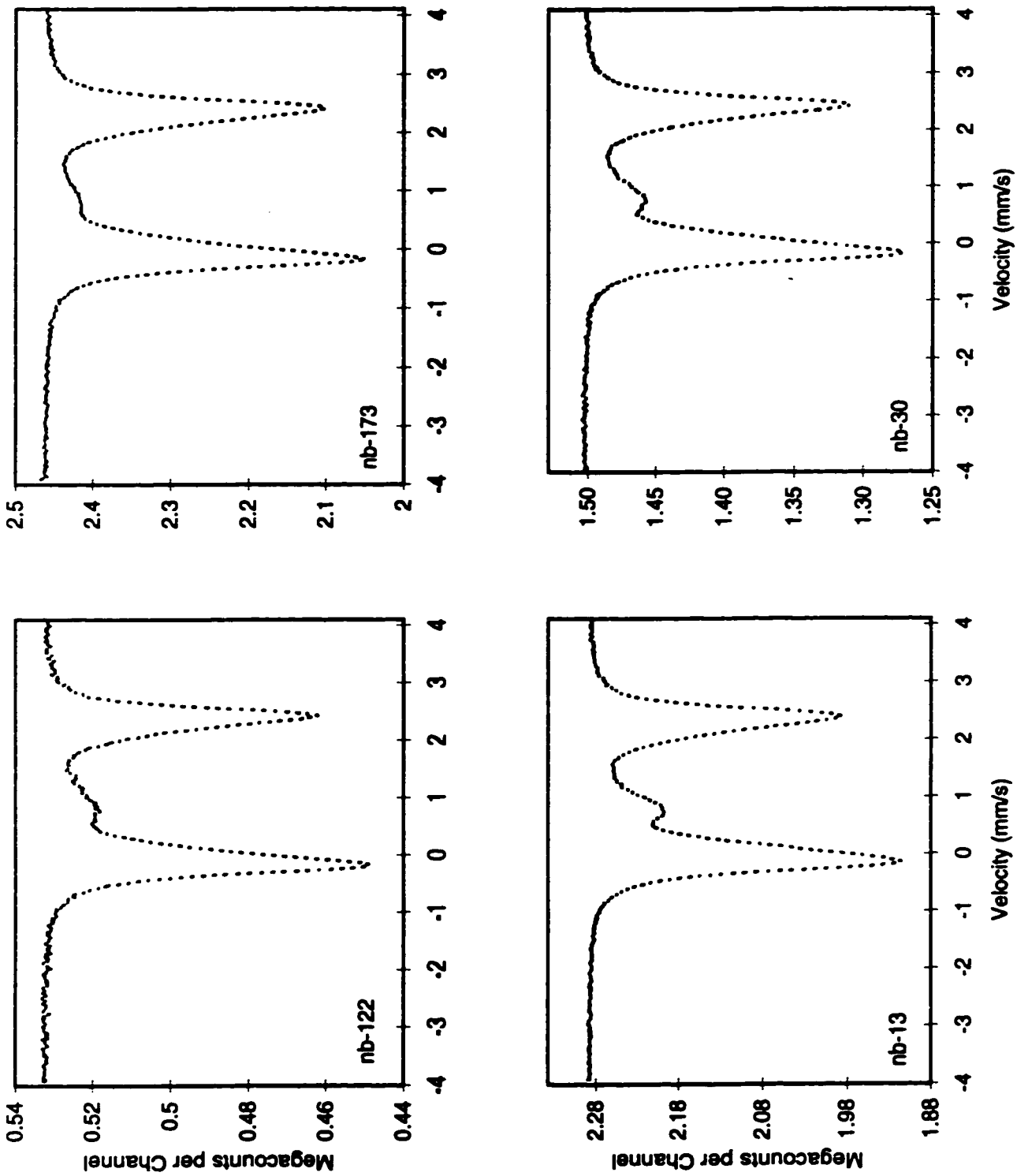
nb-173
nb-30
nb-122
nb-13
Megacounts per Channel
Velocity (mm/s)

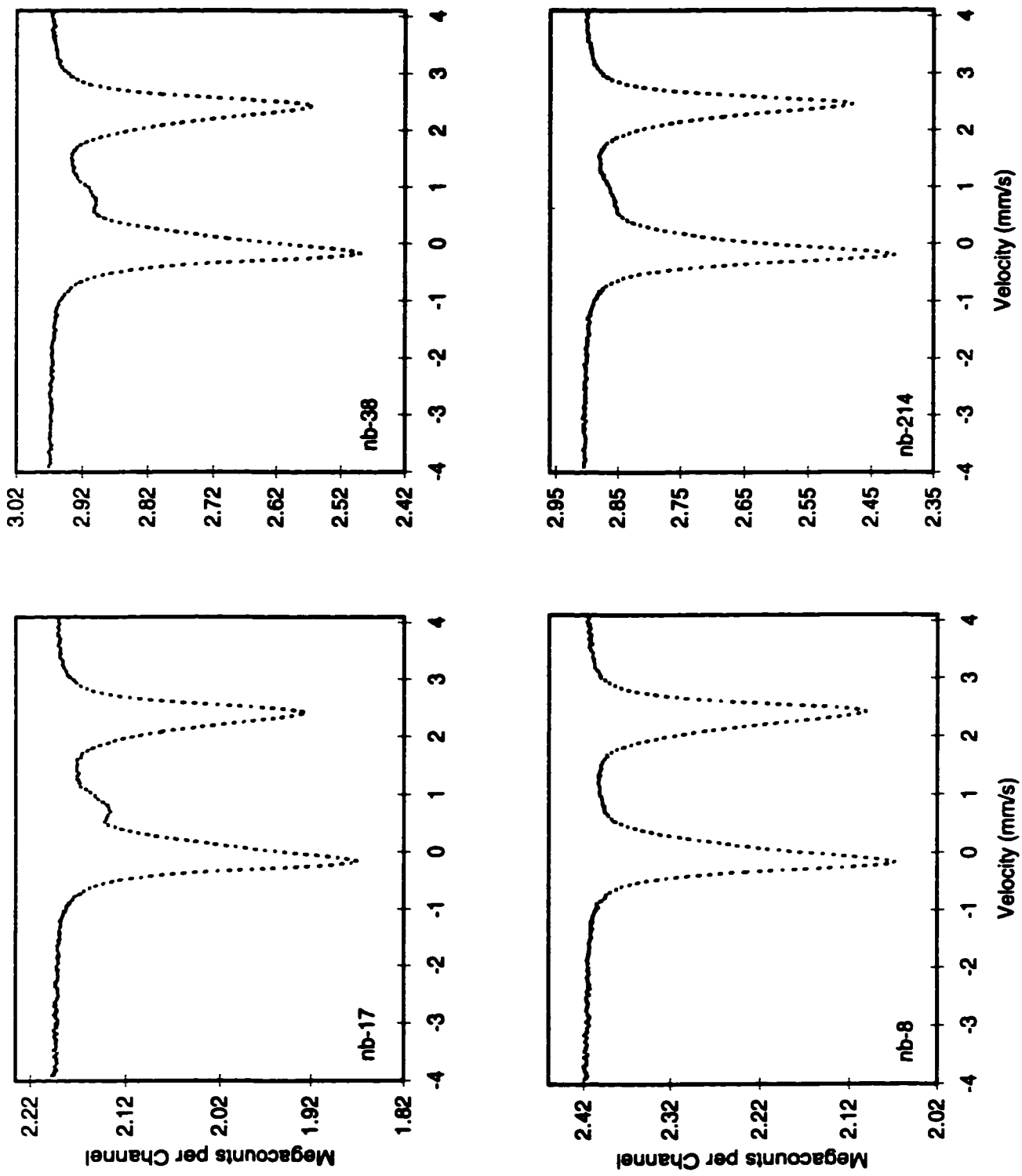
nb-38
nb-214
nb-17
nb-8
Megacounts per Channel
Velocity (mm/s)

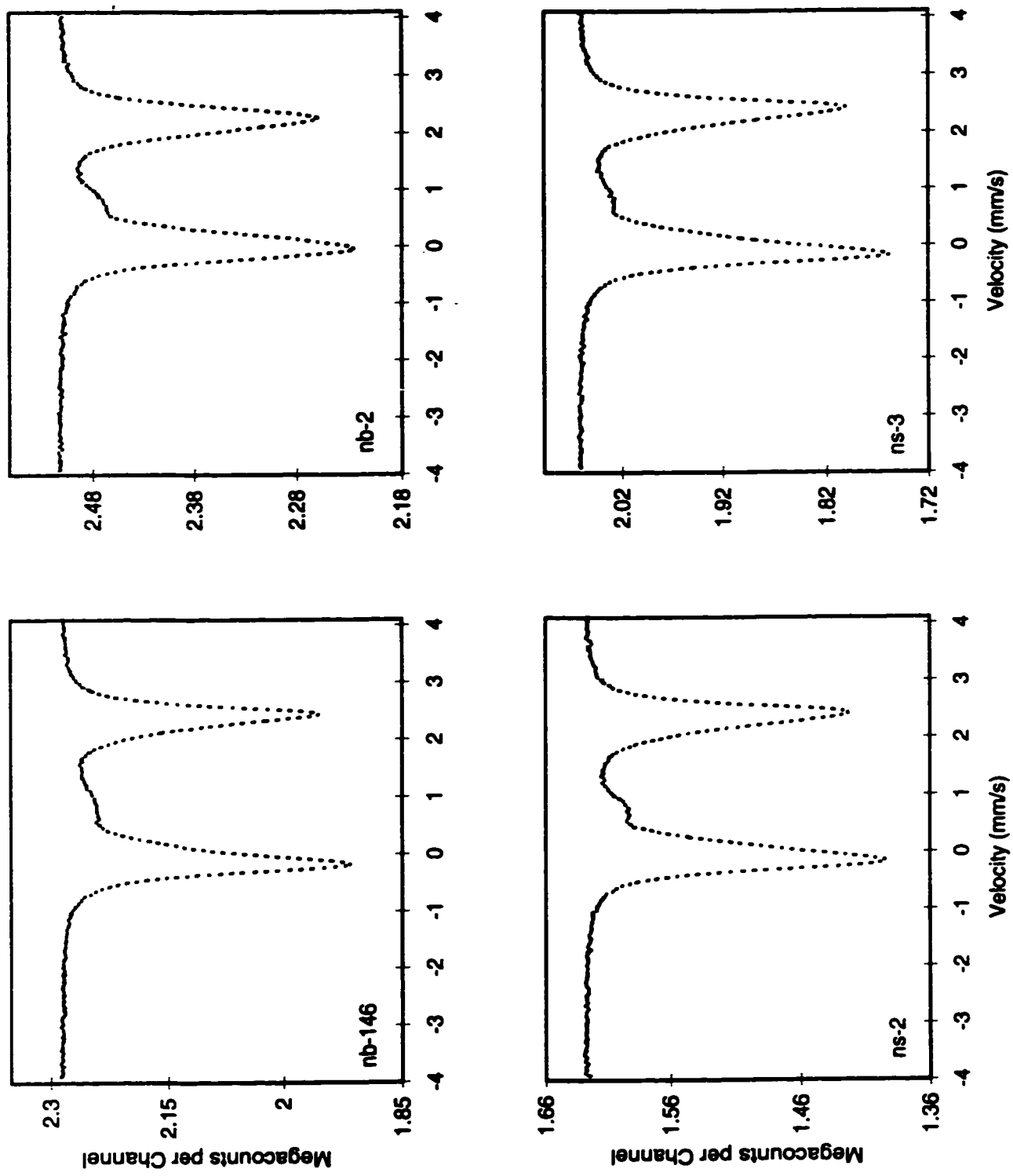
nb-2
2.48
2.38
2.28
2.18
nb-146
2.3
2.15
2
1.85
ns-3
2.02
1.92
1.82
1.72
ns-2
1.66
1.56
1.46
1.36
-4
-3
-2
-1
0
1
2
3
4
Velocity (mm/s)
Megacounts per Channel

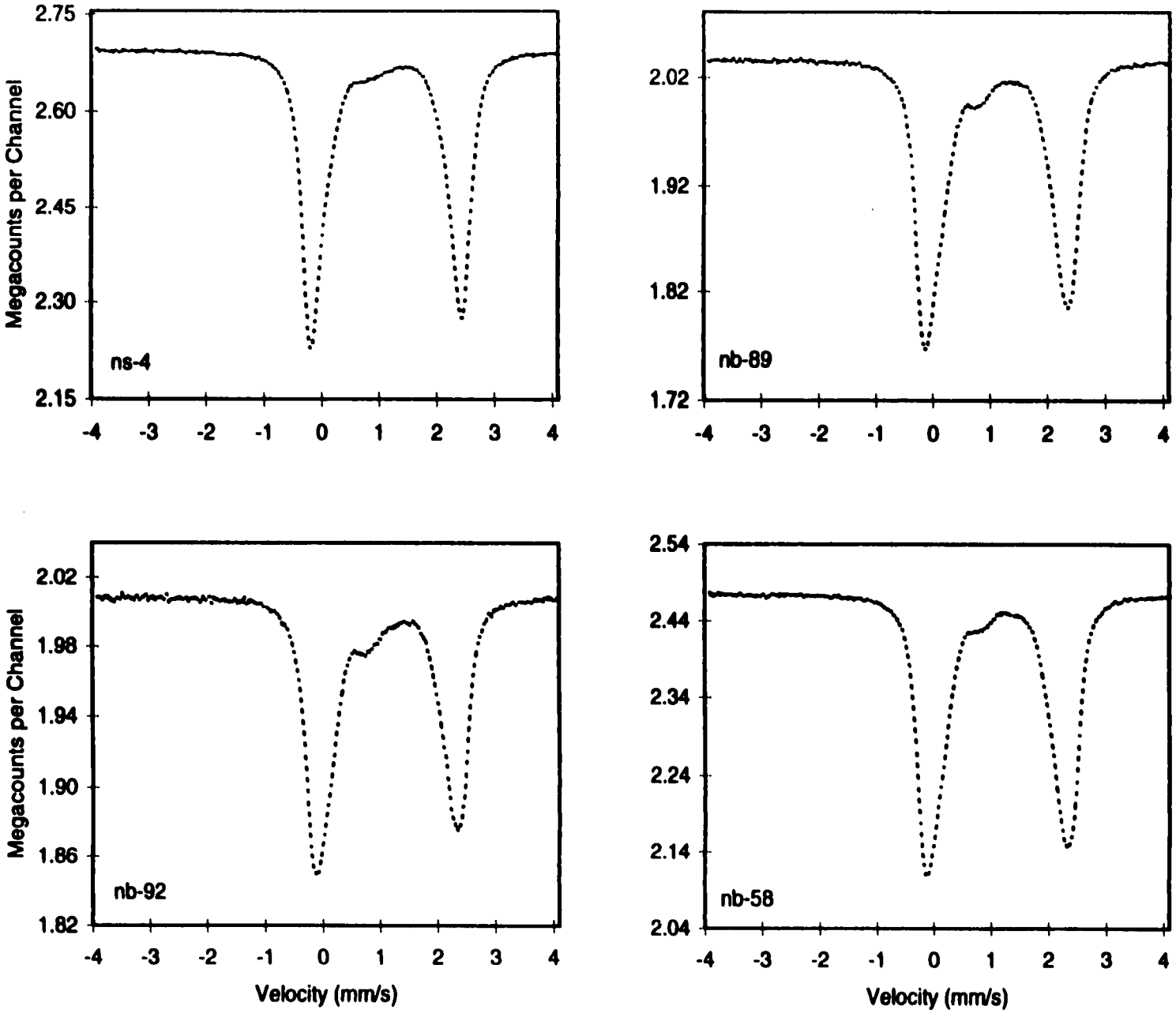
Megacounts per Channel
2.75
2.60
2.45
2.30
2.15
ns-4
-4 -3 -2 -1 0 1 2 3 4
2.02
1.92
1.82
1.72
nb-89
-4 -3 -2 -1 0 1 2 3 4
Megacounts per Channel
2.02
1.98
1.94
1.90
1.86
1.82
nb-92
-4 -3 -2 -1 0 1 2 3 4
Velocity (mm/s)
2.54
2.44
2.34
2.24
2.14
2.04
nb-58
-4 -3 -2 -1 0 1 2 3 4
Velocity (mm/s)

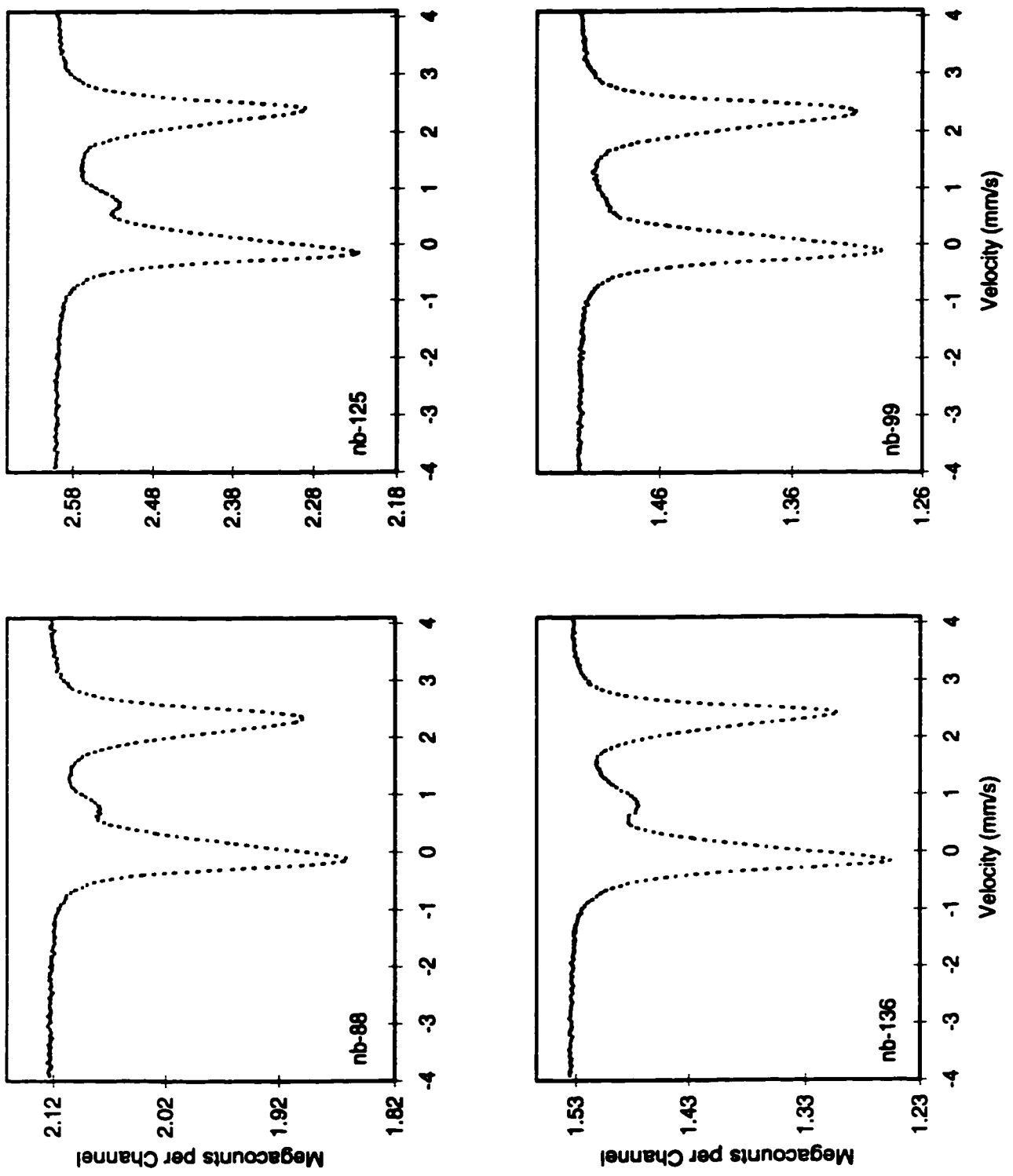
nb-88
nb-125
nb-136
nb-99
Megacounts per Channel
Velocity (mm/s)
2.12
2.02
1.92
1.82
2.58
2.48
2.38
2.28
2.18
1.53
1.43
1.33
1.23
1.46
1.36
1.26
-4
-3
-2
-1
0
1
2
3
4

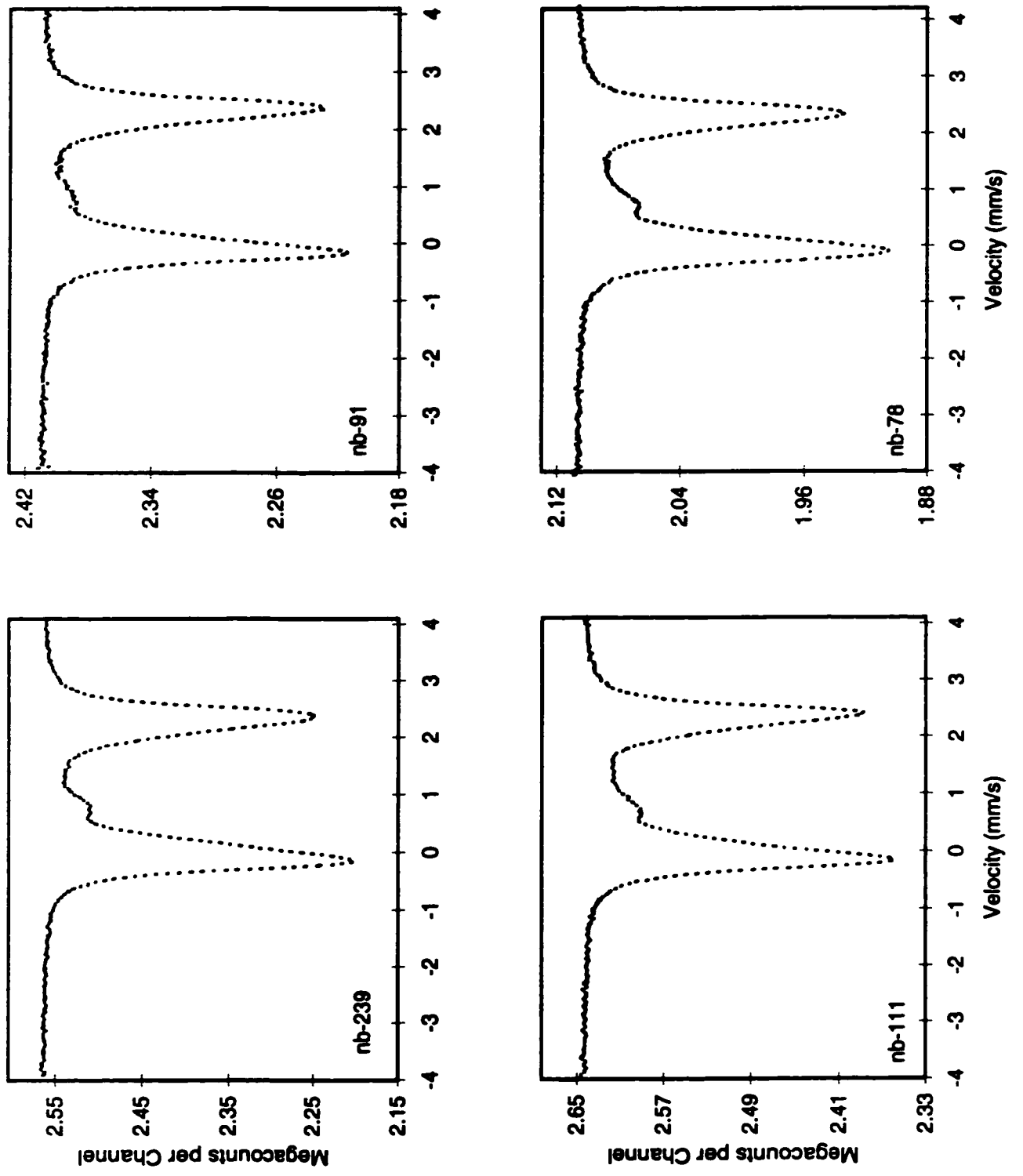
nb-91
nb-78
nb-239
nb-111
Megacounts per Channel
Velocity (mm/s)
2.42
2.34
2.26
2.18
2.12
2.04
1.96
1.88
2.55
2.45
2.35
2.25
2.15
2.65
2.57
2.49
2.41
2.33
-4
-3
-2
-1
0
1
2
3
4

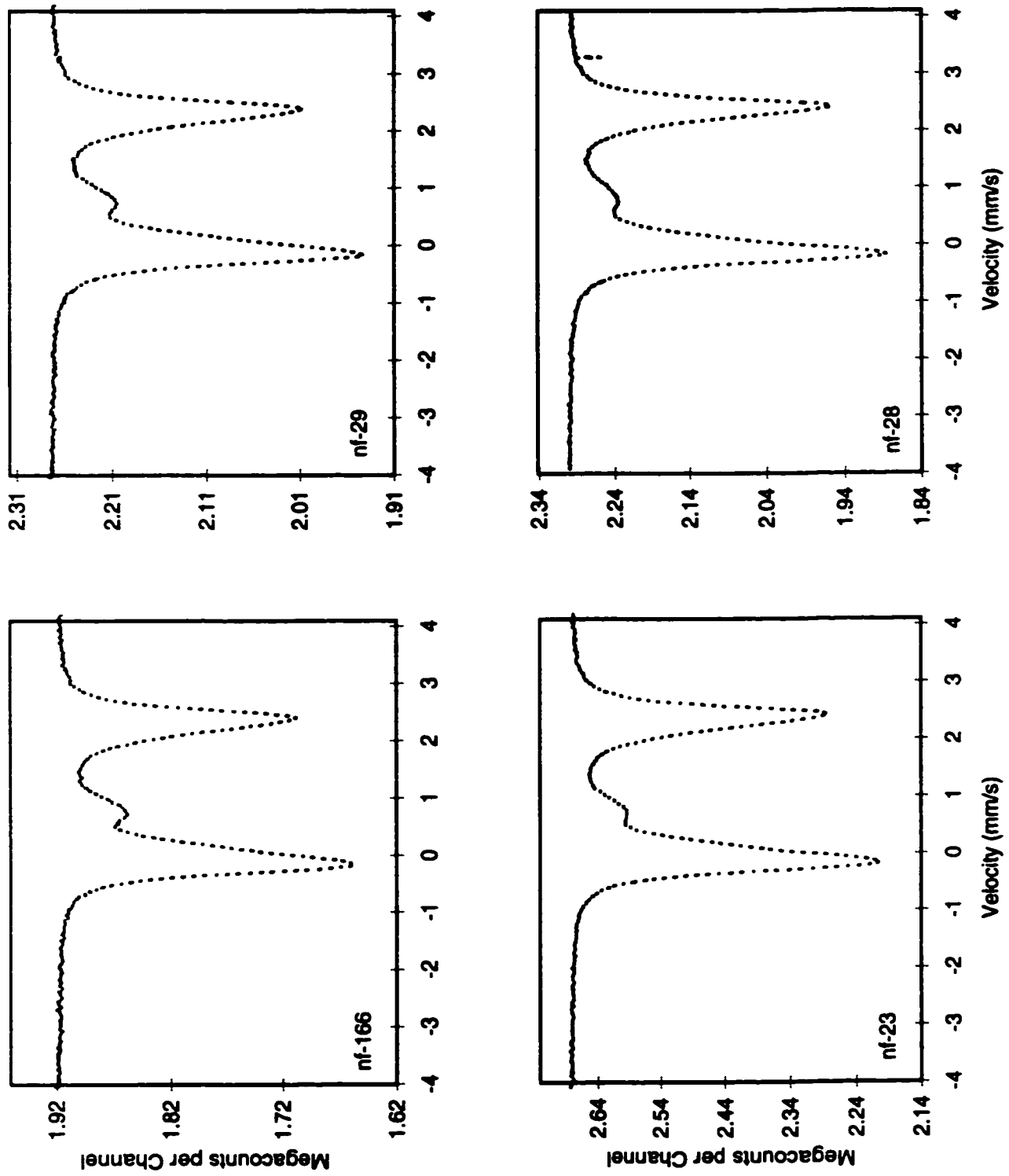
nf-29
nf-28
nf-166
nf-23
Megacounts per Channel
Velocity (mm/s)
2.31
2.21
2.11
2.01
1.91
2.34
2.24
2.14
2.04
1.94
1.84
1.92
1.82
1.72
1.62
2.64
2.54
2.44
2.34
2.24
2.14
-4
-3
-2
-1
0
1
2
3
4

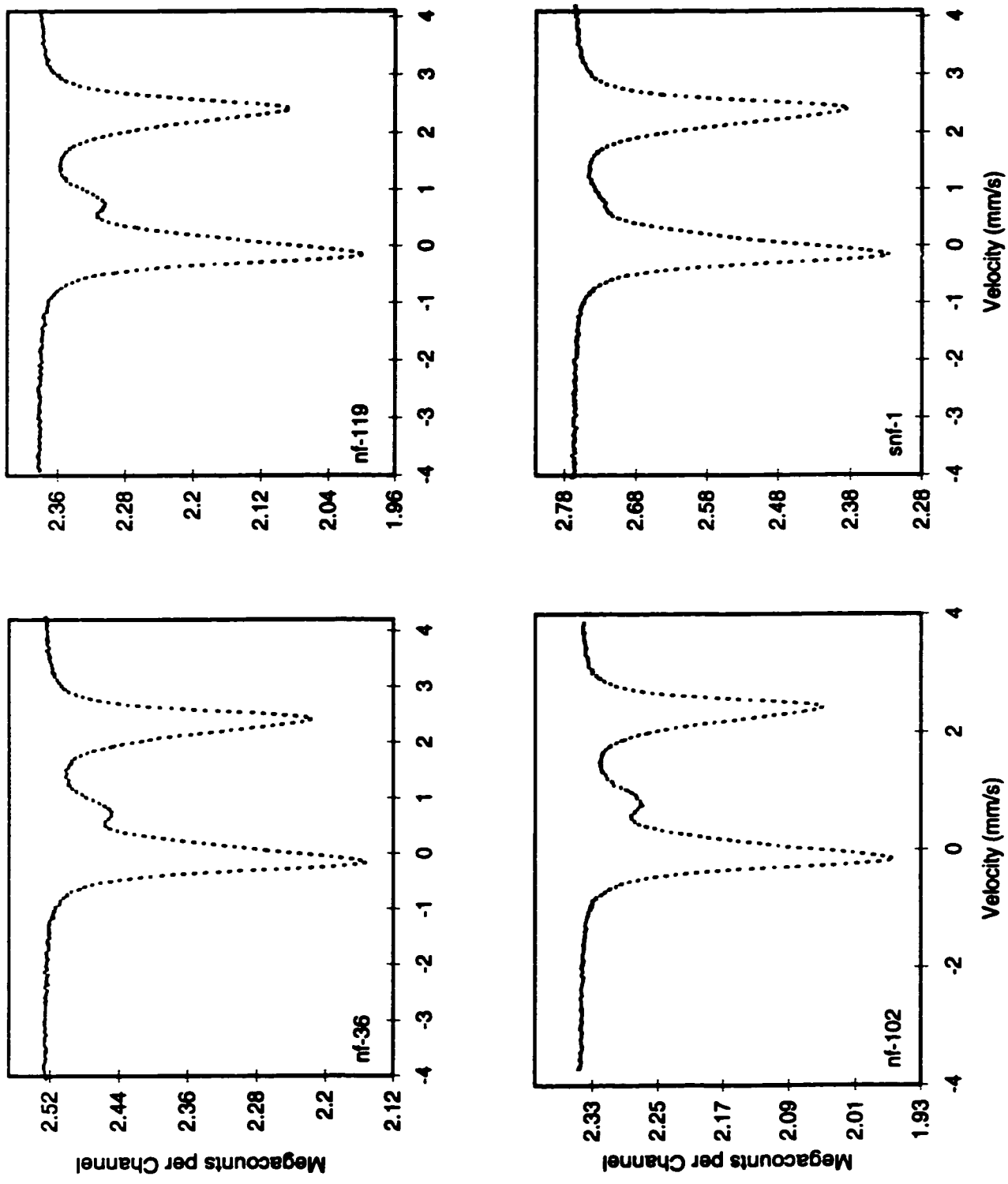
nf-119
snf-1
nf-36
nf-102
Megacounts per Channel
Velocity (mm/s)

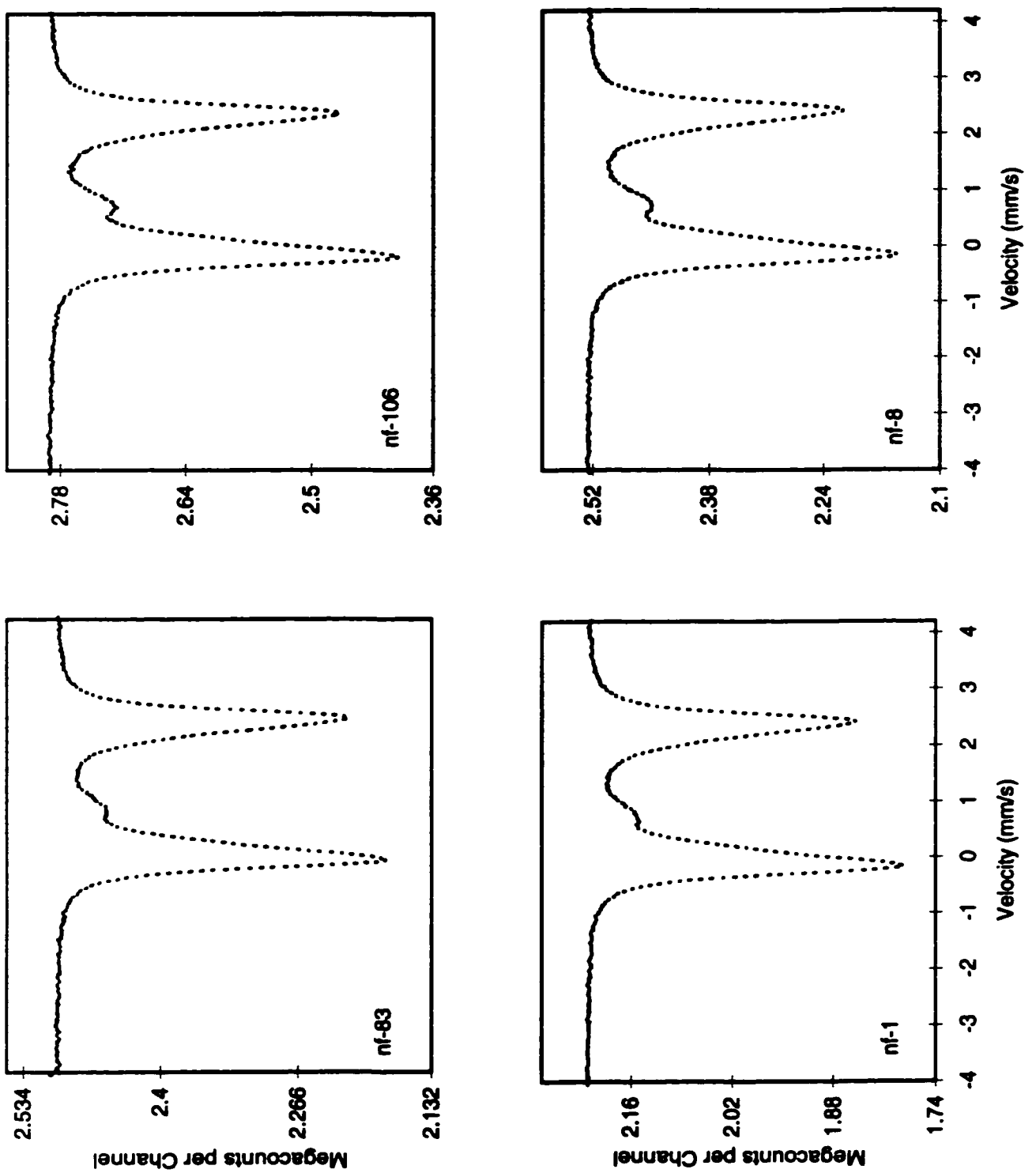
nf-106
nf-8
nf-83
nf-1
Megacounts per Channel
Velocity (mm/s)
2.78
2.64
2.5
2.36
2.52
2.38
2.24
2.1
2.534
2.4
2.266
2.132
2.16
2.02
1.88
1.74
-4
-3
-2
-1
0
1
2
3
4

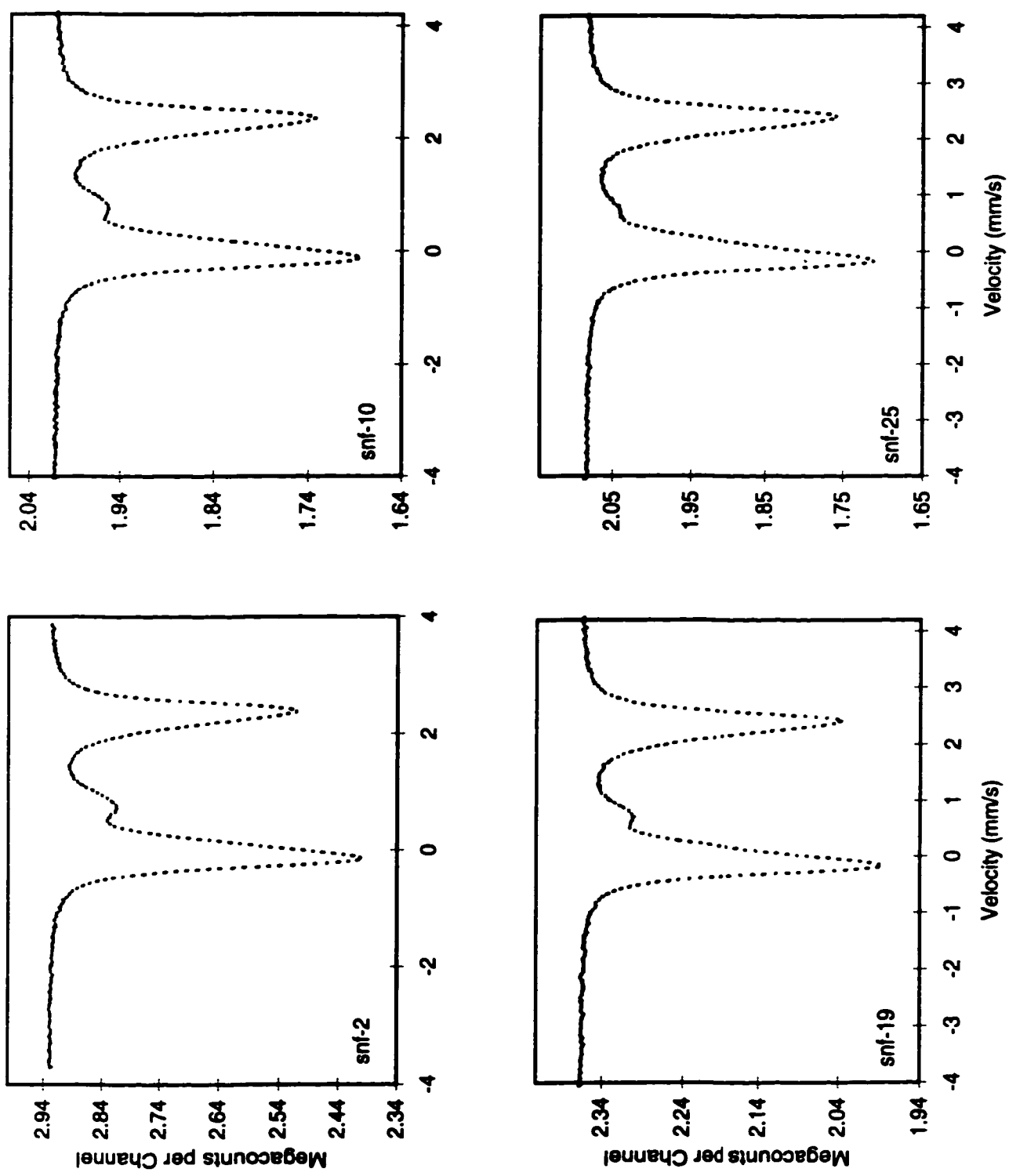
snf-10
snf-25
snf-2
snf-19
Megacounts per Channel
Velocity (mm/s)

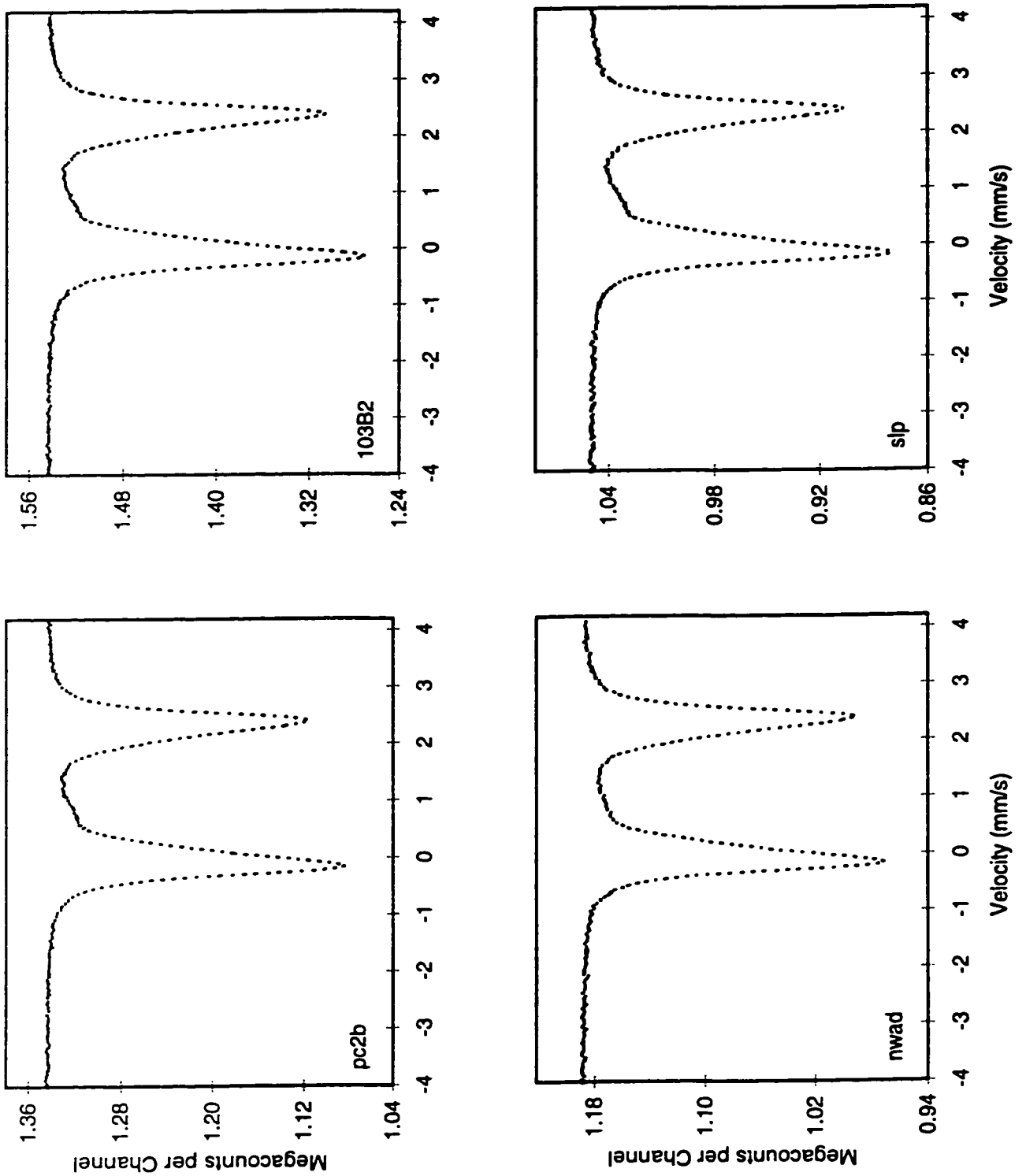
103B2
slp
pc2b
nwad
Megacounts per Channel
Velocity (mm/s)

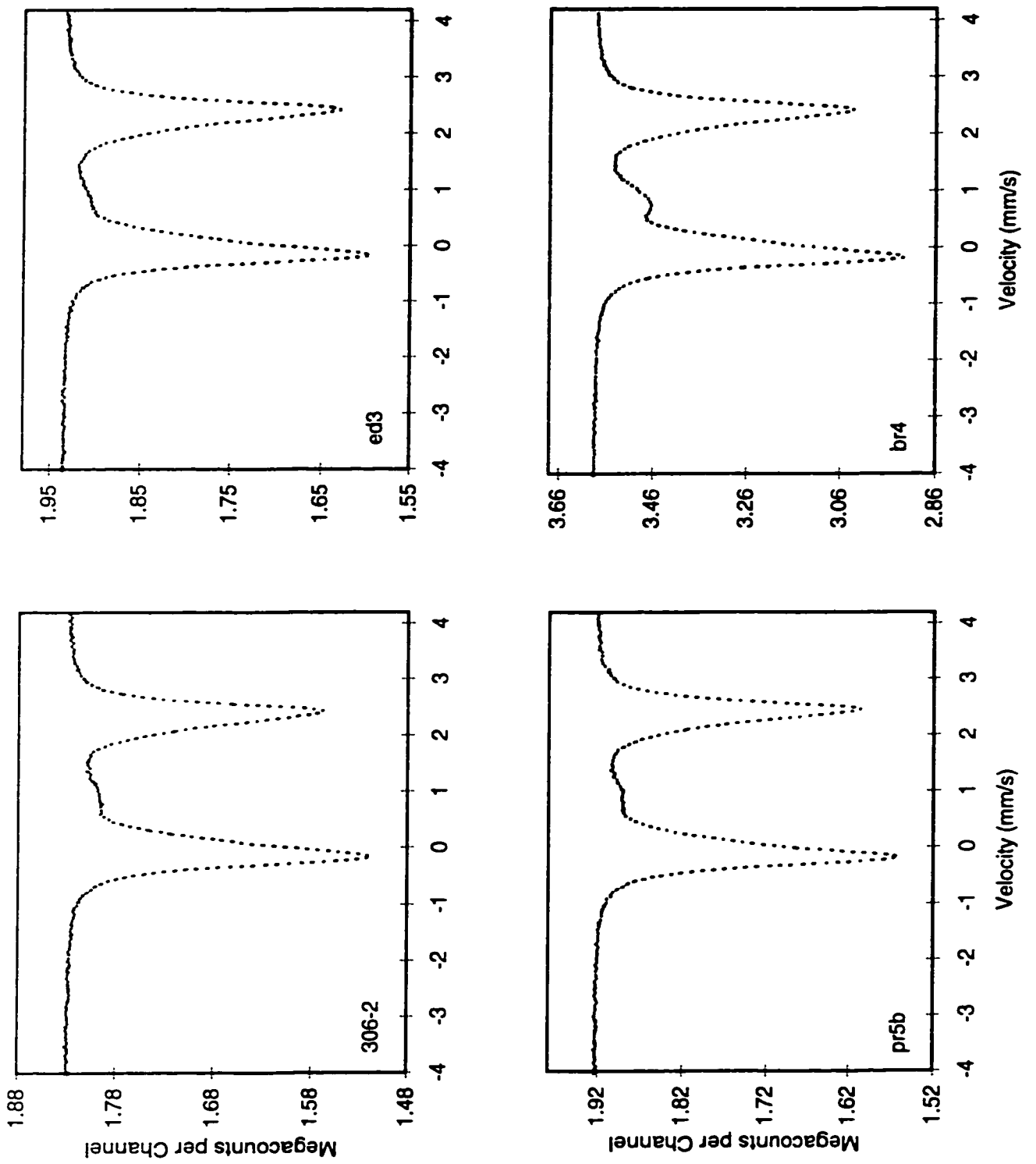
Megacounts per Channel
1.88
1.78
1.68
1.58
1.48
306-2
-4 -3 -2 -1 0 1 2 3 4
1.95
1.85
1.75
1.65
1.55
ed3
3.66
3.46
3.26
3.06
2.86
br4
1.92
1.82
1.72
1.62
1.52
pr5b
Velocity (mm/s)

Appendix V of Manuscript 1

Mössbauer Fitting Parameters for Biotite Spectra

Tabulated below are the Mössbauer fitting parameters for biotite spectra performed during this study.

Mössbauer spectrum fitting parameters for Appalachian biotites

sample	fit	BG	δ_o[3']	δ_o[2']	δ_i[2']	Δ_{Q1}[3']	$\sigma_{\Delta1}$[3']	Δ_{Q2}[3']	$\sigma_{\Delta2}$[3']	Δ_{Q1}[2']	$\sigma_{\Delta1}$[2']	Δ_{Q2}[2']	$\sigma_{\Delta2}$[2']	Δ_{Q3}[2']	$\sigma_{\Delta3}$[2']
103b2	1-3	1544.1	0.244	1.041	0.031	0.810*	0.818			2.652	0.075	2.461	0.260	1.827	0.211
306-2	2-3	1829.6	0.365	1.024	0.039	1.430	0.539	0.600*	0.720	2.660	0.085	2.475	0.278	1.811	0.185
br4	2-3	3582.7	0.389	1.078	0.017	1.463	0.616	0.756	0.385	2.642	0.107	2.449	0.319	1.738	0.202
ed3	1-3	1934.8	0.359	1.065	0.022	0.878	0.774			2.649	0.101	2.480	0.301	1.783	0.205
nb-111	2-3	2641.5	0.504	1.055	0.023	0.955	0.769	0.477	0.167	2.325	0.343	2.605	0.135	1.800*	1.053
nb-122	1-3	532.5	0.389	1.051	0.028	1.034	0.642			2.503	0.162	2.332	0.412	2.681	0.108
nb-125	2-3	2601.2	0.466	1.005	0.044	1.100*	0.765	0.575	0.238	2.265	0.416	2.504	0.209	2.669	0.070
nb-13	2-3	2288.7	0.439	1.047	0.027	1.470	0.624	0.679	0.338	2.295	0.422	2.642	0.101	2.385	0.103
nb-136	2-3	1535.2	0.376	1.138	-0.006	1.102	0.649	0.911	0.301	2.326	0.361	1.955	0.955	2.627	0.131
nb-159	1-3	2441.4	0.370	1.073	0.021	0.768	0.839			2.340	0.409	2.671	0.110	2.390	0.069
nb-161	2-3	893.4	0.453	1.016	0.040	0.648	0.175	0.810*	0.784	2.673	0.090	2.452	0.146	2.318	0.426
nb-162	1-3	2297.6	0.339	1.034	0.036	0.919	0.775			1.880	0.216	2.689	0.071	2.528	0.269
nb-166	1-3	346.1	0.342	1.070	0.023	0.833	0.876			2.670	0.072	2.509	0.281	1.842	0.210
nb-169	2-3	2931.3	0.457	1.040	0.030	0.804	0.898	0.600*	0.184	2.641	0.073	1.768	0.206	2.452	0.285
nb-17	2-3	2198.3	0.436	1.004	0.045	1.617	0.492	0.625	0.337	2.322	0.416	2.551	0.180	2.686	0.061
nb-173	2-3	2461.3	0.355	1.061	0.024	1.257	0.585	0.700*	0.805	2.609	0.183	1.936	0.254	2.210	0.103
nb-227	2-3	1668.1	0.406	1.062	0.018	1.297	0.594	0.695	0.358	2.649	0.107	2.347	0.424	2.378	0.066
nb-29	2-3	1978.5	0.398	0.995	0.045	0.617	0.315	1.100*	0.684	2.431	0.123	2.300	0.410	2.655	0.091
nb-30	2-3	1503.0	0.431	1.059	0.026	1.452	0.598	0.673	0.342	2.341	0.427	2.699	0.044	2.607	0.179
nb-38	2-3	2969.1	0.422	1.043	0.031	1.000	0.745	0.717	0.296	2.657	0.114	2.340	0.422	2.357	0.053
nb-8	1-3	2417.1	0.252	1.056	0.025	0.600	0.981			2.656	0.081	1.814	0.214	2.488	0.284
nb-91	1-3	2408.8	0.525	1.066	0.016	0.679	0.443			2.442	0.284	1.758	0.171	2.636	0.080
nf-1	2-3	2218.6	0.429	1.028	0.035	1.400*	0.641	0.584	0.349	2.231	0.376	2.647	0.802	2.615	0.166
nf-102	2-3	2349.6	0.369	1.053	0.030	0.842	0.861	0.965	0.323	2.496	0.242	1.932	0.226	2.686	0.078
nf-106	2-3	2792.2	0.432	1.013	0.040	0.633	0.333	1.400*	0.655	2.477	0.279	1.781	0.219	2.672	0.085
nf-119	2-3	2383.0	0.448	0.939	0.072	1.172	0.553	0.587	0.287	2.354	0.307	2.320	0.482	2.622	0.165
nf-166	2-3	1918.8	0.447	0.991	0.047	0.636	0.322	1.473	0.511	2.444	0.166	2.298	0.427	2.675	0.096
nf-23	2-3	2682.4	0.428	1.012	0.042	0.591	0.325	1.400*	0.565	2.441	0.133	2.320	0.428	2.693	0.097
nf-28	2-3	2301.0	0.439	1.072	0.018	1.456	0.661	0.705	0.374	2.353	0.404	2.326	0.041	2.641	0.123
nf-29	2-3	2276.0	0.430	1.013	0.037	0.656	0.353	1.407	0.580	2.317	0.080	2.303	0.409	2.625	0.115
nf-36	2-3	2526.2	0.449	1.019	0.039	1.458	0.576	0.615	0.322	2.322	0.420	2.436	0.145	2.687	0.103
nf-8	1-3	2201.2	0.294	1.049	0.028	0.586	1.001			2.680	0.084	2.460	0.279	1.813	0.195
nf-83	2-3	2500.9	0.468	1.041	0.030	0.583	0.261	1.100*	0.759	2.356	0.107	2.292	0.417	2.652	0.109
ns-3	1-3	2062.6	0.383	1.048	0.029	0.944	0.755			2.661	0.080	2.475	0.289	1.798	0.195
ns-4	1-3	2693.9	0.389	1.068	0.021	0.943	0.723			2.671	0.098	2.528	0.302	1.800*	0.194

continued

sample	a_1 [3']	a_2 [3']	a_1 [2']	a_2 [2']	a_3 [2']	χ^2_{red}	$Fe^{2+}QS_{avg}$	$Fe^{3+}QS_{avg}$	$Fe^{3+}CS_{avg}$	$Fe^{2+}CS_{avg}$	Fe^{3+}/Fe	Fe^{2+}/Fe
103b2	0.105		0.128	0.629	0.138	4.014	2.390	0.810	0.244	1.115	0.105	0.895
306-2	0.063	0.087	0.167	0.590	0.092	3.810	2.440	0.949	0.365	1.118	0.151	0.849
br4	0.063	0.133	0.226	0.519	0.059	2.832	2.452	0.984	0.389	1.119	0.196	0.804
ed3	0.096		0.207	0.612	0.085	2.074	2.453	0.878	0.359	1.119	0.096	0.904
nb-111	0.094	0.037	0.470	0.303	0.096	1.602	2.364	0.821	0.504	1.109	0.131	0.869
nb-122	0.206		0.155	0.398	0.241	1.260	2.471	1.034	0.389	1.120	0.206	0.795
nb-125	0.107	0.090	0.387	0.299	0.117	1.550	2.413	0.861	0.466	1.111	0.199	0.801
nb-13	0.065	0.172	0.445	0.226	0.092	1.296	2.408	0.896	0.439	1.113	0.237	0.763
nb-136	0.148	0.068	0.413	0.081	0.291	1.744	2.399	1.042	0.376	1.124	0.216	0.785
nb-159	0.074		0.533	0.314	0.079	1.736	2.457	0.768	0.370	1.125	0.074	0.926
nb-161	0.049	0.114	0.204	0.180	0.453	1.456	2.433	0.761	0.453	1.113	0.164	0.837
nb-162	0.139		0.102	0.141	0.618	2.486	2.478	0.919	0.339	1.124	0.139	0.861
nb-166	0.083		0.119	0.682	0.116	0.946	2.445	0.833	0.342	1.125	0.083	0.917
nb-169	0.090	0.024	0.154	0.093	0.639	2.104	2.413	0.760	0.457	1.112	0.114	0.886
nb-17	0.051	0.135	0.419	0.281	0.114	2.062	2.452	0.898	0.436	1.114	0.186	0.814
nb-173	0.058	0.072	0.614	0.172	0.083	3.624	2.437	0.949	0.355	1.120	0.130	0.870
nb-227	0.066	0.095	0.280	0.494	0.066	1.300	2.450	0.941	0.406	1.107	0.160	0.840
nb-29	0.088	0.131	0.133	0.421	0.227	4.666	2.425	0.906	0.398	1.105	0.219	0.781
nb-30	0.087	0.129	0.401	0.066	0.317	1.020	2.479	0.988	0.431	1.124	0.216	0.784
nb-38	0.122	0.039	0.313	0.475	0.051	2.414	2.459	0.932	0.422	1.120	0.161	0.840
nb-8	0.062		0.171	0.109	0.658	2.104	2.440	0.600*	0.252	1.118	0.621	0.938
nb-91	0.079		0.705	0.064	0.152	1.538	2.427	0.679	0.525	1.106	0.079	0.921
nf-1	0.051	0.102	0.412	0.020	0.415	6.248	2.429	0.858	0.429	1.114	0.153	0.847
nf-102	0.146	0.089	0.498	0.125	0.141	5.832	2.439	0.889	0.369	1.126	0.236	0.764
nf-106	0.133	0.054	0.586	0.080	0.148	2.558	2.444	0.854	0.432	1.111	0.187	0.813
nf-119	0.071	0.131	0.194	0.279	0.325	6.036	2.451	0.793	0.448	1.116	0.202	0.798
nf-166	0.168	0.051	0.185	0.410	0.185	1.496	2.422	0.832	0.447	1.105	0.220	0.781
nf-23	0.128	0.052	0.145	0.447	0.228	4.790	2.445	0.826	0.428	1.116	0.181	0.820
nf-28	0.059	0.123	0.396	0.055	0.368	3.434	2.481	0.948	0.439	1.118	0.177	0.823
nf-29	0.152	0.062	0.068	0.436	0.282	1.580	2.420	0.872	0.430	1.103	0.214	0.786
nf-36	0.051	0.143	0.440	0.145	0.222	1.304	2.443	0.835	0.449	1.115	0.193	0.807
nf-8	0.103		0.148	0.648	0.101	2.574	2.423	0.586	0.294	1.117	0.103	0.897
nf-83	0.069	0.070	0.118	0.448	0.295	1.290	2.424	0.844	0.468	1.114	0.139	0.861
ns-3	0.133		0.161	0.612	0.094	2.244	2.436	0.944	0.383	1.118	0.133	0.867
ns-4	0.115		0.213	0.611	0.060	1.732	2.513	0.943	0.389	1.122	0.115	0.885

Mössbauer spectrum fitting parameters for Appalachian biotites

sample	fit	BG	δ_0[3']	δ_0[2']	δ_1[2']	Δ_{Q1}[3']	$\sigma_{\Delta1}$[3']	Δ_{Q2}[3']	$\sigma_{\Delta2}$[3']	Δ_{Q1}[2']	$\sigma_{\Delta1}$[2']	Δ_{Q2}[2']	$\sigma_{\Delta2}$[2']	Δ_{Q1}[2']	$\sigma_{\Delta1}$[2']
nwad	1-3	1187.6	0.316	1.067	0.020	0.724	0.964			2.645	0.076	2.444	0.281	1.786	0.195
pc2b	1-3	1343.6	0.274	1.051	0.027	0.640	0.967			2.652	0.075	2.467	0.266	1.831	0.201
pr5b	1-3	1923.7	0.392	1.045	0.031	1.040	0.711			2.674	0.115	2.408	0.424	2.394	0.000
slp	1-3	1049.7	0.247	1.003	0.045	0.556	0.926	0.450*	1.000	2.599	0.414	2.607	0.165	2.204	0.344
snf-1	1-3	2767.3	0.269	1.043	0.030	0.593	0.927			2.717	0.068	2.537	0.162	2.301	0.385
snf-19	2-3	2365.7	0.438	1.022	0.037	0.577	0.283	1.591	0.489	2.450	0.149	2.318	0.417	2.691	0.092
snf-2	2-3	2929.9	0.419	0.997	0.044	1.418	0.559	0.651	0.328	2.456	0.247	1.879	0.254	2.646	0.099
snf-25	1-3	2082.0	0.299	1.054	0.026	0.545	0.924			2.694	0.077	1.812	0.192	2.454	0.275
nb-214	1-3	2905.1	0.321	1.025	0.039	0.943	0.745			2.682	0.063	2.607	0.252	1.949	0.243
nb-145	2-3	1187.9	0.415	1.053	0.029	1.388	0.646	0.650	0.410	2.650	0.079	1.819	0.226	2.500	0.284
nb-146	2-3	2285.4	0.402	1.090	0.014	0.842	0.319	1.100*	0.736	2.588	0.187	2.342	0.429	2.678	0.062
nb-92	2-3	2008.8	0.474	1.033	0.031	1.100*	0.755	0.559	0.249	2.176	0.346	2.276	0.799	2.549	0.195
nb-78	1-3	2106.7	0.386	1.094	0.012	0.879	0.616			2.556	0.186	2.196	0.291	1.800*	0.827
nb-88	2-3	2123.6	0.508	1.016	0.038	0.531	0.210	0.950*	0.850	2.478	0.248	1.986	0.326	2.660	0.044
nb-58	2-3	2474.7	0.538	1.053	0.024	0.574	0.149	0.800	0.856	2.691	0.063	2.213	0.397	2.451	0.167
nb-89	2-3	2036.6	0.492	1.033	0.033	0.771	0.899	0.601	0.137	2.472	0.255	1.917	0.288	2.677	0.033
snf-10	2-3	2011.9	0.476	1.030	0.032	1.400	0.643	0.583	0.297	2.433	0.255	1.859	0.254	2.657	0.067
nb-239	2-3	2559.6	0.518	1.032	0.032	0.577	0.161	0.810*	0.918	2.685	0.071	2.252	0.403	2.449	0.166
nb-99	1-3	1522.4	0.497	1.069	0.017	0.550	0.125	0.834	0.872	2.417	0.271	2.669	0.046	1.810	0.223

continued

sample	a_1 [3*]	a_2 [3*]	a_1 [2*]	a_2 [2*]	a_3 [2*]	χ^2_{red}	$Fe^{2+}QS_{avg}$	$Fe^{3+}QS_{avg}$	$Fe^{3+}CS_{avg}$	$Fe^{2+}CS_{avg}$	Fe^{3+}/Fe	Fe^{2+}/Fe
nwad	0.082		0.146	0.658	0.114	2.254	2.395	0.724	0.316	1.116	0.082	0.918
pc2b	0.110		0.130	0.634	0.126	3.040	2.404	0.640	0.274	1.117	0.110	0.890
pr5b	0.124		0.363	0.473	0.040	3.066	2.517	1.040	0.392	1.123	0.124	0.876
slp	0.090	0.041	0.038	0.431	0.400	2.852	2.421	0.523	0.247	1.111	0.131	0.869
snf-1	0.106		0.121	0.248	0.525	4.432	2.423	0.593	0.269	1.116	0.106	0.894
snf-19	0.114	0.032	0.192	0.438	0.223	2.208	2.445	0.797	0.438	1.113	0.146	0.854
snf-2	0.060	0.169	0.494	0.115	0.162	5.272	2.410	0.851	0.419	1.104	0.229	0.771
snf-25	0.107		0.140	0.106	0.646	4.054	2.415	0.545	0.299	1.118	0.107	0.893
nb-214	0.141		0.164	0.596	0.098	3.136	2.546	0.943	0.321	1.124	0.141	0.859
nb-145	0.095	0.088	0.199	0.077	0.542	1.432	2.473	1.034	0.415	1.124	0.183	0.817
nb-146	0.020	0.130	0.324	0.377	0.149	1.348	2.495	1.066	0.402	1.125	0.150	0.850
nb-92	0.130	0.071	0.401	0.030	0.368	1.112	2.352	0.910	0.474	1.105	0.201	0.799
nb-78	0.166		0.362	0.381	0.091	1.872	2.310	0.879	0.386	1.122	0.166	0.834
nb-88	0.065	0.070	0.541	0.268	0.057	1.742	2.338	0.749	0.508	1.105	0.134	0.866
nb-58	0.034	0.070	0.104	0.563	0.229	2.072	2.329	0.726	0.538	1.108	0.104	0.897
nb-89	0.110	0.034	0.597	0.192	0.066	1.724	2.363	0.731	0.492	1.112	0.144	0.856
snf-10	0.055	0.109	0.591	0.147	0.098	2.646	2.358	0.855	0.476	1.107	0.164	0.836
nb-239	0.041	0.076	0.149	0.517	0.216	1.516	2.373	0.728	0.518	1.108	0.118	0.883
nb-99	0.017	0.051	0.705	0.070	0.158	2.144	2.332	0.764	0.497	1.108	0.068	0.932

Note: symmetric doublets are assumed for all sites. The [3*] and [2*] refer respectively to octahedral Fe^{3+} and Fe^{2+} specific parameters. BG is in kilocounts per channel. parametes δ_0, Δ_0 and σ_Δ are in mm/s. parameter $\delta 1$ is dimensionless and $\Gamma = 0$.

*: this parameter was frozen during fitting.

Appendices for Manuscript 2

Appendix I of Manuscript 2

Locations and Host Rock Descriptions of Micas

Listed below in order of pluton code number ("Code") are locations of geochemical samples by NTS sheet ("Map"), easting ("East") and northing ("North"). Also given is a batholith or suite name, a pluton, phase or unit name, (Whalen, 1993) and a sample description. Unit letters (e.g. "Ogp") refer to map units on GSC Map 1751A (Geology of Northern Portion of the Central Plutonic Belt, New Brunswick, scale 1:100000, Geological Survey of Canada, 1990).

Key to abbreviations used in sample descriptions is after Whalen (1993):

vfg : very fine grained
fg : fine grained
mg : medium grained
cg : coarse grained
vcg : very coarse grained
eq : equigranular
porph : porphyritic
diss : disseminated
mass : massive
fol: foliated
incl : inclusion
metased : metasedimentary
alt : alteration
Hbl: hornblende
Bt : biotite
Chl : chlorite
Ep : epidote
Fld : feldspar
Kfs: K-feldspar
Ms: muscovite
Ne : nepheline
Ol : olivine
Pl : plagioclase
Pyx : pyroxene
Py : pyrite
Qtz : quartz

Location and host rock description of biotite samples from the Canadian Appalachians.

New Brunswick

sample	Code	Map	East	North	batholith/suite	Pluton, Phase or Unit	Sample Description
nb-91	G-12	21O/7	8378	4329	Mt Elizabeth Complex	Mafic suite (SEmd)	cg black Pyx-Hbl-ol-Bt gabbronorite
nb-99	G-12	21O/7	855	475	Mt Elizabeth Complex	Mafic suite (SEmd)	cg eq Hbl-Pyx-Bt gabbronorite, Plus Pl-Bt pegmatite
nb-239	G-12	21O/7	8081	4916	Mt Elizabeth Complex	Mafic suite (SEmd)	mg eq amph-Bt leuco-gabbro
nb-88	G-12	21O/7	8277	4326	Mt Elizabeth Complex	Alkaline suite (SEah)	mg amph-Bt Qtz monzonite, mafic and felsic zones
nb-89	G-12	21O/7	8320	4367	Mt Elizabeth Complex	Alkaline suite (SEaq)	mg grey amph-Bt Qtz monzodiorite, mafic incl-rich
nb-92	G-12	21O/7	8328	4222	Mt Elizabeth Complex	Alkaline suite (SEas)	mg red Bt-Hbl syenite
nb-78	G-12	21O/7	8211	4250	Mt Elizabeth Complex	Alkaline suite (SEag)?	fg pink Bt granite
nb-58	D-3	21O/16	082	085	Charlo stocks	Benjamin River complex	mg-cg eq Pyx-Hbl-Bt leuco-gabbronorite
nb-145	G-14	21O/2	619	088	North Pole Stream	granite (SNm)	fg eq grey Bt-Ms granite
nb-146	G-14	21O/2	613	091	North Pole Stream	granite (SNm)	mg eq grey Bt-Ms granite, weathered
nb-166	G-19	21J/11	441	702		Beadle Mountain	mg grey Bt-Ms granite, metased and Qtz incl
nb-214	G-28	21G/5	405	186		Tower Hill	mg eq white Ms-Bt granite
nb-159	G-17	21J/10	604	752		Lost Lake	fg-mg eq Bt granodiorite
nb-161	G-17	21J/11	468	750		Lost Lake	cg eq (larger Kfs) Bt-Ms granodiorite
nb-162	G-17	21J/10	535	707		Lost Lake	mg eq fol Bt-Ms granite
nb-122	G-14	21O/2	778	177	North Pole Stream	granite (SNm)	fg-mg white Bt-Ms granodiorite, pegmatitic clots
nb-136	G-14	21J/15	660	030	North Pole Stream	Squaw Lake	mg eq white Bt-Ms granite, rare Bt clots
nb-169	G-21	21J/11	409	529		Bogan Brook	fg grey Bt-Ms tonalite, metased incl-rich
nb-173	G-22	21J/11	497	570		Nashwaak	mg eq white Bt-Ms granodiorite
nb-227	G-22	21J/6	4867	4325		Nashwaak	cg eq pink Ms-Bt granite
nb-8	G-24	21G/13	962	688	Pokiok batholith	Skiff Lake	fg white Bt-Ms granite, Bt-rich incl
nb-13	G-24	21G/13	092	671	Pokiok batholith	Skiff Lake	banded fg-mg eq pink Bt-Ms granite
nb-29	G-24	21G/12	082	649	Pokiok batholith	Skiff Lake	cg seriate Bt-Ms granite
nb-30	G-24	21G/12	034	640	Pokiok batholith	Skiff Lake	mg-cg eq Ms-Bt granite, chl veins
nb-17	G-25	21J/3	370	966	Pokiok batholith	Hawkshaw	mg grey Kfs porph Bt-Ms granite
nb-19	G-26	21G/14	468	909	Pokiok batholith	Allandale	mg eq pink Ms-Bt granite, minor molybdenite
nb-38	G-26	21G/14	344	799	Pokiok batholith	Allandale	mg-cg seriate Bt-Ms granite
nb-111	G-6	21O/1	9370	2305	Ordovician suite	Mullin Stream Lake (Ogu	cg strongly fol grey Bt-Ms granodiorite
nb-125	G-8	21J/15	843	026	Ordovician suite	South Renous River?	mg-cg strongly fol Bt-Ms granite

Newfoundland

NF-8	GZ	12A/4	4494	53178		Buck Lake granite	vcg pink Kfs porph (1-2 cm) Bt granite
NF-106	DWZn	12A/5	4486	53585	Dashwoods - Ordovician plutonic suite		fol cg Bt-Hbl granodiorite or Qtz monzonite
NF-119	DWZn	12A/5	4308	53674	Dashwoods - Ordovician plutonic suite		fol white cg Bt granodiorite
NF-28	DWZs	11O/11	3271	52626		Red Rocks granite	pale pink mg eq Bt granite
NF-29	DWZs	11O/11	3413	52728		Port aux Basque granite	strongly fol dark pink mg eq Bt granite
NF-36	NDZs	12A/11	4809	53779	Pierre's Pond plutonic suite		slightly fol pink fg-mg eq Bt granite
NF-23	NDZs	12A/11	4749	53778	Star Lake intrusive suite		cg eq dark pk Bt-Hbl hypersolvus granite
NF-1	NDZs	12A/12	4373	53842	Pierre's Pond plutonic suite		mass mg eq Bt-Hbl granite, cut by ep and pegmatitic veins
NF-83	NDZs	12A/12	4408	53754	Star Lake intrusive suite		white slightly fol mg-cg Bt-Ms granite

Continued

sample	Code	Map	East	North	batholith/suite	Pluton, Phase or Unit	Sample Description
NF-102		12H/2	5096	54464		Hinds Brook granite	grey and pink Kfld porph (0.3-2.5 cm) mg Bt granite
NF-166		11O/11	3336	52729	Grand Bay granodiorite suite		fg-mg grey Bt granodiorite
SNF-1		12 A/4	5317796	449310		Burgeo granites	grey mg cg foliated Kfs megacrystic Bt granite
SNF-2**		11 P/12				Burgeo granites	mg cg pink Kfs megacrystic Bt granodiorite
SNF-10		1 M/15	5294810	686265		Ackley city granite	pale grey vcg pink Kfs megacrystic Bt-Hbl granodiorite
SNF-19		2 F/4	5449395	313645		Cape Freel granite	dark grey vcg foliated pink Kfs megacrystic Bt granite
SNF-25		2 E/9	5503690	700455		Fogo Island granite	mass pale grey mg eq Hbl-Bt granodiorite

Nova Scotia

pc2b	2b	11 D/5	426010	4927390	South Mountain batholith	Halifax	mg-cg Bt monzogranite
ed3	3	11 D/12	431350	4929050	South Mountain batholith	Halifax	mg-cg megacrystic Kfs Ms-Bt monzogranite
pr5b	5b	11 D/12	436420	4930140	South Mountain batholith	Halifax	mg eq Bt-Ms monzogranite
br4	4	11 D/12	441495	4933840	South Mountain batholith	Halifax	mg-cg megacrystic Kfs Bt-Ms monzogranite
103b2	b2	11 D/12	447350	4942280	South Mountain batholith	Halifax	mg-cg grey Bt-monzogranite
306-2	4	11 D/5	450150	4926800	South Mountain batholith	Halifax	fg-mg porphyritic Kfs Bt-Ms monzogranite
mwad	1	11 D/12	450180	4941175	South Mountain batholith	Halifax	mg-cg grey Bt-granodiorite
slp**						Sherbrook Lake	mg eq grey Bt-Ms monzogranite
NS-3**						Port Mouton	mg eq moderately fol Bt-Ms granite
NS-4**						Port Mouton	fg-mg fol Bt-Ms granite

* According to MacDonald and Horne (1988), rocks of the Halifax pluton are divided into two sequences (A and B) on the basis of texture and field relationships and each sequence is subdivided into units

** coordinates are not available at the moment.

Appendix II of Manuscript 2

Electron Microprobe Analyses of Biotite

Tabulated below are electron microprobe analyses of biotite and their corresponding structural formulae (based on 20 oxygens) collected during this study as well as obtained from published data in the literature. Major elements are in weight per cent oxides.

Appalachian biotite compositions.

sample	10352	306-2	br4	ed3	nb-111	nb-122	nb-125	nb-13	nb-136	nb-159	nb-161
SiO_2	35.003	34.722	34.720	34.383	33.966	34.526	35.674	34.783	34.642	34.515	35.222
TiO_2	3.865	3.426	3.726	2.970	2.736	2.825	2.896	3.125	2.787	3.312	3.001
Al_2O_3	18.631	19.569	18.773	19.467	18.618	17.967	16.563	18.419	17.274	18.821	17.064
Fe_2O_3	2.614	3.785	4.925	2.675	3.461	5.522	4.960	5.760	5.449	1.998	3.916
FeO	22.510	18.976	22.746	25.109	24.156	19.150	17.838	17.263	17.848	22.529	19.210
MnO	0.440	0.339	0.369	0.814	0.437	0.702	0.283	0.676	0.460	0.331	0.418
MgO	7.055	5.723	6.095	3.679	4.716	6.669	8.962	7.297	7.731	5.757	8.276
CaO	0.011	0.008	0.000	0.034	0.029	0.061	0.010	0.000	0.006	0.040	0.008
Na_2O	0.172	0.154	0.180	0.120	0.095	0.041	0.076	0.099	0.077	0.127	0.070
K_2O	10.094	10.101	9.881	9.832	9.696	9.551	10.275	10.253	10.061	9.805	10.149
H_2O	3.694	3.648	3.602	3.537	3.434	3.672	3.633	3.677	3.580	3.647	3.742
F	0.347	0.513	0.554	0.571	0.714	0.389	0.498	0.399	0.573	0.389	0.262
Cl	0.069	0.062	0.042	0.080	0.075	0.006	0.027	0.010	0.015	0.074	0.010
total	104.357	100.796	105.369	103.013	101.816	100.905	101.360	101.612	100.257	101.165	101.234
Si	5.202	5.277	5.137	5.243	5.234	5.273	5.389	5.246	5.311	5.285	5.350
Al	2.798	2.723	2.863	2.757	2.766	2.727	2.611	2.754	2.689	2.715	2.650
Ti	0.000	0.000	0.000	0.000	0.000	0.000	0.000	0.000	0.000	0.000	0.000
T site	8.000	8.000	8.000	8.000	8.000	8.000	8.000	8.000	8.000	8.000	8.000
Al	0.465	0.782	0.411	0.742	0.615	0.507	0.338	0.520	0.432	0.682	0.404
Ti	0.432	0.392	0.415	0.341	0.317	0.324	0.329	0.354	0.321	0.381	0.343
Fe^{+3}	0.292	0.433	0.548	0.307	0.401	0.635	0.553	0.654	0.629	0.230	0.448
Fe^{+2}	2.798	2.412	2.815	3.202	3.113	2.446	2.254	2.180	2.288	2.885	2.440
Mn^{+2}	0.055	0.044	0.046	0.105	0.057	0.091	0.036	0.086	0.060	0.043	0.054
Mg	1.563	1.297	1.344	0.836	1.083	1.518	2.018	1.641	1.767	1.314	1.874
O site	5.605	5.359	5.579	5.533	5.586	5.521	5.528	5.435	5.497	5.536	5.562
Ca	0.002	0.001	0.000	0.006	0.005	0.010	0.002	0.000	0.001	0.007	0.001
Na	0.049	0.045	0.052	0.036	0.028	0.012	0.022	0.029	0.023	0.038	0.021
K	1.914	1.958	1.865	1.913	1.906	1.861	1.980	1.973	1.968	1.916	1.966
A site	1.965	2.005	1.917	1.954	1.939	1.883	2.004	2.002	1.991	1.960	1.988
O	20.152	20.000	20.175	20.106	20.103	20.079	20.094	20.108	20.057	20.067	20.080
OH	3.662	3.737	3.555	3.598	3.529	3.741	3.661	3.699	3.661	3.725	3.791
F	0.163	0.247	0.259	0.275	0.348	0.178	0.238	0.190	0.278	0.189	0.126
Cl	0.022	0.016	0.010	0.021	0.020	0.002	0.007	0.003	0.004	0.019	0.003
Al tot	3.263	3.505	3.274	3.499	3.381	3.234	2.949	3.274	3.121	3.397	3.054
Fe/(Fe+Mg)	0.664	0.687	0.714	0.808	0.764	0.670	0.582	0.633	0.623	0.703	0.606
Fe^{3+}/Fe	0.105	0.152	0.196	0.096	0.114	0.206	0.197	0.231	0.215	0.074	0.155

Appalachian biotite compositions.

sample	nb-162	nb-166	nb-169	nb-17	nb-173	nb-227	nb-29	nb-30	nb-38	nb-8	nb-91
SiO_2	35.229	34.651	34.812	35.490	35.090	33.941	34.565	34.372	35.119	34.701	38.456
TiO_2	2.954	2.900	2.987	2.851	1.825	3.061	2.013	2.702	3.018	2.844	2.728
Al_2O_3	17.859	19.362	18.849	17.066	19.391	19.018	18.096	18.126	18.500	19.833	16.566
Fe_2O_3	3.298	1.754	2.789	4.267	3.046	4.375	5.033	5.452	3.958	1.396	0.685
FeO	18.397	18.402	19.816	17.757	18.310	20.623	16.105	17.757	18.838	20.030	7.185
MnO	0.430	0.213	0.273	0.478	0.555	0.596	0.951	0.828	0.537	0.257	0.028
MgO	8.164	8.592	8.082	8.650	8.305	6.201	9.457	6.980	7.057	7.274	20.987
CaO	0.006	0.003	0.014	0.016	0.001	0.015	0.013	0.029	0.006	0.010	0.046
Na_2O	0.064	0.224	0.234	0.056	0.085	0.084	0.073	0.075	0.151	0.207	1.660
K_2O	10.043	9.658	9.636	10.137	10.102	9.124	9.445	9.538	10.038	9.686	7.532
H_2O^-	3.587	3.741	3.729	3.558	3.617	3.619	3.650	3.673	3.457	3.781	4.068
F	0.641	0.401	0.328	0.680	0.604	0.484	0.527	0.404	0.867	0.269	0.207
Cl	0.009	0.007	0.035	0.011	0.005	0.009	0.008	0.006	0.026	0.030	0.151
total	100.408	99.738	101.438	100.729	100.678	100.947	99.715	99.772	101.199	100.197	100.178
Si	5.360	5.271	5.252	5.387	5.312	5.187	5.269	5.282	5.320	5.282	5.463
Al	2.640	2.729	2.748	2.613	2.688	2.813	2.731	2.718	2.680	2.718	2.537
Ti	0.000	0.000	0.000	0.000	0.000	0.000	0.000	0.000	0.000	0.000	0.000
T site	8.000	8.000	8.000	8.000	8.000	8.000	8.000	8.000	8.000	8.000	8.000
Al	0.563	0.742	0.603	0.440	0.771	0.612	0.521	0.565	0.623	0.841	0.237
Ti	0.338	0.332	0.339	0.325	0.208	0.352	0.231	0.312	0.344	0.326	0.291
Fe^{+3}	0.378	0.201	0.317	0.487	0.347	0.503	0.577	0.631	0.451	0.160	0.073
Fe^{+2}	2.341	2.341	2.500	2.254	2.318	2.636	2.053	2.282	2.386	2.550	0.854
Mn^{+2}	0.055	0.027	0.035	0.061	0.071	0.077	0.123	0.108	0.069	0.033	0.003
Mg	1.852	1.948	1.818	1.957	1.874	1.413	2.149	1.599	1.594	1.651	4.445
O site	5.527	5.591	5.611	5.525	5.589	5.593	5.654	5.497	5.466	5.560	5.903
Ca	0.001	0.001	0.002	0.003	0.000	0.002	0.002	0.005	0.001	0.002	0.007
Na	0.019	0.066	0.068	0.017	0.025	0.025	0.022	0.022	0.044	0.061	0.457
K	1.949	1.874	1.855	1.963	1.951	1.779	1.837	1.870	1.940	1.881	1.365
A site	1.969	1.941	1.925	1.982	1.976	1.806	1.861	1.897	1.985	1.944	1.829
O	20.049	20.010	20.082	20.068	20.057	20.075	20.032	20.037	20.085	20.024	20.016
OH	3.640	3.795	3.753	3.602	3.652	3.689	3.711	3.765	3.493	3.839	3.855
F	0.308	0.193	0.157	0.327	0.289	0.234	0.254	0.197	0.415	0.130	0.093
Cl	0.002	0.002	0.009	0.003	0.001	0.002	0.002	0.002	0.007	0.008	0.036
Al tot	3.203	3.471	3.351	3.053	3.459	3.425	3.252	3.283	3.303	3.558	2.774
Fe/(Fe+Mg)	0.595	0.566	0.608	0.583	0.587	0.690	0.550	0.646	0.640	0.621	0.173
Fe^{3+}/Fe	0.139	0.079	0.112	0.178	0.130	0.160	0.219	0.216	0.159	0.059	0.079

Appalachian biotite compositions.

sample	nf-1	nf-102	nf-106	nf-119	nf-166	nf-23	nf-28	nf-29	nf-36	nf-8	nf-83
SiO_2	34.334	36.954	37.379	35.471	36.459	35.463	36.337	37.122	36.151	36.022	35.263
TiO_2	3.120	2.858	2.658	2.445	2.709	2.472	1.767	2.946	3.260	3.892	2.819
Al_2O_3	15.577	14.106	15.376	16.989	16.264	15.000	16.263	15.982	16.086	16.486	16.536
Fe_2O_3	4.886	4.548	3.769	4.805	5.430	5.856	5.023	4.756	4.483	2.545	3.246
FeO	26.116	13.278	15.408	17.069	17.375	23.924	18.183	15.747	16.825	19.899	19.277
MnO	0.544	0.419	0.554	0.514	0.550	0.476	0.454	0.618	0.612	0.353	0.455
MgO	3.233	14.437	12.288	9.840	8.780	4.735	9.312	9.343	9.198	8.086	8.982
CaO	0.015	0.047	0.028	0.034	0.027	0.103	0.016	0.043	0.002	0.011	0.006
Na_2O	0.051	0.092	0.085	0.086	0.063	0.047	0.077	0.089	0.086	0.069	0.070
K_2O	9.689	9.468	10.097	9.954	10.135	9.823	9.915	10.258	10.175	10.214	10.127
H_2O	3.675	3.647	3.755	3.741	3.782	3.603	3.475	3.507	3.794	3.795	3.572
F	0.090	0.647	0.362	0.268	0.217	0.299	0.829	0.857	0.226	0.216	0.614
Cl	0.026	0.054	0.086	0.103	0.006	0.031	0.024	0.014	0.005	0.022	0.021
total	101.314	100.269	101.673	101.181	101.704	101.698	101.319	100.899	100.805	101.513	100.723
Si	5.404	5.514	5.541	5.348	5.475	5.507	5.489	5.572	5.463	5.447	5.384
Al	2.596	2.481	2.459	2.652	2.525	2.493	2.511	2.428	2.537	2.553	2.616
Ti	0.000	0.005	0.000	0.000	0.000	0.000	0.000	0.000	0.000	0.000	0.000
T site	8.000	8.000	8.000	8.000	8.000	8.000	8.000	8.000	8.000	8.000	8.000
Al	0.293	0.000	0.227	0.366	0.353	0.253	0.384	0.399	0.328	0.384	0.359
Ti	0.369	0.321	0.296	0.277	0.306	0.289	0.201	0.333	0.370	0.442	0.324
Fe^{+3}	0.579	0.506	0.420	0.545	0.614	0.684	0.571	0.537	0.510	0.290	0.373
Fe^{+2}	3.437	1.657	1.910	2.152	2.182	3.107	2.297	1.977	2.126	2.516	2.461
Mn^{+2}	0.073	0.053	0.070	0.066	0.070	0.063	0.058	0.079	0.078	0.045	0.059
Mg	0.759	3.211	2.715	2.212	1.965	1.096	2.097	2.091	2.072	1.823	2.044
O site	5.510	5.747	5.638	5.618	5.489	5.492	5.608	5.414	5.485	5.500	5.621
Ca	0.002	0.008	0.004	0.005	0.004	0.017	0.003	0.007	0.000	0.002	0.001
Na	0.016	0.027	0.024	0.025	0.018	0.014	0.022	0.020	0.025	0.020	0.021
K	1.945	1.802	1.909	1.914	1.941	1.946	1.911	1.964	1.962	1.970	1.972
A site	1.964	1.837	1.938	1.945	1.964	1.977	1.936	1.991	1.987	1.992	1.994
O	20.090	20.052	20.096	20.084	20.107	20.113	20.096	20.078	20.066	20.000	20.061
OH	3.858	3.630	3.712	3.762	3.788	3.732	3.501	3.511	3.825	3.891	3.638
F	0.045	0.305	0.170	0.128	0.103	0.147	0.396	0.407	0.108	0.103	0.296
Cl	0.007	0.014	0.022	0.026	0.001	0.008	0.006	0.004	0.001	0.006	0.005
Al tot	2.889	2.481	2.686	3.019	2.878	2.745	2.895	2.827	2.865	2.938	2.975
Fe/(Fe+Mg)	0.841	0.403	0.462	0.549	0.587	0.776	0.578	0.546	0.560	0.606	0.581
Fe^{3+}/Fe	0.144	0.236	0.180	0.202	0.219	0.180	0.199	0.214	0.193	0.103	0.132

Appalachian biotite compositions.

sample	ns-3	ns-4	nwab	pc2b	pr5b	slp	snf-1	snf-19	snf-2	snf-25	nb-214
SiO_2	34.316	34.913	34.873	34.833	34.601	34.902	35.586	36.175	36.994	36.312	34.649
TiO_2	3.070	2.200	3.786	3.569	3.814	4.015	3.722	3.315	2.745	4.555	2.648
Al_2O_3	18.789	18.495	18.482	18.591	19.611	19.409	16.771	15.248	15.138	13.341	19.346
Fe_2O_3	3.426	3.029	1.984	2.688	3.201	3.428	2.566	3.577	5.092	3.388	3.917
FeO	20.081	21.223	21.868	22.205	20.396	23.159	19.390	18.825	15.434	25.392	21.453
MnO	0.266	0.895	0.398	0.389	0.467	0.443	0.382	0.557	0.419	0.280	0.639
MgO	7.248	6.043	7.009	6.976	4.833	5.613	8.498	8.965	11.443	5.736	4.469
CaO	0.006	0.000	0.010	0.025	0.003	0.002	0.019	0.014	0.018	0.007	0.003
Na_2O	0.052	0.052	0.172	0.138	0.110	0.130	0.052	0.075	0.125	0.082	0.062
K_2O	10.225	9.791	9.977	10.078	10.232	10.334	10.365	10.169	10.168	9.835	9.423
H_2O	3.805	3.834	3.711	3.739	3.541	3.752	3.780	3.531	3.778	3.476	3.648
F	0.089	0.049	0.318	0.259	0.700	0.230	0.254	0.754	0.364	0.428	0.421
Cl	0.069	0.001	0.113	0.091	0.038	0.046	0.012	0.021	0.013	0.344	0.005
total	101.387	100.504	102.542	103.452	101.243	105.354	101.286	100.902	101.574	102.918	100.504
Si	5.216	5.369	5.256	5.219	5.267	5.158	5.392	5.508	5.515	5.576	5.326
Al	2.784	2.631	2.744	2.781	2.733	2.842	2.608	2.492	2.485	2.415	2.674
Ti	0.000	0.000	0.000	0.000	0.000	0.000	0.000	0.000	0.000	0.009	0.000
T site	8.000	8.000	8.000	8.000	8.000	8.000	8.000	8.000	8.000	8.000	8.000
Al	0.582	0.721	0.539	0.503	0.786	0.539	0.386	0.245	0.175	0.000	0.831
Ti	0.351	0.254	0.429	0.402	0.437	0.446	0.424	0.380	0.308	0.526	0.306
Fe^{+3}	0.392	0.350	0.225	0.303	0.367	0.381	0.293	0.410	0.571	0.382	0.453
Fe^{+2}	2.553	2.729	2.756	2.783	2.597	2.862	2.457	2.397	1.924	3.261	2.758
Mn^{+2}	0.034	0.117	0.051	0.049	0.060	0.055	0.049	0.072	0.053	0.036	0.083
Mg	1.642	1.385	1.575	1.558	1.097	1.237	1.919	2.035	2.543	1.313	1.024
O site	5.554	5.557	5.575	5.598	5.343	5.521	5.528	5.538	5.574	5.518	5.455
Ca	0.001	0.000	0.002	0.004	0.000	0.000	0.003	0.002	0.003	0.001	0.001
Na	0.015	0.015	0.050	0.040	0.032	0.037	0.015	0.022	0.036	0.024	0.019
K	1.983	1.921	1.918	1.927	1.987	1.949	2.003	1.975	1.934	1.927	1.848
A site	1.999	1.936	1.970	1.971	2.020	1.986	2.022	2.000	1.973	1.952	1.867
O	20.082	20.043	20.089	20.117	20.000	20.182	20.000	20.000	20.000	20.142	20.054
OH	3.858	3.932	3.730	3.737	3.653	3.699	3.875	3.631	3.825	3.560	3.740
F	0.043	0.024	0.152	0.123	0.337	0.107	0.122	0.363	0.172	0.208	0.205
Cl	0.018	0.000	0.029	0.023	0.010	0.012	0.003	0.005	0.003	0.090	0.001
Al tot	3.366	3.352	3.283	3.283	3.519	3.381	2.995	2.736	2.660	2.415	3.505
Fe/(Fe+Mg)	0.642	0.690	0.654	0.664	0.730	0.724	0.589	0.580	0.495	0.736	0.758
Fe^{3+}/Fe	0.133	0.114	0.082	0.110	0.124	0.134	0.106	0.146	0.229	0.107	0.141

Appalachian biotite compositions.

sample	nb-145	nb-146	nb-92	nb-78	nb-68	nb-58	nb-69	snf-10	nb-239	nb-99
SiO_2	34.513	34.465	38.719	39.648	36.162	36.085	36.327	36.238	36.833	35.116
TiO_2	2.483	3.052	3.147	1.774	4.546	5.058	4.325	3.500	4.478	5.572
Al_2O_3	18.575	18.439	12.052	12.396	12.632	12.830	13.075	12.984	13.598	13.611
Fe_2O_3	4.630	3.877	3.707	2.728	3.427	2.302	3.455	4.135	2.623	1.897
FeO	18.598	20.242	15.364	12.335	23.093	20.641	19.099	19.860	20.896	23.028
MnO	0.502	0.538	0.173	0.265	0.140	0.119	0.127	0.516	0.138	0.150
MgO	7.624	6.912	14.135	17.330	8.126	9.988	10.963	9.690	10.251	7.658
CaO	0.035	0.021	0.002	0.007	0.026	0.007	0.522	0.016	0.021	0.008
Na_2O	0.074	0.082	0.071	0.117	0.067	0.261	0.092	0.092	0.232	0.173
K_2O	9.774	9.570	10.069	10.329	9.787	9.574	9.262	9.918	9.389	9.170
H_2O	3.562	3.609	2.702	1.942	3.282	3.417	3.355	3.241	3.741	3.634
F	0.642	0.517	2.375	4.284	0.649	0.641	0.812	1.259	0.094	0.073
Cl	0.012	0.016	0.403	0.113	0.775	0.564	0.493	0.066	0.343	0.599
total	100.751	101.119	101.830	101.439	102.264	101.088	101.455	100.970	102.519	100.522
Si	5.254	5.251	5.747	5.813	5.554	5.525	5.506	5.564	5.531	5.454
Al	2.746	2.749	2.108	2.142	2.287	2.315	2.336	2.350	2.406	2.492
Ti	0.000	0.000	0.145	0.045	0.159	0.159	0.159	0.086	0.063	0.054
T site	8.000	8.000	8.000	8.000	8.000	8.000	8.000	8.000	8.000	8.000
Al	0.587	0.562	0.000	0.000	0.000	0.000	0.000	0.000	0.000	0.000
Ti	0.284	0.350	0.206	0.151	0.366	0.423	0.334	0.318	0.443	0.597
Fe^{+3}	0.530	0.444	0.414	0.301	0.396	0.265	0.394	0.478	0.296	0.222
Fe^{+2}	2.368	2.579	1.907	1.512	2.966	2.643	2.421	2.550	2.624	2.991
Mn^{+2}	0.065	0.069	0.022	0.033	0.018	0.015	0.016	0.067	0.018	0.020
Mg	1.730	1.570	3.128	3.788	1.861	2.280	2.477	2.218	2.295	1.773
O site	5.564	5.576	5.677	5.786	5.607	5.627	5.643	5.631	5.676	5.602
Ca	0.006	0.003	0.000	0.001	0.004	0.001	0.085	0.003	0.003	0.001
Na	0.022	0.024	0.021	0.033	0.020	0.078	0.027	0.027	0.067	0.052
K	1.898	1.860	1.907	1.932	1.918	1.870	1.791	1.943	1.799	1.817
A site	1.926	1.888	1.927	1.967	1.942	1.949	1.903	1.973	1.869	1.870
O	20.071	20.079	20.108	20.086	20.120	20.000	20.092	20.000	20.121	20.042
OH	3.617	3.668	2.675	1.900	3.363	3.543	3.392	3.372	3.747	3.765
F	0.309	0.249	1.115	1.986	0.315	0.310	0.389	0.611	0.045	0.036
Cl	0.003	0.004	0.101	0.028	0.202	0.146	0.127	0.017	0.087	0.158
Al tot	3.333	3.311	2.108	2.142	2.287	2.315	2.336	2.350	2.406	2.492
Fe/(Fe+Mg)	0.626	0.658	0.426	0.324	0.644	0.561	0.532	0.577	0.560	0.644
Fe^{3+}/Fe	0.183	0.147	0.178	0.166	0.118	0.091	0.140	0.158	0.101	0.069

Compositions of biotites from the Hepburn and Bishop intrusive suites.

sample	HL125	HL200	HL204	HL14	HL341	HS29	BL313	BL315	BL531	BZ53	BL255
SiO_2	34.000	35.660	34.430	35.140	34.240	35.340	37.290	36.930	36.540	34.280	35.510
TiO_2	3.390	3.440	2.670	3.380	2.930	3.550	2.730	3.020	3.130	4.270	4.690
Al_2O_3	15.130	15.800	16.150	16.490	19.160	15.860	13.660	13.860	14.640	13.810	12.990
Fe_2O_3	1.800	1.710	1.980	2.040	1.070	2.260	3.410	3.340	3.470	3.970	2.330
FeO	26.730	22.120	23.690	21.090	20.910	21.120	14.270	16.520	16.750	17.200	20.410
MnO	0.310	0.280	0.410	0.270	0.290	0.290	0.410	0.390	0.340	0.350	0.240
MgO	4.440	6.740	6.260	7.400	6.370	7.600	13.200	12.370	11.100	11.300	9.780
CaO	0.010	0.020	0.020	0.010	0.010	0.010	0.030	0.030	0.030	0.010	0.020
Na_2O	0.070	0.050	0.060	0.040	0.140	0.060	0.070	0.070	0.060	0.080	0.090
K_2O	9.840	9.830	9.690	9.930	9.260	9.870	9.780	9.620	9.760	9.830	9.820
H_2O	3.365	3.424	3.224	3.109	3.512	3.186	3.368	3.512	3.588	3.305	3.109
F	0.490	0.840	1.070	1.330	0.630	1.220	1.240	0.880	0.690	1.150	1.410
Cl	0.570	0.130	0.280	0.440	0.320	0.340	0.050	0.060	0.090	0.100	0.270
total	99.810	99.661	99.420	100.010	98.505	100.126	98.975	100.217	99.877	99.148	100.014
Si	5.441	5.545	5.433	5.440	5.333	5.468	5.659	5.584	5.554	5.320	5.506
Al	2.559	2.455	2.567	2.560	2.667	2.532	2.341	2.416	2.446	2.526	2.374
Ti	0.000	0.000	0.000	0.000	0.000	0.000	0.000	0.000	0.000	0.154	0.121
T site	8.000	8.000	8.000	8.000	8.000	8.000	8.000	8.000	8.000	8.000	8.000
Al	0.295	0.441	0.437	0.449	0.850	0.359	0.101	0.054	0.176	0.000	0.000
Ti	0.408	0.402	0.317	0.394	0.343	0.413	0.312	0.343	0.358	0.344	0.426
Fe^{+3}	0.217	0.200	0.235	0.238	0.125	0.263	0.389	0.380	0.397	0.464	0.272
Fe^{+2}	3.577	2.877	3.126	2.731	2.724	2.732	1.811	2.089	2.129	2.232	2.646
Mn^{+2}	0.042	0.037	0.055	0.035	0.038	0.038	0.053	0.050	0.044	0.046	0.032
Mg	1.059	1.562	1.473	1.708	1.479	1.752	2.986	2.788	2.515	2.614	2.261
O site	5.598	5.519	5.643	5.554	5.560	5.558	5.652	5.705	5.619	5.700	5.637
Ca	0.002	0.003	0.003	0.002	0.002	0.002	0.005	0.005	0.005	0.002	0.003
Na	0.022	0.015	0.018	0.012	0.042	0.018	0.021	0.021	0.018	0.024	0.027
K	2.009	1.950	1.951	1.961	1.840	1.948	1.893	1.856	1.892	1.946	1.942
A site	2.032	1.968	1.972	1.975	1.884	1.967	1.919	1.881	1.915	1.972	1.973
O	20.000	20.000	20.000	20.000	20.000	20.000	20.000	20.000	20.000	20.000	20.000
OH	3.597	3.553	3.391	3.233	3.605	3.314	3.392	3.564	3.645	3.409	3.238
F	0.248	0.413	0.534	0.651	0.310	0.597	0.595	0.421	0.332	0.564	0.691
Cl	0.155	0.034	0.075	0.115	0.084	0.089	0.013	0.015	0.023	0.026	0.071
Al tot	2.854	2.896	3.004	3.009	3.517	2.891	2.443	2.470	2.623	2.526	2.374
Fe/(Fe+Mg)	0.782	0.663	0.695	0.635	0.658	0.631	0.424	0.470	0.501	0.508	0.564
Fe^{3+}/Fe	0.057	0.065	0.070	0.080	0.044	0.088	0.177	0.154	0.157	0.115	0.052

continued

sample	BL246	BL243
SiO_2	36.110	34.970
TiO_2	3.690	5.640
Al_2O_3	13.090	13.320
Fe_2O_3	3.170	3.030
FeO	17.400	19.980
MnO	0.350	0.220
MgO	11.380	9.760
CaO	0.010	0.020
Na_2O	0.050	0.080
K_2O	9.630	9.630
H_2O	3.426	3.363
F	0.960	0.930
Cl	0.100	0.220
total	98.939	100.721
Si	5.575	5.377
Al	2.382	2.414
Ti	0.044	0.209
T site	8.000	8.000
Al	0.000	0.000
Ti	0.385	0.443
Fe^{+3}	0.368	0.351
Fe^{+2}	2.246	2.569
Mn^{+2}	0.046	0.029
Mg	2.619	2.237
O site	5.664	5.629
Ca	0.002	0.003
Na	0.015	0.024
K	1.897	1.889
A site	1.913	1.916
O	20.000	20.000
OH	3.505	3.490
F	0.469	0.452
Cl	0.026	0.057
Al tot	2.382	2.414
Fe/(Fe+Mg	0.500	0.566
Fe^{3+}/Fe	0.124	0.048

Compositions of micas from Mont Saint-Hilaire.

sample	Bt-b	Bt-c	Bt-d	Ann
SiO_2	37.220	38.670	34.280	33.820
TiO_2	2.540	2.530	1.070	1.250
Al_2O_3	10.030	9.330	8.740	9.950
Fe_2O_3	3.220	3.390	5.490	7.590
FeO	21.030	21.720	24.470	32.180
MnO	2.100	1.750	5.190	2.470
MgO	8.470	8.540	4.540	0.590
CaO	0.000	0.000	0.010	0.000
Na_2O	0.240	0.220	0.220	0.460
K_2O	8.960	9.410	7.740	8.780
H_2O	2.736	2.777	2.983	3.282
F	2.200	2.040	1.350	0.560
Cl	0.020	0.220	0.010	0.030
total	97.835	99.689	95.522	100.719
Si	5.952	6.074	5.864	5.653
Al	1.806	1.709	1.686	1.959
Fe^{+3}	0.241	0.216	0.450	0.388
T site	8.000	8.000	8.000	8.000
Al	0.084	0.019	0.076	0.002
Ti	0.305	0.299	0.138	0.157
Fe^{+3}	0.147	0.184	0.257	0.567
Fe^{+2}	2.813	2.853	3.501	4.499
Mn^{+2}	0.284	0.233	0.752	0.350
Mg	2.021	2.000	1.158	0.147
O site	5.653	5.587	5.881	5.721
Ca	0.000	0.000	0.002	0.000
Na	0.074	0.067	0.073	0.149
K	1.828	1.886	1.689	1.872
A site	1.902	1.953	1.764	2.021
O	20.000	20.000	20.000	20.000
OH	2.882	2.928	3.267	3.695
F	1.113	1.013	0.730	0.296
Cl	0.005	0.059	0.003	0.008
Al tot	1.890	1.727	1.762	1.960
Fe/(Fe+Mg	0.613	0.619	0.784	0.974
Fe^{3+}/Fe	0.121	0.123	0.168	0.175

Appendix III of Manuscript 2

Mössbauer Fitting Parameters for Biotite Spectra

Tabulated below are the Mössbauer fitting parameters for biotite spectra performed during this study and those collected from published papaers.

Mössbauer spectrum fitting parameters for Appalachian biotites

sample	fit	BG	δ_0[3']	δ_0[2']	δ_1[2']	Δ_{Q1}[3']	σ_{A1}[3']	Δ_{Q2}[3']	σ_{A2}[3']	Δ_{Q1}[2']	σ_{A1}[2']	Δ_{Q2}[2']	σ_{A2}[2']	Δ_{Q3}[2']	σ_{A3}[2']
103b2	1-3	1544.1	0.244	1.041	0.031	0.810*	0.818			2.652	0.075	2.461	0.260	1.627	0.211
306-2	2-3	1829.6	0.365	1.024	0.039	1.430	0.539	0.600*	0.720	2.660	0.085	2.475	0.278	1.811	0.185
br4	2-3	3582.7	0.389	1.078	0.017	1.463	0.616	0.756	0.385	2.642	0.107	2.449	0.319	1.738	0.202
ed3	1-3	1934.8	0.359	1.065	0.022	0.878	0.774			2.649	0.101	2.480	0.301	1.783	0.205
nb-111	2-3	2641.5	0.504	1.055	0.023	0.955	0.769	0.477	0.167	2.325	0.343	2.605	0.135	1.800*	1.053
nb-122	1-3	532.5	0.389	1.051	0.028	1.034	0.642			2.503	0.162	2.332	0.412	2.681	0.108
nb-125	2-3	2601.2	0.466	1.005	0.044	1.100*	0.765	0.575	0.238	2.265	0.416	2.504	0.209	2.669	0.070
nb-13	2-3	2288.7	0.439	1.047	0.027	1.470	0.624	0.679	0.338	2.295	0.422	2.642	0.101	2.385	0.103
nb-136	2-3	1535.2	0.376	1.138	-0.006	1.102	0.649	0.911	0.301	2.326	0.361	1.955	0.955	2.627	0.131
nb-159	1-3	2441.4	0.370	1.073	0.021	0.768	0.839			2.340	0.409	2.671	0.110	2.390	0.069
nb-161	2-3	893.4	0.453	1.016	0.040	0.648	0.175	0.810*	0.784	2.673	0.090	2.452	0.146	2.318	0.426
nb-162	1-3	2297.6	0.339	1.034	0.036	0.919	0.775			1.880	0.216	2.689	0.071	2.528	0.269
nb-166	1-3	346.1	0.342	1.070	0.023	0.833	0.876			2.670	0.072	2.509	0.281	1.842	0.210
nb-169	2-3	2931.3	0.457	1.040	0.030	0.804	0.898	0.600*	0.184	2.641	0.073	1.768	0.206	2.452	0.285
nb-17	2-3	2198.3	0.436	1.004	0.045	1.617	0.492	0.625	0.337	2.322	0.416	2.551	0.180	2.686	0.061
nb-173	2-3	2461.3	0.355	1.061	0.024	1.257	0.585	0.700*	0.805	2.609	0.183	1.936	0.254	2.210	0.103
nb-227	2-3	1668.1	0.406	1.062	0.018	1.297	0.594	0.695	0.358	2.649	0.107	2.347	0.424	2.378	0.066
nb-29	2-3	1978.5	0.398	0.995	0.045	0.617	0.315	1.100*	0.684	2.431	0.123	2.300	0.410	2.655	0.091
nb-30	2-3	1503.0	0.431	1.059	0.026	1.452	0.598	0.673	0.342	2.341	0.427	2.699	0.044	2.607	0.179
nb-38	2-3	2969.1	0.422	1.043	0.031	1.000	0.745	0.717	0.296	2.657	0.114	2.340	0.422	2.357	0.053
nb-8	1-3	2417.1	0.252	1.056	0.025	0.600	0.981			2.656	0.081	1.814	0.214	2.488	0.284
nb-91	1-3	2408.8	0.525	1.066	0.016	0.679	0.443			2.442	0.284	1.758	0.171	2.636	0.080
nf-1	2-3	2218.6	0.429	1.028	0.035	1.400*	0.641	0.584	0.349	2.231	0.376	2.647	0.802	2.615	0.166
nf-102	2-3	2349.6	0.369	1.053	0.030	0.842	0.861	0.965	0.323	2.496	0.242	1.932	0.226	2.686	0.078
nf-106	2-3	2792.2	0.432	1.013	0.040	0.633	0.333	1.400*	0.655	2.477	0.279	1.781	0.219	2.672	0.085
nf-119	2-3	2383.0	0.448	0.939	0.072	1.172	0.553	0.587	0.287	2.354	0.307	2.320	0.482	2.622	0.165
nf-166	2-3	1918.8	0.447	0.991	0.047	0.636	0.322	1.473	0.511	2.444	0.166	2.298	0.427	2.675	0.096
nf-23	2-3	2682.4	0.428	1.012	0.042	0.591	0.325	1.400*	0.565	2.441	0.133	2.320	0.428	2.693	0.097
nf-28	2-3	2301.0	0.439	1.072	0.018	1.456	0.661	0.705	0.374	2.353	0.404	2.326	0.041	2.641	0.123
nf-29	2-3	2276.0	0.430	1.013	0.037	0.656	0.353	1.407	0.580	2.317	0.080	2.303	0.409	2.625	0.115
nf-36	2-3	2526.2	0.449	1.019	0.039	1.458	0.576	0.615	0.322	2.322	0.420	2.436	0.145	2.687	0.103
nf-8	1-3	2201.2	0.294	1.049	0.028	0.586	1.001			2.680	0.084	2.460	0.279	1.813	0.195
nf-83	2-3	2500.9	0.468	1.041	0.030	0.583	0.261	1.100*	0.759	2.356	0.107	2.292	0.417	2.652	0.109
ns-3	1-3	2062.6	0.383	1.048	0.029	0.944	0.755			2.661	0.080	2.475	0.289	1.798	0.195
ns-4	1-3	2693.9	0.389	1.068	0.021	0.943	0.723			2.671	0.098	2.528	0.302	1.800*	0.194

continued

sample	a_1 [3+]	a_2 [3+]	a_1 [2+]	a_2 [2+]	a_3 [2+]	χ^2_{red}	$Fe^{2+}QS_{avg}$	$Fe^{3+}QS_{avg}$	$Fe^{3+}CS_{avg}$	$Fe^{2+}CS_{avg}$	Fe^{3+}/Fe	Fe^{2+}/Fe
103b2	0.105		0.128	0.629	0.138	4.014	2.390	0.810	0.244	1.115	0.105	0.895
306-2	0.063	0.087	0.167	0.590	0.092	3.810	2.440	0.949	0.365	1.118	0.151	0.849
br4	0.063	0.133	0.226	0.519	0.059	2.832	2.452	0.984	0.389	1.119	0.196	0.804
ed3	0.096		0.207	0.612	0.085	2.074	2.453	0.878	0.359	1.119	0.096	0.904
nb-111	0.094	0.037	0.470	0.303	0.096	1.602	2.364	0.821	0.504	1.109	0.131	0.869
nb-122	0.206		0.155	0.398	0.241	1.260	2.471	1.034	0.389	1.120	0.206	0.795
nb-125	0.107	0.090	0.387	0.299	0.117	1.550	2.413	0.861	0.466	1.111	0.199	0.801
nb-13	0.065	0.172	0.445	0.226	0.092	1.296	2.408	0.896	0.439	1.113	0.237	0.763
nb-136	0.148	0.068	0.413	0.081	0.291	1.744	2.399	1.042	0.376	1.124	0.216	0.785
nb-159	0.074		0.533	0.314	0.079	1.736	2.457	0.768	0.370	1.125	0.074	0.926
nb-161	0.049	0.114	0.204	0.180	0.453	1.456	2.433	0.761	0.453	1.113	0.164	0.837
nb-162	0.139		0.102	0.141	0.618	2.486	2.478	0.919	0.339	1.124	0.139	0.861
nb-166	0.083		0.119	0.682	0.116	0.946	2.445	0.833	0.342	1.125	0.083	0.917
nb-169	0.090	0.024	0.154	0.093	0.639	2.104	2.413	0.760	0.457	1.112	0.114	0.886
nb-17	0.051	0.135	0.419	0.281	0.114	2.062	2.452	0.898	0.436	1.114	0.186	0.814
nb-173	0.058	0.072	0.614	0.172	0.083	3.624	2.437	0.949	0.355	1.120	0.130	0.870
nb-227	0.066	0.095	0.280	0.494	0.066	1.300	2.450	0.941	0.406	1.107	0.160	0.840
nb-29	0.088	0.131	0.133	0.421	0.227	4.666	2.425	0.906	0.398	1.105	0.219	0.781
nb-30	0.087	0.129	0.401	0.066	0.317	1.020	2.479	0.988	0.431	1.124	0.216	0.784
nb-38	0.122	0.039	0.313	0.475	0.051	2.414	2.459	0.932	0.422	1.120	0.161	0.840
nb-8	0.062		0.171	0.109	0.658	2.104	2.440	0.600*	0.252	1.118	0.621	0.938
nb-91	0.079		0.705	0.064	0.152	1.538	2.427	0.679	0.525	1.106	0.079	0.921
nf-1	0.051	0.102	0.412	0.020	0.415	6.248	2.429	0.858	0.429	1.114	0.153	0.847
nf-102	0.146	0.089	0.498	0.125	0.141	5.832	2.439	0.889	0.369	1.126	0.236	0.764
nf-106	0.133	0.054	0.586	0.080	0.148	2.558	2.444	0.854	0.432	1.111	0.187	0.813
nf-119	0.071	0.131	0.194	0.279	0.325	6.036	2.451	0.793	0.448	1.116	0.202	0.798
nf-166	0.168	0.051	0.185	0.410	0.185	1.496	2.422	0.832	0.447	1.105	0.220	0.781
nf-23	0.128	0.052	0.145	0.447	0.228	4.790	2.445	0.826	0.428	1.116	0.181	0.820
nf-28	0.059	0.123	0.396	0.055	0.368	3.434	2.481	0.948	0.439	1.118	0.177	0.823
nf-29	0.152	0.062	0.068	0.436	0.282	1.580	2.420	0.872	0.430	1.103	0.214	0.786
nf-36	0.051	0.143	0.440	0.145	0.222	1.304	2.443	0.835	0.449	1.115	0.193	0.807
nf-8	0.103		0.148	0.648	0.101	2.574	2.423	0.586	0.294	1.117	0.103	0.897
nf-83	0.069	0.070	0.118	0.448	0.295	1.290	2.424	0.844	0.468	1.114	0.139	0.861
ns-3	0.133		0.161	0.612	0.094	2.244	2.436	0.944	0.383	1.118	0.133	0.867
ns-4	0.115		0.213	0.611	0.060	1.732	2.513	0.943	0.389	1.122	0.115	0.885

Mössbauer spectrum fitting parameters for Appalachian biotites

sample	fit	BG	δ_0[3']	δ_0[2']	δ_1[2']	Δ_{Q1}[3']	σ_{A1}[3']	Δ_{Q2}[3']	σ_{A2}[3']	Δ_{Q1}[2']	σ_{A1}[2']	Δ_{Q2}[2']	σ_{A2}[2']	Δ_{Q1}[2']	σ_{A1}[2']
nwad	1-3	1187.6	0.316	1.067	0.020	0.724	0.964			2.645	0.076	2.444	0.281	1.786	0.195
pc2b	1-3	1343.6	0.274	1.051	0.027	0.640	0.967			2.652	0.075	2.467	0.266	1.831	0.201
pr5b	1-3	1923.7	0.392	1.045	0.031	1.040	0.711			2.674	0.115	2.408	0.424	2.394	0.000
slp	1-3	1049.7	0.247	1.003	0.045	0.556	0.926	0.450*	1.000	2.599	0.414	2.607	0.165	2.204	0.344
snf-1	1-3	2767.3	0.269	1.043	0.030	0.593	0.927			2.717	0.068	2.537	0.162	2.301	0.385
snf-19	2-3	2365.7	0.438	1.022	0.037	0.577	0.283	1.591	0.489	2.450	0.149	2.318	0.417	2.691	0.092
snf-2	2-3	2929.9	0.419	0.997	0.044	1.418	0.559	0.651	0.328	2.456	0.247	1.879	0.254	2.646	0.099
snf-25	1-3	2082.0	0.299	1.054	0.026	0.545	0.924			2.694	0.077	1.812	0.192	2.454	0.275
nb-214	1-3	2905.1	0.321	1.025	0.039	0.943	0.745			2.682	0.063	2.607	0.252	1.949	0.243
nb-145	2-3	1187.9	0.415	1.053	0.029	1.388	0.646	0.650	0.410	2.650	0.079	1.819	0.226	2.500	0.284
nb-146	2-3	2285.4	0.402	1.090	0.014	0.842	0.319	1.100*	0.736	2.588	0.187	2.342	0.429	2.678	0.062
nb-92	2-3	2008.8	0.474	1.033	0.031	1.100*	0.755	0.559	0.249	2.176	0.346	2.276	0.799	2.549	0.195
nb-78	1-3	2106.7	0.386	1.094	0.012	0.879	0.616			2.556	0.186	2.196	0.291	1.800*	0.827
nb-88	2-3	2123.6	0.508	1.016	0.038	0.531	0.210	0.950*	0.850	2.478	0.248	1.986	0.326	2.660	0.044
nb-58	2-3	2474.7	0.538	1.053	0.024	0.574	0.149	0.800	0.856	2.691	0.063	2.213	0.397	2.451	0.167
nb-89	2-3	2036.6	0.492	1.033	0.033	0.771	0.899	0.601	0.137	2.472	0.255	1.917	0.288	2.677	0.033
snf-10	2-3	2011.9	0.476	1.030	0.032	1.400	0.643	0.583	0.297	2.433	0.255	1.859	0.254	2.657	0.067
nb-239	2-3	2559.6	0.518	1.032	0.032	0.577	0.161	0.810*	0.918	2.685	0.071	2.252	0.403	2.449	0.166
nb-99	1-3	1522.4	0.497	1.069	0.017	0.550	0.125	0.834	0.872	2.417	0.271	2.669	0.046	1.810	0.223

continued

sample	a_1 [3⁺]	a_2 [3⁺]	a_1 [2⁺]	a_2 [2⁺]	a_3 [2⁺]	χ^2_{red}	$Fe^{2+}QS_{avg}$	$Fe^{3+}QS_{avg}$	$Fe^{3+}CS_{avg}$	$Fe^{2+}CS_{avg}$	Fe^{3+}/Fe	Fe^{2+}/Fe
nwad	0.082		0.146	0.658	0.114	2.254	2.395	0.724	0.316	1.116	0.082	0.918
pc5b	0.110		0.130	0.634	0.126	3.040	2.404	0.640	0.274	1.117	0.110	0.890
pr5p	0.124		0.363	0.473	0.040	3.066	2.517	1.040	0.392	1.123	0.124	0.876
slp	0.090	0.041	0.038	0.431	0.400	2.852	2.421	0.523	0.247	1.111	0.131	0.869
snf-1	0.106		0.121	0.248	0.525	4.432	2.423	0.593	0.269	1.116	0.106	0.894
snf-19	0.114	0.032	0.192	0.438	0.223	2.208	2.445	0.797	0.438	1.113	0.146	0.854
snf-2	0.060	0.169	0.494	0.115	0.162	5.272	2.410	0.851	0.419	1.104	0.229	0.771
snf-25	0.107		0.140	0.106	0.646	4.054	2.415	0.545	0.299	1.118	0.107	0.893
nb-214	0.141		0.164	0.596	0.098	3.136	2.546	0.943	0.321	1.124	0.141	0.859
nb-145	0.095	0.088	0.199	0.077	0.542	1.432	2.473	1.034	0.415	1.124	0.183	0.817
nb-146	0.020	0.130	0.324	0.377	0.149	1.348	2.495	1.066	0.402	1.125	0.150	0.850
nb-92	0.130	0.071	0.401	0.030	0.368	1.112	2.352	0.910	0.474	1.105	0.201	0.799
nb-78	0.166		0.362	0.381	0.091	1.872	2.310	0.879	0.386	1.122	0.166	0.834
nb-88	0.065	0.070	0.541	0.268	0.057	1.742	2.338	0.749	0.508	1.105	0.134	0.866
nb-58	0.034	0.070	0.104	0.563	0.229	2.072	2.329	0.726	0.538	1.108	0.104	0.897
nb-89	0.110	0.034	0.597	0.192	0.066	1.724	2.363	0.731	0.492	1.112	0.144	0.856
snf-10	0.055	0.109	0.591	0.147	0.098	2.646	2.358	0.855	0.476	1.107	0.164	0.836
nb-239	0.041	0.076	0.149	0.517	0.216	1.516	2.373	0.728	0.518	1.108	0.118	0.883
nb-99	0.017	0.051	0.705	0.070	0.158	2.144	2.332	0.764	0.497	1.108	0.068	0.932

Mössbauer spectrum fitting parameters for Hepburn and Bishop biotites (data from Lalonde et al. 1998).

sample	fit	BG	δ_p[3']	δ_p[2']	δ_i[2']	Δ_{p1}[3']	σ_{A1}[3']	Δ_{p2}[3']	σ_{A2}[3']	Δ_{p1}[2']	σ_{A1}[2']	Δ_{p2}[2']	σ_{A2}[2']	Δ_{p3}[2']	σ_{A3}[2']
HL125	1-3	2367.6	0.251	0.993	0.049	0.621	0.763			2.484	0.268	2.672	0.081	1.820	0.201
HL200	1-3	1599.5	0.325	1.135	-0.001	0.968	0.512			2.343	0.381	2.659	0.148	1.800*	1.322
HL204	1-3	1891.1	0.505	1.103	0.008	0.781	0.408			2.332	0.358	2.649	0.163	2.215	0.800
HL14	1-3	2143.5	0.434	1.074	0.016	1.077	0.656			2.247	0.382	2.611	0.168	2.635	0.837
HL341	1-3	1202.8	0.593	1.071	0.018	0.731	0.412			2.247	0.359	2.608	0.168	2.338	0.734
HS29	1-3	1484.5	0.437	1.107	0.004	0.892	0.526			2.257	0.380	2.610	0.165	2.027	1.216
BL255	1-3	1219.0	0.326	1.161	-0.011	1.016	0.340			2.217	0.368	2.634	0.165	1.800*	1.173
BL313	2-3	878.5	0.418	1.130	-0.004	0.801	0.370	1.582	0.701	2.281	0.326	2.631	0.143	2.079	0.794
BL315	2-3	1686.1	0.444	1.092	0.101	0.716	0.335	1.487	0.608	2.314	0.356	2.639	0.159	2.059	0.930
BL531	2-3	1462.9	0.445	1.103	0.004	0.731	0.342	1.408	0.582	2.282	0.312	2.617	0.149	2.069	0.744
BZ53	2-3	1028.6	0.462	1.049	0.023	0.690	0.349	1.45*	0.668	2.444	0.137	2.679	0.080	2.283	0.403
BL246	2-3	1326.4	0.475	1.047	0.021	0.669	0.304	1.45*	0.698	2.225	0.331	2.587	0.180	2.066	0.780
HL243	2-3	1316.2	0.487	1.054	0.025	0.599	0.261	1.253	0.734	2.541	0.197	2.704	0.066	2.283	0.417

Mössbauer spectrum fitting parameters for Mont Saint-Hilaire micas (data from Lalonde et al. 1996).

sample	fit	BG	a <3'>	a [3']	a_1 [2']	a_2 [2']	a_3 [2']	δ_i<3'>	δ_p[3']	δ_p[2']	δ_i[2']	Δ_q<3'>	σ_q<3'>	Δ_p[3']	σ_A[3']
Bt-b	1-1-3	839	0.075	0.046	0.282	0.371	0.226	0.152	0.467	1.204	-0.033	0.467	0.080	0.746	0.319
Bt-c	1-1-3	8536	0.066	0.057	0.313	0.507	0.058	0.152	0.470	1.252	-0.050	0.478	0.000	0.800	0.323
Bt-d	1-1-3	1331	0.107	0.061	0.278	0.414	0.140	0.258	0.431	1.134	-0.006	0.344	0.181	0.778	0.403
Ann	1-1-3	397	0.071	0.104	0.284	0.425	0.116	0.190	0.521	1.232	-0.043	0.452	0.091	0.736	0.373

continued

sample	a_1 [3⁺]	a_2 [3⁺]	a_1 [2⁺]	a_2 [2⁺]	a_3 [2⁺]	χ^2_{red}	$Fe^{2+}QS_{av}$	$Fe^{3+}QS_{avg}$	$Fe^{3+}CS_{avg}$	$Fe^{2+}CS_{avg}$	Fe^{3+}/Fe	Fe^{2+}/Fe
HL125	0.130	0.000	0.577	0.208	0.084	2.446	2.464	0.621	0.251	1.112	0.130	0.870
HL200	0.055	0.000	0.515	0.360	0.069	1.892	2.424	0.968	0.325	1.132	0.055	0.945
HL204	0.063	0.000	0.433	0.378	0.125	2.700	2.445	0.781	0.505	1.123	0.063	0.937
HL14	0.124	0.000	0.482	0.367	0.027	2.914	2.412	1.077	0.434	1.113	0.124	0.876
HL341	0.049	0.000	0.399	0.425	0.126	1.992	2.421	0.731	0.593	1.116	0.049	0.951
HS29	0.070	0.000	0.516	0.346	0.068	2.564	2.371	0.892	0.437	1.117	0.070	0.930
BL255	0.076	0.000	0.492	0.318	0.114	2.17	2.309	1.016	0.326	1.135	0.076	0.924
BL313	0.149	0.036	0.359	0.324	0.131	1.136	2.387	0.954	0.418	1.120	0.186	0.814
BL315	0.130	0.065	0.414	0.326	0.065	1.612	2.425	0.972	0.444	1.116	0.195	0.805
BL531	0.117	0.043	0.367	0.332	0.140	1.544	2.379	0.914	0.445	1.113	0.161	0.839
BZ53	0.136	0.080	0.163	0.161	0.460	0.986	2.398	0.971	0.462	1.104	0.216	0.784
BL246	0.120	0.054	0.404	0.342	0.080	1.440	2.359	0.912	0.475	1.097	0.174	0.826
HL243	0.076	0.088	0.261	0.096	0.478	1.178	2.412	0.949	0.487	1.115	0.165	0.835

continued

sample	Δ_{a1}[2⁺]	σ_{a1}[2⁺]	Δ_{a2}[2⁺]	σ_{a2}[2⁺]	Δ_{a3}[2⁺]	σ_{a3}[2⁺]	χ^2_{red}	$^{IV}Fe^{3+}QS_{avg}$	$^{IV}Fe^{3+}CS_{avg}$	$Fe^{2+}QS_{avg}$	$Fe^{2+}CS_{avg}$	$^{VI}Fe^{3+}QS_{avg}$	$Fe^{3+}CS_{avg}$	Fe^{3+}/Fe	Fe^{2+}/Fe
Bt-b	2.642	0.067	2.353	0.194	1.962	0.284	1.320	0.467	0.152	2.345	1.127	0.746	0.467	0.121	0.879
Bt-c	2.618	0.086	2.243	0.307	1.705	0.671	5.000	0.478	0.152	2.342	1.135	0.800	0.470	0.123	0.878
Bt-d	2.626	0.083	2.389	0.236	2.042	0.464	1.530	0.344	0.206	2.410	1.120	0.778	0.431	0.168	0.833
Ann	2.607	0.070	2.311	0.262	1.793	0.610	1.200	0.452	0.190	2.340	1.131	0.736	0.521	0.175	0.825

Note: symmetric doublets are assumed for all sites. The <3⁺>, [3⁺] and [2⁺] refer respectively to tetrahedral Fe^{3+}, octahedral Fe^{3+} and Fe^{2+} specific parameters respectively.

BG is in kilocounts per channel, parametes δ_a, Δ_a and σ_a are in mm/s, parameter δ1 is dimensionless and Γ = 0 for Hepburn and Bishop and is a free parameter for Mont Saint-Hilaire spectra.

*: this parameter was frozen during fitting.

Appendix for Manuscript 3

Tabulated below are the XRD data for muscovites. Powder XRD patterns were obtained using a Philips X'Pert PW3710 automated powder diffractometer (CuK_{α} radiation). The calculations of d-spacings were done using a wavelength of 1.5418 Å for CuK_{α}. The intensities were evaluated with the PC-APD software package provided on the Philips diffractometer. For unit-cell refinements, the indexing of the muscovite peaks was done on the basis of a XRD powder pattern of synthetic $2M_1$ muscovite reported by Bailey (1984).

XRD peaks observed for muscovite (nb-173)

Angle (°2 θ)	d-spacing (Å)	peak width (°2 θ)	peak intensity (counts)	relative intensity (%)
8.910	0.0865	0.1	36100	41.9
12.450	0.0619	0.1	49	0.1
13.160	0.0586	0.24	25	0
16.240	0.0475	0.12	26	0
17.810	0.0433	0.1	25857	30
18.330	0.0421	0.1	353	0.4
19.950	0.0386	0.1	1024	1.2
20.240	0.0381	0.1	246	0.3
20.730	0.0372	0.14	279	0.3
21.640	0.0356	0.1	286	0.3
22.040	0.0350	0.1	190	0.2
22.440	0.0344	0.2	231	0.3
22.940	0.0336	0.12	795	0.9
23.860	0.0323	0.12	858	1
25.575	0.0301	0.14	1576	1.8
26.810	0.0288	0.14	86084	100
27.890	0.0276	0.16	2007	2.3
28.665	0.0269	0.12	424	0.5
29.915	0.0258	0.14	2362	2.7
31.275	0.0246	0.16	1747	2
32.090	0.0240	0.14	1436	1.7
32.770	0.0235	0.16	154	0.2
33.130	0.0233	0.12	182	0.2
33.470	0.0230	0.12	151	0.2
34.080	0.0226	0.12	151	0.2
34.660	0.0222	0.16	692	0.8
35.060	0.0220	0.16	1832	2.1
35.985	0.0214	0.1	10363	12
36.470	0.0211	0.1	882	1
37.325	0.0207	0.16	317	0.4
37.850	0.0204	0.1	502	0.6
38.960	0.0198	0.16	56	0.1
40.045	0.0193	0.16	188	0.2
40.365	0.0191	0.16	188	0.2
41.060	0.0188	0.1	216	0.3
41.425	0.0186	0.1	172	0.2
42.040	0.0183	0.1	361	0.4
42.445	0.0182	0.16	645	0.7
43.440	0.0177	0.12	276	0.3
44.150	0.0175	0.16	262	0.3
45.410	0.0170	0.2	36941	42.9
46.115	0.0167	0.2	625	0.7
46.665	0.0165	0.16	328	0.4
48.635	0.0159	0.12	114	0.1
49.935	0.0154	0.12	108	0.1
50.755	0.0152	0.16	32	0
52.845	0.0146	0.32	317	0.4
55.165	0.0140	0.2	824	1
55.905	0.0138	0.24	745	0.9

XRD peaks observed for muscovite (nb-173)

Angle (°2 θ)	d-spacing (Å)	peak width (°2 θ)	peak intensity (counts)	relative intensity (%)
56.500	0.0136	0.12	190	0.2
56.905	0.0135	0.12	169	0.2
57.525	0.0134	0.16	180	0.2
59.195	0.0130	0.1	272	0.3
60.670	0.0127	0.2	408	0.5
61.740	0.0125	0.32	424	0.5
63.195	0.0122	0.1	182	0.2
64.040	0.0120	0.2	534	0.6
65.385	0.0118	0.1	1962	2.3
65.935	0.0117	0.12	266	0.3
66.195	0.0116	0.12	177	0.2
67.040	0.0115	0.1	286	0.3
67.780	0.0114	0.1	114	0.1
68.365	0.0113	0.16	180	0.2
69.390	0.0111	0.12	751	0.9
70.200	0.0110	0.1	520	0.6
70.450	0.0109	0.12	454	0.5
71.000	0.0109	0.12	250	0.3
71.260	0.0108	0.12	199	0.2
72.210	0.0107	0.12	202	0.2
73.065	0.0106	0.48	174	0.2
74.250	0.0104	0.2	219	0.3
76.245	0.0101	0.14	2560	3
78.480	0.0098	0.48	41	0
79.735	0.0097	0.1	66	0.1

XRD peaks observed for muscovite (nb-29).

Angle (°2 θ)	d-spacing (Å)	peak width (°2 θ)	peak intensity (counts)	relative intensity (%)
8.195	10.7888	0.1	199	0.3
8.895	9.9412	0.12	41820	52.7
12.530	7.0642	0.1	72	0.1
13.265	6.6744	0.24	24	0
17.810	4.9801	0.1	21993	27.7
19.885	4.4649	0.12	445	0.6
20.880	4.2543	0.12	169	0.2
21.595	4.1150	0.16	125	0.2
22.115	4.0194	0.1	132	0.2
22.885	3.8859	0.14	299	0.4
23.815	3.7362	0.14	346	0.4
25.470	3.4971	0.16	571	0.7
26.810	3.3252	0.12	79355	100
27.535	3.2393	0.12	751	0.9
27.900	3.1978	0.1	1136	1.4
29.915	2.9868	0.2	900	1.1
31.220	2.8649	0.1	767	1
32.040	2.7934	0.14	610	0.8
34.975	2.5654	0.2	876	1.1
35.990	2.4954	0.1	8226	10.4
37.785	2.3808	0.2	225	0.3
38.460	2.3406	0.12	58	0.1
40.325	2.2365	0.1	94	0.1
41.965	2.1529	0.1	161	0.2
42.410	2.1313	0.1	243	0.3
43.430	2.0836	0.12	161	0.2
45.420	1.9968	0.1	25792	32.5
49.970	1.8251	0.1	100	0.1
52.890	1.7310	0.1	76	0.1
55.175	1.6646	0.16	692	0.9
55.820	1.6469	0.28	262	0.3
57.520	1.6022	0.1	36	0
58.240	1.5841	0.1	61	0.1
59.150	1.5619	0.1	83	0.1
61.050	1.5178	0.1	132	0.2
61.730	1.5027	0.1	161	0.2
64.025	1.4542	0.28	234	0.3
65.425	1.4265	0.12	1429	1.8
66.060	1.4143	0.1	106	0.1
67.070	1.3954	0.16	119	0.1
68.185	1.3753	0.12	67	0.1
69.485	1.3527	0.1	196	0.2
70.370	1.3379	0.16	188	0.2
71.295	1.3228	0.12	98	0.1
72.240	1.3078	0.24	69	0.1
74.515	1.2734	0.1	90	0.1
76.265	1.2485	0.12	1731	2.2
76.520	1.2449	0.1	942	1.2
78.390	1.2199	0.12	36	0

XRD peaks observed for muscovite (nb-166).

Angle (°2 θ)	d-spacing (Å)	peak width (°2 θ)	peak intensity (counts)	relative intensity (%)
8.875	9.9636	0.1	15277	34.3
12.395	7.1409	0.12	610	1.4
17.785	4.9870	0.1	12188	27.4
19.870	4.4682	0.1	1632	3.7
20.660	4.2991	0.1	534	1.2
20.835	4.2634	0.1	847	1.9
21.635	4.1075	0.16	376	0.8
22.435	3.9628	0.16	266	0.6
22.905	3.8825	0.1	1296	2.9
23.840	3.7323	0.1	1296	2.9
24.385	3.6501	0.1	234	0.5
24.895	3.5765	0.14	967	2.2
25.510	3.4917	0.18	1731	3.9
26.800	3.3265	0.14	44521	100
27.910	3.1966	0.16	2304	5.2
28.615	3.1195	0.1	697	1.6
29.895	2.9888	0.1	4083	9.2
31.260	2.8613	0.1	2798	6.3
32.050	2.7925	0.12	1936	4.3
33.450	2.6788	0.1	562	1.3
34.645	2.5891	0.1	1414	3.2
35.015	2.5626	0.1	3114	7
35.985	2.4957	0.1	6194	13.9
36.525	2.4600	0.1	936	2.1
37.280	2.4119	0.12	471	1.1
37.745	2.3833	0.16	734	1.6
39.505	2.2811	0.1	310	0.7
40.200	2.2432	0.1	534	1.2
41.035	2.1995	0.1	424	1
42.095	2.1465	0.1	801	1.8
42.465	2.1287	0.2	1043	2.3
44.060	2.0552	0.4	320	0.7
45.410	1.9972	0.16	26050	58.5
46.015	1.9724	0.16	841	1.9
46.585	1.9495	0.1	590	1.3
48.155	1.8896	0.24	156	0.4
48.660	1.8712	0.12	182	0.4
49.355	1.8464	0.16	85	0.2
50.145	1.8192	0.1	350	0.8
52.875	1.7315	0.32	458	1
53.555	1.7111	0.1	253	0.6
55.225	1.6633	0.1	1406	3.2
55.815	1.6471	0.1	1444	3.2
57.595	1.6003	0.1	424	1
59.265	1.5592	0.1	590	1.3
59.990	1.5420	0.12	396	0.9
60.730	1.5250	0.16	778	1.7
61.770	1.5018	0.2	718	1.6
63.370	1.4677	0.14	207	0.5

XRD peaks observed for muscovite (nb-166).

Angle (°2 θ)	d-spacing (Å)	peak width (°2 θ)	intensity (counts)	intensity (%)
64.030	1.4541	0.14	894	2
65.405	1.4269	0.16	1901	4.3
65.970	1.4160	0.12	428	1
67.055	1.3957	0.12	404	0.9
68.210	1.3749	0.1	310	0.7
69.470	1.3530	0.1	1347	3
70.290	1.3392	0.1	930	2.1
71.180	1.3246	0.1	511	1.1
72.225	1.3080	0.16	331	0.7
73.135	1.2940	0.1	552	1.2
74.250	1.2773	0.24	328	0.7
76.285	1.2482	0.18	2372	5.3
78.500	1.2184	0.28	237	0.5
79.650	1.2037	0.12	317	0.7

XRD peaks observed for muscovite (nb-19).

Angle (°2 θ)	d-spacing (Å)	peak width (°2 θ)	peak intensity (counts)	relative intensity (%)
8.915	9.9190	0.1	23963	34.4
17.795	4.9842	0.12	13202	18.9
19.870	4.4682	0.24	1030	1.5
20.165	4.4035	0.1	250	0.4
20.660	4.2991	0.1	445	0.6
21.625	4.1094	0.1	506	0.7
22.395	3.9698	0.16	216	0.3
22.920	3.8800	0.12	864	1.2
23.815	3.7362	0.16	912	1.3
25.505	3.4923	0.14	1781	2.6
26.820	3.3240	0.1	69749	100
27.880	3.2000	0.18	2343	3.4
28.635	3.1173	0.1	586	0.8
29.885	2.9897	0.16	2788	4
31.250	2.8622	0.14	2362	3.4
32.065	2.7913	0.12	1989	2.9
34.555	2.5956	0.1	992	1.4
34.945	2.5675	0.2	2411	3.5
36.000	2.4947	0.1	9604	13.8
36.460	2.4643	0.2	454	0.7
37.340	2.4082	0.1	756	1.1
37.745	2.3833	0.16	676	1
40.130	2.2470	0.1	342	0.5
41.005	2.2010	0.1	396	0.6
41.270	2.1875	0.1	342	0.5
42.070	2.1477	0.1	650	0.9
42.440	2.1299	0.1	1239	1.8
43.450	2.0827	0.1	320	0.5
43.960	2.0597	0.24	324	0.5
45.435	1.9962	0.1	38652	55.4
46.525	1.9519	0.1	600	0.9
49.945	1.8260	0.2	196	0.3
52.870	1.7317	0.1	718	1
53.510	1.7124	0.16	185	0.3
55.205	1.6638	0.1	1584	2.3
55.815	1.6471	0.1	1325	1.9
57.485	1.6031	0.1	317	0.5
59.210	1.5605	0.18	361	0.5
60.730	1.5250	0.1	841	1.2
61.675	1.5039	0.16	581	0.8
64.040	1.4539	0.22	812	1.2
65.445	1.4261	0.14	2430	3.5
65.990	1.4156	0.16	420	0.6
67.125	1.3944	0.16	376	0.5
69.460	1.3531	0.2	1096	1.6
70.260	1.3397	0.2	734	1.1
71.055	1.3266	0.16	350	0.5
72.235	1.3078	0.16	369	0.5
73.115	1.2943	0.16	188	0.3

XRD peaks observed for muscovite (nb-19).

Angle (°2 θ)	d-spacing (Å)	peak width (°2 θ)	peak intensity (counts)	relative intensity (%)
74.255	1.2772	0.16	269	0.4
76.300	1.2480	0.14	3080	4.4
78.380	1.2200	0.24	106	0.2
79.730	1.2027	0.1	237	0.3

XRD peaks observed for muscovite (nb-127).

Angle (°2 θ)	d-spacing (Å)	peak width (°2 θ)	peak intensity (counts)	relative intensity (%)
9.035	9.7875	0.12	44690	75.6
12.665	6.9892	0.1	74	0.1
17.935	4.9457	0.18	20022	33.9
20.075	4.4230	0.28	686	1.2
20.795	4.2715	0.12	190	0.3
21.765	4.0833	0.12	202	0.3
22.525	3.9472	0.2	139	0.2
23.080	3.8535	0.2	462	0.8
24.000	3.7078	0.12	595	1
25.655	3.4723	0.1	858	1.5
26.955	3.3077	0.18	59146	100
28.065	3.1793	0.12	1204	2
28.615	3.1195	0.16	8556	14.5
30.075	2.9713	0.18	1332	2.3
31.450	2.8444	0.2	912	1.5
32.270	2.7740	0.18	795	1.3
34.695	2.5855	0.1	353	0.6
35.115	2.5555	0.14	949	1.6
36.155	2.4843	0.18	5991	10.1
37.475	2.3998	0.12	228	0.4
38.030	2.3661	0.1	286	0.5
40.270	2.2395	0.1	207	0.4
41.205	2.1908	0.1	88	0.1
41.555	2.1731	0.1	172	0.3
42.200	2.1414	0.12	272	0.5
42.530	2.1256	0.2	328	0.6
43.600	2.0758	0.1	272	0.5
45.590	1.9898	0.18	21727	36.7
47.505	1.9139	0.1	6115	10.3
50.115	1.8202	0.14	76	0.1
53.025	1.7270	0.28	139	0.2
55.395	1.6586	0.14	571	1
55.900	1.6448	0.1	416	0.7
56.285	1.6344	0.12	1537	2.6
57.680	1.5982	0.1	77	0.1
59.300	1.5583	0.1	121	0.2
60.965	1.5197	0.1	713	1.2
61.630	1.5049	0.16	149	0.3
64.200	1.4507	0.18	303	0.5
65.600	1.4231	0.16	1156	2
66.125	1.4131	0.14	154	0.3
67.215	1.3928	0.1	169	0.3
68.390	1.3717	0.1	94	0.2
69.330	1.3554	0.1	372	0.6
69.590	1.3509	0.1	595	1
70.405	1.3373	0.1	253	0.4
70.585	1.3343	0.1	210	0.4
71.200	1.3243	0.2	139	0.2
72.310	1.3067	0.12	102	0.2

XRD peaks observed for muscovite (nb-127).

Angle (°2 θ)	d-spacing (Å)	peak width (°2 θ)	peak intensity (counts)	relative intensity (%)
73.195	1.2930	0.12	53	0.1
74.325	1.2762	0.1	83	0.1
76.435	1.2461	0.2	1467	2.5
78.600	1.2171	0.2	27	0
79.825	1.2015	0.1	177	0.3

XRD peaks observed for muscovite (nb-13).

Angle (°2 θ)	d-spacing (Å)	peak width (°2 θ)	peak intensity (counts)	relative intensity (%)
8.880	9.9580	0.14	23470	100
17.780	4.9884	0.16	6432	27.4
19.870	4.4682	0.16	449	1.9
20.615	4.3084	0.16	154	0.7
21.610	4.1122	0.24	144	0.6
22.285	3.9891	0.12	112	0.5
22.855	3.8909	0.2	269	1.1
23.775	3.7424	0.24	259	1.1
25.505	3.4923	0.2	515	2.2
26.795	3.3271	0.12	15525	66.1
27.825	3.2062	0.24	552	2.4
29.835	2.9946	0.12	605	2.6
31.260	2.8613	0.16	428	1.8
32.035	2.7938	0.1	529	2.3
34.970	2.5658	0.1	718	3.1
35.980	2.4960	0.14	1632	7
37.295	2.4110	0.12	123	0.5
37.720	2.3848	0.1	219	0.9
42.430	2.1303	0.28	110	0.5
43.320	2.0886	0.1	142	0.6
45.405	1.9974	0.14	4007	17.1
52.615	1.7394	0.1	94	0.4
55.145	1.6655	0.12	142	0.6
55.795	1.6476	0.12	149	0.6
57.465	1.6036	0.1	71	0.3
59.240	1.5598	0.12	21	0.1
60.710	1.5255	0.16	44	0.2
61.615	1.5052	0.16	55	0.2
64.000	1.4547	0.28	38	0.2
65.410	1.4268	0.16	204	0.9
67.070	1.3954	0.1	45	0.2
68.160	1.3757	0.12	23	0.1
69.450	1.3533	0.32	64	0.3
70.180	1.3410	0.16	44	0.2
71.040	1.3269	0.2	21	0.1
76.265	1.2485	0.12	193	0.8

Analytical uncertainty

1. Electron Microprobe Analysis

Mineral analyses were obtained by wavelength-dispersive X-ray spectrometry for 11 elements (K, Na, Ca, Mg, Mn, Fe, Al, Ti, Si, F, and Cl) using the JEOL 8900 Superprobe of the McGill University Microprobe Laboratory. Typical beam operating conditions were 15 kV and 20 nA.

Below is an estimate of analytical precision for each element of a typical biotite analysis by the electromicroprobe during the periode of operation. However, it would be incorrect to comment on the accuracy of the microprobe data, due to various interacting sources of errors, i.e., surface roughness, geometrical effects, incorrect concentration values for standards, poor matrix corrections, etc. (personnal communication with Glenn Poirier, McGill University Microprobe Laboratory).

Specimen NB-195

Oxides	wt%	STD
SiO2	36.41	0.10
TiO2	2.70	0.04
Al2O3	14.08	0.06
FeO	22.12	0.13
MnO	0.52	0.09
MgO	13.91	0.07
CaO	0.18	0.00
Na2O	0.10	0.01
K2O	9.23	0.07
F	0.66	0.05
Cl	0.03	0.00

2. Mössbauer Spectroscopy

Transmission ^{57}Fe Mössbauer spectra of 67 mica specimens were obtained at room temperature (RT=22°C) using a ^{57}Co rhodium matrix source on a velocity range of ±4 mm/s with a constant acceleration transducer. Data were collected on 1024 channels, which covered twice the Doppler velocity range of ±4 mm/s. Calibrations of spectra were obtained with a ^{57}Fe-enriched iron foil, both before and after each experiment. All positions are reported with respect to this calibration spectrum, i.e., with respect to the centre shift (CS) of metallic α-Fe at RT. All spectra were folded to give a flat background (BG). The new Voigt-based model of arbitrary-shape quadrupole splitting distributions (QSD) of Rancourt and Ping (1991) was used to fit the spectra.

Recently, Lalonde et al. (1998) have examined the accuracy of Fe^{3+}/Fe^{2+} ratios in micas and compared Mössbauer spectroscopy with conventional wet-chemical methods. It has been shown that the best alternative to wet-chemical techniques is Mössbauer spectroscopy. When absorber preparation is optimized, full absorber thickness corrections are made and QSD analysis is used, it can give precision on Fe^{3+}/Fe^{2+} ratios of about 0.2% of total Fe (Lalonde et al. 1998).